UNIVERSIDAD POLITÉCNICA DE MADRID

ESCUELA TÉCNICA SUPERIOR DE INGENIEROS AERONÁUTICOS

# ANALYSIS OF THE GEOMETRIC ALTIMETRY TO SUPPORT AIRCRAFT OPTIMAL TRAJECTORIES WITHIN THE FUTURE 4D TRAJECTORY MANAGEMENT

TESIS DOCTORAL / DISSERTATION

JAVIER GARCÍA-HERAS CARRETERO

INGENIERO AERONÁUTICO / M.S. AERONAUTICAL ENGINEER

2014

DEPARTAMENTO DE INFRAESTRUCTURA, SISTEMAS AEROSPACIALES Y AEROPUERTOS

ESCUELA TÉCNICA SUPERIOR DE INGENIEROS AERONÁUTICOS

# Título:

ANALYSIS OF THE GEOMETRIC ALTIMETRY TO SUPPORT AIRCRAFT OPTIMAL TRAJECTORIES WITHIN THE FUTURE 4D TRAJECTORY MANAGEMENT

# Autor:

JAVIER GARCÍA-HERAS CARRETERO

Ingeniero Aeronáutico / M.S. Aeronautical Engineer

# Director de Tesis:

Francisco Javier Sáez Nieto

Doctor en Ciencias Físicas / Doctor of Science

U.D. Navegación y Circulación Aérea

Luís Pérez Sánz

Doctor en Ciencias Físicas / Doctor of Science

U.D. Navegación y Circulación Aérea

2014

Tribunal nombrado por el Sr. Rector Magfco. de la Universidad Politécnica de Madrid, el dia.....de.....de 20.....

Presidente: _____

Vocal: _____

Vocal: _____

Vocal: _____

Secretario: _____

Suplente: _____

Suplente: _____

Realizado el acto de defensa y lectura de la Tesis el día.....de.....de 2014 en la E.T.S.I. Aeronáuticos

Calificación.....

EL PRESIDENTE LOS VOCALES

EL SECRETARIO

## ABSTRACT

Over the past few years, the common practice within air traffic management has been that commercial aircraft fly by following a set of predefined routes to reach their destination. Currently, aircraft operators are requesting more flexibility to fly according to their preferences, in order to achieve their business objectives. Due to this reason, much research effort is being invested in developing different techniques which evaluate aircraft optimal trajectory and traffic synchronisation. Also, the inefficient use of the airspace using barometric altitude overall in the landing and takeoff phases or in Continuous Descent Approach (CDA) trajectories where currently it is necessary introduce the necessary reference setting (QNH or QFE). To solve this problem and to permit a better airspace management born the interest of this research. Where the main goals will be to evaluate the impact, weakness and strength of the use of geometrical altitude instead of the use of barometric altitude. Moreover, this dissertation propose the design a simplified trajectory simulator which is able to predict aircraft trajectories. The model is based on a three degrees of freedom aircraft point mass model that can adapt aircraft performance data from Base of Aircraft Data, and meteorological information. A feature of this trajectory simulator is to support the improvement of the strategic and pre-tactical trajectory planning in the future Air Traffic Management. To this end, the error of the tool (aircraft Trajectory Simulator) is measured by comparing its performance variables with actual flown trajectories obtained from Flight Data Recorder information. The trajectory simulator is validated by analysing the performance of different type of aircraft and considering different routes. A fuel consumption estimation error was identified and a correction is proposed for each type of aircraft model.

In the future Air Traffic Management (ATM) system, the trajectory becomes the fundamental element of a new set of operating procedures collectively referred to as Trajectory-

Based Operations (TBO). Thus, governmental institutions, academia, and industry have shown a renewed interest for the application of trajectory optimisation techniques in commercial aviation. The trajectory optimisation problem can be solved using optimal control methods. In this research we present and discuss the existing methods for solving optimal control problems focusing on direct collocation, which has received recent attention by the scientific community. In particular, two families of collocation methods are analysed, i.e., Hermite-Legendre-Gauss-Lobatto collocation and the pseudospectral collocation. They are first compared based on a benchmark case study: the minimum fuel trajectory problem with fixed arrival time. For the sake of scalability to more realistic problems, the different methods are also tested based on a real Airbus 319 El Cairo-Madrid flight. Results show that pseudospectral collocation, which has shown to be numerically more accurate and computationally much faster, is suitable for the type of problems arising in trajectory optimisation with application to ATM. Fast and accurate optimal trajectory can contribute properly to achieve the new challenges of the future ATM.

As atmosphere uncertainties are one of the most important issues in the trajectory planning, the final objective of this dissertation is to have a magnitude order of how different is the fuel consumption under different atmosphere condition. Is important to note that in the strategic phase planning the optimal trajectories are determined by meteorological predictions which differ from the moment of the flight. The optimal trajectories have shown savings of at least 500 [kg] in the majority of the atmosphere condition (different pressure, and temperature at Mean Sea Level, and different lapse rate temperature) with respect to the conventional procedure simulated at the same atmosphere condition.This results show that the implementation of optimal profiles are beneficial under the current Air traffic Management (ATM).

## RESUMEN

Durante los últimos años, la práctica habitual en el control de tráfico aéreo ha sido que las aeronaves puedan volar solamente por unas rutas predefinidas para poder alcanzar sus destinos. Actualmente, los operadores requieren disponer de más flexibilidad para volar de acuerdo a sus necesidades y así poder conseguir también sus objetivos de negocio. Por esta razón, se debe realizar un esfuerzo mayor en la investigación de nuevas técnicas que evalúen las trayectorias óptimas y la sincronización del tráfico. Además, el uso ineficiente del espacio aéreo debido al uso de la altitud barométrica tanto en las fase de despegue y aterrizaje como en los descensos de pendiente continua donde es necesario proporcionar el correcto reglaje del altímetro (QNH o QFE). Para resolver este problema y también para permitir un mejor aprovechamiento del espacio aéreo nace el interés de la presente investigación. Donde el principal objetivo será evaluar el impacto, fortalezas y debilidades del uso de la altitud geométrica en lugar de la altitud barométrica. Además, esta tesis presenta un simplificado simulador de trayectorias capaz de predecir las trayectorias de las aeronaves con la suficiente precisin. Está basado en un modelo de tres grados de libertad que puede emplear datos de cualquier tipo de aeronaves a través de la base de datos aeronáutica (BADA), así como de información meteorológica. El futuro de este simulador de trayectorias es apoyar a la mejora del diseño de las trayectorias en la fase estratégica y pre-táctica del futuro control de tráfico aéreo. Para este respecto, se ha medido el error cometido por la herramienta mediante la comparación directa con un flujo de trayectorias reales de aeronaves obtenidas a través de grabaciones de datos del vuelo. El simulador de trayectorias es validado evaluando las prestaciones de la herramienta para diferentes tipos de aeronaves y considerando diferentes rutas. Un error en el consumo de combustible ha sido identificado así como se ha propuesto un factor de corrección cada tipo de aeronave.

En el futuro sistema de gestión del trafico aéreo, las trayectorias toman un lugar fun-

damental de un nuevo conjunto de procedimientos operativos llamados colectivamente como Trajectory-Based Operations (TBO). Por lo tanto gobiernos, universidades, y la industria han visto un renovado interés por la aplicación de las técnicas de optimización de las trayectorias en la aviación comercial. El problema de optimización de trayectorias puede resolverse mediante el uso de métodos de control óptimo. En esta investigación se presenta y se discute los métodos existentes para la resolución de dichos problemas haciendo mayor hincapié en los métodos de colocación directa, los cuales han sido de gran interés para la comunidad científica. En concreto se han analizado dos familias de métodos de colocación: Hermite-Legendre-Gauss-Lobatto collocation y los pseudospectral collocation. Han sido primeramente comparados en un problema de Benchmark: mínimo consumo de combustible con un tiempo fijo de llegada. Para un mayor acercamiento con problemas reales, se han analizado los anteriores métodos para un Airbus 319 en su ruta El Cairo-Madrid. Los resultados muestran que los métodos pseudospectrales son mucho mas rápidos, e interesantes para los problemas de optimización de trayectorias con aplicación en la gestión del tráfico aéreo. Rápidas y precisas trayectorias pueden contribuir adecuadamente a conseguir los retos de la futura gestión del tráfico aéreo.

Como las incertidumbres atmosféricas son una de las cosas más relevantes en el diseño de trayectorias, el objetivo final de esta tesis doctoral es tener un orden de magnitud del valor del consumo de combustible para diferentes condiciones atmosféricas. Es importante resaltar que en la fase estratégica las trayectorias son determinadas mediante predicción de trayectorias que son diferentes de la existente en el momento del vuelo. Las trayectorias óptimas calculadas han mostrado ahorros de gasto de combustible de al menos 500 [kg] en la mayoría de las condiciones atmosféricas (diferentes presiones y temperaturas al nivel medio del mar, y diferentes valores de la pendiente de temperatura con la altura) con respecto a los procedimientos convencionales simulados con la misma condición atmosférica. Los resultados

muestran que la implementación de perfiles óptimos son beneficiosos bajo el actual sistema de gestión del tráfico aéreo.

## ACKNOWLEDGMENTS

He soñado tantos días con que llegaba el momento de tener que escribir esta sección en mi tesis y ahora que ha llegado me quedo sin palabras. Son tantas las personas que me han ayudado y tantos los momentos buenos y no tan buenos vividos durante los años dedicados a esta tesis, a esta etapa de mi vida, que no puedo evitar emocionarme al recordarlos.

En primer lugar y por méritos propios le quería agradecer al Dr. Francisco Javier Sáez Nieto. Paco me distes la oportunidad, me ofreciste una tesis interesantísima y me has ayudado en todo el camino, ¿Qué más puedo pedir? Pues sí hay más, pienso en el niño que entró en tu despacho antes de comenzar esta aventura hablándote sobre mi sueño de llegar a ser doctor y me miro al espejo ahora y no sólo tengo más canas y más años sino que he cambiado mucho, he madurado, he aprendido. Gracias por ayudarme a ser la persona que soy hoy día, trabajando día a día contigo uno no es consciente de todo lo que llega a desarrollar su potencial habiendo estado a tu lado, pero ahora lo soy. Siempre que en mi trabajo no encuentro la respuesta pienso ¿Qué me diría Paco? Sigo tus consejos y encuentro lo que buscaba: la solución. Gracias también por confiar siempre en mi, dándome responsabilidades que me hacían sentir como tu mano derecha. Y eso es mucho decir ya que como siempre te he dicho para mi eras más que un jefe, eras ese "gran gurú" que todo lo sabe, que con 5 minutos de su tiempo te podía ahorrar semanas. Finalmente gracias por concederme el honor de trabajar a tu lado ya que siempre podré decir "Sí, yo trabajé con el gran Sáez Nieto".

En segundo lugar porque sin ti no hubiera terminado esta tesis, quería agradecerle al Dr. Manuel Soler todo lo que ha aportado en el desarrollo de esta tesis. Llegaste en el momento en el que más perdido estaba iluminando mi camino y haciendo que viera la luz al final del túnel, ofreciendo tu trabajo, tiempo y conocimientos de forma totalmente desinteresada. De

la colaboración contigo no sólo he sacado papers y publicaciones en congresos, al trabajar contigo he aprendido mucho más que optimal control, he aprendido a trabajar y he ganado un compañero y amigo. Aunque fueron momentos de mucho agobio y trabajo, han sido sin duda los momentos más provechosos y bonitos que he sacado de esta tesis.

Al Groupe de Recherche en Automatique du Laboratoire MAIAA de la ENAC y muy especialmente al Dr. Félix Mora-Camino por toda la ayuda prestada no sólo al permitirme la realización de la estancia, sino que en todo momento que he necesitado algo de su parte nunca he recibido un no por respuesta, gracias por estar siempre ahí.

A mis queridos compañeros del GINA que han aguantado cada momento que he pasado peleando con esta tesis. Gracias Ricardo, Rocío, Lawrence, Elena, Cristina, Enrique, Mikel... Nunca un despacho tan pequeño concentró tanto conocimiento. Sin animo de menospreciar a nadie ya que todos habéis sido muy importantes, quisiera resaltar la figura del futuro Dr. Lawrence Kyei Asante porque siempre has tenido tiempo para revisarme un articulo y echarme una mano cuando lo necesitaba, siempre has tenido tiempo para darme esos consejos de sabio que tanto me han ayudado, gracias bro!. Así como a Elena Justel que me ayudó en el proceso de validación del predictor de trayectorias haciendo que esta ardua tarea resultase super gratificante y amena.

A mi familia, ¿Qué puedo decir? Que aunque la vida nunca ha sido justa con nosotros y año tras año se supera, seguimos estando unidos y superando todos los baches del camino, porque si algo he aprendido de vosotros es que todos unidos somos invencibles. Gracias por todo el apoyo que he recibido durante estos años y sin el cual me hubieran faltando las fuerzas para llegar a esta parte. Esta tesis te la dedico a ti Irene, porque sería injusto si no lo hiciera porque has moldeado a esta persona desde bien pequeño haciéndole que fuera responsable, constante, cabezota y obstinado con las cosas que se proponga, por recordarme todos los días que iba a venir Paco con las rebajas. Gracias porque si de algo estoy seguro

es que sin ti no hubiera hecho Aeronáutica y sin ti no hubiera sabido que todo esfuerzo tiene su recompensa y que para conseguir lo que uno quiere hay que dejarse la piel. GRACIAS POR SER SIEMPRE ESE ESPEJO AL QUE MIRARME.

Quisiera también hacer una mención especial a mi mujer Lucía, porque no sólo eres mi a alma gemela y amiga sino que me has demostrado en todo este tiempo que darías la vida por mi, has aguantado mis interminables jornadas de trabajo, todos mis desplantes, por hacer tuyo este mi sueño de ser doctor y poner tanto empeño en ello como el mío propio. Gracias por sentarte a escribir conmigo cuando ya no me quedaban fuerzas. Gracias porque cuando no me quedan fuerzas ni para seguir caminando siempre me ofreces tu regazo permitiéndome dar un paso más. Y como ya dije en su día GRACIAS POR SER MI SUEÑO MÁS REAL.

> *"Your time is limited, so don't waste it living someone else's life. Don't be trapped by dogma - which is living with the results of other people's thinking. Don't let the noise of others' opinions drown out your own inner voice. And most important, have the courage to follow your heart and intuition."* Steve Jobs.

## DEDICATION

*A mi hermana Irene.*

## Contents

## List of Tables

**Table** **Page**

## List of Figures

**Figure** **Page**

**Figure** **Page**

**Figure** **Page**

# CHAPTER 1

## General Introduction

### 1.1 Motivation

Aircraft barometric altimeters have been, basically, the only sensor used to determine aircraft altitude for many years. As a consequence, any intention of using any other sensor which applies a fixed reference geometric vertical altitude has been somehow against the current aeronautical heritage.

Airspace vertical organisation is based on isobaric surfaces (Flight Levels (FLs)) following ICAO rules [1]. From this structure, aircraft vertical separation is obtained by maintaining 1000ft as nominal separation minima in flight level. This standard has safety issues which have been extensively studied in the last decade [2, 3].

However, when aircraft is ascending or descending near airports, close to or below transition altitude/level, required vertical separation minima is greater, mainly due to uncertainties about the vertical profile flown by the aircraft and the required change of the altimeter reference. Therefore, barometric altimetry requires specific procedures in terms of aircraft and Air Traffic Control (ATC) operations which come with associated pilot and controller workload. The extra workload and operations could lead to an inefficient use of the airspace and potential occurrence of human error [4].

Barometric altimetry provides an altitude based on International Standard Atmosphere (ISA) model, which assumes not only a given pressure and temperature at Mean Sea Level (MSL) but also a defined law, establishing temperature and pressure evolution with altitude. Nonetheless, this estimated altitude is affected by temperature variation. For example, when temperature given is below from the established by standard atmosphere; the altimeter provides an altitude higher than geometric altitude. This fact could be critical at places where the standard temperature profile is significantly different from the real profile. Young and Erik Yee [5] have shown that in Canada differences in altitude can reach up to 340 [m].

Moreover, over the past few years, the common practice within ATM has been that commercial aircraft must fly by following a set of predefined routes for the horizontal profile to reach their destinations. Currently, Aircraft Operator Companies (AOCs) are requesting for more flexibility to fly according to their preferences, in order to help them to achieve their business objectives (to keep the cost of a flight as low as possible, these costs depend mainly on: the amount of fuel needed; the actual time of flight and also the over flight charges). However, due to uncertainties in trajectory prediction these trajectories are further modified by air traffic controller to ensure separation rules are not infringed upon. As a result, flown trajectories are usually far from optimal and thereby increasing airline operational cost, yet environmental impact [6, Section 3.5]. This challenge calls for the development of new and practical concept of operation that reduce air transport cost which is the main objective of SESAR [7] and NextGen [8] programs.

In the future envisioned Air Traffic Management (ATM) system, the trajectory becomes the fundamental element of a new set of operating procedures collectively referred to as Trajectory Based Operation (TBO) [9]. Under this concept, TBO will replace the classical airspace based management principle. AOCs will be able to select their preferred trajectory [9] and fly these same routes with no or little modification that fulfils their cost objectives. Improved capabilities in trajectory management, i.e., planning, sharing, agreeing, and synchronising, will result in enhanced ATM performances in terms of capacity, efficiency, safety, and environmental impact. The implementation of TBO will require as enablers: Performance Based Navigation (PBN), Air/Ground Data Link (AGDL) to enable the required information exchange between aircraft and Air Traffic Control, improved surveillance such as Automatic Dependent Surveillance-Broadcast (ADS-B) to up-date aircraft and/or atmosphere information [10] to be used in certain autonomous systems. Besides that, this implementation will be supported by the so called System Wide Information Management (SWIM) to ensure all required information is available for the different agents serving the

flight.

Opposite to conventional procedures, it is widely known that the best aircraft performance is that resulting from continuous climb, cruise, and descent operations. These might be also referred to as Continuos Climb Departure (CCD), Continuous Climb Cruise (CCC), and Continuous Descent Approach (CDA), referred, as a whole, as "continuous operations". Extensive research related to the potential benefits derived from the application of continuous operations has been recently made both numerically simulated and in real-trials. Unfortunately, the real implementation of continuous operations is in turn still far from implementation due to, among other issues, lack of automation and human decision support tools.

Therefore, the use of geometric reference will permit to predefine any vertical (optimal) profile, as is done for horizontal routes, in the Flight Management System (FMS), based on best available atmospheric and aircraft data. The planned profile will then be flown under predefined required vertical navigation performance. As an example, today's CDAs for a complete descent, with close to idle engines regime is not practicable mainly due to the lack of FMS defined geodetic flyable trajectories for vertical profile. In addition, aerodynamic induced forces in steady flight remain constant by isodensity surfaces rather than isobaric surfaces. The maximum lift/drag ratio is density independent, and so the maximum efficiency for steady flight can be easily followed by isodensity surfaces. Besides, considering that aircraft continuously losing mass, the required lift for steady flight also decreases, demanding altitude changes for optimal vertical profiles.

At present, positioning sensors and associated avionics on board (Global Positioning System (GPS)/Inertial Navigation System (INS) and Radioaltimeter) are able to estimate 3/4D position referred to a geodetic reference, local coordinates and time deviations within certain statistical limit. Authors such as Robert A. Gray and Peter S. Maybeck [11] researched on the possible use of GPS/INS/BARO and Radar Altimeter System in Category

I/II precision approach and based on this, Instrumental Landing System (ILS) look alike approaches are being implemented today.

## 1.2 Objective

The main objective of this dissertation is to explore the benefits and drawbacks of using a non barometric reference in the vertical navigation profile.

To achieve the previous main objective the following more specific objectives are pursued:

- To establish the difference between the barometric and geometric altitude, not only in a theoretical way but also quantitatively.
- To explore new ways for better weather information using aircraft as an additional atmospheric sensor.
- To develop an aircraft trajectory predictor. Based on a 3 Degrees of Freedom (DoF) aircraft Point Mass Model (PMM), where environmental and aircraft performance information are introduced as user preference.
- To explore for more appropriate trajectory optimisation methods for trajectory design based on geometric reference. And quantify in terms of fuel/time saved the new proposed trajectory.
- To study the sensitivity of the new optimal trajectory proposed to new/real weather condition.

## 1.3 Methodology

To reach the above goals an atmosphere study has been accomplished in order to achieve a measure of the maximum differences between barometric and geometric references. Moreover, the new proposed trajectory will need an accurate meteorological information. For this purpose, ADS-B used for atmospheric behaviour determination has been deeply studied.

Among other reasons, the comparison between current trajectories and the ones based on geometric reference, has demanded an aircraft de development of a trajectory simulator.

This trajectory simulation gives flexibility for simulating the behaviour of different types of aircraft and physical scenarios. The aircraft trajectory simulator has been implemented using MATLAB® and SIMULINK® Software. The simulator is composed by four main blocks: FMS, Flight Control System (FCS), 3DoF PMM Aircraft Kinematic and Dynamic Equation and Geographic Reference. The FMS gives the references values for velocity and 3D aircraft coordinates (longitude, latitude, altitude). This information will be derived from Flight Data Recorder (FDR) information or results from the trajectory optimisation problem. The FCS block is based on three interdependent control loops to regulate: velocity deviation, altitude deviation and lateral deviation from the defined mission. These control loops will act on Throttle Lever Percentage (TLP), desired altitude derivative and roll angle, respectively, which are the inputs in the aircraft dynamic model. In the 3DoF PMM Aircraft Kinematic and Dynamic Equation section, as its name indicates, the kinematic, dynamic and the fuel consumption equations are implemented without taking into account the wind vector value. That section needs, besides the inputs, the aircraft performances, power plant information and aircraft initial condition. Finally, in the Geographic Reference section aircraft variables are evaluated referred to a geographic reference, that is the wind vector is include into de kinematic equation and also $x, y$ are converted into longitude and latitude coordinates using the WGS-84 reference ellipsoid.

Aircraft kinematic and dynamic equations is modelled as a 3 DoF aircraft PMM with the following considerations: flight path angle small, angle of attack negligible, fixed engines, thrust pointing into the longitudinal aircraft axis direction, and climb acceleration angle negligible. Aircraft performances, such as: polar coefficients, aircraft maximum thrust or specific fuel consumption, become from BADA 3.9 information. Besides that, physical environment is also estimated into the aircraft trajectory simulator tool, not only ISA model

could be introduced but also a deviation from the ISA model or real one becomes from e.g.: ADS-B estimation or other weather institution, could be introduced.

The geometric reference trajectory used in this dissertation is the optimal trajectory with a required time of arrival minimising the fuel consumption. Firstly, an exhaustive revision of the trajectory optimisation methods has been made, mainly: singular arc solution belonging to the analytical optimal solution group, collocation methods which are direct methods of the numerical optimal control methods.

Lastly, the trajectory optimisation is introduced into the aircraft trajectory simulator and the atmosphere conditions are modify in order of study how atmosphere prediction could affect on the optimal trajectory.

## 1.4 State of the art

The topic of this dissertation has currently a great interest since more efficient and environmentally friendly trajectories are desired. Also, projects such as SESAR and NextGen have put a lot effort to accomplish these goals.

### 1.4.1 Vertical navigation overview

Current commercial aircraft flies following predefined routes for the horizontal profile and using flight level or isobars surfaces for the vertical profile following ICAO Annex 2 rules [1]. That means that cruising flight involves a sequence of level segments increasing in altitude as fuel is burned. The steps in altitude are typically 1000, 2000, or 4000 [ft] depending on the constraints of the airspace in which the aircraft is flying. The aircraft is changing the flight level when the flight efficiency between two candidate altitudes is approximately equal. As a result, flown trajectories are usually far from optimal increasing the operational cost. Therefore it is demanded a new operational concept to reduce the cost per flight as much as practicable.

Currently, the called Continuous Climb Operations (CCOs) are being deeply studied as

a solution of the previously exposed new operational concept, for instance [12], [13], [14], and [15]. Other examples can be found in, [16], [17], [18], [19], and projects RETA-CDA [20] and Atlantic Interoperability initiative to Reduce Emissions (AIRE) [21].

In a CCD aircraft flies reducing noise and local air quality impacts on the ground, and also this procedure will allow getting the more fuel efficient cruise altitudes earlier. However, there is a need to compromise with aircraft desires and flight levels to keep them separated from each other. These compromises mean that aircraft often climb in a series of steps followed by periods of level flight, so the trajectory is far form the optimal.

In average, cruise phase is around the 90% of a whole commercial aircraft trajectory and, therefore, where more fuel is consumed. As aircraft is continuously losing mass, demanded lift for steady flight also decreases, changes in altitude are then required for optimal vertical profiles, the resulting optimal profile is called CCC.

SESAR launched the project AIRE studying the advantages of CCC in trial scenarios for North Atlantic flights [21].

In [18] analysed cruise climb, direct routing and variable speed to get a better flight profiles by aircraft flying through Reykjavik control area. Estimation of benefits of cruise climb is around 0.1%-0.4% compared to 1000 [ft] step climb and around 0%-0.5% of total en-route fuel burn for variable speed according to analysis.

In [19] several trial scenarios in the Santa Maria Area Control Center (ACC) were developed to enhance the current aircraft trajectories in the vertical profile through cruise climb, as well as the lateral profile, with more direct routes, and longitudinal analysing the different cost index. The result of this project showed that a vertical profile based on steps in altitude of 100 [ft] saves 29 [kg] of fuel compared to a 2,000 [ft] step climb or 12 [kg] to two 1,000 [ft] steps climb, if an A340 at 0.8 Mach with an average climb rate of 250 [ft/min] is used.

Several airlines have estimated from their experience that cruise climb, in the case of

B747-400, could save up to approximately 1% in fuel consumption in non Reduced Vertical Separation Minima (RVSM) airspace and a bit less in RVSM [18]. Because of the limitations of current aircraft avionics, flying CCC is an arduous process of continuous configuration while climbing. Currently cruise climb is done manually, applying vertical speed in steps and by manual speed selection and is therefore not operationally feasible. Airlines and pilots believe that if vertical speed is manually applied, the procedure become infeasible due to human errors during the manoeuvre. Therefore, the procedure needs to be fully automated within the cockpit.

On the contrary, flying with variable speed, airlines are currently a more familiar procedure for crews. This is performed by variable speed schedule as a function of gross weight, cruise altitude, Cost Index (CI), and headwind component. It is calculated to provide minimum operating cost for the entered CI, defined as the ratio of the time-related cost of an airplane operation and the cost of fuel.

In a CDA procedure, the main aim is to enable aircraft to descend with low engine thrust setting, thereby reducing fuel consumption and $CO_2$ emissions. These procedures are in use at many airports, under "ad-hoc" ATC clearances and a restricted operational schedule.

The problem for applying CDA procedures in medium/high density traffic airports is that each aircraft while in continuous descent has a different optimum speed and, as a result, current ATC techniques to ensure a minimum distance between aircraft (issuing radar vectors, speed restrictions and waiting manoeuvres) cannot be applied, reducing significantly the airport throughput.

Then, new techniques are required for CDA implementation into high traffic scenarios. In this sense, SESAR is developing several project to find technical solutions to this problem based on ATC support tools such as Arrivals Managers (AMAN) [22].

### 1.4.2 Trajectory optimisation overview

From a strategic trajectory planning perspective, ideal performance result to the solution of a flight planning problem, which can be regarded as a trajectory optimisation problem. The trajectory optimisation problem can be studied as an optimal control problem of a dynamic system in which the goal is to find the trajectory and the corresponding control inputs that steer the state of the system between two configurations satisfying a set of constraints on the state and/or control variables while minimising an objective functional.

Typically, optimal control problems are highly non-linear where it is very difficult to find an analytical solution, even for simple cases. The common practice used is to implement numerical methods to obtain solutions. Three fundamental approaches exist to solve numerically continuos time optimal control problems: Dynamic Programming (DP) methods, whose optimality criteria in continuous time is based on the Hamilton-Jacobi-Bellman partial differential equation [23]; indirect methods, that rely on the necessary conditions of optimality that can be derived from the Pontryagin's maximum principle [24]; direct methods, that are based on a finite dimensional parameterization of the infinite-dimensional problem [25].

In the scope of commercial aircraft trajectory optimisation using optimal control, all above methods have been used in the literature. For instance, in [26] the authors analyse the minimum fuel trajectory for an aircraft flying at constant altitude and with fixed arrival time. The problem is solved as a singular arc, an analytical solution based on the above mentioned indirect approach. This solution provides a smooth profile, very suitable from an operational perspective. However, it does not consider constrained arcs, i.e., situations in which some of the inequality constraints are saturated. Singular arc trajectories have been also analysed for more complex instances, as it is the case for climb performances [27].

Dynamic Programming has been also used very recently to solve a minimum fuel vertical profile [28]. Nevertheless, direct methods have been shown to be more suitable for solving more realistic commercial aircraft trajectory optimisation problems in a highly constrained

environment as it is ATM.

For instance, since the 90's, Hermite-Legendre-Gauss-Lobatto (HLGL) direct collocation methods [29, 30] have been used to solve different commercial aircraft trajectory planning problems. To name a few, in [31, 32, 13] minimum fuel vertical profiles under ATM procedure constraints are analyzed. Also, minimum fuel 3D profiles have been also solved [33]. Moreover, a recent approach has shown that binary decision variables can be combined into optimal control problems, resulting in a so-called multiphase mixed-integer optimal control problem, which can be solved using HLGL collocation methods [34, 35]. Therefore, these methods are mature for solving commercial aircraft trajectory optimization problems in ATM environment.

Very recently, the scientific community have shifted the attention to the so-called pseudospectral collocation methods, which have shown very promising results. The basis of these methods lays on spectral methods [36]. Two recent, thorough publications on the matter are [37, 38]. The attention gained in the last years is in part due to the development of two commercial off-the-shelf software packages that implement different pseudospectral methods for solving optimal control problems in a user friendly and widely used interface as it is Matlab. One of these software packages is GPOPS [39], which implements a Legendre Pseudospectral Method. The other one is DIDO [40], which implements a Legendre-Gauss-Lobatto (LGL) pseudospectral collocation method. Both software packages have been extensively used with success for solving optimal control problems, particularly with application to space and unmanned vehicles [41, 39, 42, 43].

### 1.5 Document Structure

This dissertation is structured as follows:

In chapter 2 the atmospheric assessment is presented. The goal of this chapter is to analyse the differences between barometric and geometric references in order to clarify what are the implication of saying that aircraft could use better a geometric reference. Also, the

necessity of having a more accurate atmospheric parameters to a better optimal trajectory design, the used of ADS-B for this purpose was analysed.

In chapter 3 the aircraft Trajectory Simulator is presented. The focus is first on define the aircraft model used where all the hypothesis and simplification is described. Then, a validation with real FDR aircraft information is carried out. Finally, the corresponding calibration is also proposed.

In chapter 4 the optimisation assessment is put forward. A brief overview of the optimal control problem and the different optimisation techniques is performed with a more deeply study into the Hermite-Legendre-Gauss-Lobatto and pseudoospectral collocation methods. Eventually, two cases of studies (1D and 2D optimal trajectory) are performed to compare collocation method performances.

In chapter 5 the effects of how atmospheric characteristics affect to the optimal trajectory is presented. A sample real trajectory is employed with different pressure at MSL, lapse rate temperature conditions and temperature at MSL. The objective of this chapter is to quantify fuel saving with optimal trajectory and also how the optimal trajectory evaluated at ISA standard condition is affected by the cases studied mentioned above.

In chapter 6 the conclusion and future work are described.

**List of References**


[1] International Civil Aviation Organization (ICAO), "Rules of the Air," ICAO, Tech. Rep., 10th Edtion. 2005.

[2] S. E. Steve Creamer and N. Haase, "Reduced vertical separation minima in u.s. airspace: Air traffic control issues and answers," *Journal of Air Traffic Control*, 2003.

[3] A. Malwitz, S. Balasubramanian, G. Fleming, T. Yoder, and I. Waitz, "Impact of the reduced vertical separation minimum on the domestic united states," *Journal of Aircraft*, vol. 46, no. 1, pp. 148–156, 2013/05/02 2009. [Online]. Available: http://arc.aiaa.org/doi/abs/10.2514/1.36776

[4] M. C. Benoît Roturier, "Analysis of baro vnav safety issues," in *Proc. Navigation Systems Panel (NSP) meeting, Working Group 1&2*, Brussels, BE, 8-19 May 2006, pp. 1–10.

[5] E. Y. Young Yee, "A study of barometric altimeter in high latitude regions," in *A13th conference on aviation, range and aerospace meteorology (ARAM)*, New Orleans, LA, 2008.

[6] Eurocontrol, Performance Review Comission, "Performance review report an assessment of air traffic management in europe during the calendar year 2011: Eurocontrol PRR 2011," Eurocontrol, Tech. Rep., May 2012. http://www.eurocontrol.int/prc [Retrieved 01/09/2012].

[7] Thales ATM, "Analysis of sesar 4d trajectory activities-trajectory decomposition for se-2020 task order 0022 international harmonization of 4d trajectory activities," September 2012.

[8] Federal Aviation Administration Office of NextGen, *NextGen Implementation Plan*, Washington, DC 20591, 2013.

[9] Sesar Consortium, "The ATM target concept, SESAR definition phase milestone deliverable 3," September 2007.

[10] J. F. A. Alarcón, F. J. S. Nieto, and J. G.-H. Carretero, "Aircraft used as a sensor for atmospheric behaviour determination. practical case: pressure estimation using automatic dependent surveillance-broadcast," *Proceedings of the Institution of Mechanical Engineers, Part G: Journal of Aerospace Engineering*, vol. 227, no. 5, pp. 778–797, 2013. [Online]. Available: http://pig.sagepub.com/content/227/5/778.abstract

[11] R. Gray and P. Maybeck, "An integrated gps/ins/baro and radar altimeter system for aircraft precision approach landings," in *Aerospace and Electronics Conference, 1995. NAECON 1995., Proceedings of the IEEE 1995 National*, vol. 1, 1995, pp. 161–168 vol.1.

[12] S. Shresta, D. Neskovic, and S. Williams, "Analysis of continuous descent benefits and impacts during daytime operations," in *8th USA/Europe Air Traffic Management Research and Development Seminar (ATM2009), Napa, CA*, 2009.

[13] M. Soler, D. Zapata, A. Olivares, and E. Staffetti, "Framework for aircraft 4D trajectory planning towards an efficient air traffic management," *Journal of Aircraft*, vol. 49, no. 1, pp. 341–348, 2012.

[14] L. Jin, Y. Cao, and D. Sun, "Investigation of potential fuel savings due to continuous-descent approach," *Journal of Aircraft*, vol. 50, no. 3, pp. 807–816, 2013.

[15] R. Dalmau and X. Prats, "How much fuel and time can be saved in a perfect flight trajectory?" in *International Conference on Research in Air Transportation (ICRAT)*, 2014.

[16] J.-P. B. Clarke, N. T. Ho, L. Ren, J. A. Brown, K. R. Elmer, K. Zou, C. Hunting, D. L. McGregor, B. N. Shivashankara, K.-O. Tong, *et al.*, "Continuous descent approach: Design and flight test for louisville international airport," *Journal of Aircraft*, vol. 41, no. 5, pp. 1054–1066, 2004.

[17] R. A. Coppenbarger, R. W. Mead, and D. N. Sweet, "Field evaluation of the tailored arrivals concept for datalink-enabled continuous descent approach," *Journal of Aircraft*, vol. 46, no. 4, pp. 1200–1209, 2009.

[18] European Comission, the FAA and the project AIRE, "Reduction of Emissions on the North Atlantic by the Implementation of ADS-B. Final Report," SESAR Joint Undertaking, Tech. Rep., 2010.

[19] European Comission, the FAA and the project AIRE, "North atlantic cruise climb, lateral deviation, and mach number flight trials demonstration. Final Report (D1)," SESAR Joint Undertaking, Tech. Rep., 2010.

[20] RETA-CDA Consortium, "RETA-CDA: Reduction of Emissions in Terminal Areas using Continuous Descent Apporaches. Final Report." SESAR Joint Undertaking, Tech. Rep., 2010.

[21] European Comission, the FAA and the project AIRE, "Atlantic Interoperability Initiative to Reduce Emission (AIRE). Summary results 2010/2011," SESAR Joint Undertaking, Tech. Rep., 2012.

[22] S. J. Undertaking., "Sesar (single european sky atm research)," http://www.sesarju.eu/, 2007.

[23] R. Bellman, *Dynamic Programming*. Princeton UP, 1957.

[24] L. S. Pontryagin, V. Boltyanskii, R. V. Gamkrelidze, and E. F. Mishchenko, *The Mathematical Theory of Optimal Processes*. Interscience Publishers, 1962.

[25] J. T. Betts, *Practical Methods for Optimal Control and Estimation using Nonlinear Programming*. Advances in Design and Control. Society for Industrial and Applied Mathematics, 2010.

[26] A. Franco, D. Rivas, and A. Valenzuela, "Minimum-fuel cruise at constant altitude with fixed arrival time," *Journal of Guidance, Control, and Dynamics*, vol. 33, no. 1, pp. 280–285, 2010.

[27] N. Nguyen, *Singular Arc Time-Optimal Climb Trajectory of Aircraft in a Two-Dimensional Wind Field*. American Institute of Aeronautics and Astronautics, 2013/09/16 2006.

[28] Y. Miyazawa, N. K. Wickramashinghe, A. Harada, and Y. Miyamoto, "Dynamic programming application to airliner four dimensional optimal flight trajectory," in *Guidance, Navigation, and Control Conference*, 2013.

[29] C. R. Hargraves and S. W. Paris, "Direct trajectory optimization using nonlinear programming and collocation," *Journal of Guidance, Control, and Dynamics*, vol. 10, no. 4, pp. 338–342, 1987.

[30] P. Williams, "Hermite-Legendre-Gauss-Lobatto direct transcription methods in trajectory optimization," *Advances in the Astronautical Sciences*, vol. 120, Part I, pp. 465–484, 2005.

[31] J. T. Betts and E. J. Cramer, "Application of direct transcription to commercial aircraft trajectory optimization," *Journal of Guidance, Control, and Dynamics*, vol. 18, no. 1, pp. 151–159, 1995.

[32] M. Soler, A. Olivares, and E. Staffetti, "Hybrid optimal control approach to commercial aircraft trajectory optimization," *Journal of Guidance, Control, and Dynamics*, vol. 33, no. 3, pp. 985–991, 2010.

[33] M. Soler, A. Olivares, and E. Staffetti, "Multiphase optimal control framework for commercial aircraft four dimensional flight planning problems," *Journal of Aircraft*, Acceppted for publicaton. DOI:10.2514/1.C032697.

[34] P. Bonami, A. Olivares, M.Soler, and E. Staffetti, "Multiphase mixed-integer optimal control approach to aircraft trajectory optimization," *Journal of Guidance, Control, and Dynamics*, vol. 36, no. 5, pp. 1267–1277, 2013.

[35] M. Soler, "Commercial aircraft trajectory planning based on multiphase mixed-integer optimal control," Ph.D. dissertation, Universidad Rey Juan Carlos, 2013. [Online]. Available: http://www.aerospaceengineering.es/publications/phd-thesis/

[36] C. Canuto, *Spectral methods: Fundamentals in single domains*. Springer Verlag, 2006.

[37] D. Garg, M. Patterson, W. Hager, A. Rao, D. Benson, and G. Huntington, "A unified framework for the numerical solution of optimal control problems using pseudospectral methods," *Automatica*, vol. 46, no. 11, pp. 1843–1851, 2010.

[38] I. Ross and M. Karpenko, "A review of pseudospectral optimal control: from theory to flight," *Annual Reviews in Control*, vol. 36, no. 2, pp. 182–197, 2012.

[39] A. V. Rao, D. A. Benson, C. Darby, M. A. Patterson, C. Francolin, I. Sanders, and G. T. Huntington, "Algorithm 902: Gpops, a matlab software for solving multiple-phase optimal control problems using the gauss pseudospectral method," *ACM Transactions on Mathematical Software (TOMS)*, vol. 37, no. 2, p. 22, 2010.

[40] I. M. Ross, *A Beginner's Guide to DIDO. A MATLAB Application Package for Solving Optimal Control Problems*, September 2010.

[41] R. F. de Oliveira and C. Büskens, *Emergency flight replanning for minimum loss of life risk using a decoupled trajectory optimization approach*. American Institute of Aeronautics and Astronautics, 2014/04/25 2013. [Online]. Available: http://dx.doi.org/10.2514/6.2013-4238

[42] F. Fahroo and I. M. Ross, "Pseudospectral methods for infinite-horizon nonlinear optimal control problems," *Journal of Guidance, Control, and Dynamics*, vol. 31, no. 4, pp. 927–936, 2014/04/15 2008. [Online]. Available: http://dx.doi.org/10.2514/1.33117

[43] F. Fahroo and I. M. Ross, *Advances in Pseudospectral Methods for Optimal Control*. American Institute of Aeronautics and Astronautics, 2014/04/15 2008. [Online]. Available: http://dx.doi.org/10.2514/6.2008-7309

# CHAPTER 2

## Atmospheric behaviour

The use of barometric altimetry is to some extent a limiting factor on safety, predictability and efficiency of aircraft operations, and reduces the potential of the Trajectory based operations capabilities. But geodetic altimetry could be used to improve all of these aspects. Nowadays aircraft altitude is estimated applying the International Standard Atmosphere which may differs from real altitude up to 340 [m]. At different temperatures for an assigned barometrical altitude, aerodynamic forces are different and this has a direct relationship with time, fuel consumption and range of the flight. It will be relevant to explore the feasibility of use sensors providing geodetic reference altitude, in particular, to provide capabilities to the optimisation of vertical profiles and, on the other hand, their impact on the vertical ATM separation assurance processes.

Atmosphere is essential in air navigation because it is the domain where aircraft flies. To develop a safe and correct flight, it is necessary to know its characteristics, such as: temperature, pressure, wind vector, etc.

This section includes an barometric and geometric altitudes study, as well as the use of ADS-B information to estimate horizontal and vertical pressure and wind vector.

### 2.1 Barometric and geometric altitudes analysis

International Civil Aviation Organization (ICAO) Standard Atmosphere [1], which was established in 1952, is based on ideal gas, without dust, humidity and water vapor and stable relative to the Earth. With these hypotheses, it is possible to apply the hydrostatic Equation 1 for an air column.

$$\frac{dp}{p} = -\frac{g_0}{R_a T} dh, \tag{1}$$

where:

- $p$ is the pressure,
- $g_0$ is the acceleration of gravity at MSL which is equal to $9.80665 m/s^2$,
- $R_a$ is is the gas constant which is equal to 287.0531J/kgK,
- $T$ is the temperature, and
- $h$ is the altitude.

When aircraft are in the approach phase at the altitude of transition, ATC sends them the QNH information so that all aircraft have the same reference in order to maintain a secure vertical separation.

To separate aircraft using altimeter information, it is important that the altimeters have a great accuracy in their static pressure measurements. The pressure error or the position error, as it is sometimes called, is determined experimentally. It is a function of the Mach [2] and in the worst case produces an error value of 180 [Pa] (150 [Pa] due to uncertainty error and 30 [Pa] due to sensor). Aircraft traveling at the tropopause give equivalent error in altitude of 69 [m] (227 [ft]). At lower altitudes this error is around 30 [Pa], which gives an altitude error of less than 3.3 [m] (11[ft]) [2].

ISA considers a linear dependency (-6.5 degree per 1000 [m]) of temperature with altitude in the troposphere (MSL- 11.000 [m]) and constant values in the tropopause (11.000 [m]- 20.000 [m]) [1]. Having this temperature model, the hydrostatic equation denoted as in Equation 1 can be solved. To evaluate the difference between barometric altitude and geometric altitude, the next step will be to determine the temperature deviation from the ISA temperature model.

Many researches have measured atmospheric characteristics in terms of the vertical profile with different instruments, such as: balloons, Laser Imaging Detection and Ranging (LIDAR), radar, sounding rocket, Thermosphere Ionosphere Mesosphere Energetics and Dynamics (TIMED) spacecraft. In Hainn (China) on June 3, 2011, the vertical temperature

profile was measured [3] using some the above mentioned instruments. From this research a maximum temperature deviation of 25 [K] at 17.000 [m] was observed. In an urban area of Beijing (China) on November 2, 2009 a similar experiment was performed and the maximum temperature deviation was 15 degree at 16.000 [m] [4]. Again, in Kyotanable (Japan) on May 13, 2000, the temperature difference was about 10 degrees [5]. Research performed by National Aeronautics and Space Administration (NASA) on the US Standard Atmosphere [6] shows a global maximum temperature deviation from the ISA model of 65 [K] at MSL. Another study undertaken by Garrido-López and Gómez [7], showed the relationship between barometric and geometric altitude using the hydrostatic and ideal gas equation as shown in Equation 2:

$$\frac{dH_b}{dh} = \frac{T_{ISA}}{T_{ISA} + T_{Dev}} \simeq 1 - \frac{T_{Dev}}{T_{ISA}}, \tag{2}$$

where:

- $H_b$ is the pressure altitude,
- $h$ is the geometric altitude,
- $T_{ISA}$ is the temperature from ISA model, and
- $T_{Dev}$ is the difference from the ISA temperature model to the actual temperature.

To evaluate the $T_{Dev}$ from the Equation 2, a statistical study using information from about 95 radiosondes stations of World Meteorological Organization (WMO) [8] collected between July to September, 1996 was performed. The study was based on the calculation of the standard deviation of the collected temperature data for each FL, as shown by the dots in Figure 1.

A continuous relationship between FLs and temperature deviation from the ISA temperature was achieved using quadratic polynomial approximation by applying Least Mean Square (LMS) calculation. The result from the calculation can be seen in Equation 3.

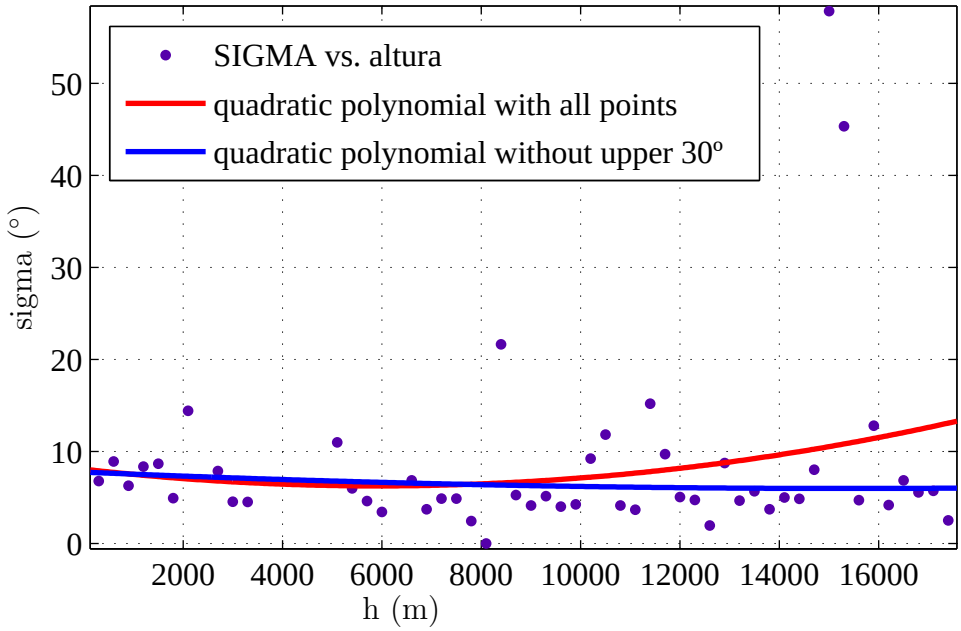


Figure 1: Temperature standard deviation vs. Geometric altitude

$$\frac{T_{Dev}}{T_{ISA}} \simeq \frac{5.184 \cdot 10^{-8} h^2\,(m) - 6.141 \cdot 10^{-4} h\,(m) + 8.069}{288.15 - \frac{6.5}{1000} H_b\,(m)} \tag{3}$$

Equation 3 shows the mathematical expression for the ratio of temperature deviation with respect to ISA temperature as a function of geometric altitudes below 11,000 [m].

Substituting Equation 3 into Equation 2, a differential equation is denoted by Equation 4, which relates the geometric and the barometric altitude. This differential equation is solved by assuming that MSL pressure is equal to ISA pressure at MSL.

$$\frac{dH_b}{dh} \simeq 1 - \frac{5.184 \cdot 10^{-8} h^2\,(m) - 6.141 \cdot 10^{-4} h\,(m) + 8.069}{288.15 - \frac{6.5}{1000} h\,(m)} \tag{4}$$

Figure 2 shows a nearly linear relationship between the relative barometric altitude to the geometric altitude from 0 to 300 [m]. This relationship is relevant for the development of the thesis, because most of the information from aircraft is given based on barometric altitude but the research seeks to analyze trajectories based on geometric altitude.

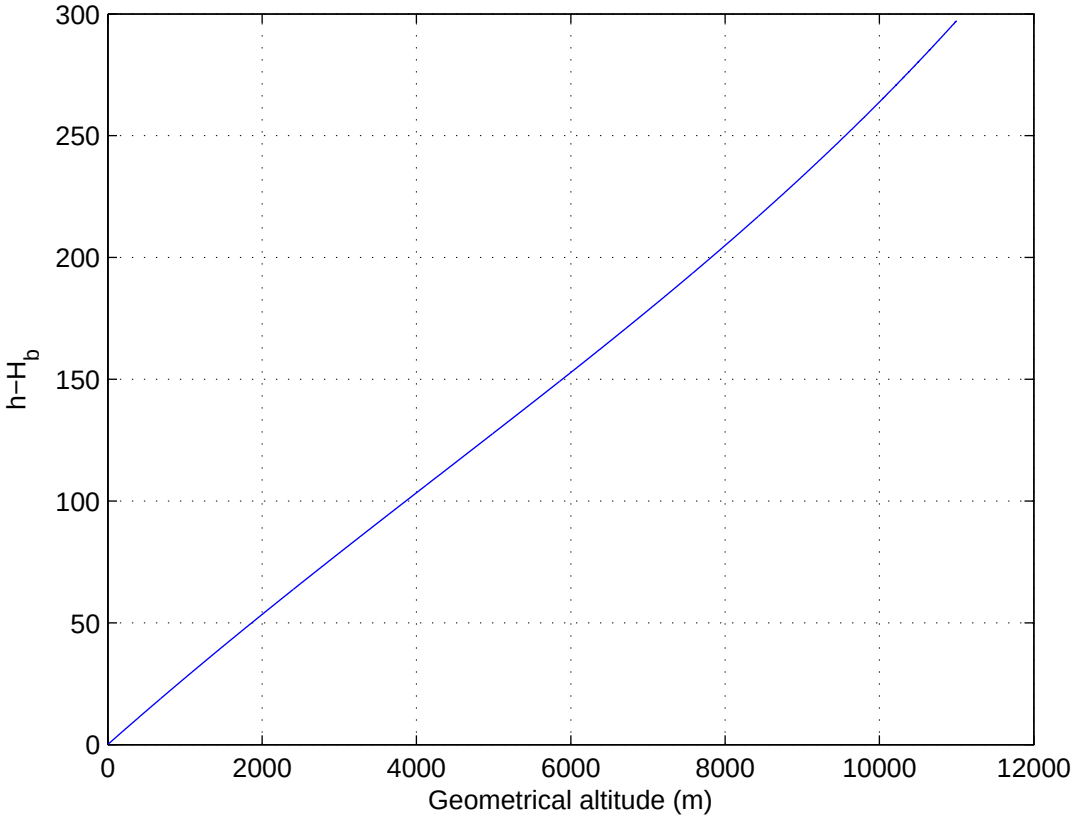


Figure 2: Relative barometric altitude vs. geometric altitude

### 2.2 ADS-B used for atmospheric behaviour determination

The cornerstone of the future ATM system is four dimensional (4D) trajectory management [9, 10] which will rely on accurate trajectory prediction to produce flyable, efficient and de-conflicted trajectories for all involved aircraft.

Considering the fact that the flight of aircraft is a product of induced forces from the air, flight trajectories can be said to be closely related to the physical state of the atmosphere. Thus, any realistic trajectory prediction algorithm should take this into account, with focus on variables such as air pressure, wind velocity and temperature, as well as clouds/visibility, gusts/microbursts and the concentration of particles or other elements that affect aircraft travel through the atmosphere.

The number of aircraft that currently fly simultaneously has resulted in a high aircraft

density within continental airspace. Managing this situation is a high priority for the future ATM system. For example, in Western Europe, approximately 2000 aircraft are simultaneously in operation on daily basis [11]. The spatial distribution of the population of aircraft presents the opportunity to use the aircraft as atmospheric sensors that could increase and improve the input data that are supplied to tools devoted to monitoring and predicting the status of the atmosphere.

Most of today's commercial aircraft are equipped with ADS-B system [12, 13]. The system broadcasts messages with information related to the atmosphere that could serve the purposes discussed above.

Atmospheric behaviour is currently established by using information provided by peripheral sensors located on the ground and by satellites in space as the primary inputs. This implies that there are no additional sensors within the atmosphere (except some balloons and other specialised flying systems), even though it is the area of interest for ATM.

The purpose of the analysis presented in this article was to explore the characteristics of the information supplied by the ADS-B system, which broadcast by using 1090MHz Extended Squitter (1090 ES) messages. Activities performed in the study covered analysis of the ADS-B messages supported by 1090 ES, including a review of the relevant regulatory framework [12, 13] for these messages and empirical test that were conducted with a representative sample of aircraft to obtain valuable results.

The study provides information regarding the strengths and weaknesses of ADS-B as a source of relevant data for atmospheric status estimation, as well as on the differences between the regulatory framework and the information currently available from aircraft.

After analysing the ADS-B messages and determining which information was available and useful, further studies were conducted to estimate the pressure field within a specified volume of airspace.

The altitude information (barometric and geometric) from the appropriate ADS-B down-

link messages was used to derive the real time pressure at all positions of aircraft, i.e. the local universal transverse mercator x and y coordinates plus altitude (z).

From the information obtained, a scalar field estimate of the pressure was obtained for a given time within the airspace volume which was determined by the ADS-B receiver coverage used for the study.

The pressures at the MSL surface were estimated by projecting or extrapolating each aircraft pressure by using ISA model. As a result, a set of estimated pressures at different points on the surface were obtained by vertical projection of the pressures from all aircraft. The validity of this approach is based on the assumption that the pressure follows the variation of the ISA model.

The results were evaluated extensively to identify elements that could help to achieve the goal of improving knowledge of the characteristics of the atmosphere with data derived from aircraft equipment. In the final section, conclusions and proposed further study are also presented.

Safe and efficient 4D trajectory management has always been the goal of ATM. In the future ATM system, this will be the basis for solving capacity limitations which are associated with human-centred concept of operation. The new paradigm for ATM is presented in NextGen [14] and SESAR [15].

Current navigation systems permit aircraft to fly following the horizontal two dimensional (2D) component of the trajectory Required Navigation Performance (RNP)/PBN concept by maintaining a given performance, related to lateral deviations from the trajectory reference line, when this component of the trajectory has been planned and defined as a sequential set of waypoints, straight segments between them and a rule of turning at each waypoint.

The current vertical profile of the aircraft trajectories three dimensional (3D), only exhibits a given performance for vertical deviations when the aircraft is flying following a

precision approach and also when it is in level flight. Other descent and climbing phases are flown without a reference line, but by using different profiles based on efficiency criteria and some restrictions or limitations (upper and/or lower), imposed by ATC, or established by the operational navigation procedure. Flight profiles are directly dependent on atmospheric variables such as pressure, temperature and especially the wind speed. For example, when an aircraft performs a climb or descent, it does not only depend on the aircraft performances but knowledge of the atmosphere to achieve the right altitude, hence the importance of having information on the behaviour of the atmosphere at all times.

3D trajectory with incorporated vertical deviations, still have important issues to be resolved before full implementation. This makes the concept of 4D trajectory looks like a far away concept from implementation because though acceptable the present development still does not provide navigational information at all times. In some references today, the terminology $3^1/_2$-D is used to remark on present 4D trajectories development.

4D trajectories with its defined standards in vertical and along track deviations, is a paradigmatic objective that will bring about a new complex scenario in ATM in which automation shall play an important role in both, autonomous and centric involved places of decision making.

According to SESAR, several changes will be necessary to fully meet the safety, capacity and other performance targets by set for 2020/2025. A shift from airspace-based operations towards trajectory- based operations will ensure that the airspace user flies close to its intended trajectory in the most efficient manner possible.

Moreover a shift from tactical management towards a more strategic system will involve the implementation of different planning layers, where decision about trajectories can be made in advance to accommodate user needs, eliminate conflict amongst trajectories and reduce human tactical control over the aircraft as much as possible.

This shift will facilitate a move from a controller-based system towards a more dis-

tributed system, in which decision about aircraft trajectories could be made by the actor that is in the best place at each moment and for each scenario.

To achieve all of these requirements, improved predictability of 4D trajectories will be needed, and to arrive at this, it would be essential to obtain an improved knowledge of the behaviour of the physical atmosphere. NextGen and SESAR programmes assign great importance to meteorological information. For example, SESAR has dedicated Work Package number 8 (WP-8) (information management) to defining the ATM information reference model and the information service model, which will include information for modelling the meteorological domain and enable the best information to be used for the 4D scenario. In addition, SESAR Work Package number 11 (WP-11), which is devoted to Flight and Wing Operations Centres/Meteorological Services, will address the meteorological service component of improving ATM performance.

At present, there are various initiatives aimed at obtaining better information about the physical behaviour of the atmosphere. One of these is related to air pollution and the dispersion of other particles. Meteorology stations are used to determine the wind velocity at these points and to estimate this variable through the use of finite difference methods [16, 17, 18].

Furthermore, unmanned aerial systems have also been used for studying air pollution dispersion, weather prediction and wind power harvesting by measuring the atmospheric variables (temperature, humidity, pressure and wind speed) at a flexible position and altitude in real time [19]. There are also commercial software tools such as WindStation [20], which uses an airflow simulator to solve the full 3D Navier-Stokes equations and can help to improve the 3D models of physical atmospheric behaviour.

Additionally, aircraft could provide valuable information (i.e. temperature, pressure, ground speed and air speed). For example, aircraft can receive information from the Aircraft Communications, Addressing, and Reporting System (ACARS) [21, 22, 23, 24] through

110 types of different messages [25]. Although meteorological information could be sent by aircraft, current messages transmit information only from ground stations (obtained from meteorological centres) that is uplinked to aircraft (weather messages).

A study of the spatial statistics of the atmosphere was conducted by Frehlich et al. [26] using a rawinsonde, ACARS and the aircraft meteorological data relay. Schwartz et al. [18], Benjamin et al. [25] and Cole et al.[27] used ACARS data to study the accuracy of the wind vectors predicted by the rapid update cycles 1 and 2, two systems from the National Oceanic and Atmospheric Administration (NOAA)/National Centers for Environmental Prediction.

The ADS-B systems [13, 28, 29] which are supported by 1090 ES as the physical layer, provides information that could be used to improve our understanding of atmospheric physical states. 1090 ES is currently in operation because most aircraft are equipped with a mode-S transponder. The ADS-B messages were analysed through 1090 ES in Steen et al. [30] to determine wind information.

For RVSM airspace it is essential for all aircraft to keep their assigned vertical altitude. The Altimetry System Error (ASE) is not detectible in normal operations, as such another set of equipment is needed to assess its magnitude. In Martin et al. [31] and Falk et al. [32] an in-depth analysis was performed for ASE estimation by employing the use of ADS-B supported by two of its transmission technologies, 1090 ES and universal access transceiver. These studies concluded that by using ADS-B technology, it is feasible to collect atmospheric data.

However, one of the problems presented by the authors was the lack of information about the vertical reference surface employed by aircraft which was also encountered in this study.

Different studies have been carried out to demonstrate ADS-B technology capabilities in the meteorological information dissemination. In Heuwinkel [33] ADS-B was used as crosslink of meteorological information from one aircraft to another. Actually many studies including

Yanovsky and Bokal [34] and Dunstone [35] are focused on the possibility of transmitting extra meteorological data on the ADS-B datalink.

### 2.2.1 ADS-B 1090 Extended Squitter data

The ADS-B system is a cooperative surveillance technology for ATM. This system provides flight data, including position, aircraft identification, velocity and barometric/geometric altitude, through ADS-B messages using mode-S transponders. Currently, ADS-B systems are regulated as shown in RTCA [13] and ICAO [28, 29]. ADS-B messages relevant to this study are those defined in Downlink Format (DF) 17 [13]. All messages have 112 bits with 56 bits of the Message (ME) field inserted between the 24 bit aircraft address and the parity information. The first 5 bits of the ME field define 32 possible messages types, which are classified into six groups [13]:

- no position information (type 0);
- identification and category (type 1-4);
- surface position (type 5-8);
- airborne position (types 9-18 and 20-22);
- airborne velocity (type 19); and
- ADS-B periodic status and event-driven (type 23-31).

Table 1: Airborne position message

| ME bit | 1-5 | 6-7 | 8 | 9-20 | 21 |
|---|---|---|---|---|---|
| Field name | Type code | Surveillance status | NIC supplemnt-B | Altitude | Time (T) |
| ME bit | 22 | 23-39 | 40-56 | | |
| Field name | CPR format (F) | CPR encoded latitude | CPR encoded longitude | | |

This article considers only the airborne position, airborne velocity and identification and category messages. For airborne position, Table 1 presents the bit structure of the

Table 2: Airborne velocity message subtipe 1 and 2

| ME bit | 1-5 | 6-8 | 9 | 10 | 11-13 |
|---|---|---|---|---|---|
| Field name | Type code | Subtype | Intent change flag | Reserved-A | $NAC_v$ |
| ME bit | 14 | 15-24 | 25 | 26-35 | 36 |
| Field name | E/W direction bit | E/W velocity | N/S direction bit | N/S velocity | Vert. rate soruce |
| ME bit | 37 | 38-46 | 47-48 | 49 | 50-56 |
| Field name | Vert. rate sign | Vert. rate | Reserved-B | Difference from barometric altitude sign | Difference from barometric altitude |

different fields that contain longitude, latitude and barometric altitude information. As presented in Table 2, the airborne velocity message contains, among other information, the difference from barometric altitude, which indicates the difference between the barometric and geometric altitudes.

Table 3: Maximum MSG rates

| Group of ADS-B MSG | MSG interval (s) |
|---|---|
| No position information | Variable |
| Airborne position | 0.4-0.6 |
| Airborne velocity | 0.4-0.6 |
| Surface position | 0.4-0.6 (high); 4.8-5.2 (low) |
| Identification and category | 4.8-5.2[a]; 9.8-10.2[b] |
| ADS-B periodic status and even-driven | variable |

[a] When the ADS-B transmitting subsystems is reporting the airborne position message, or when it is reporting the surface position message at the high surface rate, or when neither the airborne position message nor the surface position message is being transmitted.

[b] When the surface position message is being reported at the low surface rate.

Finally, the identification and category messages are used to identify the company and the type of aircraft that sent the message. This message contains eight identification characters that are encoded as a 6 bit subset of the international alphabet number 5. The standard MSG rates [13] for different messages are presented in Table 3.

Those standards use 25 or 100 ft as the resolution for the altitude information contained in the airborne position Message (MSG). Additionally, the velocity information resolution is 1 [kt] and the difference from the barometric altitude resolution is 25 [ft].

### 2.2.2 Processed data and criteria

ADS-B allows equipped aircraft to automatically broadcast their position, velocity, barometric and geometric altitudes and other information. This information can be processed by any receiver within the coverage volume and used for various purposes in relation to aircraft surveillance. Aircraft equipped with ADS-B use on-board positioning systems, such as GPS receivers, to determine their WGS84 [36] geographical coordinates ($\varphi$,$\lambda$,$h$). Other sensors, such as an air data computer, are used to determine the indicated air speed and barometric altitude. Broadcasted information can be collected on the ground by using low-cost ADS-B receivers. For this research study, the ADS-B data were acquired with a Kinetic SBS-1 commercial 1090MHz receiver. Ad-hoc software that does not permit raw data recording is supplied with this equipment. However, in order to store the raw data, a modified communication dynamic library (dll) was used. This "dll" acts as a middleman between the receiver and the display application software because the data stream processed by the receiver is split into two groups.

All messages received as raw data were saved as text file, including mode-S standard/extended length communications replies and 1090 ES type DF 17 messages, which contained the ADS-B information. This text file was then processed using Matlab software environment [37]. As a first step, the saved text strings were transformed into binary strings for further decoding.

The decoded information was analysed according to message type. The message types of interest were 4, 9-18 and 19. Message type 4 contained the ADS-B emitter category and the airline flight number. Message types 9-18 contained the barometric pressure altitude, synchronisation time type and Compact Position Reporting (CPR) encoded latitude and longitude. Finally, message type 19 contained the difference between the geometric and barometric altitudes. To obtain the aircraft latitude and longitude, it was necessary to decode two squitters that were separated in time by less than 10 [s]. Then, because the

mean frequency at which the position messages were received was 2 [MSG/s], a new aircraft position was typically obtained once per second.

The high number of received messages prevented continuous recording. For this reason, the recording periods were limited to a maximum of 30-40 [min].

Three recording sessions were post processed; the first two were processed to estimate the aircraft population over the central area of the Spanish airspace on a typical day and the third recording session used to estimate the atmospheric pressure field.

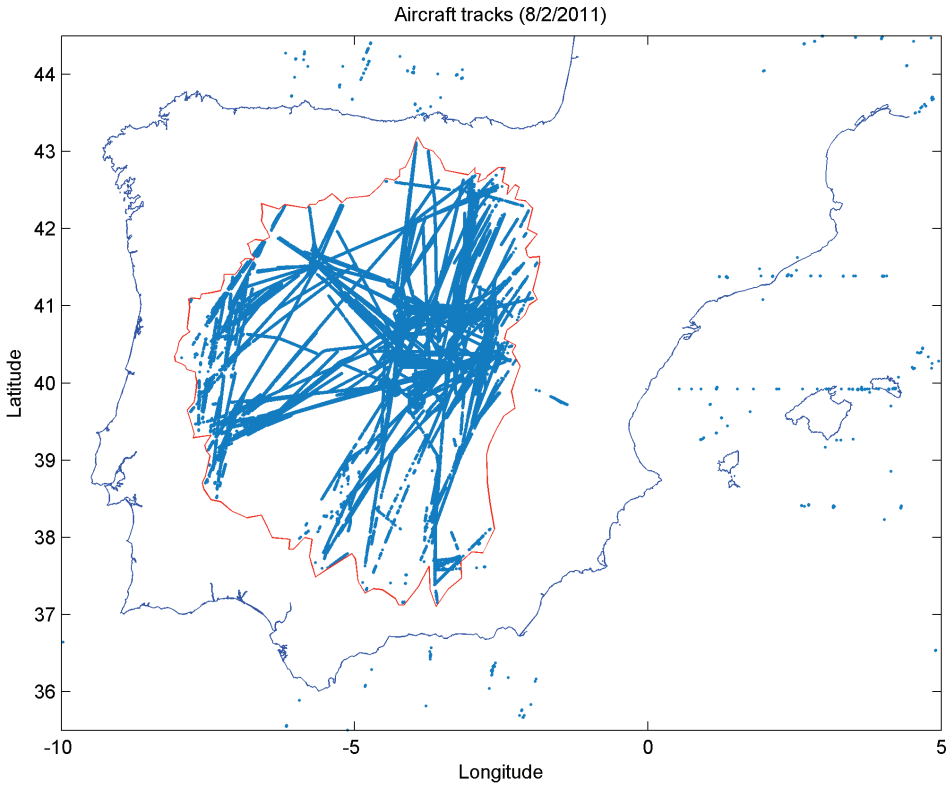


Figure 3: Coverage area and received aircraft tracks

Figure 3 illustrates the 1090 ES coverage area for the receiver located at the Technical University of Madrid. The contour line indicates the limit of receiver coverage for aircraft flying at FL300 or above and inside this area are the representations of the aircraft tracks that were received during the first recording session. From Figure 3 it was inferred that most aircraft tracks have a length of about 200 Nautical Miles (NM) within the coverage area and

remain in this area for approximately 30 [min].

The dynamics of the atmosphere are governed by fluid mechanics equations. However, to evaluate the characteristic parameters in this study, these equations were simplified according to the geostrophic wind hypothesis [38]. Following this hypothesis, aircraft were assumed to be located at altitudes where the effect of the friction term was negligible. Geostrophic velocity is defined by Equation 5.

$$\omega = -(\rho f)^{-1} \nabla p_n \tag{5}$$

where $\omega$ is the wind speed; $\rho$ the characteristic density of the air; $f$ the Coriolis parameter, which is defined as $2\Omega \cdot \sin \varphi_c \sim 0.35 \cdot 10^{-5}$ [rad/s], where $\Omega$ is the angular speed of Earth; $\varphi_c$ the latitude of the area in question ($\sim 40°$)and $\nabla p_n$ the air pressure gradient normal to the air velocity vector.

From Equation 5, the characteristic distance and time was broadly estimated as a function of the characteristic wind speed ($\omega_\infty$) and a desired resolution for $\nabla p$ of 1 [hPa], as shown in Equation 6 and 7

Using the ISA model, the density ($\rho$) at 6000 [m] is approximately 0.66 [kg/m$^3$]. For this density value, the characteristic distance ($l_c$) and time ($t_c$) were expressed as a function of wind speed ($\omega_c$).

Table 4: Recording parameters

| Recording data | Total aircraft number | Total squitter number | Position squitter number | Velocity squitter number | Aircraft identification squitter number | Total recording minutes |
|---|---|---|---|---|---|---|
| February 8 | 567 | 1,470,685 | 697,829 | 698,971 | 70,745 | 261 |
| February 16 | 609 | 2,100,829 | 996,156 | 998,902 | 100,795 | 354 |
| March 14 | 467 | 213,940 | 101,188 | 101,693 | 10,511 | 57 |

$$l_c \cdot \omega_c \approx \frac{\nabla p_n}{\rho \cdot f} = \frac{100[hPa]}{0.66[kg/m^3] \cdot 9.35 \cdot 10^{-5}[rad/s]} = 1620480[m^2/s] \tag{6}$$

which gave the results

$$l_c = \frac{1620480}{\omega_c} m; \quad t_c = \frac{1620480}{\omega_c^2} s \tag{7}$$

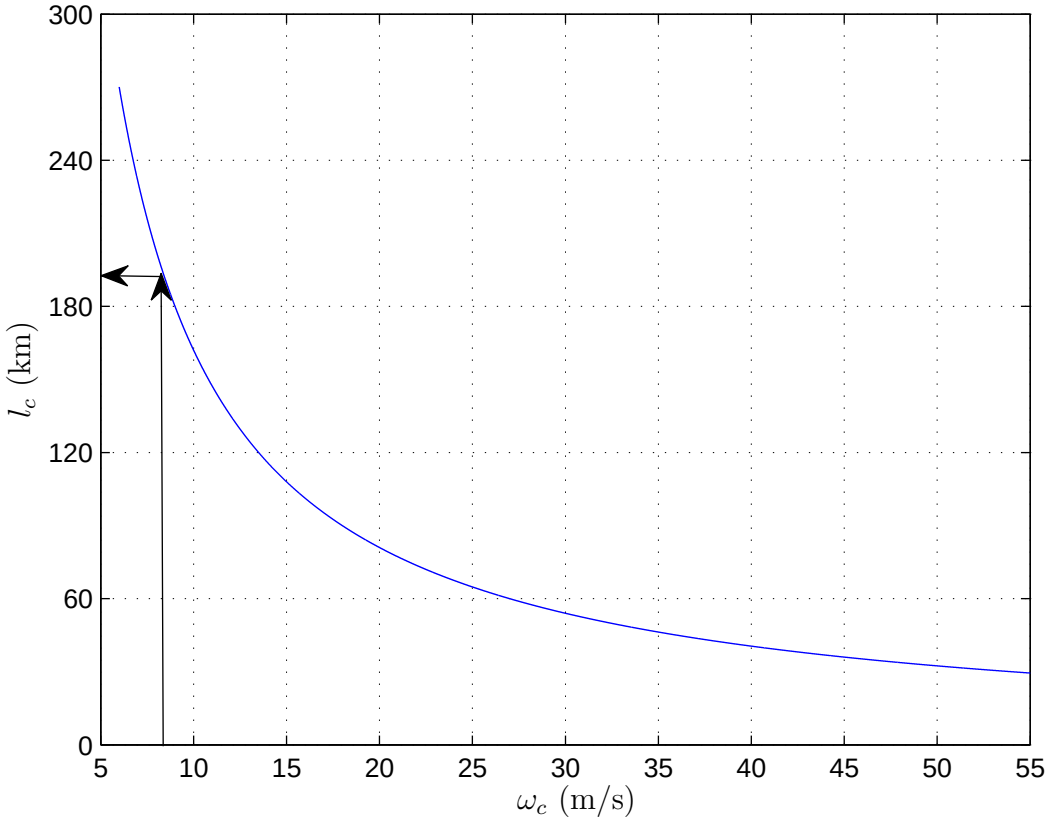


Figure 4: Characteristic longitude versus characteristic speed

Figure 4 and 5 show the resulting characteristic longitude and time as a function of the characteristic wind speed, respectively.

The arrows in Figure 4 and 5 show the characteristic parameters on the 14th of March that were used in the following analysis.

A representative wind speed of 10 [m/s] was used as an example, which took into account [39] the fact that although the highest wind speed ever recorded in Madrid is approximately 36 [m/s], the mean wind speed is 8.8 [m/s]. Thus, a speed of 10 [m/s] is an acceptable example of a typical value. Following the Hellmann power law [39, 40] with a rough land

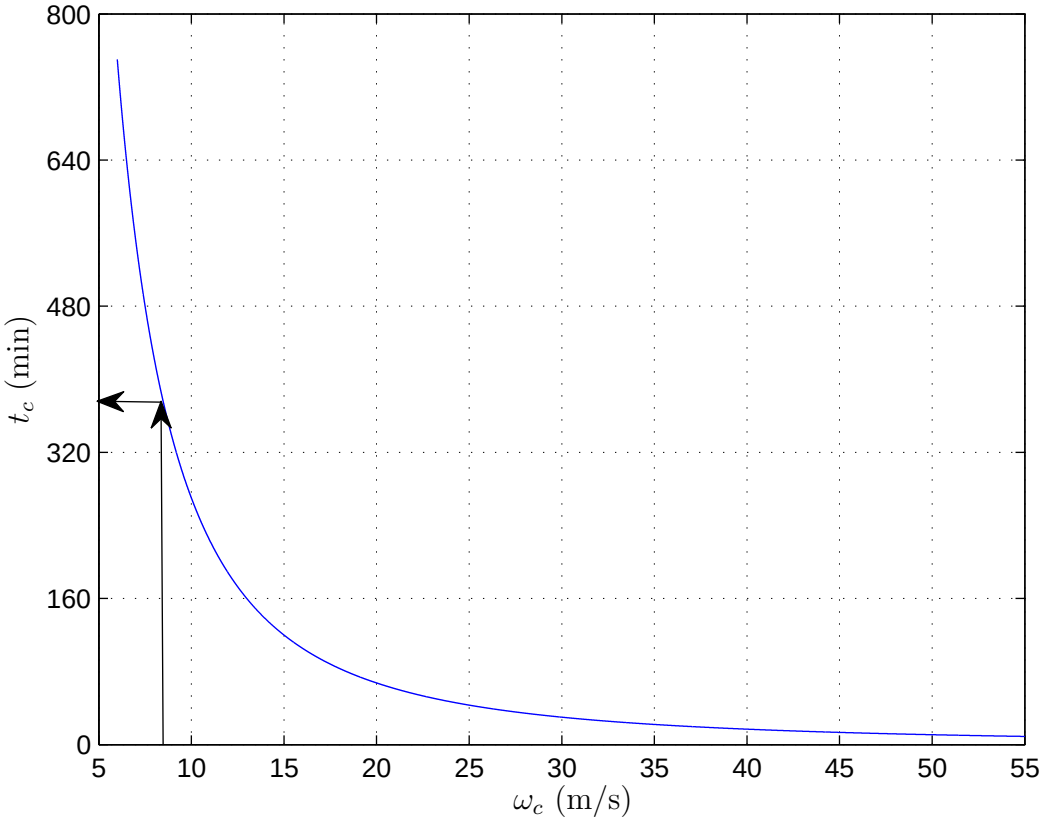


Figure 5: Characteristic time versus characteristic speed

representative value of $\alpha = 0.25$ (such as for cities), the wind speed at 6000 [m] for this surface was calculated in Equation 8.

$$\frac{v_2}{v_1} = \left(\frac{h_2}{h_1}\right)^{\alpha} \rightarrow v_2 = v_1 \left(\frac{h_2}{h_1}\right)^{\alpha} = 10 \cdot \left(\frac{6000[m]}{10[m]}\right)^{0.25} \approx 50[m/s] \tag{8}$$

When this value was used as the characteristic speed ($\omega_c$) in Figure 4 and 5, the result was a characteristic distance of approximately 30 [km] and a characteristic time of 10 [min]. This implies that lower values of air speed will result in higher values for both the characteristic distance and the time.

### 2.2.3 Element-Free Galerkin Method

Element-Free Galerkin Method (EFGM) has been used in the pressure and wind vector estimation. It was developed by Belytschko in 1994 [41] and it is based in the called Diffuse Element Method (DEM) developed by Nayroles [42] in 1992. The EFGM is a mesh-free method where a set of polynomial approximation function are adjusted to determine the estimation function with the inputs of the observation of the variable value in the observation points of the area of study. The adjustment of the polynomial approximation function makes use of the Moving Least-Squares (MLS) with the weighted function which gives more importance to the closest points.

Although EFGM is considered a mesh-free in to the function approximation, it needs a mesh to solve the partial differential equation. This is because the weak integral evaluation needs a domain division at least as far as nodal quadrature is used [43].

The EFGM main idea is to replace the Finite Element Method (FEM) by part typical interpolation by a local less squares adjustment. The resultant function is more regular than the FEM function because their discontinuous coefficients are replaced by continuous weighted functions [44].

The MLS $u^h(\mathbf{x})$ interpolation of the $u(\mathbf{x})$ function defined in the study domain is approximated around $\mathbf{x}$ point:

$$u^h(\mathbf{x}) = \sum_{j}^{m} p_j(\mathbf{x}) \cdot a_j(\mathbf{x}) = \mathbf{p}^T(\mathbf{x}) \cdot \mathbf{a}(\mathbf{x}) \tag{9}$$

where $\mathbf{p}(\mathbf{x})_{m\times 1}$ is the basis functions vector of the polynomial approximation. $\mathbf{p}^T(\mathbf{x}) = \{1, x, y, xy, x^2, y^2, \cdots, x^r, y^r\}$; $m$ are the terms number of the basis function vector $\mathbf{p}(\mathbf{x})$; $\mathbf{a}(\mathbf{x})_{m\times 1}$ are the polynomial approximation parameters, whose extended notation is: $\mathbf{a}^T(\mathbf{x}) = \{a_0(\mathbf{x}), a_1(\mathbf{x}), \cdots, a_m(\mathbf{x})\}$. These parameters have the goal of minimizing the cost function $(J(\mathbf{x})_{1\times 1})$ denoted by:

$$J(\mathbf{x}) = \sum_{I=1}^{n} w(\mathbf{d_I}) \cdot (u^h(\mathbf{x}, \mathbf{x}_I) - u(\mathbf{x}_I))^2 \tag{10}$$

where in the Equation 10: $w(\mathbf{d_I})$ is the weighted function defined by Equation 13; $\mathbf{d}_I = \left|\mathbf{x} - \mathbf{x_I}\right|$ is the distance between the point at which the pressure is estimated ($\mathbf{x}$) and the known pressure point (A/C location) ($\mathbf{x_I}$); $\mathbf{x}_I (I = 1, 2, \cdots, n)$ are the observation points inside the domain of influence around $\mathbf{x}$.

Substituting Equation 9 into Equation 10, the cost function result as it is denoted by Equation 11, which shows the cost function summatory in a vector notation way.

$$J(\mathbf{x}) = \sum_{I=1}^{n} w(\mathbf{x} - \mathbf{x}_I) \cdot (\mathbf{p}^T(\mathbf{x}) \cdot \mathbf{a}(\mathbf{x}) - u(\mathbf{x}_I))^2 \tag{11}$$

If the Equation 11 is rewritten including all the observation points the resultant is the cost function matricial equation as denotes Equation 12.

$$J(\mathbf{x}) = (\mathbf{P} \cdot \mathbf{a} - \mathbf{u})^T \cdot \mathbf{W}(\mathbf{x}) \cdot (\mathbf{P} \cdot \mathbf{a} - \mathbf{u}) \tag{12}$$

In Equation 12:

- $\mathbf{P}_{n \times m} = \begin{pmatrix} p_1(\mathbf{x}_1) & p_2(\mathbf{x}_1) & \cdots & p_m(\mathbf{x}_1) \\ p_1(\mathbf{x}_2) & p_2(\mathbf{x}_2) & \cdots & p_m(\mathbf{x}_2) \\ \vdots & \vdots & \ddots & \vdots \\ p_1(\mathbf{x}_n) & p_2(\mathbf{x}_n) & \cdots & p_m(\mathbf{x}_n) \end{pmatrix}$ are the monomials evaluated on each of the $n$ observation points.
- $\mathbf{u}_{1 \times n} = \{u_1(\mathbf{x}), u_2(\mathbf{x}), \cdots, u_n(\mathbf{x})\}^T$ are the observation value of the function $u$ at the $n$ observation points.
- $\mathbf{W}(\mathbf{x})_{n \times n} = \begin{pmatrix} w(\mathbf{x} - \mathbf{x}_1) & 0 & \cdots & 0 \\ 0 & w(\mathbf{x} - \mathbf{x}_2) & \cdots & 0 \\ \vdots & \vdots & \ddots & \vdots \\ 0 & 0 & \cdots & w(\mathbf{x} - \mathbf{x}_n) \end{pmatrix}$ is the weighted functions matrix.

$$
\begin{aligned}
w(d_I) &= \frac{e^{-\left(\frac{d_I}{c}\right)^{2k_f}} - \left(\frac{d_{mI}}{c}\right)^{2k_f}}{1-\left(\frac{d_{mI}}{c}\right)^{2k_f}} && d_I \leq d_{mI} \\
w(d_I) &= 0 && d_1 \leq d_{mI}
\end{aligned}
\tag{13}
$$

In the above, $d_{mI}$ is the influence distance, which is the distance that allows the use of points that are far from the evaluation pressure point, $c = \beta \cdot c_I$, where $\beta$ has a value between 1 and 2, $c_I$ the characteristic distance of the area. When $c$ decreases, the closest points to $\mathbf{x}$ become more relevant; and $k_f$ is equal to 1, it provides the faraway points relevance in the analysis.

The polynomial approximation parameters $(\mathbf{a}(\mathbf{x})_{m\times 1})$ are determined as them whose minimize/maximize the cost function denoted by Equation 12, resulting as follows:

$$
\mathbf{a}(\mathbf{x}) = \mathbf{A}(\mathbf{x})^{-1} \cdot \mathbf{B}(x) \cdot \mathbf{u}(\mathbf{x}) \tag{14}
$$

where $\mathbf{A}(\mathbf{x})$ and $\mathbf{B}(\mathbf{x})$ are the matrices defined by Equation 15 and 16, respectively.

$$
\mathbf{A}(\mathbf{x})_{m\times m} = \mathbf{P}^T \cdot \mathbf{W}(\mathbf{x}) \cdot \mathbf{P} \tag{15}
$$

$$
\mathbf{B}(\mathbf{x})_{m\times n} = \mathbf{P}^T \cdot \mathbf{W}(\mathbf{x}) \tag{16}
$$

Finally, the function $(u)$ can be expressed including the polynomial approximation parameters defined by Equation 14 into the interpolated function Equation 9 the resultant equation appears in Equation 17.

$$
\mathbf{u}^h(\mathbf{x}) = \sum_I^n \sum_j^m p_j(\mathbf{x}) \cdot (\mathbf{A}^{-1}(\mathbf{x}) \cdot \mathbf{B}(\mathbf{x}))_{jI} \cdot u_I = \sum_I^n \phi_I(\mathbf{x}) \cdot u_I \tag{17}
$$

### 2.2.4 Empirical horizontal pressure estimate

An example of a method by which ADS-B messages could be used to analyse the state of the atmosphere is presented below. For this purpose, a reference pressure was acquired

from GRIB.US [45] with atmospheric variables at 10 [m] above MSL and these values were corrected to correspond to MSL.

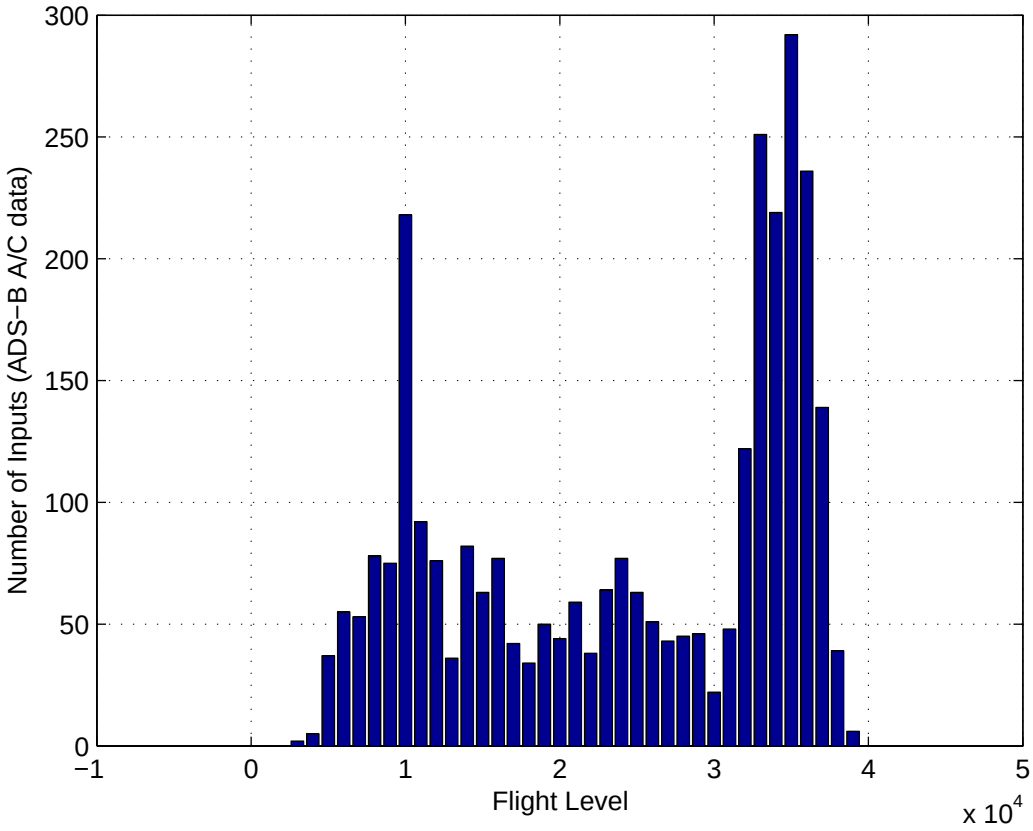


Figure 6: Aircraft messages received on the 14th of March during 9:00-12:00 UTC

The estimated pressure at MSL was derived from stored messages on the 14th of March. The altitude distribution for the different flight levels is shown in Figure 6. Considering that these messages were obtained during a 1 [min] period (less than the characteristic time; see Figure 5), it was assumed that the pressure remained constant within this time interval. Therefore, the time interval 9:00-12:00 Universal Time Coordinated (UTC) was used in this example.

The data from aircraft within an altitude range of 15,000-38,000 [ft] were used. Aircraft that were close to or under the transition altitude of Madrid-Barajas were eliminated. Before applying the Galerkin method [41], the pressure was extrapolated to MSL using the ISA

atmospheric model (see Equation 18 and Equation 19).

According to ICAO [1], the following Equation 18 and Equation 19 gave the pressure at troposphere and tropopause atmosphere layer, respectively. These equations assume a linear variation of the temperature with altitude in the troposphere of 6.5°/km and remain constant above tropopause (11,000 [m]). They also follow static air and perfect gas law.

$$p = p_2 \left(1 - \frac{LR}{T_1}(h - h_1)\right)^{g_0/LR \cdot R_a} \qquad MSL \leq h, h_1 \leq 11,000m \tag{18}$$

$$p = p_1 \cdot e^{g_0(h-h2)/T_2 R_a} \quad 11,000 \leq h, h_2 \leq 22,000m \tag{19}$$

where

- h is the altitude;
- $LR = 0.0065$ [K/m] the temperature gradient with altitude between MSL and 11,000 [m];
- $g_0 = 9.81$ [m/s$^2$] the acceleration of gravity at MSL;
- $R_a = 287$ [J/kg/K] the gas constant;
- $h_1$ and $h_2$ are the aircraft altitude located in the troposphere and in the tropopause, respectively;
- $T_1(K) = 288.15 - 0.66(h_1(m)/1000) = 288.15 - 1.98(h_1(ft)/1000)$ the temperature at $h_1$ altitude;
- $T_2 = -56.5$ [° C] $= 216.65$ [K] the temperature at the tropopause;
- $p_1$ the pressure at $h_1$ altitude; and
- $p_2$ the pressure at $h_2$ altitude.

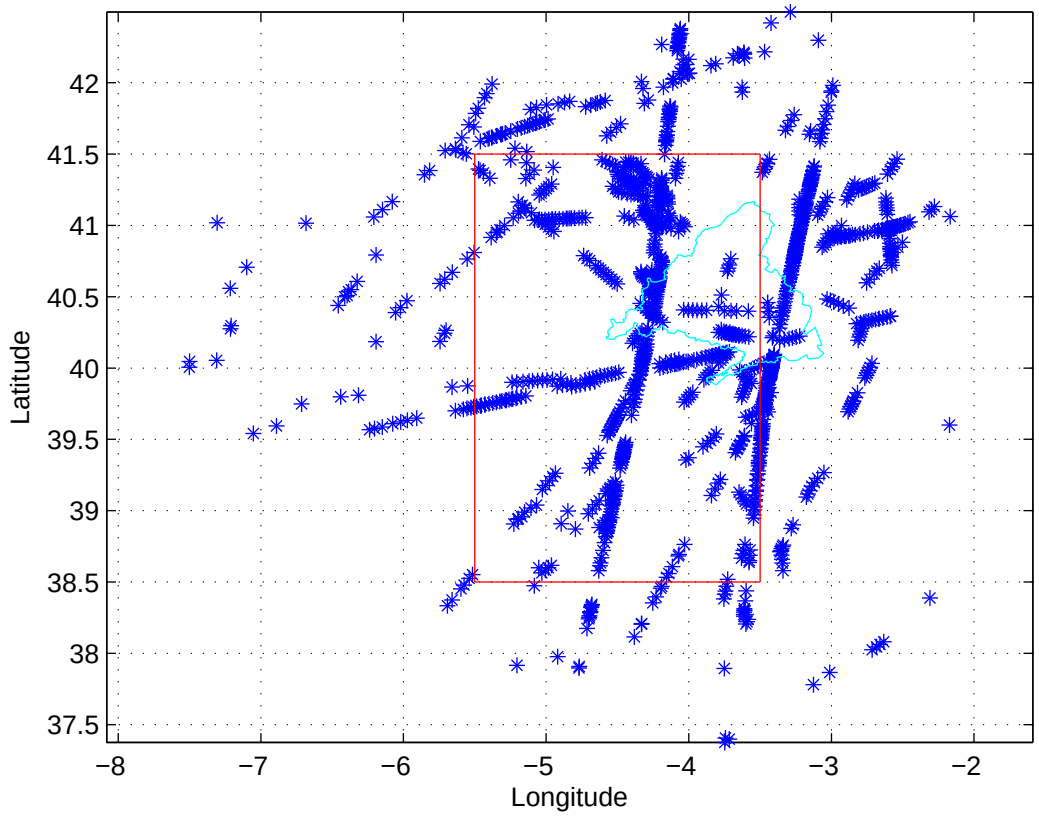


Figure 7: Locations of aircraft messages received on the 14th of March during 9:00-12:00 UTC

Figure 7 shows the positions from which the ADS-B messages were received and the red square indicates the area for which the pressure was estimated.

Figure 8 shows the distribution of the aircraft pressures obtained from ADS-B messages at different MSL altitudes, where the data used in this estimate are marked in circles. Filtered data are marked with circles while the solid line represents the ISA pressure model.

The mathematical model chosen to estimate the pressure was the EFGM. In 1915 Galerkin [46] published an approximate method to solve the Laplace equation. This method gives an approximate solution as a linear combination of elements from a given linearly independent system.

The primary reason why this model was chosen is due to the meshless method it employs,

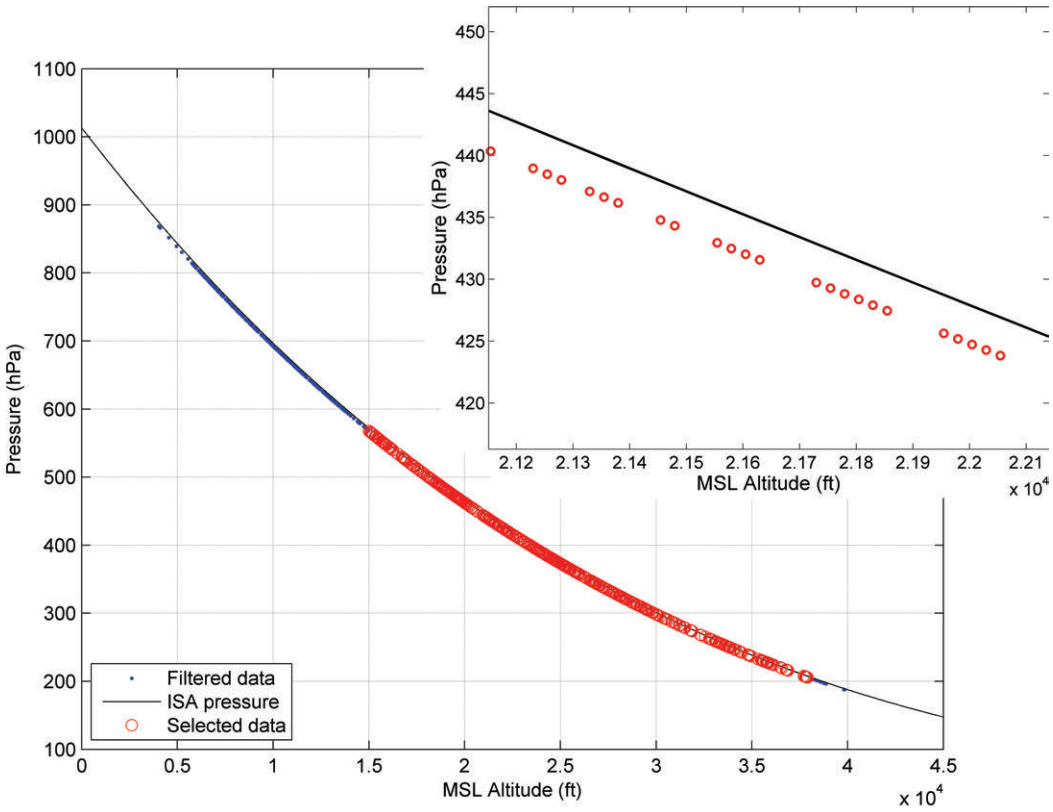


Figure 8: Locations of aircraft messages received on the 14th of March during 9:00-12:00 UTC

which facilitates its application to modelling data from moving points. Furthermore, it has been used in other applications, such as elasticity and heat conduction problems [47, 48, 49], which yielded realistic results. The pressure model was developed by applying a moving least squares approximation to the EFGM, as in Belytschko et al. [41], and using the pressure information sent from the aircraft ADS-B. In this method, a local polynomial estimate of the parameter ($p$) was performed by computing a Gaussian weighted function of the distance from each input to the point where the estimate was being made, as in Equation 13 which is a Gaussian weighted function centred at the point where the approximation was made. This function provides more relevance for closer points.

For each point within the grid, a second-order polynomial approximation was applied. Equation 20 is the expression for this approximation, where $a_{ij}(x, y)$ are the parameters to

be estimated.

$$\hat{p}(x,y) = a_{00}(x,y) + a_{01}(x,y)\cdot x + a_{01}(x,y)\cdot y + a_{11}(x,y)\cdot xy + a_{02}(x,y)\cdot x^2 + a_{20}(x,y)\cdot y^2 \quad (20)$$

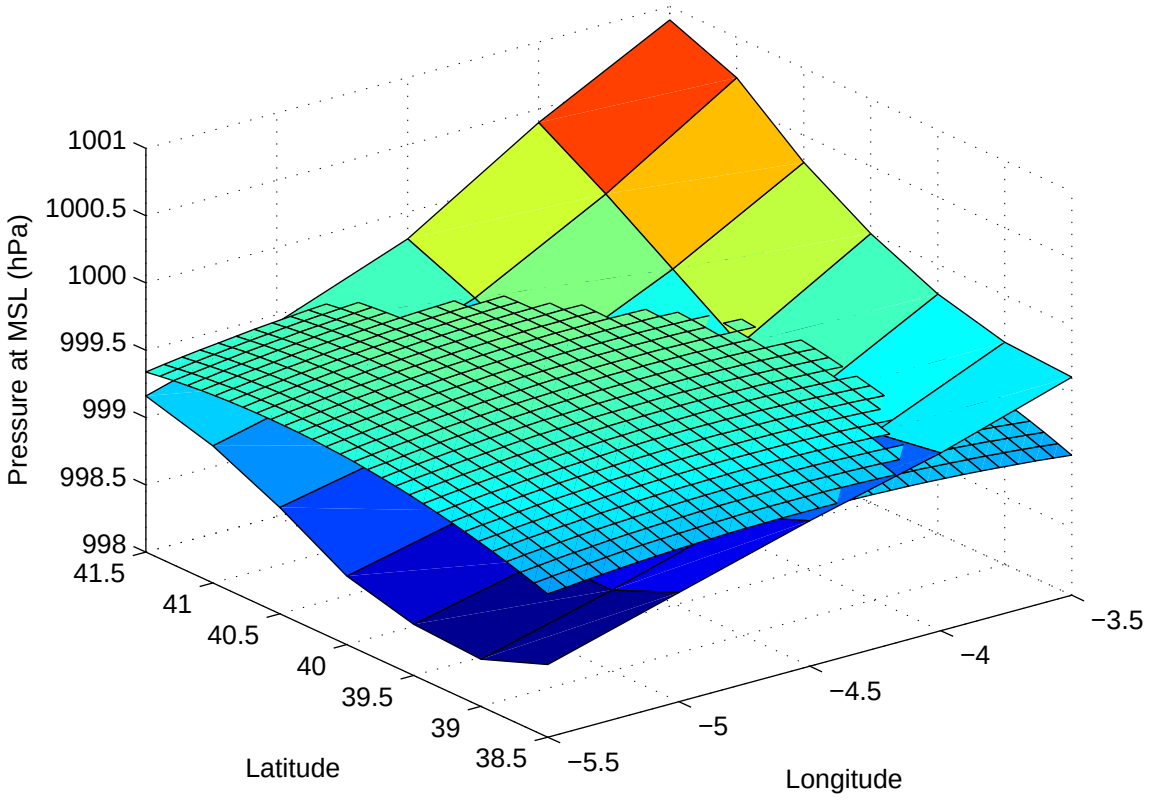


Figure 9: Pressure estimate

Figure 9 shows the pressure derived from the stored ADS-B data at MSL and the pressure obtained from NOAA [45]. The pressure obtained from [45] is less granular (6 points) than the surface, showing the pressure obtained from the Galerkin method. In comparing both surfaces, an error of around 1 hPa (∼10 [m] in height) was observed.

### 2.2.5 Empirical vertical pressure estimate

Stored data can also be used to analyse the agreement between the ISA model and the pressure derived from ADS-B messages. The assessment of the standard atmospheric model

was conducted using the pressure derived from the ADS-B as a reference. Stored data was filtered to exclude any aircraft located outside of a tube with a minimum altitude of the transition level of Madrid Terminal Management Area (TMA) (13,000 [ft]) and a radius of 50 [km]. This volume was chosen, based on the recording session, in different locations to get a representative number of aircraft.

Because of the reduced physical dimensions of the analysed surface and the small time interval (1 h), it was assumed that the pressure variations with position and time were both negligible.

This pressure assumption was supported by the fact that the recording days were characterised by a low variation in the pressure as a function of time and position; the variation was lower than 0.7 [hPa] in this case. Therefore, it was assumed that the pressure was constant for each altitude and during the time interval of the study.

Comparisons of the altitudes and the pressures were conducted. To make the altitude comparison possible, the same reference surface was used for all altitude data.

One of the parameters used in this comparison was the pressure altitude, which was calculated on-board from the static pressure measured by the pitot tube using the expressions from the standard atmospheric model. The other parameter is the difference between the aircraft geometric altitude and the pressure altitude (difference from barometric altitude) [13, 50], which is transmitted when the pressure and geometric altitudes are available and valid.

Not all aircraft use the same reference surface to determine the geometric height. Modern avionics always use Height Above Ellipsoid (HAE) and can be distinguished because they transmit the squitter types 9 and 10. Aircraft transmitting squitters types 11-18 may also refer to the geometric height over MSL reference, so it is not possible a priori to determine the type of reference they are using. Although it is preferable to express this difference using the World Geodetic System (WGS)84 ellipsoid, not all aircraft follow this convention.

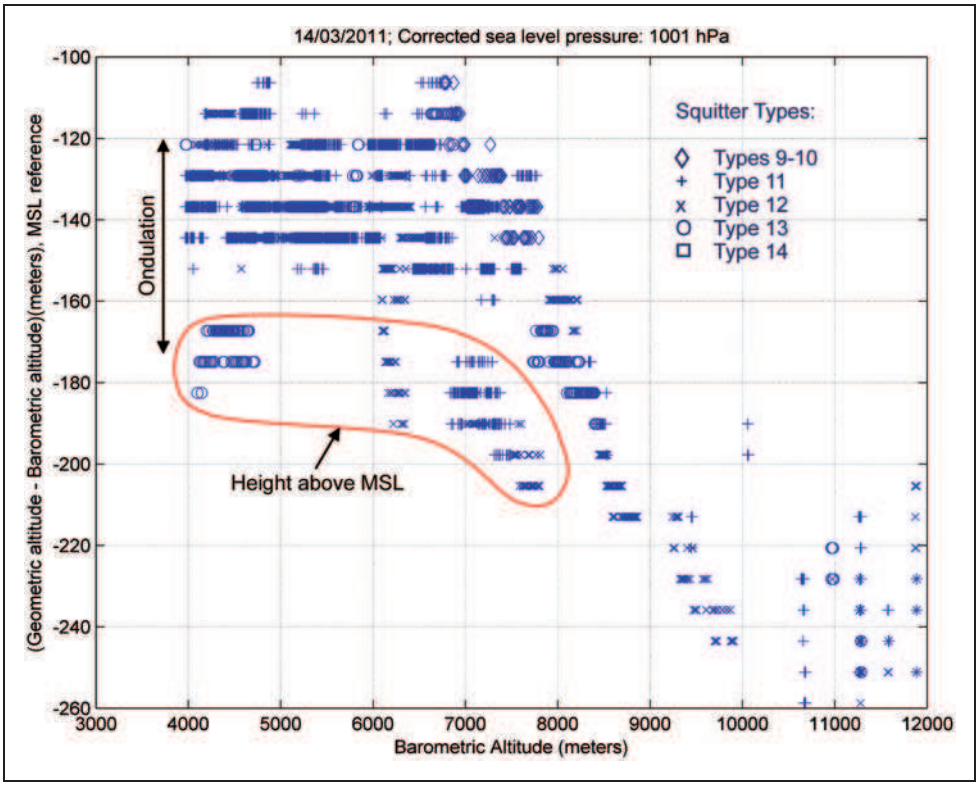


Figure 10: Difference between geometric and pressure altitude (14/03/2011)

Since both the first parameter and the atmospheric model were expressed in reference to MSL, all heights that referred to the ellipsoid were transformed to refer to MSL as well. To transform the heights, the value of the ondulation was subtracted from the heights that referred to the ellipsoid (for the position of the study volume, the ondulation had a mean value of 53 [m]). The ondulation correction was used to modify the difference in the altitude values by subtracting the mean ondulation value at the study area. It was later observed that this correction produced an error (shown in Figure 10) because some aircraft used MSL instead of the ellipsoidal reference.

The difference between the aircraft geometric and pressure altitudes versus the barometric altitude for March 14th is as shown in Figure 10. The collected squitter types 9 and 10 were always referenced to the ellipsoid; they are shown as diamonds in Figure 10 and were used as reference data. Below these points appears a group enclosed by a line that exhibits

a significant deviation, which is close to the ondulation value.

It was inferred that the information for those data points were transmitted from aircraft that used MSL as a reference. This information which is the least precise amongst the filtered data was provided mainly by squitter type 13.

Table 5: Corrected atmospheric pressure and temperature at sea level

| Recording day | MSL pressure (hPa) | MSL temperature |
|---|---|---|
| February 8 | 1028 | 11°C |
| February 16 | 998 | 7°C |
| March 14 | 1001 | 13°C |

Different types of filters were applied to exclude aircraft transmitting MSL altitude information, but with an ondulation value that was similar to the data dispersion, it was practically impossible. The best option for this assessment was to use only squitter types 9-12. The corrected atmospheric pressure and temperature at sea level were obtained within the study area, and the values were as presented in Table 5.

Figure 11 presents the altitude differences versus the barometric altitude, for the three recording days using the filtered data. There was a significant difference between the aircraft geometric and pressure altitudes for all stored data; these differences were positive for high pressure days and negative for low pressure days. Furthermore, the trend in the data was that these differences decreased as a function of altitude.

On low-pressure days, it was observed that this negative trend changed close to the bottom of the tropopause zone, which is where the expressions for the ISA model also change.

Figure 12 shows a scheme of the process followed by the aircraft and ground analysis. To check the accuracy of the ISA model two pressures were compared; the pressure measured by the aircraft and that obtained from the geometric altitude using the ISA model (ISA model pressure).

As the aircraft transmitted their barometric altitude, this was converted to pressure using the same model that is used on-board the aircraft (ISA 1013.25 [hPa] MSL reference and 15 [°C]).

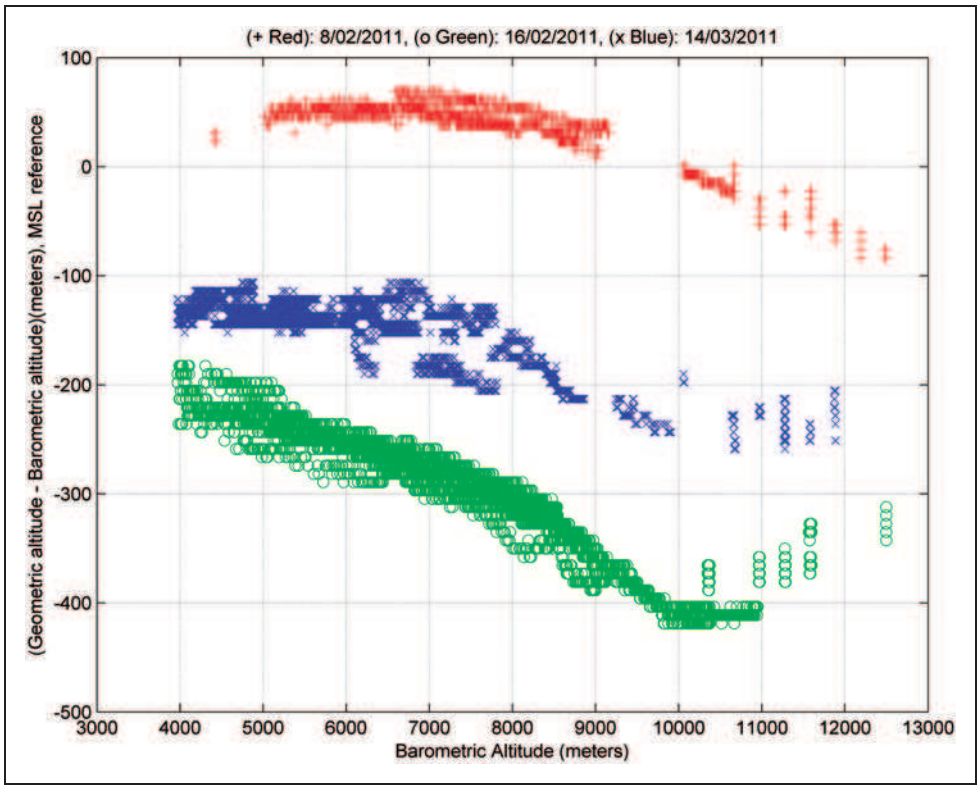


Figure 11: Difference between geometric and pressure altitude (three days)

Two methods were used to calculate the ISA model pressure. The first uses as the reference pressure ($p_0$) only, the corrected pressure at sea level that exists near the centre of the study volume, and 15 [°C] as temperature at sea level. The second uses the pressure and temperature corrected at sea level from the closest meteorological stations.

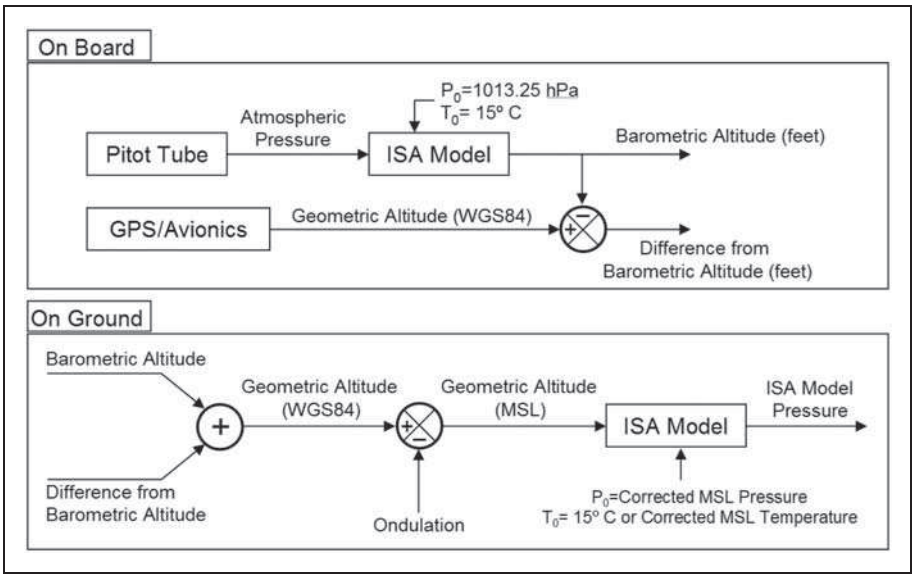


Figure 12: Data processing

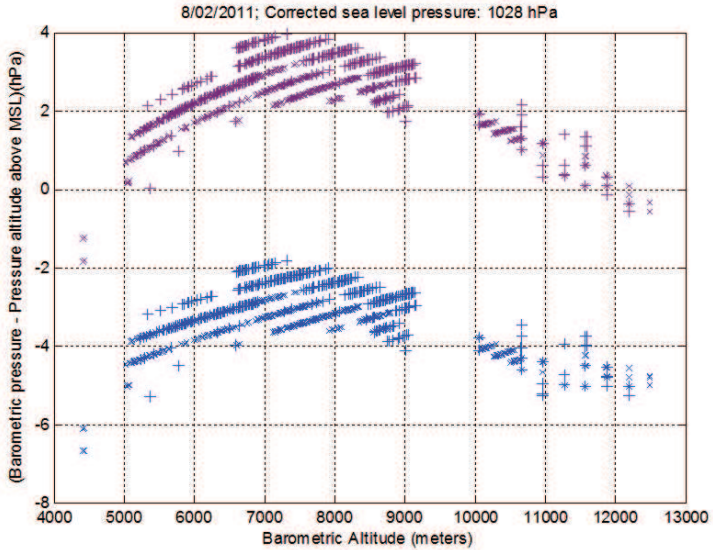


Figure 13: Difference between geometric and pressure altitude (08/02/2011)

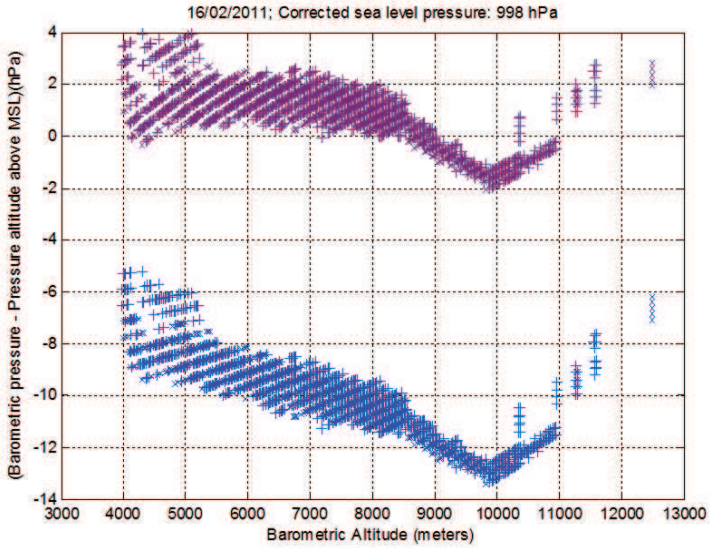


Figure 14: Difference between geometric and pressure altitude (16/02/2011)

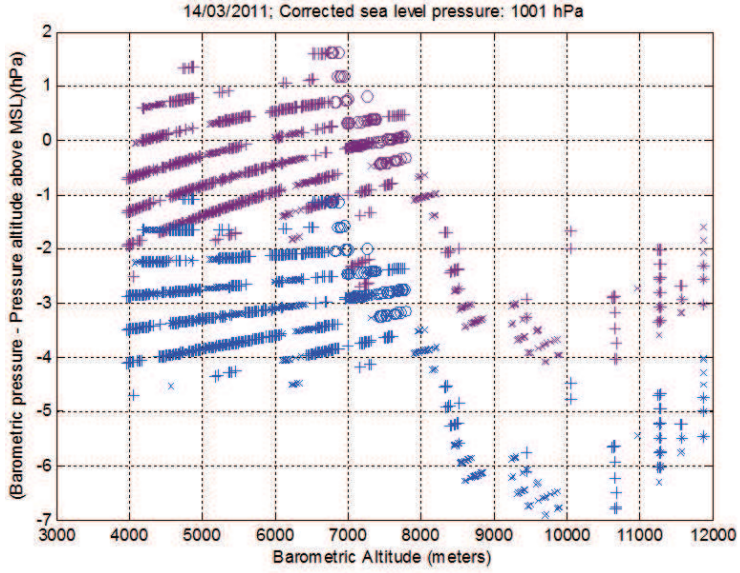


Figure 15: Difference between geometric and pressure altitude (14/03/2011)

The differences between the pressures measured by the aircraft and the pressures that were calculated using the ISA model are shown in Figure 13, 14 and 15, for the three recording days. The use of temperature adjustment provided more accurate results, with only small errors in the tropopause region (altitudes around 10,000 [m]). This is depicted by the plus samples in Figure 14 and 15 . The circles samples are obtained when only a pressure ad-

justment is used, and it was observed that the error increases as the temperature differences from the ISA (15°C) also increase.

However, in Figure 13, there is a larger error despite the temperature correction, which probably occurred because no meteorological stations data were available close to the centre of the study volume and that the interpolated temperature might have been obtained from distant stations.

### 2.2.6 Wind vector possible estimation

Moreover, ADS-B data could serve to evaluate a better wind vector estimation. In this section, a wind vector approximation with EFGM is evaluated making use of two different scenarios: non rotational and cyclonic wind flow. These scenarios are shown in Figure 16, where the red arrows denote the wind vector estimation, the blue ones the real wind vector and the stars the observation points. Real wind vector information is collected from [45], where the non rotational wind flow scenario is composed by 99 observation points and the cyclonic by 49 ones.

This objective has been fulfilled under certain hypothesis:

- **Incompressible fluid**: Most of the time wind speed is less than 100 [km/h] and therefore air density can be considered as a constant. As a result, the continuity equation flow can be simplified as it is shown in the following expression:

$$\frac{\partial \rho}{\partial t} + \nabla \cdot (\rho \mathbf{v}) \rightarrow \nabla \cdot \mathbf{v} = 0 \tag{21}$$

- **Hydrostatic equilibrium**: gravity force is balanced by the vertical component of the pressure gradient denoted by the following equation:

$$\frac{\partial p}{\partial z} = -\rho g \tag{22}$$

That vertical pressure assumption is considered good enough in real atmosphere mesoscale model and higher.

- **Stationary problem**: No time dependence due to the fact that a diagnostic meteorological numerical model type is used thus the wind estimated is the result of the interpolation and extrapolation of information from aircraft in a particular moment.

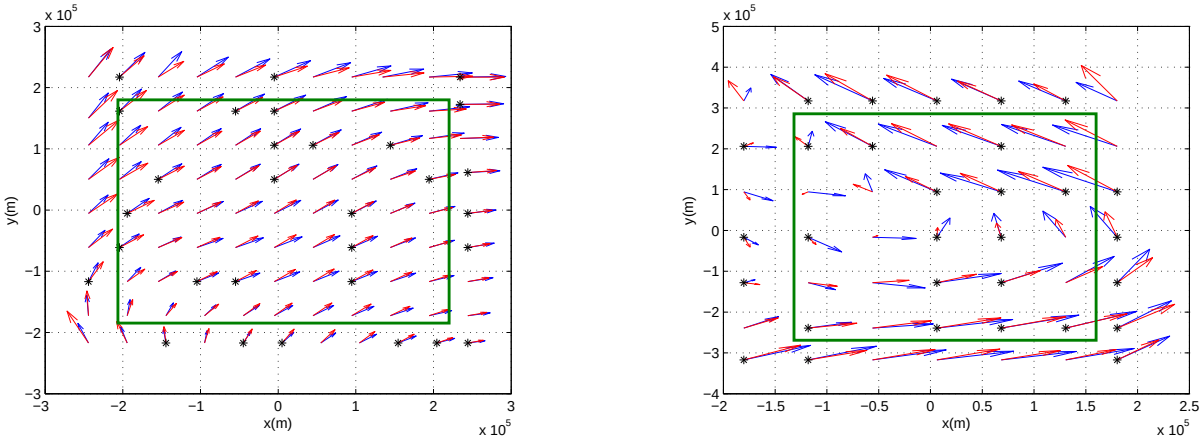


(a) non rotational wind flow scenario

(b) cyclonic wind flow scenario

Figure 16: Wind approximation for a 5 degree functional approximation and 30 observation points

The first hypothesis cited above (incompressible fluid) allows us to write the wind vector components ($\omega_x$, $\omega_y$) approximated through the following potential function:

$$\Phi = \sum_{\substack{i=0 \\ j=0}}^{N} a_{ij} \cdot x^i \cdot y^j \tag{23}$$

Therefore, wind vector components approximate polynomials are defined by:

$$\omega_x^h(\mathbf{x}) = \frac{\partial \Phi}{\partial y} = \sum_{\substack{i=0 \\ j=1 \\ i+j \leq N}}^{N} j \cdot a_{ij} \cdot x^i \cdot y^{j-1} \tag{24}$$

$$\omega_y^h(\mathbf{x}) = -\frac{\partial \Phi}{\partial x} = -\sum_{\substack{i=1 \\ j=0 \\ i+j \leq N}}^{N} i \cdot a_{ij} \cdot x^{i-1} \cdot y^j \tag{25}$$

where $N$ is the maximum potential function monomial degree.

These equations are right described if the polynomial approximation parameters ($a_{ij}$) are not $x$ e $y$ dependent. It assumption is achieved under the evaluation scenarios since there

is an uniform number of observation points around the point where the wind component is going to be approximated.

$\omega_x$ and $\omega_y$ approximation functions are based in the Pascal triangle, as it is shown in Figure 17, e.g.: in a 2nd degree of potential function $\Phi = a_{00} + a_{10}x + a_{01}y + a_{20}x^2 + a_{11}xy + a_{02}y^2$, $\omega_x = a_{01} + a_{11}x + 2a_{02}y$ and $\omega_y = -(a_{10} + a_{11}y + 2a_{20}x)$.

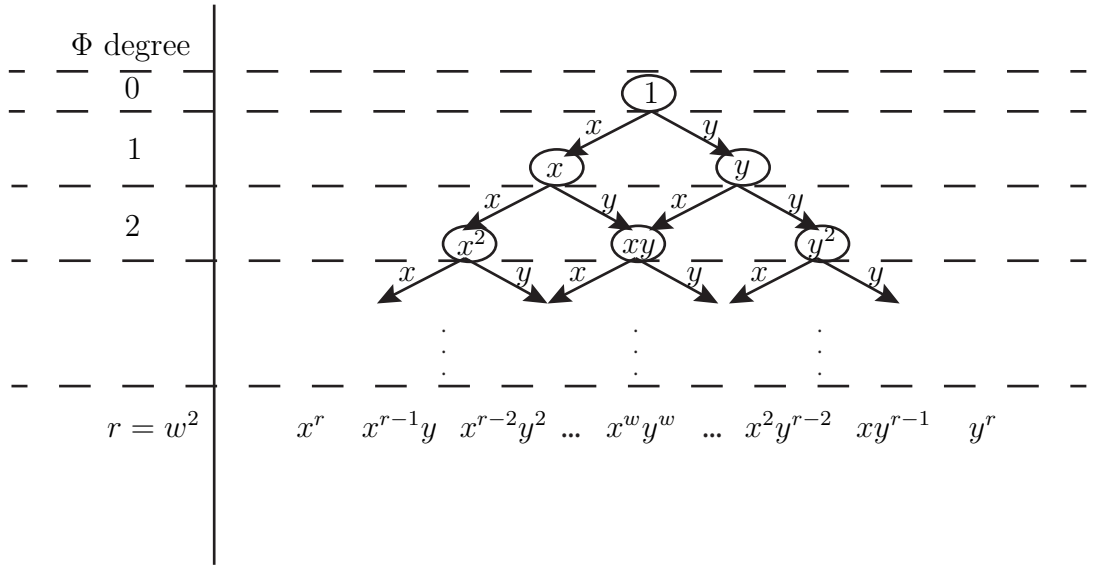


Figure 17: Functional approximation polynomial building

In order to approximate the wind vector, polynomial approximation parameters have to be determine following the procedure described in subsection 2.2.3. As an example, Figure 16 shows the non rotational and cyclonic wind vector estimation, respectively, to a 5th degree potential function and 30 observation points. Where red arrows are the estimated wind, blue arrows the measured one, stars are the observation points and area selected is established to the boundary effect study, as it was mentioned above.

Estimation is evaluated through the arithmetic mean of the difference between the estimation wind vector component and their real values for each , as it is denoted by:

$$E\left[(\omega^{\mathbf{h}} - \omega) \cdot (\omega^{\mathbf{h}} - \omega)^T\right] = \begin{bmatrix} \varepsilon_{xx} & \varepsilon_{xy} \\ \varepsilon_{xy} & \varepsilon_{yy} \end{bmatrix} \tag{26}$$

where $\epsilon_{xx}$, $\epsilon_{xy}$ and $\epsilon_{xx}$ are the arithmetic mean error values in the $x$, $y$ and $xy$ components

defined by:

$$\varepsilon_{xx} = \frac{\sum_{i=1}^{n}(\omega_x^h|_i - \omega_x|_i)^2}{n} \tag{27}$$

$$\varepsilon_{xy} = \frac{\sum_{i=1}^{n}(\omega_x^h|_i - \omega_x|_i)((\omega_y^h)_i - \omega_y|_i)}{n} \tag{28}$$

$$\varepsilon_{yy} = \frac{\sum_{i=1}^{n}(\omega_y^h|_i - \omega_y|_i)^2}{n} \tag{29}$$

The analysed elements are the trace of the Equation 26, because it provides a representative value of the estimation quality. Then, a potential function polynomial degree and a number of observation points are selected, after that the wind vector is estimated for each of the 99 or 49 of the non rotational and cyclonic wind flow mesh scenarios, and finally the trace of arithmetic mean error matrix are evaluated.

The main goals of this study is to analyze wind estimation performances. To accomplish this, the two scenarios have been used to determine the accuracy of the wind estimation function as a dependency of the number of observation points selected and the potential function polynomial degree.

Firstly, observation points selection influence into the wind estimation error is analyzed. For this purpose, 10 different simulations have been used, where observation points have been selected in a random way.

Figure 18 and 19 show the trace of the error matrix for different number of observation points and functional polynomials degree in the non rotational and cyclonic wind flow scenarios, respectively.

This figures exhibit an important observation points location dependence, nevertheless a minimum tendency value of the wind estimation error is observed which decreases in value with a higher functional polynomial degree. Moreover, as functional polynomial degree is increased a more important observation points location dependence is observed. Considering 6.8404 [m/s] and 3.3460 [m/s] of average real wind speed of the cyclonic and non rotational wind flow escenarios, respectively, a $73 - 34\%$ range error percentage is observed in the cyclonic scenario and a $23 - 15\%$ range error percentage in the non rotational one. In sort,

non rotational scenario estimation shows not only a more accurate approximation but also a higher level of observation point location dependence.

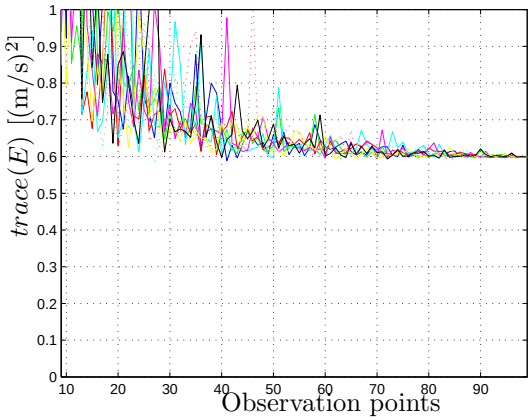


(a) 3rd degree functional polynomial approximation

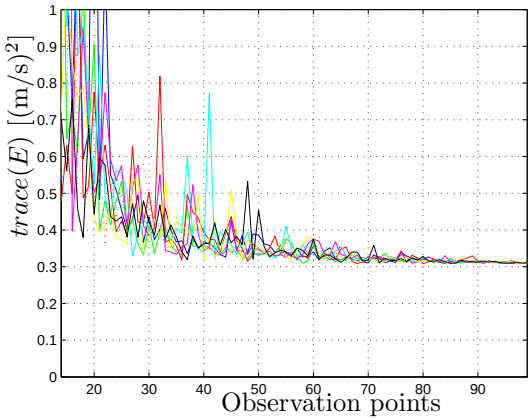


(b) 4th degree functional polynomial approximation

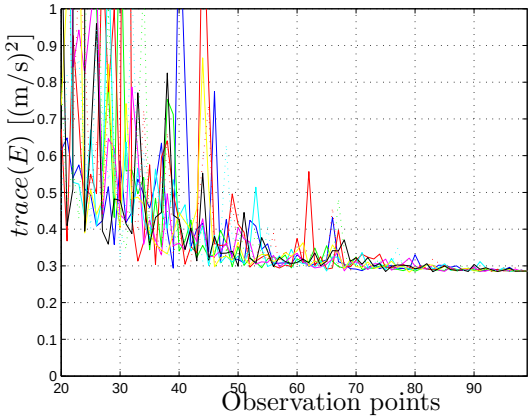


(c) 5th degree functional polynomial approximation

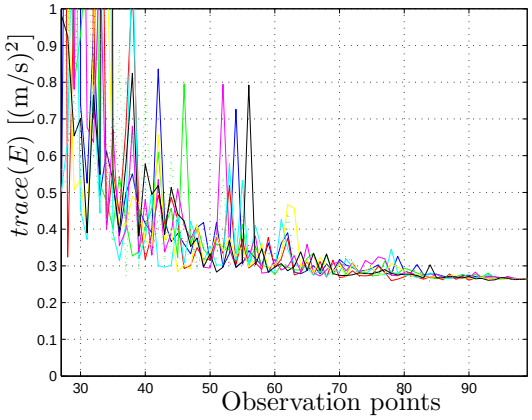


(d) 6th degree functional polynomial approximation

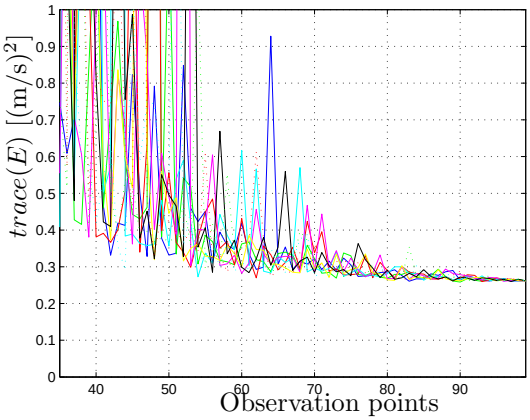


(e) 7th degree functional polynomial approximation

Figure 18: Trace wind vector arithmetic mean error matrix value representation of the different functional polynomial approximation degrees and observation points in the non rotational wind flow scenario

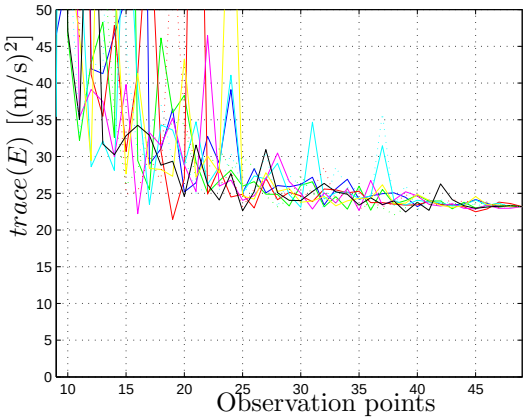


(a) 3rd degree functional polynomial approximation

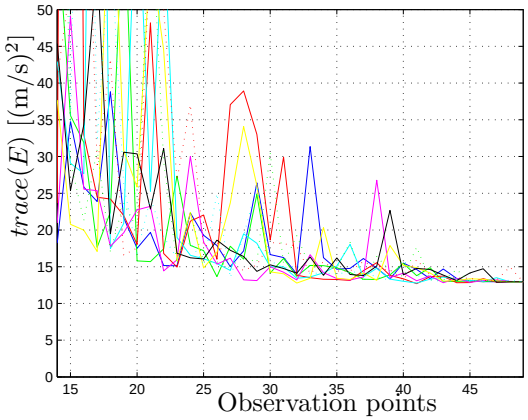


(b) 4th degree functional polynomial approximation

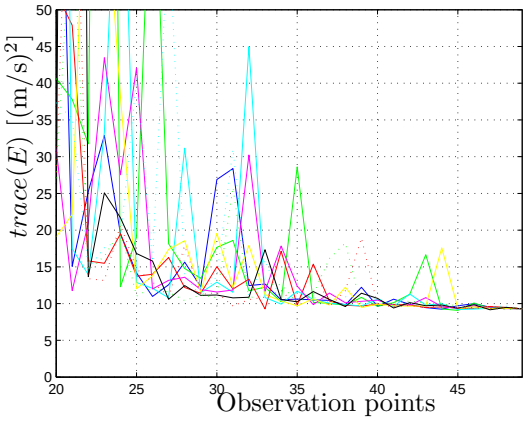


(c) 5th degree functional polynomial approximation

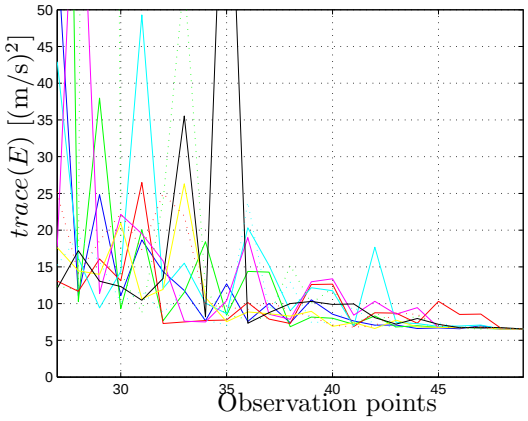


(d) 6th degree functional polynomial approximation

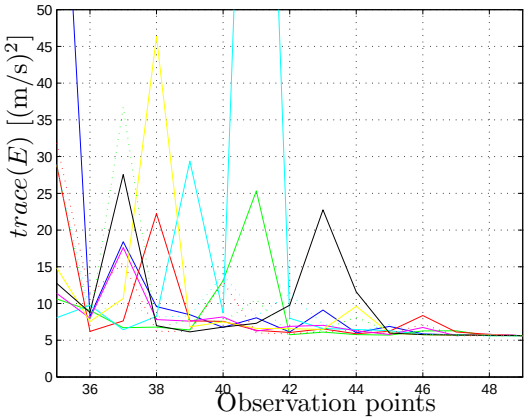


(e) 7th degree functional polynomial approximation

Figure 19: Trace wind vector arithmetic mean error matrix value representation of the different functional polynomial approximation degrees and observation points in the cyclonic wind flow scenario

As wind vector is estimate through a polynomial expression, which is a function of unknown parameters $a_{ij}$, and therefore, other estimator accuracy indicator is the Dilution of Precision (DOP) of each point into the analyzed scenario. Error in the polynomial approximation parameters is expressed as follows:

$$\boldsymbol{\varepsilon}_{m\times 1}(\mathbf{x}_I) = \hat{\mathbf{a}}(\mathbf{x}_I) - \mathbf{a}(\mathbf{x}_I) \tag{30}$$

where $\hat{\mathbf{a}}$ are the estimated polynomial approximation parameters and $\mathbf{a}$ the real ones.

Including Equation 14 in Equation 30:

$$\boldsymbol{\varepsilon}_{m\times 1}(\mathbf{x}_I) = \mathbf{A}(\mathbf{x})^{-1} \cdot \mathbf{B}(x) \cdot \hat{\mathbf{u}}(\mathbf{x}) - \mathbf{A}(\mathbf{x})^{-1} \cdot \mathbf{B}(x) \cdot \mathbf{u}(\mathbf{x}) \tag{31}$$

Considering that real $\mathbf{u}$ values are denoted as the estimated as the measured value $\hat{\mathbf{u}}$ plus the measurement error $\boldsymbol{\eta}$, Equation 31 is rewritten as follows:

$$\boldsymbol{\varepsilon}_{m\times 1}(\mathbf{x}_I) = \mathbf{A}(\mathbf{x})^{-1} \cdot \mathbf{B}(x) \cdot \boldsymbol{\eta} \tag{32}$$

Therefore, covariance matrix estimation errors obey the expected value of the error vector multiply by the same vector error transposed:

$$\boldsymbol{\sigma}_{m\times m}(\mathbf{x}_I) = E[\boldsymbol{\varepsilon} \cdot \boldsymbol{\varepsilon}^T] \tag{33}$$

After operate the Equation 34, the covariance matrix estimation errors become:

$$\boldsymbol{\sigma}_{m\times m}(\mathbf{x}_I) = \left(\mathbf{A}(\mathbf{x})^{-1} \cdot \mathbf{B}(x)\right) \left(\mathbf{A}(\mathbf{x})^{-1} \cdot \mathbf{B}(x)\right)^T \cdot \boldsymbol{\sigma}_m^2 \tag{34}$$

where $\boldsymbol{\sigma}_m^2$ is the measure error covariance denotes by $\boldsymbol{\sigma}_m^2\mathbf{I} = E[\boldsymbol{\eta} \cdot \boldsymbol{\eta}^T]$.

Consequently, DOP is evaluated as:

$$DOP(\mathbf{x}_I) = \sqrt{trace((G) \cdot (G)^T)} \tag{35}$$

where $\mathbf{G}$ is defined as $\left(\mathbf{A}(\mathbf{x})^{-1} \cdot \mathbf{B}(x)\right) \left(\mathbf{A}(\mathbf{x})^{-1} \cdot \mathbf{B}(x)\right)^T$.

As an example Figure 20 and 21 show the DOP value for 30 observation points and 3rd and 5th polynomial approximations in the non rotational and cyclonic wind flow scenario, respectively. When wind estimation error for each scenario point is analysed, is observed that boundary observation points have bigger error than the inside points. This effect is produced because boundary observation points have just information from a section of their round area, meanwhile inside observation points have surrounding area information.

For this reason, if boundary points are extracted from the trace of arithmetic mean error matrix calculation, estimation are substantially improved, not very appreciable in the estimation quality but above all in the selection point dependence, as it is shown in Figure 22 and 23. Where the range percentage wind error are 20-12% in the non rotational wind flow and 75-38% in the cyclonic wind flow considering 6.8404 [m/s] and 3.3460 [m/s] of average real wind speed, as in the previous study.

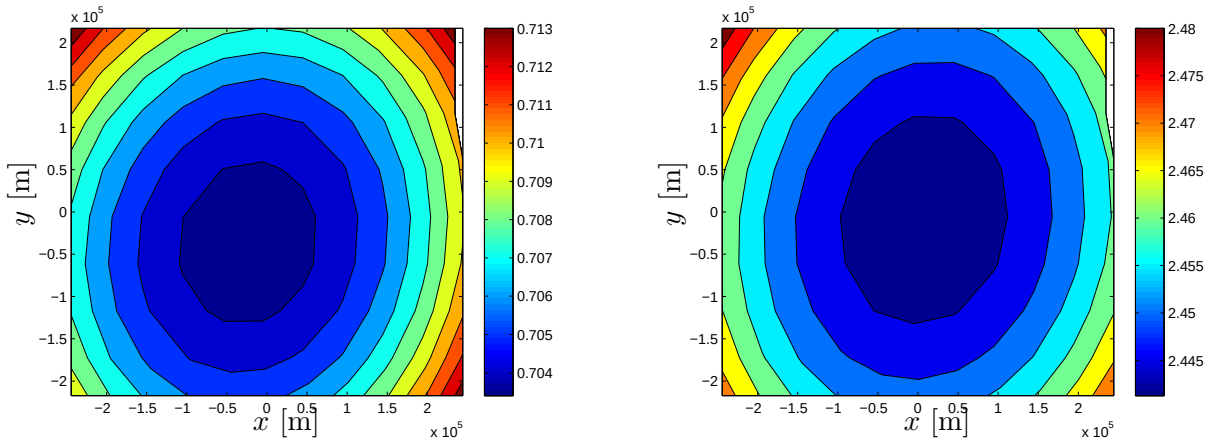


(a) Boundary effect 3rd order in $\Phi$ and 35 observation points in a non rotational wind flow scenario

(b) Boundary effect 5th order in $\Phi$ and 35 observation points in a non rotational wind flow scenario

Figure 20: DOP value in the non rotational wind flow scenario

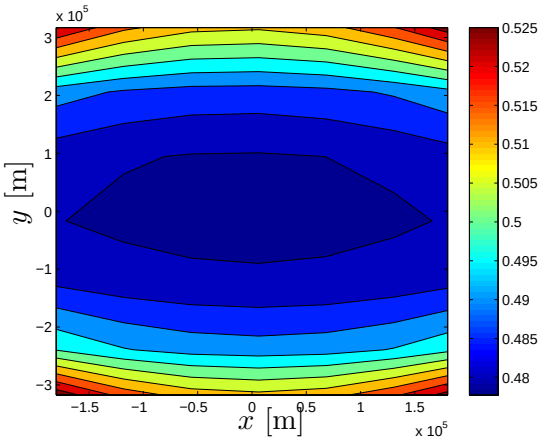


(a) Boundary effect 3rd order in $\Phi$ and 35 observation points in a cyclonic wind flow scenario

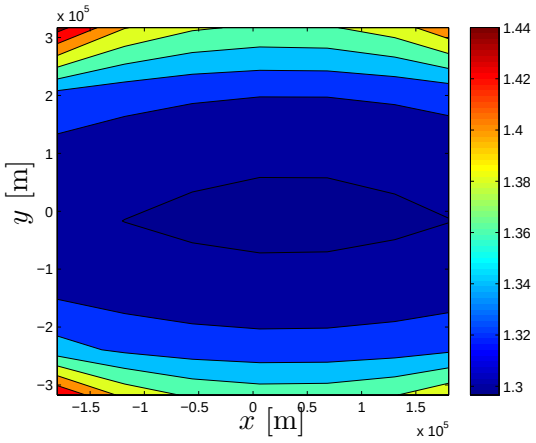


(b) Boundary effect 5th order in $\Phi$ and 35 observation points in a cyclonic wind flow scenario

Figure 21: DOP value in the cyclonic wind flow scenario

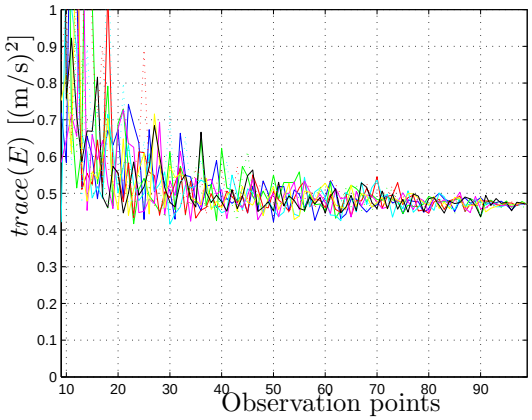


(a) Trace value green area with a 3rd degree functional polynomial approximation

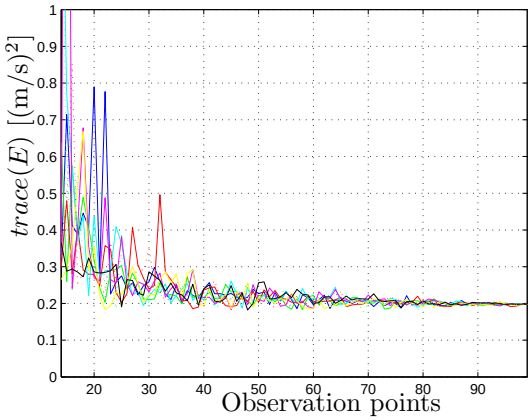


(b) Trace value green area with a 4th degree functional polynomial approximation

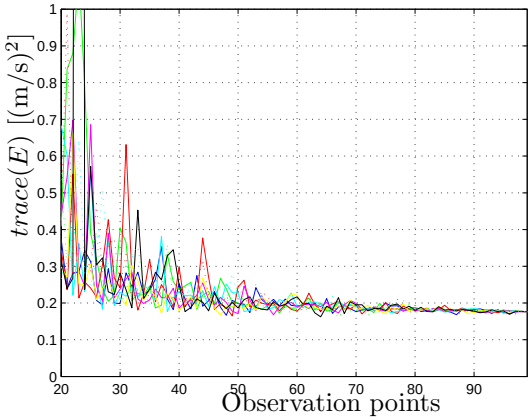


(c) Trace value green area with a 5th degree functional polynomial approximation

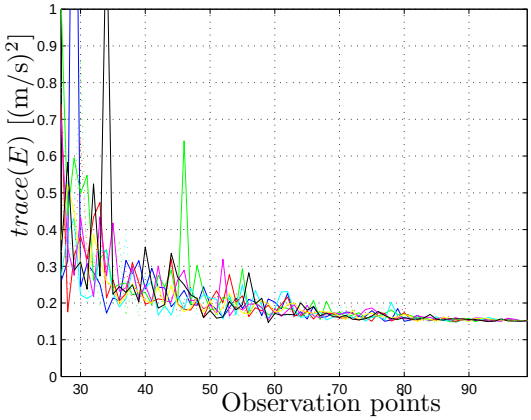


(d) Trace value green area with a 6th degree functional polynomial approximation

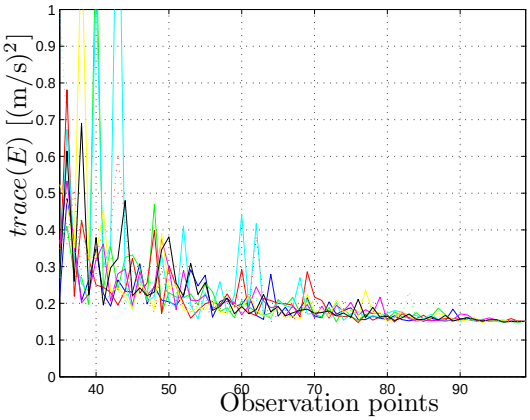


(e) Trace value green area with a 7th degree functional polynomial approximation

Figure 22: Trace variance matrix value representation of the different functional polynomial approximation degrees in the green zone of the non rotational wind flow scenario

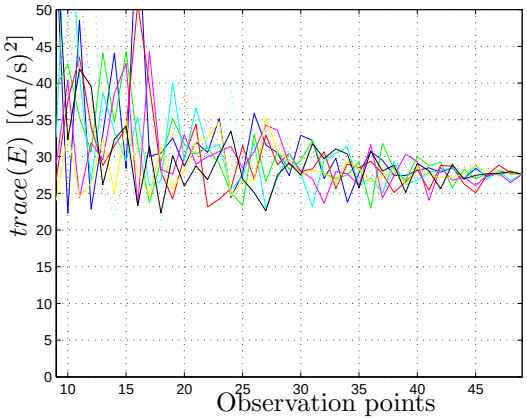


(a) Trace value green area with a 3rd degree functional polynomial approximation

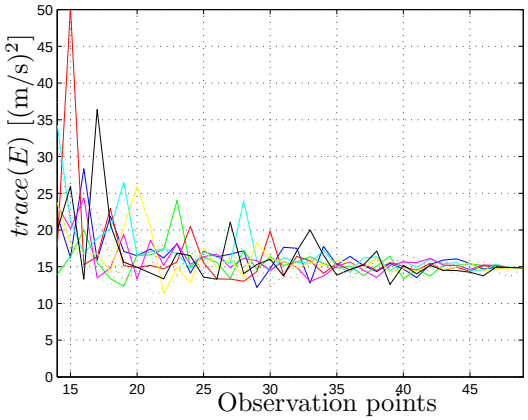


(b) Trace value green area with a 4th degree functional polynomial approximation

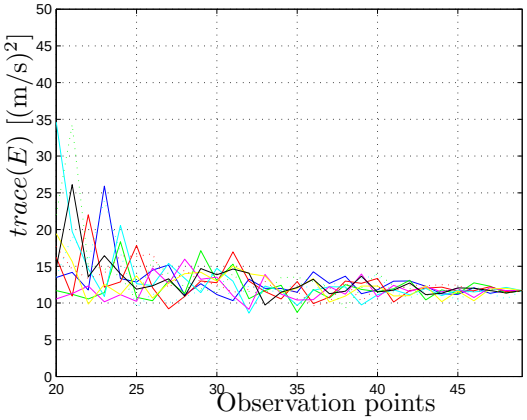


(c) Trace value green area with a 5th degree functional polynomial approximation

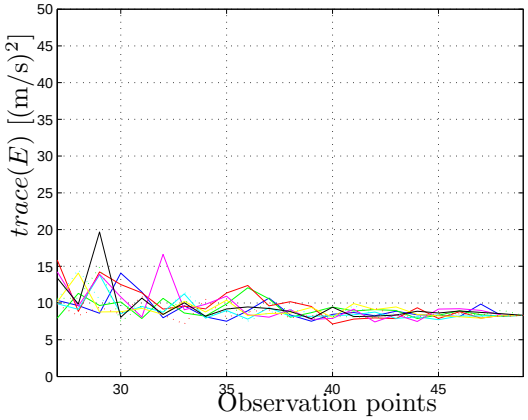


(d) Trace value green area with a 6th degree functional polynomial approximation

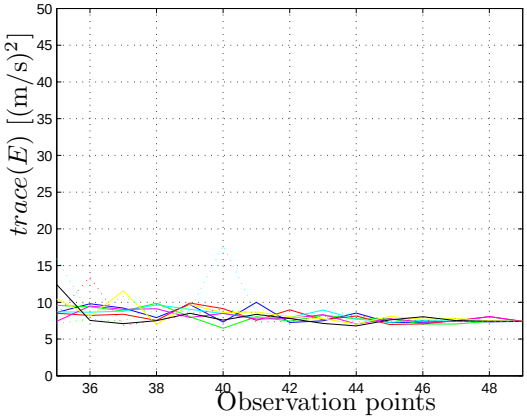


(e) Trace value green area with a 7th degree functional polynomial approximation

Figure 23: Trace variance matrix value representation of the different functional polynomial approximation degrees in the green zone of the cyclonic wind flow scenario

## 2.3 Discussion on the results

This study explored the characteristics of the information supplied by an ADS-B receiver, the report types currently transmitted by aircraft equipped with this technology and particularly its capability for providing information related to the atmosphere behaviour. After analysing the types of available information, the study focused on the estimation of the pressure fields and the assessment of the accuracy of the ISA model.

For these purposes two pressure fields (in the horizontal and the vertical planes) and wind vector analysis were carried out. The horizontal plane analysis showed that the free Galerkin method results provided close to the values obtained from NOAA, with a maximum difference of less than 1 hPa in the pressure estimation and less than 20% of the mean wind speed in the non rotational scenario. This method was only valid for high traffic density areas, where important set of data are available.

The pressure data processing in the vertical plane initially showed error dispersion greater than the expected. It was inferred that this dispersion was not due to the resolution of the data but to the different altitude references used by the on-board avionics.

After the observation was made, a second analysis was performed on the data which led to the discovery that certain aircraft provided data having values close to the geoid undulation. Critical analysis of the data revealed that some aircraft refer their altitude data to the MSL instead of ellipsoidal reference altitude. This ambiguity in the reference surface used by aircraft made it difficult to correctly use the information, especially when the geoid undulation value was close to the deviation value of the data.

The ISA model corrected by the pressure and temperature at sea level obtained from the METAR website was used to determine the estimated pressure at a given altitude. It was observed that when both corrections were applied more accurate estimates were obtained.

The lack of information about the avionics of the aircraft made it difficult establishing the accuracy of the data used for the study. It was possible to weight the information only as

a function of the squitter NIC. Nevertheless, considering the amount of information available and that the RVSM standard was used, the results are sufficiently accurate.

The reference surface ambiguity could easily be removed by using a single bit to specify the type of reference that is employed. There are three free bits still available in the speed squitter, in fields Reserved-A and Reserved-B (message bits 42 and 79-80), that do not carry any type of information.

The results also indicated that accuracy increased when temperature information was also added to the ADS-B message. For example, by multiplexing this value with the difference from the baroaltitude, taking into account that this difference evolves very slowly with time and not demanding any extra bits in the velocity messages.

**List of References**


[1] ICAO, *Manual of the ICAO Standard Atmosphere. ICAO-Doc 7488/3*, Montreal, Canada, 1993.

[2] R. Collinson, *Introduction to Avionics Systems*. Springer, 2002.

[3] J. GuoYing, X. JiYao, S. DongBo, W. Feng, and W. LianZhong, "Observations of the first meteorological rocket of the meridian space weather monitoring project," *Chinese Science Bulletin*, vol. 56, no. 20, p. 2131, 2011. [Online]. Available: http://csb.scichina.com:8080/kxtbe/EN/abstract/article_503801.shtml

[4] S. Chen, Z. Qiu, Y. Zhang, H. Chen, and Y. Wang, "A pure rotational raman lidar using double-grating monochromator for temperature profile detection," *Journal of Quantitative Spectroscopy and Radiative Transfer*, vol. 112, no. 2, pp. 304 – 309, 2011, ¡ce:title¿International Symposium on Atmospheric Light Scattering and Remote Sensing (ISALSaRS09)¡/ce:title¿. [Online]. Available: http://www.sciencedirect.com/science/article/pii/S0022407310002815

[5] R. Wilson, H. Luce, F. Dalaudier, and J. Lefrère, "Turbulence patch identification in potential density or temperature profiles," *Journal of Atmospheric and Oceanic Technology*, vol. 27, no. 6, pp. 977–993, 2013/05/02 2010. [Online]. Available: http://dx.doi.org/10.1175/2010JTECHA1357.1

[6] U. S. N. Oceanic, A. Administration, U. S. C. on Extension to the Standard Atmosphere, U. S. N. Aeronautics, S. Administration, and U. S. A. Force, *U.S. standard atmosphere, 1976*, ser. NOAA–S/T. U.S. Govt. Print. Off., 1976.

[7] D. Garrido-López, R. G. Ledesma, G. Gershzohn, and S. Moore, *Analysis of Aircraft Descent Predictability: Implications for Continuous Four-Dimensional Navigation*. American Institute of Aeronautics and Astronautics, 2013/05/02 2011. [Online]. Available: http://dx.doi.org/10.2514/6.2011-6217

[8] National Aeronautics and Space Administration. "Radiosonde stations information." Last checked: 09 March 2012. 1996. [Online]. Available: ftp://ftp-gte.larc.nasa.gov/pub/PEMTROPICSA/RADIOSONDES/

[9] J. K. Klooster, *4D Trajectory based operations*. GE Aviation Systems, 2009.

[10] S. Puechmorel and D. Delahaye, "4d trajectories: A functional data perspective," in *Digital Avionics Systems Conference, 2007. DASC '07. IEEE/AIAA 26th*, Oct 2007, pp. 1.C.6–1–1.C.6–12.

[11] EUROCONTROL, "EUROCONTROL Medium-Term Forecast: IFR Flight Movements 2011–2017," STATFOR, the EUROCONTROL Statistics and Forecast Service, Tech. Rep. Doc 442, Oct. 2011.

[12] EUROCONTROL, "Automatic dependent surveillance requirements," EUROCONTROL, Tech. Rep. Edition number 0.65, Jan. 2000.

[13] RTCA, *DO 260B standard: minimum operational performance standards for 1090MHz extended squatter ADS-B and Traffic Information Services-Broadcast (TIS-B)*, Washington, USA, 2009.

[14] Federal Aviation Administration Office of NextGen, *NextGen Implementation Plan*, Washington, DC 20591, 2013.

[15] S. J. Undertaking., "Sesar (single european sky atm research)," http://www.sesarju.eu/, 2007.

[16] G. Montero and N. Sanin, "3-d modelling of wind field adjustment using finite differences in a terrain conformal coordinate system," *Journal of Wind Engineering and Industrial Aerodynamics*, vol. 89, no. 5, pp. 471 – 488, 2001. [Online]. Available: http://www.sciencedirect.com/science/article/pii/S0167610500000751

[17] N. Sanín and G. Montero, "A finite difference model for air pollution simulation," *Advances in Engineering Software*, vol. 38, no. 6, pp. 358 – 365, 2007, advances in Numerical Methods for Environmental Engineering. [Online]. Available: http://www.sciencedirect.com/science/article/pii/S0965997806001372

[18] B. E. Schwartz, S. G. Benjamin, S. M. Green, and M. R. Jardin, "Accuracy of ruc-1 and ruc-2 wind and aircraft trajectory forecasts by comparison with acars observations," *Weather and Forecasting*, vol. 15, no. 3, pp. 313–326, 2014/05/05 2000. [Online]. Available: http://dx.doi.org/10.1175/1520-0434(2000)015⟨0313:AORARW⟩2.0.CO;2

[19] H. Chao and Y.-Q. Chen, "Surface wind profile measurement using multiple small unmanned aerial vehicles," in *American Control Conference (ACC), 2010*, June 2010, pp. 4133–4138.

[20] WindStation, "Windstation - a software for the numerical simulation of wind flow over complex topography. easycfd - educational user-friendly ccd (computational fluid dynamics) software," http://www.easycfd.net/wind-station/, 2011 (accessed May 2011).

[21] A. R. Inc and A. E. E. Committee, *Air-ground Character-oriented Protocol Specification*, ser. ARINC specification. Aeronautical Radio, Incorporated, 1993.

[22] A. R. Inc and A. E. E. Committee, *ACARS protocols for avionics end systems*, ser. ARINC specification. Aeronautical Radio, Incorporated, 2009.

[23] A. R. Inc and A. E. E. Committee, *ATS data link applications over ACARS air-ground network*, ser. ARINC specification. Aeronautical Radio, Incorporated, 2001.

[24] A. R. Inc and A. E. E. Committee, *Character-oriented Air Traffic Service (ATS) applications*, ser. ARINC specification. Aeronautical Radio, Incorporated, 2005.

[25] S. G. Benjamin, B. E. Schwartz, and R. E. Cole, "Accuracy of acars wind and temperature observations determined by collocation," *Weather and Forecasting*, vol. 14, no. 6, pp. 1032–1038, 2014/05/05 1999. [Online]. Available: http://dx.doi.org/10.1175/1520-0434(1999)014⟨1032:AOAWAT⟩2.0.CO;2

[26] R. Frehlich and R. Sharman, "Climatology of velocity and temperature turbulence statistics determined from rawinsonde and acars/amdar data," *Journal of Applied Meteorology and Climatology*, vol. 49, no. 6, pp. 1149–1169, 2014/05/06 2010. [Online]. Available: http://dx.doi.org/10.1175/2010JAMC2196.1

[27] R. Cole, S. Green, M. Jardin, B. Schwartz, and S. Benjamin, "Wind prediction accuracy for air traffic management decision support tools," in *3rd USA/Europe Air Traffic Management R&D Seminar, Napoli, Italy*, 2000.

[28] I. C. A. Organization, *Technical Provisions for Mode S Services and Extended Squitter. Doc 9871*, ser. Doc (International Civil Aviation Organization). International Civil Aviation Organization, 2008.

[29] ICAO, *Aeronautical telecommunication*, Montreal, Canada, 2007.

[30] M. Steen, S. Schönhals, J. Polvinen, P. Drake, J.-P. Cariou, and F. Barbaresco, "Candidate technologies survey of airport wind & wake-vortex monitoring sensors," in *9th Innovative Research Workshop & Exhibition, Eurocontrol Experimental Centre Brétigny-sur-Orge, France*, 2010, pp. 7–9.

[31] L. Martin, C. Falk, and J. L. Perez, "Investigation into the use of automatic dependent surveillance-broadcast data for monitoring aircraft altimetry system error," in *AIAA Guidance, Navigation and Control Conference and Exhibit*, 2008, pp. 18–21.

[32] C. Falk, J. Gonzalez, and J. Perez, "Using automatic dependent surveillance-broadcast data for monitoring aircraft altimetry system error," in *Proceedings of the AIAA guidance, navigation, and control conference*, 2010, pp. 2–5.

[33] H. R., "Meteorological information data link study group (metlinksg) ninth meeting," in *Proceedings of the ninth meeting of Meteorological Information Data Link Study Group (METLINKSG)*, 2006.

[34] Y. F.J. and B. Z.M., "Weather data obtaining and dissemination using ads-b," in *Proceedings of the 9th Innovative Research Workshop & Exhibition, Eurocontrol Experimental Centre Brétigny-sur-Orge, France*, 2010.

[35] D. G., "Use of mode s extended squitter in automatic met air-reporting," in *Proceedings of the 5th meeting of Automatic Dependent Surveillance-Broadcast (ADS-B) Study and Implementation Task Force (ADS-B SITF/5), New Delhi, India*, 2006.

[36] U. S. D. M. Agency, *Supplement to Department of Defense World Geodetic System 1984 Technical Report*, ser. Supplement to Department of Defense World Geodetic System 1984 Technical Report. Defense Mapping Agency, 1987, no. v. 2.

[37] MATLAB, *version 7.10.0 (R2010a)*. Natick, Massachusetts: The MathWorks Inc., 2010.

[38] G. K. Vallis, *Atmospheric and oceanic fluid dynamics: fundamentals and large-scale circulation*. Cambridge University Press, 2006.

[39] I. Tullot, *Climatología de España y Portugal*, ser. Acta Salmanticensia. Ediciones Universidad de Salamanca, 2000.

[40] M. Hussain, "Dependence of power law index on surface wind speed," *Energy conversion and management*, vol. 43, no. 4, pp. 467–472, 2002.

[41] T. Belytschko, Y. Y. Lu, and L. Gu, "Element-free galerkin methods," *International Journal for Numerical Methods in Engineering*, vol. 37, no. 2, pp. 229–256, 1994. [Online]. Available: http://dx.doi.org/10.1002/nme.1620370205

[42] B. Nayroles, G. Touzot, and P. Villon, "Generalizing the finite element method: Diffuse approximation and diffuse elements," *Computational Mechanics*, vol. 10, no. 5, pp. 307–318, 1992. [Online]. Available: http://dx.doi.org/10.1007/BF00364252

[43] Z. Zhang, "Numerical development of an improved element-free galerkin method for engineering analysis," Ph.D. dissertation, City University of Hong Kong, Hong Kong, China, 2009.

[44] J. L. Cuesta Molina, "Estudio de dos metodos sin malla para la resolucion de ecuaciones elipticas," Ph.D. dissertation, Technical University of Madrid, Madrid, Spain, 2003.

[45] GRIB.US, "(accessed february 2011)," http://www.GRIB.US/, 2005.

[46] B. Galerkin, *On electrical circuits for the approximate solution of the Laplace equation citation.* Vestnik Inzh, 1915, vol. 19.

[47] X. Pan and H. Yuan, "Computational algorithms and applications of element-free galerkin methods for nonlocal damage models," *Engineering Fracture Mechanics*, vol. 77, no. 14, pp. 2640 – 2653, 2010. [Online]. Available: http://www.sciencedirect.com/science/article/pii/S001379441000353X

[48] L. Zhang, J. Ouyang, X. Wang, and X. Zhang, "Variational multiscale element-free galerkin method for 2d burgers' equation," *Journal of Computational Physics*, vol. 229, no. 19, pp. 7147 – 7161, 2010. [Online]. Available: http://www.sciencedirect.com/science/article/pii/S0021999110003190

[49] M. Pant, I. Singh, and B. Mishra, "Numerical simulation of thermo-elastic fracture problems using element free galerkin method," *International Journal of Mechanical Sciences*, vol. 52, no. 12, pp. 1745 – 1755, 2010. [Online]. Available: http://www.sciencedirect.com/science/article/pii/S0020740310002195

[50] EUROCADE, *ED-102A standard: minimum operational performance standards for 1090MHz extended squatter ADS-B and Traffic Information Services-Broadcast (TIS-B)*, 2009.

# CHAPTER 3

## Aircraft Trajectory Simulator

Over the past few years, the common practice within ATM has been that commercial aircraft must fly by following a set of predefined routes to reach their destinations. Currently, AOCs are requesting for more flexibility to fly according to their preferences, in order to help them achieve their business objectives. AOCs generally wish to keep the cost of a flight as low as possible. These costs depend mainly on: the amount of fuel needed; the actual time of flight and also the over flight charges.

To support these challenges, this chapter presents a trajectory predictor using a 3 DoF aircraft PMM implemented in Matlab® Simulink® software, where environmental and aircraft performance information are introduced as user preference. The model uses aircraft performance variables established in Base of Aircraft Data (BADA) 3.9 [1].

Similar models have been developed by different authors and used for aircraft trajectory optimization problem, for instance, Soler et al. in [2] established an approach to commercial aircraft optimal trajectory for different flight phases and operational procedures from a hybrid optimal control point of view. Similar 3 DoF aircraft PMM for optimisation of aircraft trajectories have been used in [3, 4]. These studies do not only provide improvement in trajectory optimisation but also highlight the sensitivity of the optimization processes to uncertainties of input parameters. Additional references can be found in [5, 6].

The main contribution of this chapter is to present the design and validation of an aircraft Trajectory Simulator (TS) based on the simplest aircraft model capable of serving as trajectory predictor for the planning layers of the TBO concept. To achieve this goal, a direct comparison is performed for aircraft TS performance and FDR for long and short haul flight. The model was adapted to also utilize inputs taken from the FDR so that it could run both the TS and FDR trajectory concurrently to provide a congrous base for the analysis.

Flight data taken from aircraft: A340-600, A319-111 and A321, were used to validate the aircraft TS.

This chapter has been divided into the following sections: Description of the aircraft Trajectory Simulator (TS) is presented in section 3.1, the Flight Data Recorder content used for the validation is analysed in section 3.2, results and explanation of the validation process is presented in section 3.3, and finally the conclusion and recommendations are specified in section 3.4.

### 3.1 Simulator Definition

Two main aircraft dynamics models are in use, namely 6 DoF or a 3 DoF [7]. In the case of 6DoF model, the aircraft is considered as a rigid solid, where it takes into consideration both rotational and translational dynamics. On the other hand, the 3DoF model assumes that the rotational variables and their rates are small. This assumption is supported by the fact that that commercial aircraft trajectories involve small aircraft rotation which are insignificant in long trajectory analysis. The analysis in this chapter is based on commercial aircraft long trajectory analysis making the 3DoF the most appropriate model. For more detailed information about aircraft models the reader is referred to [7, 8]. The 3 DoF dynamic equation for a symmetric flight over a flat surface is expressed as Equation 36.The three first equations describe the kinematic relationship, the following three represent the dynamics and the final one is the weight equation.

$$\begin{aligned}
\dot{x} &= V\cos\gamma\cos\psi + \omega_x \\
\dot{y} &= V\cos\gamma\sin\psi + \omega_y \\
\dot{h} &= V\sin\gamma + \omega_z \\
\dot{V} &= (g/m)\left[Thr\cdot\cos\epsilon - D - m\sin\gamma\right] \\
\dot{\psi} &= (g\sin\phi/mV\cos\gamma)\left[L + Thr\cdot\sin\alpha\right] \\
\dot{\gamma} &= (g/mV)\left[(L + Thr\cdot\sin\epsilon)\cos\phi - m\cos\gamma\right] \\
\dot{m} &= -\eta\cdot Thr
\end{aligned} \tag{36}$$

Where in the Equation 36: $x[m], y[m], h[m]$ are the longitudinal position, lateral position and altitude respectively; $V[m/s]$ is the speed of the aircraft relative to the air; $\gamma[rad], \phi[rad], \psi[rad]$ are the airplane flight path, bank and heading angles respectively; $m[kg]$

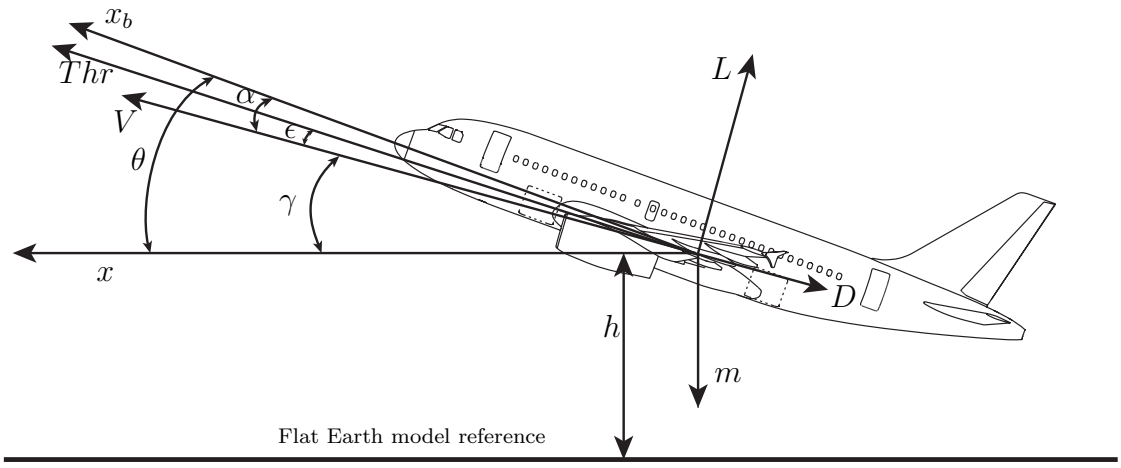


Figure 24: Sketch of the vertical layer aircraft forces and angles. $x_b$ is the longitudinal axis of the plane.

is the weight; $\omega_x[m/s], \omega_y[m/s], \omega_z[m/s]$ are the component of the wind vector along $XYZ$; $\epsilon[rad]$ is the thrust angle of attack; $g[m/s^2]$ is the gravity of value $9.81 m/s^2$; $\alpha[rad]$ is the angle of attack; $L[kg]$ is the aircraft lift force, which is considered equal to $m/\cos\phi$; $D[kg]$ is the aircraft drag force, which is evaluated in each phase of flight with drag polar coefficients from BADA 3.9 [1]; $\eta[1/s]$ and $Thr[kg]$ are the specific fuel consumption and the engine thrust respectively, determined as well using BADA 3.9 information [1].

In this chapter, the following assumptions are made in establishing the 3 DoF PMM aircraft TS:

- flight path angle is small ($\sin\gamma \approx \gamma$ and $\cos\gamma \approx 1$),
- angle of attack ($\alpha$) is negligible, and therefore the flight path angle ($\gamma$) has considered approximately equal to the pitch angle ($\theta$), see Figure 24,
- fixed engines with thrust pointing into the longitudinal aircraft axis direction ($\epsilon = 0$),
- climb acceleration angle ($\dot{\gamma}$) this is negligible,
- ISA applicable, thus altitude ($h$) is considered as pressure altitude,
- vertical wind speed ($\omega_z$) is approximated to zero,

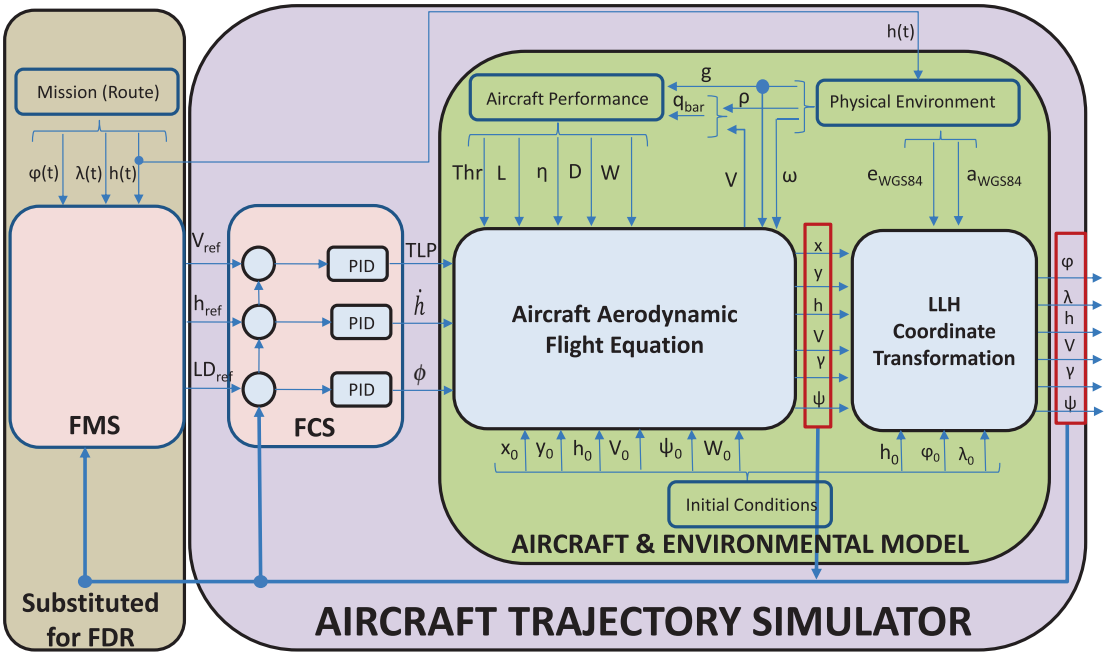


Figure 25: Aircraft Trajectory Simulator scheme

- no wind accelerations are considered.

As a consequence of these assumptions Equation 36 is simplified to the following:

$$\begin{aligned} \dot{x} &= V\cos\psi + \omega_x \\ \dot{y} &= V\sin\psi + \omega_y \\ \dot{h} &= V\gamma \\ \dot{V} &= (g/m)\,[Thr - D - m\gamma] \\ \dot{\psi} &= gL\sin\phi/mV \\ \dot{m} &= -\eta \cdot Thr \end{aligned} \tag{37}$$

A general aircraft simulator is composed of three main subsystem: FMS, FCS, and the block containing aircraft dynamics and environmental model, as is depicted in Figure 25. The aircraft TS described in this dissertation is implemented in MATLAB® SIMULINK® [9].

### 3.1.1 Flight Management System

The FMS provides flight planning and route determination for the aircraft. The inputs of the FMS are the planed trajectories. The system makes use of the aircraft guidance law

information to determine the desired values of True Air Speed (TAS), altitude and lateral deviation. However, the FMS has been substituted for FDR data in this study. The reason for this substitution is to establish a common reference value and condition for the TS and the FDR generated trajectory for the comparison. The output from the substitute FDR system and fed to the FCS as input are explained below:

- **Altitude reference ($h_{ref}$)** is the barometric altitude from the FDR,
- **TAS reference ($V_{ref}$)** is derived from the Mach number and temperature as follows:

$$TAS = M \cdot \sqrt{\kappa \cdot R_g \cdot T} \tag{38}$$

  where: M is the Mach number from the FDR data, $\kappa$ is the ratio specific heats ratio considered 1.4 in this kind of problems, $R_g$ is the ideal gas constant of 287.0531 J/kg/K and T is the air temperature from the FDR data.

- **Lateral deviation ($LD_{ref}$)** is the distance from the aircraft to the desired trajectory.

The FDR data have been introduced in a form of a lookup-table with each data time interval. The planed trajectory taken form the FDR has been estimated as segmented trajectory. Each segment is either a straight line or an arc.

The lateral deviation is calculated by the minimum distance to a straight or curved lines, as is denoted by the Equation 39 and Equation 40, respectively. To this end, the initial and final Waypoint (WP) of each segments is required.

The straight line segment is defined by the initial and final WP. Therefore, the minimum distance is determined as the cross product of the vector director of the straight line segment and the aircraft TS vector referred to the first WP of the segment, as follows:

$$LD_{straight} = \|\vec{a} \times \vec{b}\| \tag{39}$$

Where:

- $\vec{a}$ is the vector director of the current segment,
- $\vec{b}$ is the aircraft TS vector referred to the beginning WP of the current segment.

Meanwhile, the curved lines is calculated as an arc of a circle as explained in [10].

$$LD_{turn} = d_{center} - Radius \tag{40}$$

Where:

- $Radius$ is the Radius value of the circle arc segment,
- $d_{center}$ is the distance from the aircraft TS position to the circle arc centre,

### 3.1.2 Flight Control System

The FCS uses three different interdependent control loops to regulate speed, altitude, and lateral deviations taken from the FDR. The control loops evaluate the FCS input to produce TLP, vertical speed ($\dot{h}$) and bank angle ($\phi$), respectively. The control outputs are saturated to a maximum/minimum to consider that conventional aircraft operate within a range of values, in our case the considered saturation values are: TLP between 0 and 1, $\dot{h}$ between $\pm$3500 [ft/min] and $\phi$ between $\pm 35°$. These variables are the inputs for the aircraft & environmental model block.

To calibrate the FCS behaviour, aircraft in nominal flight and flying in stable conditions have been assumed. Under this assumption the three control loops (speed, altitude and relative position to the planed route) have been considered independently with Proportional-Integral-Derivative (PID) controller [11], as shown in Figure 26.

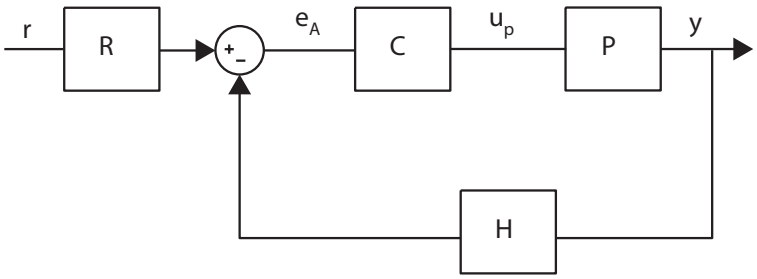


Figure 26: General configuration for feedback control single-loop. Where: $r$ is the command input control, $e_A$ is the control error, $u_p$ is the plant input, $y$ is the output variable, $R$ is the command pre-filter, $H$ is an additional compensator or a measurement transducer, $C$ is the compensator, and $P$ is the plant.

To avoid the maximum possible extent reaching saturated situation, the PID design should provide small error signal amplitude. To this end, an ad-hoc controller tuning has been chosen, in spite of poor transient response.

**Speed control tuning:**

Dynamic equation for the plant (see Equation 37), $\dot{h}$ is considered equal to zero which implies that the flight path angle also zero, and the resulting speed equation becomes:

$$\dot{V} = \frac{g}{m}(Thr - D) \tag{41}$$

Aircraft has been considered as flying in a stable condition at FL350 and the standard performance values used becomes from an A319 BADA 3.9 information:

- $V_r$ is equal to 231.2994 [m/s] (449.61 [kt]),
- $Thr_max$ is equal to 140720 [N] (14345 [kg]),
- $m$ is equal to 48000 [kg],
- $\rho$ is the density of the ISA model at 35000 [ft] which is equal to 0.3796 [kg/m$^3$],
- $S$ is the wing alar surface of 122.6 [m$^2$],
- $D$ is the drag force which is equal to 3,763.1 [kg],

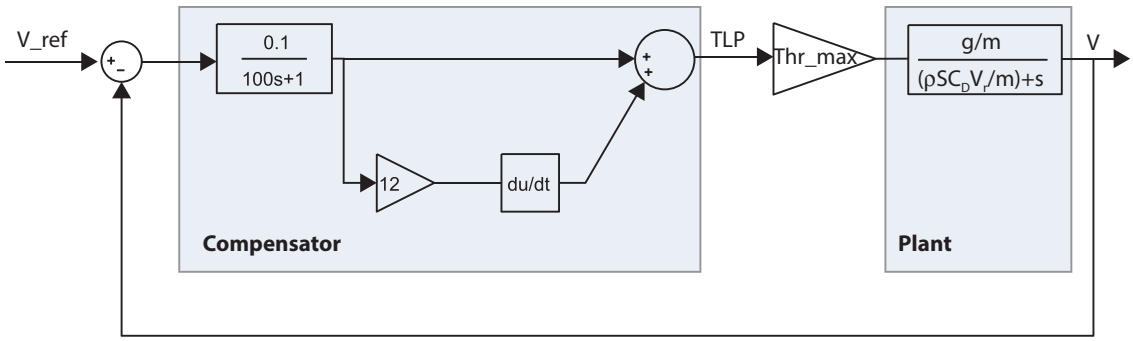


Figure 27: FCS PID speed control tuning. Speed values given in [m/s] and thrust value in [kg].

- $C_D$ is the drag coefficient which is equal to 0.0297 evaluated as $2D/\rho SV_r^2$.

As drag force is speed dependent ($0.5\rho SV^2C_D$), the Equation 41 speed equation has to be differentiate before applying Laplace transform to evaluate the transfer function of the speed controller:

$$\frac{V}{Thr} = \frac{g/m}{(s + (\rho SC_D V_r)/m)} \tag{42}$$

where $s$ denotes the Laplace complex variable.

The compensator is based on a low pass filter and a proportional and derivative control, as shown in Figure 27. It produces the subsequent root locus Figure 28 showing the system stability for all possible gain values. The squared dot in the Figure 28 denotes the selected gain.

The closed-loop transfer function is:

$$\frac{V}{V_c} = \frac{0.063324(s + 0.08333)}{(s^2 + 0.07997s + 0.005344)} \tag{43}$$

The closed-loop of the speed regulator step response and Bode diagram representation are shown Figure 29. The response has a 21.5% of overshoot and a setting time of 99.3 [s], and without stationary error. Bode diagram shows a cut-off frequency of 0.0583 [rad/s] where phase change 90° and amplitude is decreasing in 20 [dB/decade].

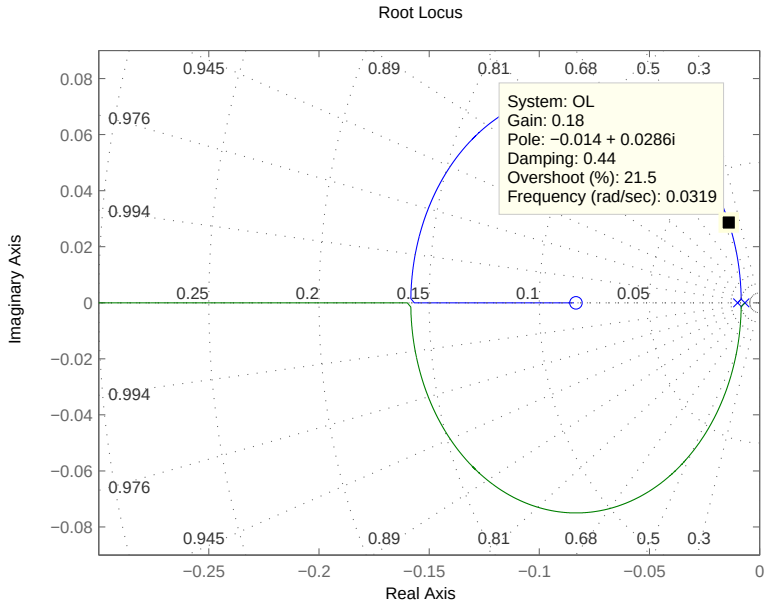


Figure 28: Rlocus speed control

**Altitude control tuning:**

In this control loop the altitude is controlled by the vertical speed, and therefore the plant transfer function is given by:

$$\frac{h}{\dot{h}} = \frac{1}{s} \tag{44}$$

The compensator is based on a proportional and integral control shown in Figure 30. It produces the subsequent root locus given in Figure 31 which indicates the system stability for all possible gain values. The square dot in the Figure 31 denotes the selected gain.

The closed-loop transfer function is:

$$\frac{h}{h_c} = \frac{0.08(s+1)}{(s^2 + 0.08s + 0.08)} \tag{45}$$

The closed-loop of the speed regulator step response and Bode diagram representation are shown Figure 32. The response has a 66.4% of overshoot, a setting time of 91.7 [s], and no stationary error. Bode diagram shows a cut-off frequency of 0.277 [rad/s] where phase change 90° and amplitude is decreasing in 20 [dB/decade].

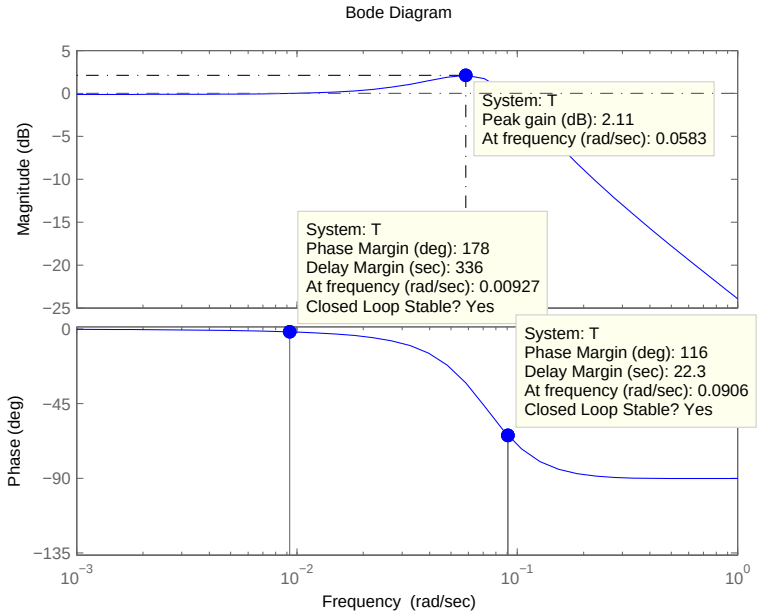


(a) Bode diagram for open loop speed control

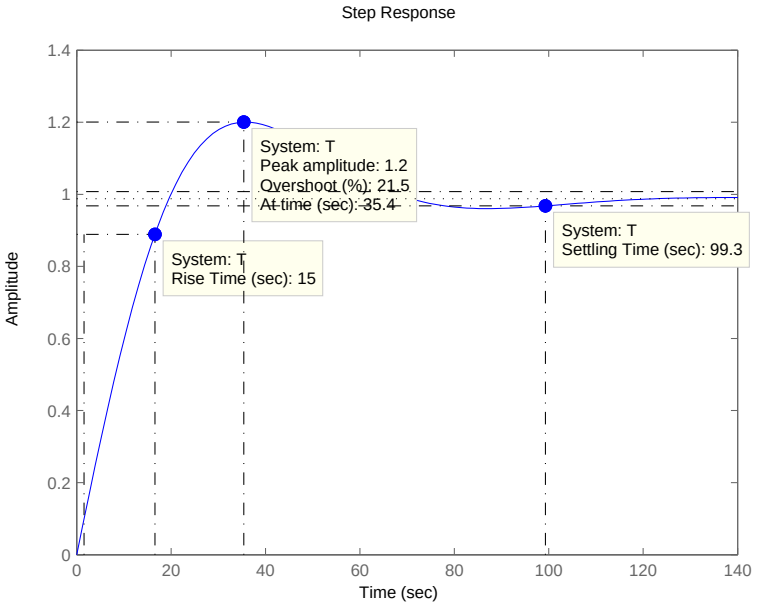


(b) Step response for open loop speed control

Figure 29: FCS Speed control tuning

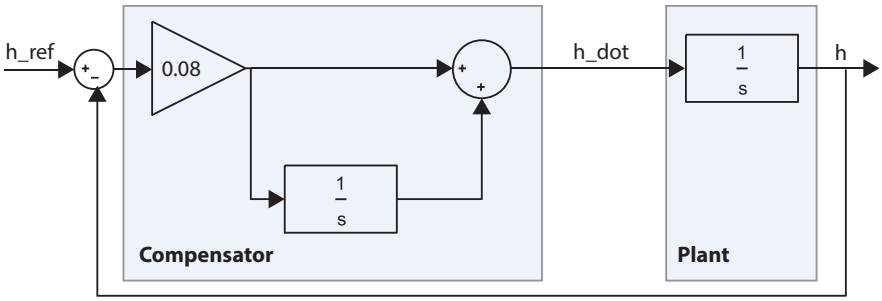


Figure 30: FCS PID altitude control tuning. Altitude values given in [m] and vertical speed value given in [m/s]

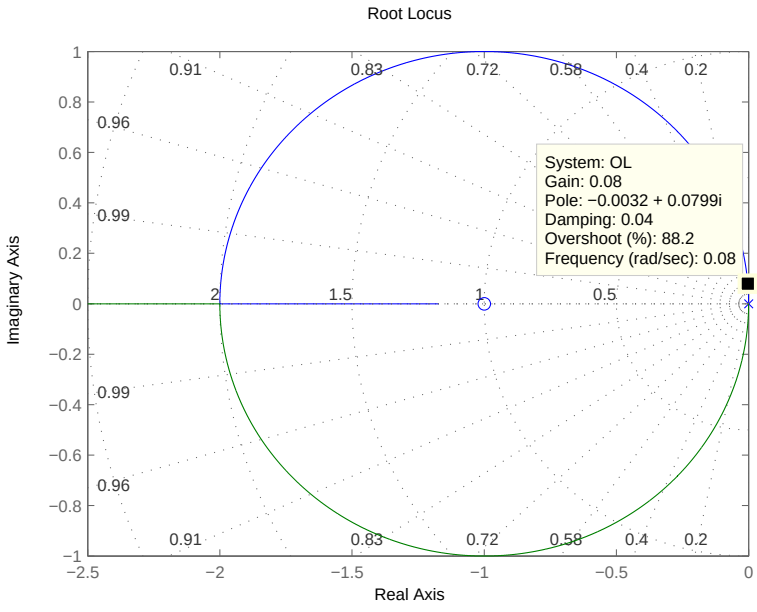


Figure 31: Rlocus altitude control

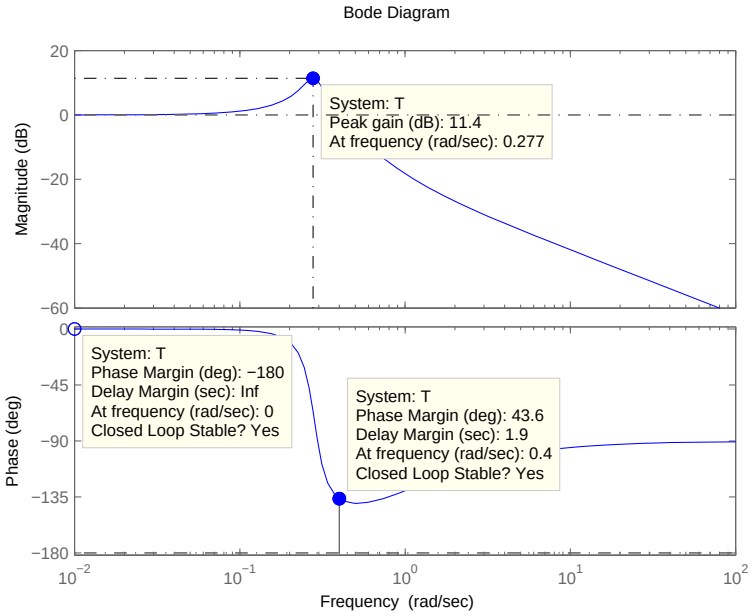


(a) Bode diagram for open loop altitude control

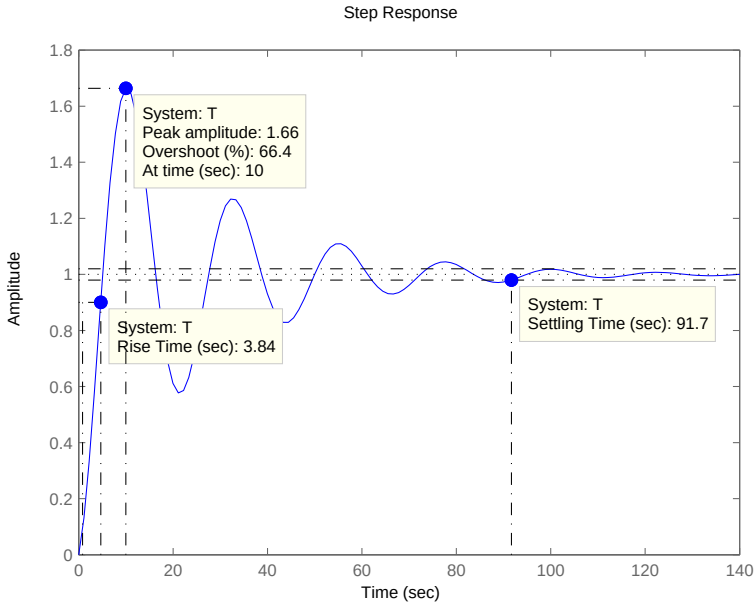


(b) Step response for open loop altitude control

Figure 32: FCS Altitude control tuning

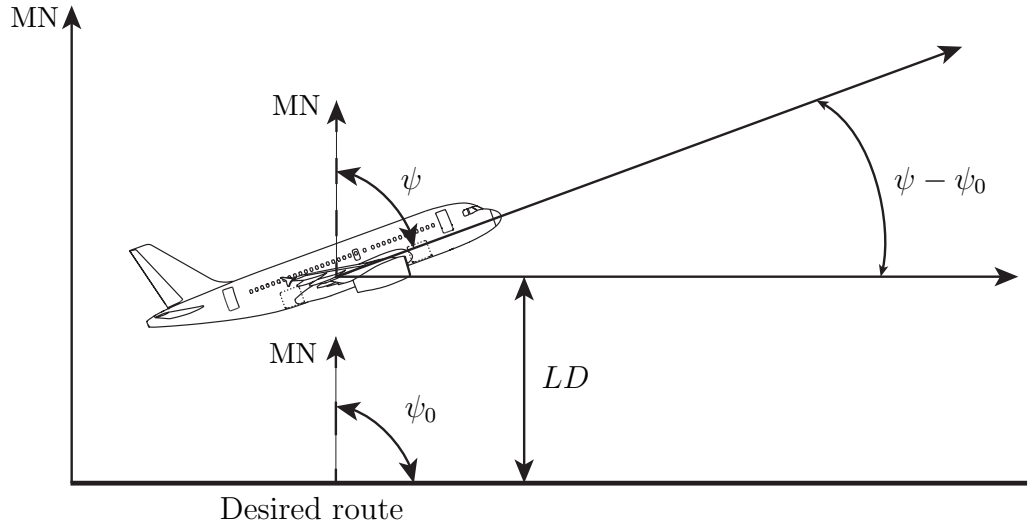


Figure 33: Aircraft movement relative to the desired route. NM is the magnetic north, $\psi$ is the aircraft heading, $\psi_0$ is the desired heading and LD is the lateral deviation form the desired route.

**Lateral deviation control tuning**

The first, second and fifth equations from the aircraft dynamic equation (Equation 37) represent the lateral aircraft dynamic. Considering velocity as a constant value, lateral deviation is only controlled by the bank angle, for instance, a change in flight path angle produces a heading change which modifies the aircraft coordinates $(x, y)$.

If a change of coordinates is made as shown Figure 33 the heading angle is substituted by the difference between the real and the desired heading and the lateral aircraft dynamic equation can be rewritten as:

$$\frac{d}{dt}\begin{bmatrix} X \\ LD \\ \psi - \psi_0 \end{bmatrix} = \begin{bmatrix} V \cdot cos(\psi - \psi_0) \\ V \cdot sin(\psi - \psi_0) \\ g \cdot tan(\phi)/V \end{bmatrix} \tag{46}$$

Assuming the aircraft is located close to the planing route, therefore $\psi - \psi_0$ and $\phi$ can be considered to be a small. Following the conditions of these assumptions lateral navigation equations are:

$$\frac{d}{dt}\begin{bmatrix} LD \\ \psi - \psi_0 \end{bmatrix} = \begin{bmatrix} 0 & V \\ 0 & 0 \end{bmatrix}\begin{bmatrix} LD \\ \psi - \psi_0 \end{bmatrix} + \begin{bmatrix} 0 \\ g/V \end{bmatrix}\begin{bmatrix} \phi - \phi_0 \end{bmatrix} \tag{47}$$

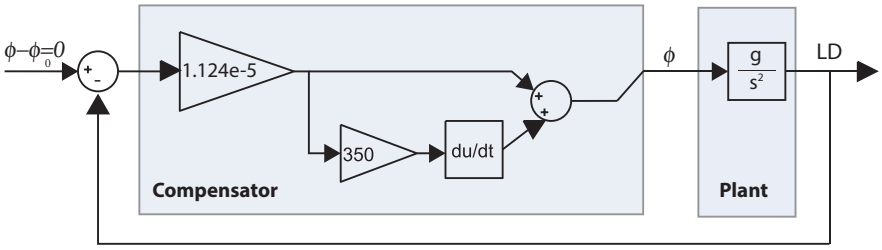


Figure 34: FCS PID Lateral deviation control tuning. Lateral deviation values given in [m], bank angle values given in [rad], and $\phi - \phi_0$ is the difference between the current and the planing bank angles.

The transfer functions after applying the Laplace transform is given by:

$$\frac{LD}{\psi - \psi_0} = \frac{V}{s} \tag{48}$$

$$\frac{\psi - \psi_0}{\phi - \phi_0} = \frac{g}{sV} \tag{49}$$

And therefore the lateral deviation control loop plant tranfer function can be written as:

$$\frac{LD}{\phi - \phi_0} = \frac{g}{s^2} \tag{50}$$

The compensator is based on a proportional and derivative control as shown Figure 34. IIt produces the subsequent root locus given in Figure 35 which indicates the system stability for all possible gain values. The square dot in the Figure 31 denotes the selected gain.

The closed-loop transfer function is:

$$\frac{LD}{\phi - \phi_0} = \frac{0.038598(s + 0.002857)}{(s + 0.03549)(s + 0.003107)} \tag{51}$$

The closed-loop of the speed control step response and Bode diagram representation are shown in Figure 36. The response has an overshoot of 5.49%, a setting time of 505 [s], and no stationary error. Bode diagram shows a cut-off frequency of 0.0148 [rad/s] where amplitude is decreasing in 20 [dB/decade] and phase is tending to 90°.

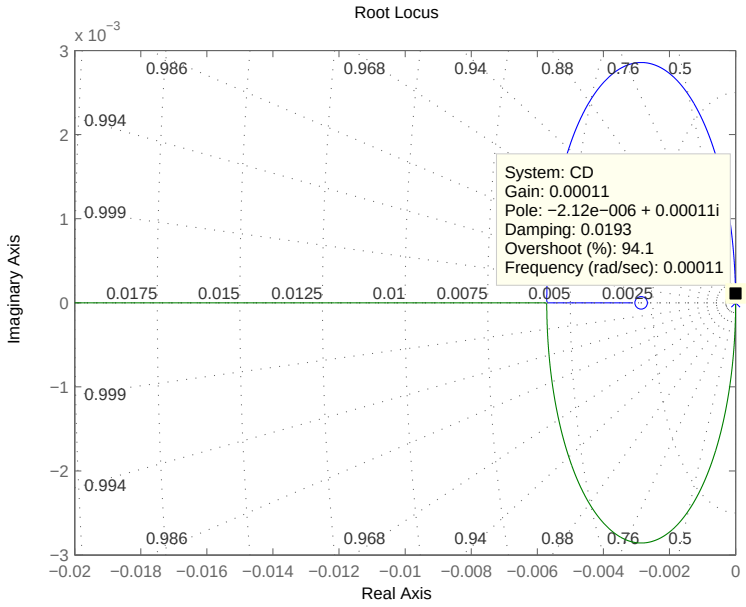


Figure 35: Rlocus lateral deviation control

### 3.1.3 Aircraft and environmental model

The Aircraft and environmental model block is divided into five sub-blocks:

- **Aircraft performance**: Aircraft forces - drag, thrust and weight, are calculated by the aircraft performance sub-block. BADA 3.9 [1] is used to feed the drag polar, thrust and fuel consumption for each phase of flight. A quasi-stationary assumption that makes $\dot{\gamma}$ negligible is made. This implies that the lift is balanced by the opposite component - weight. The weight equation that appears in Equation 37 are integrated making use of the continuous-time integrator SIMULINK block with an ode5 fixed step solver. Furthermore, it was observed that fuel consumption was not only TAS and thrust dependent but also initial aircraft weight, thus some fuel consumption corrections were introduced which is discussed later in subsequent section.

- **Physical environment**: Wind velocity, dynamic pressure and gravity are calculated in the physical environment sub-block. In order to reduce meteorological errors on the predicted track, wind and density have been computed from FDR data. Wind speed

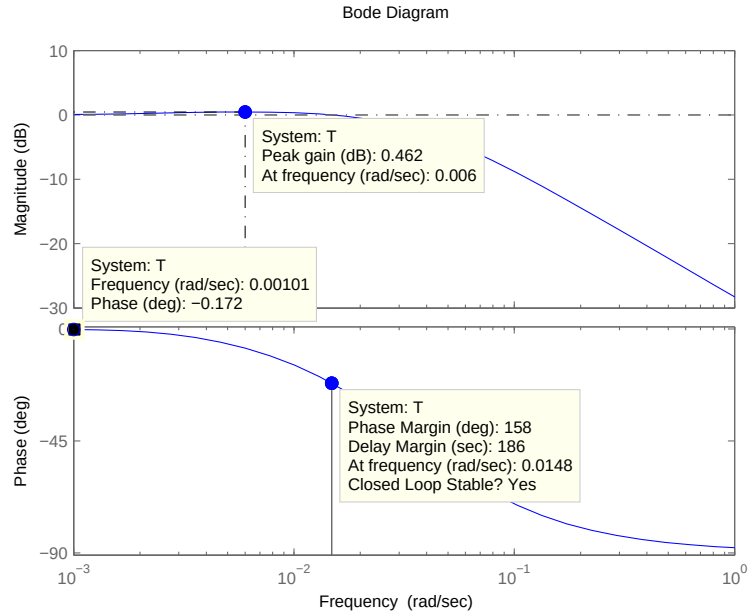


(a) Bode diagram for open loop lateral deviation control

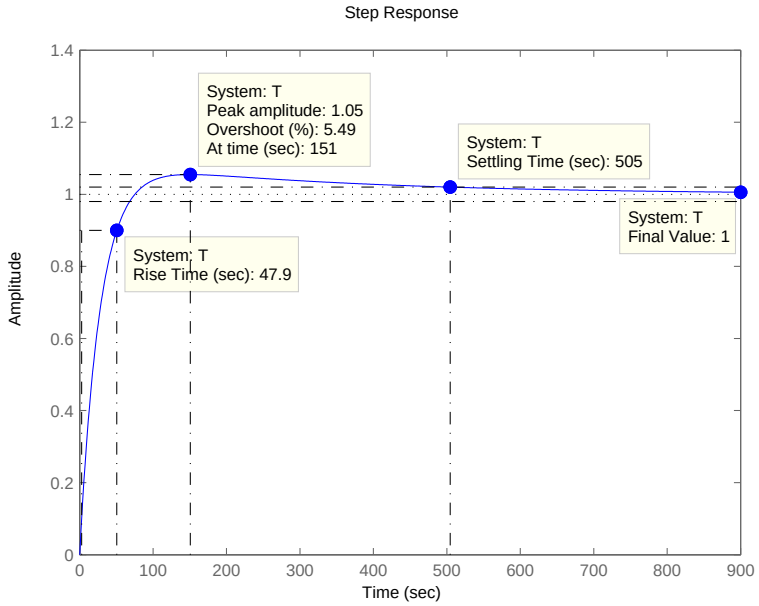


(b) Step response for open loop lateral deviation control

Figure 36: FCS Lateral deviation control tuning

at the aircraft longitudinal axis is estimated by taking the difference between TAS and Ground Speed (GS). The density is obtained by applying Equation 52 using the temperature values taken from FDR and the current pressure from the altitude.

$$\rho = \frac{p}{RT} \tag{52}$$

where: $\rho$ is the atmosphere density, $p$ is the atmosphere pressure, $T$ is the atmosphere temperature, and $R$ is the characteristic gas constant of value $287.0531 J/kg/K$.

- **Initial conditions**: They are the initial state variable values taken form the FDR data in such a way that both the FDR trajectory and the TS can be simulated from the same initial point and under the same initial conditions.

- **Aircraft aerodynamic flight equation**: the kinematics and dynamics equations were used to evaluate the state vector of the system (see Equation 37). The block requires the aircraft performance variables, and aircraft initial conditions. FCS outputs, aircraft performance, and initial conditions are inputs for this sub-block. On the contrary, the output is the aircraft state vector. All the flight equation are integrated making used of the continuous-time integrator SIMULINK block with an ode5 fixed step solver.

- **LLH coordinates transformation**: This block converts from Local Level System (LLS) coordinates to Longitude Latitude and barometric Height (LLH) coordinates [12]. The inputs for this block are: the eccentricity and the major axis of the ellipsoid WGS-84 system; the initial longitude, latitude and barometric altitude; and the dynamic aircraft equations. As the time step used is small, the following transformation is considered and integrated making used of the continuous-time integrator SIMULINK block with an ode5 fixed step solver:

$$\dot{\varphi} = \frac{\dot{x}}{R_n + h} \tag{53}$$

where: $\dot{\varphi}$ is the latitude derivative and $R_n$ the prime vertical radius of curvature denotes by:

$$R_n = \frac{a_{WGS84}}{\sqrt{1 - sin^2\varphi \cdot e^2_{WGS84}}} \tag{54}$$

$$\dot{\lambda} = \frac{\dot{y}}{(R_n + h)cos\varphi} \tag{55}$$

where: $\dot{\lambda}$ is the longitude derivative.

### 3.2 Flight Data Recorder

FDR is an on-board element to store the main aircraft variables. The information collected by the different aircraft sensors and computers are transfered to the FDR through a serial link ARINC 573 or 717 [13, 14]. Data acquisition system output has a binary file sequenced in four frames, each of them is divided into four one second subframes, each subframe is further divided into 64, 128, 256 or 512 words of 12 bits each depending on the used FDR technology [14]. Data acquisition is managed to provide a continuous parameters information. There are four FDR types [10]: type I, IA, II and IIA. The first two record parameters that determine the aircraft speed, flight path, engine power, configuration and operation. However, the II and IIA types record parameters of the first two types in addition to the configuration of lift and drag devices. The mandatory parameters that have to be recorded by the FDR are:

- The flight path and speed: barometric altitude; Indicated Air Speed (IAS) or Calibrated Air Speed (CAS); Air-ground status and each landing gear air-ground sensor; total or outside air temperature; heading; normal, lateral and longitudinal accelerations; time or relative time count .
- The aircraft attitude: pitch and roll attitude.
- The engine power: propulsive thrust/power on each engine, cockpit thrust/power lever position.

- The aircraft configuration: pitch trim surface position.
- The aircraft operation status: Warnings; Primary flight control surface and primary flight control pilot input: pitch axis, roll axis, yaw axis; Marker beacon passage; Each navigation receiver frequency selection; Manual radio transmission keying and Cockpit Voice Recorder (CVR)/FDR synchronization reference.

Other parameters could be registered if the aircraft and the recorder system allow it. The main performance data provided by the FDR used in the present chapter are presented in Table 6, more detailed information about FDR specification data can befound in [10].

Table 6: Main Flight Data Recorders data contained

| Parameter | Recording resolution | Accuracy limits | Maximum sampling and recording interval (seconds) |
|---|---|---|---|
| Aircraft position (Latitude/Longitude) | 0.00005° | 0.00015° | 2 |
| Aircraft weight | 0.01 Tones | - | 4 |
| Phase of flight | - | - | 1 |
| Pressure altitude | 1.5 ft | ±30 m to ±200 m | 1 |
| CAS or IAS | 1 kt | ±5% | 1 |
| GS | 1 kt | ±5 kt | 2 or 1 if is available |
| Mach | 0.001 | - | 1 |
| Pitch | 0.5° | ±2° | 0.25 |
| Roll | 0.5° | ±2° | 0.25 |
| Heading | 0.5° | ±2° | 1 |
| Flaps position | 0.5° | As installed | 2 |
| Landing gear position | Up/Down | As installed | 2 each gear |
| Power on each engine | 0.2% of full range | ±2% | 1 per engine |
| Outside air temperature | 0.3°C | ±2°C | 2 |

### 3.3 Simulator Validation

The validation is based on a comparison between FDR trajectories and those obtained from the aircraft TS. Two different scenarios were studied to get a more complete vision of the aircraft TS behavior. The first scenario includes assessment of a whole flight profile-take-off, climb, cruise, approach, and landing, to identify the error distribution between the FDR variables and those of the aircraft TS. The second scenario was focused on analyzing specific manoeuvres - straight line, arc and changing of flight level. The scenarios were run for three different aircrafts - A340 for long range routes, and A319 and A321 for short range routes. A sequence of the validation process is shown in figure Figure 37.

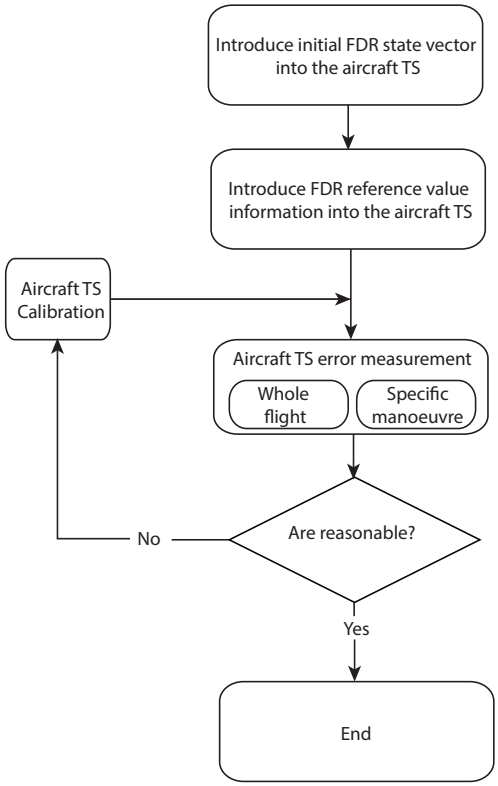


Figure 37: Sequence of the validation process

The error analysis was performed base on mean error ($\mu$) and variance ($\sigma$) of the aircraft TS (pitch, bank angle, fuel consumption, relative final mass, altitude and TAS):

$$\mu = \frac{\sum_{i=1}^{N} \xi_i}{N} \tag{56}$$

where: $N$ is the sample space, and $\xi$ is the variable to be analyzed.

$$\sigma = \sqrt{\frac{\sum_{i=1}^{N} (\xi_i - \mu)^2}{N}} \tag{57}$$

It is important to observe that the error analysis from TAS ($\varepsilon_{TAS}$) and altitude indicate the quality of the FCS. Also, the relative final mass $\left(\frac{\varepsilon_m|_{t_f}}{fuel_{used}}\right)$ is calculated as the percentage ratio between the final mass and the fuel consumption in the scenario.

Table 7: FDRs from the aircraft used in the validation process

| FDR number | Origin | Destination | Duration | Aircraft type / Engine |
|---|---|---|---|---|
| 1628303 | Buenos Aires (EZE-11) | Madrid (MAD-33R) | 11:48:32 | A340-642/RR RB 211 Tren |
| 1628336 | México (MEX-05R) | Madrid (MAD-33R) | 10:50:47 | A340/CFM56-5C4 |
| 1629008 | Buenos Aires (EZE-11) | Madrid (MAD-33R) | 11:35:58 | A340-642/RR RB 211 Tren |
| 1629399 | Santiago de Chile (SCL-17R) | Madrid (MAD-33R) | 12:25:07 | A340-642/RR RB 211 Tren |
| 1631203 | Dakar (DKR-36) | Madrid (MAD-33R) | 03:57:12 | A321-211/CFM56-5B3 |
| 1629858 | Cairo (CAI-05R) | Madrid (MAD-33R) | 05:14:04 | A319-111/CFM56-5B5 |
| 1629874 | Cairo (CAI-23L) | Madrid (MAD-33R) | 05:03:45 | A319-111/CFM56-5B5 |
| 1630306 | Cairo (CAI-05R) | Madrid (MAD-33R) | 04:57:10 | A319-111/CFM56-5B5 |
| 1633358 | Cairo (CAI-05R) | Madrid (MAD-33R) | 04:57:29 | A319-111/CFM56-5B5 |
| 1633400 | Cairo (CAI-23R) | Madrid (MAD-33R) | 05:03:17 | A319-111/CFM56-5B5 |
| 1633476 | Cairo (CAI-05R) | Madrid (MAD-33R) | 05:02:17 | A319-111/CFM56-5B5 |
| 1629850 | Cairo (CAI-23L) | Madrid (MAD-33R) | 05:17:49 | A319-111/CFM56-5B5 |
| 1633449 | Cairo (CAI-05R) | Madrid (MAD-33R) | 05:12:05 | A319-111/CFM56-5B5 |

### 3.3.1 Whole flight analysis

In this part of the analysis the whole trajectories flown by different flights, obtained from FDR, are compared with the TS trajectories. Their different phases of flight have been analyzed separately due to the fact that the aircraft forces and configuration are not the same for each phase of flight.

#### Take-off and climb phase of flight

Take-off is characterized by the maximum weight, and acceleration. Due to this, the assumptions that $\dot{\gamma}$ and $\alpha$ are negligible are not applicable.

Flaps change configuration time for the take-off and climb phase is obtained from the FDR. The applicable thrust, and fuel consumption equations, and $Cd0$ and $k$ specific values are obtained from [1].

The error analysis for the aircraft TS and FDR trajectories are shown in Table 8.

Table 8: Mean ($\mu$) and Variance ($\sigma$) of the Aircraft Trajectory simulator validation variables errors (pitch $\theta$, bank angle $\phi$, fuel consumption $\dot{m}$ and final mass) and the Flight Control System variables errors (altitude and TAS) for take-off phase of flight

| FDR N$^o$ | n | $\varepsilon_\theta$[deg] | | $\varepsilon_\phi$[deg] | | $\varepsilon_{\dot{m}}$[kg/s] | | $\frac{\varepsilon_m\|_{t_f}}{fuel_{used}}$[%] | $\varepsilon_h$[ft] | | $\varepsilon_{TAS}$[kt] | |
|---|---|---|---|---|---|---|---|---|---|---|---|---|
| | | $\mu$ | $\sigma$ | $\mu$ | $\sigma$ | $\mu$ | $\sigma$ | | $\mu$ | $\sigma$ | $\mu$ | $\sigma$ |
| 1628303 | 1411 | -3.856 | 1.225 | 0.052 | 5.670 | 0.182 | 2.243 | 3.959 | 0.002 | 5.267 | 0.337 | 3.011 |
| 1628336 | 1222 | -3.509 | 1.372 | 0.139 | 2.489 | 0.607 | 3.379 | 15.403 | 0.001 | 4.043 | -4.213 | 6.065 |
| 1629008 | 1820 | -3.507 | 1.727 | 0.043 | 4.343 | 0.574 | 2.845 | 11.725 | 0.004 | 3.762 | 1.372 | 1.525 |
| 1629399 | 973 | -4.983 | 1.319 | -0.069 | 8.544 | 0.335 | 2.951 | 6.096 | -0.046 | 3.967 | -14.680 | 7.410 |
| 1631203 | 1942 | -2.295 | 1.591 | 0.011 | 2.415 | 0.109 | 0.391 | 7.035 | -0.003 | 4.000 | 0.494 | 2.506 |
| 1629858 | 1338 | -1.580 | 1.110 | 0.379 | 7.232 | 0.074 | 0.207 | 5.644 | -0.014 | 4.241 | -11.492 | 8.645 |
| 1629874 | 1043 | -2.556 | 1.950 | 0.353 | 5.436 | 0.066 | 0.478 | 4.680 | -0.031 | 7.268 | -4.061 | 10.011 |
| 1630306 | 1264 | -2.167 | 1.208 | 0.450 | 5.139 | 0.069 | 0.237 | 5.443 | 0.011 | 5.315 | -6.723 | 4.710 |
| 1633358 | 1303 | -2.025 | 1.443 | -0.318 | 4.397 | 0.100 | 0.241 | 7.751 | -0.013 | 6.435 | -12.344 | 9.316 |
| 1633400 | 1180 | -1.995 | 1.384 | 0.334 | 6.957 | 0.063 | 0.237 | 4.941 | -0.006 | 6.284 | -9.358 | 3.583 |
| 1633476 | 1297 | -2.603 | 1.546 | 0.251 | 2.022 | 0.100 | 0.180 | 7.785 | 0.007 | 6.113 | -7.243 | 5.196 |
| 1629850 | 1284 | -2.525 | 1.157 | 0.166 | 6.376 | 0.085 | 0.168 | 6.673 | -0.015 | 4.355 | -5.852 | 5.897 |
| 1633449 | 826 | -1.923 | 1.380 | 0.552 | 6.354 | 0.014 | 0.604 | 1.089 | -0.011 | 5.427 | -8.058 | 4.055 |
| A346 FDRs | 5426 | -3.863 | 1.556 | 0.047 | 5.400 | 0.437 | 2.861 | 9.296 | -0.006 | 4.296 | -3.033 | 7.441 |
| A319 FDRs | 9535 | -2.173 | 1.446 | 0.254 | 5.681 | 0.074 | 0.306 | 5.501 | -0.008 | 5.723 | -8.264 | 7.392 |
| All FDRs | 16903 | -2.729 | 1.690 | 0.159 | 5.314 | 0.195 | 1.651 | 6.786 | -0.007 | 5.122 | -5.579 | 7.727 |

The errors in the kinematic variables were close to zero, the maximum error is note in 1629399 FDR which gave a mean TAS error of 14 kt. This was because a non-typical trajectory profile was flown - high sharp turn was performed. Considering the performance of different aircraft, the A319 exhibited large errors especially in TAS. Altitude error were however negligible and relatively the same for all the aircraft types.

Two observations were made on the variables used for implementing the aircraft TS. The first was that even though the fuel flow ($\dot{m}$) using BADA 3.9 [1] exhibited good performance there was a need to apply a correction. This aspect will further be discussed in subsection 3.3.3. The second observation was that there was significant pitch error. This large error was due to our assumption that alpha was negligible and therefore $\alpha$ was considered equal to zero.

Figure 38 and 39 show the 1628303 FDR variables for the take-off and climb phase of flight.

**Cruise phase of flight**

The cruise phase is characterize by a stabilized aircraft, flying at a close to constant mach value almost all the time, and simultaneously maintaining vertical speed of zero. Ac-

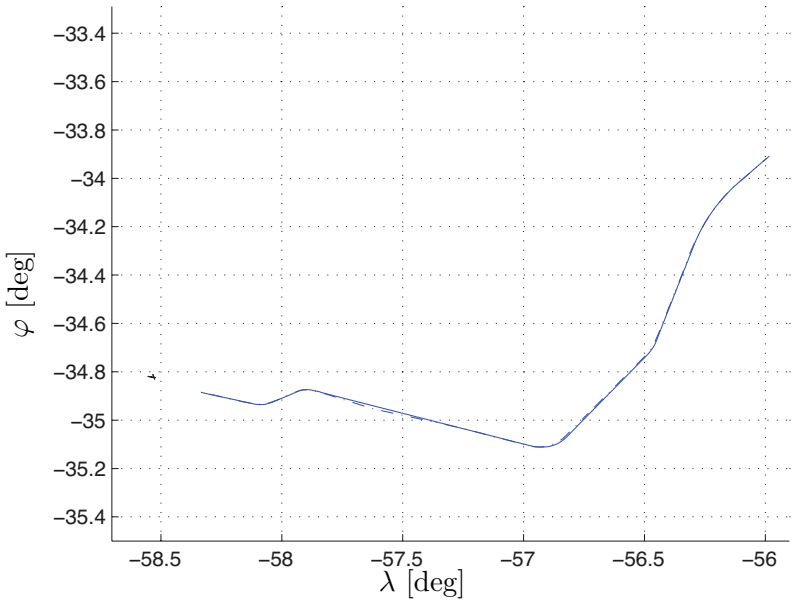


(a) Horizontal profile. FDR values are denoted by doted line and aircraft TS values by the solid line.

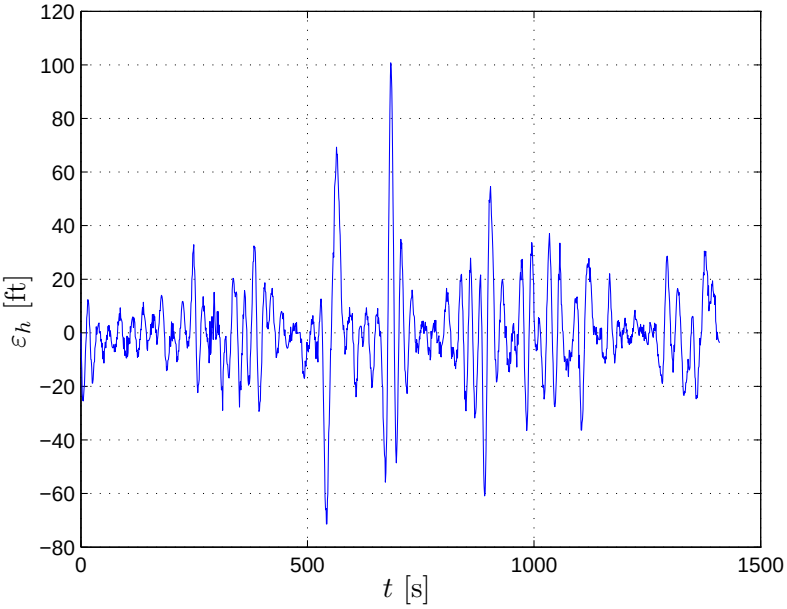


(b) Aircraft TS altitude - FDR altitude vs time

Figure 38: Take-off and climb phase of flight representation for 1628303 FDR.

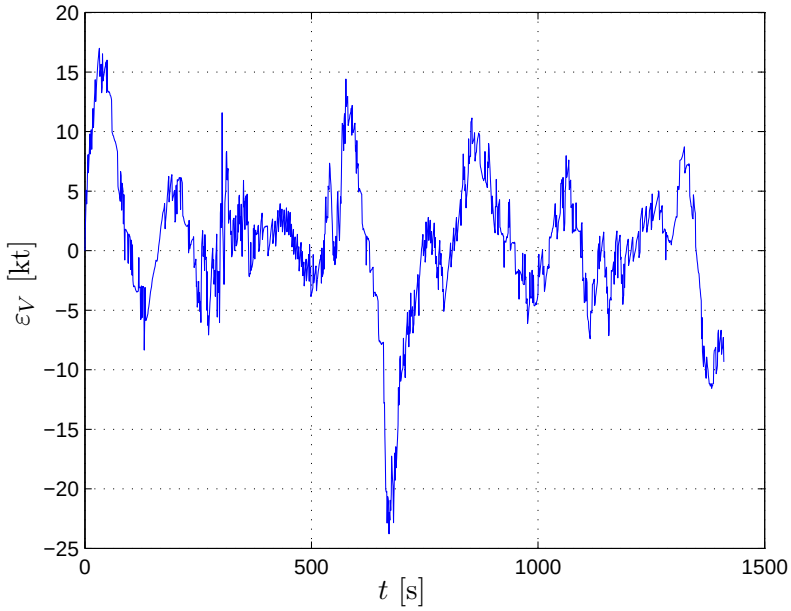


(a) Aircraft TS TAS - FDR TAS vs time

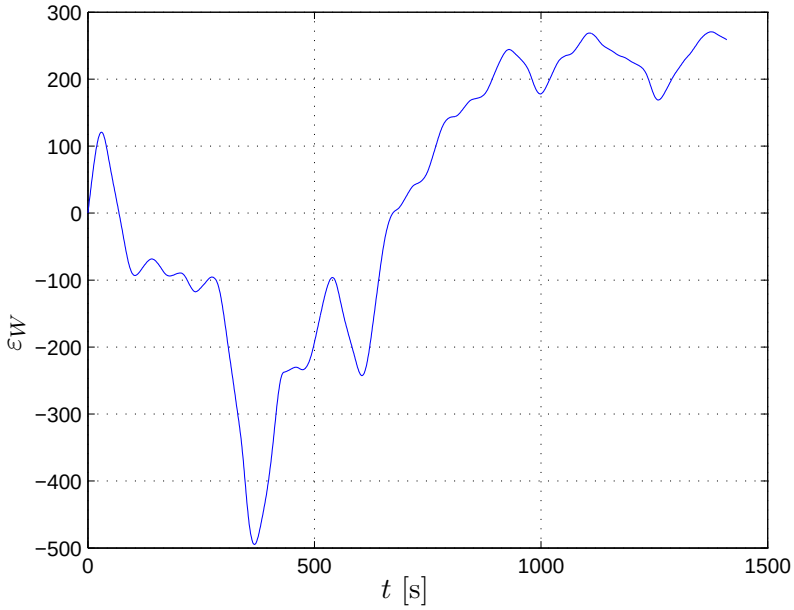


(b) Aircraft TS weight - FDR weight vs time

Figure 39: Take-off and climb phase of flight representation for 1628303 FDR

Table 9: Mean ($\mu$) and Variance ($\sigma$) of the Aircraft Trajectory simulator validation variables errors (pitch $\theta$, bank angle $\phi$, fuel consumption $\dot{m}$ and final mass) and the Flight Control System variables errors (altitude and TAS) for cruise phase of flight

| FDR N$^o$ | n | $\varepsilon_\theta$[deg] | | $\varepsilon_\phi$[deg] | | $\varepsilon_{\dot{m}}$[kg/s] | | $\frac{\varepsilon_m\|_{t_f}}{fuel_{used}}$[%] | $\varepsilon_h$[ft] | | $\varepsilon_{TAS}$[kt] | |
|---|---|---|---|---|---|---|---|---|---|---|---|---|
| | | $\mu$ | $\sigma$ | $\mu$ | $\sigma$ | $\mu$ | $\sigma$ | | $\mu$ | $\sigma$ | $\mu$ | $\sigma$ |
| 1628303 | 37960 | -2.341 | 0.290 | 0.137 | 2.902 | 0.098 | 0.871 | 4.155 | 0.003 | 1.185 | 0.097 | 1.167 |
| 1628336 | 34987 | -2.287 | 0.249 | 0.224 | 2.145 | 0.030 | 0.783 | 1.844 | 0.003 | 0.972 | -0.228 | 1.428 |
| 1629008 | 37032 | -2.293 | 0.290 | 0.202 | 2.949 | 0.090 | 0.822 | 3.824 | 0.004 | 1.262 | 0.047 | 1.142 |
| 1629399 | 37960 | -2.874 | 0.246 | 0.166 | 3.146 | 0.104 | 1.149 | 4.043 | 0.004 | 1.174 | 0.813 | 1.242 |
| 1631203 | 9835 | -2.174 | 0.180 | 0.018 | 3.359 | -0.008 | 0.100 | -0.927 | 0.003 | 0.973 | -0.380 | 2.380 |
| 1629858 | 14762 | -1.985 | 0.293 | 0.218 | 1.786 | 0.061 | 0.094 | 9.283 | 0.005 | 1.388 | 0.028 | 1.244 |
| 1629874 | 14476 | -1.906 | 0.327 | 0.262 | 1.887 | 0.075 | 0.097 | 11.146 | 0.004 | 2.457 | 0.013 | 1.737 |
| 1630306 | 13802 | -1.758 | 0.379 | 0.370 | 2.163 | 0.053 | 0.098 | 7.989 | 0.006 | 1.681 | 0.174 | 1.332 |
| 1633358 | 14004 | -1.902 | 0.164 | -0.352 | 1.807 | 0.040 | 0.081 | 6.466 | 0.003 | 0.940 | 0.138 | 0.824 |
| 1633400 | 14317 | -1.967 | 0.203 | 0.314 | 2.109 | 0.054 | 0.093 | 8.447 | 0.003 | 1.266 | 0.115 | 1.270 |
| 1633476 | 14037 | -1.991 | 0.245 | 0.184 | 1.828 | 0.059 | 0.089 | 9.100 | 0.003 | 1.087 | -0.002 | 0.916 |
| 1629850 | 15415 | -1.984 | 0.226 | -0.014 | 2.058 | 0.084 | 0.095 | 11.985 | 0.004 | 1.341 | -0.242 | 1.019 |
| 1633449 | 14872 | -1.413 | 0.493 | 0.138 | 1.778 | 0.038 | 0.097 | 5.483 | 0.003 | 14.170 | 0.014 | 3.610 |
| A346 FDRs | 147939 | -2.453 | 0.367 | 0.181 | 2.822 | 0.082 | 0.921 | 3.467 | 0.004 | 1.156 | 0.191 | 1.305 |
| A319 FDRs | 115685 | -1.863 | 0.361 | 0.139 | 1.944 | 0.058 | 0.094 | 8.737 | 0.004 | 5.276 | 0.026 | 1.732 |
| All FDRs | 273459 | -2.193 | 0.460 | 0.158 | 2.513 | 0.069 | 0.681 | 6.372 | 0.004 | 3.540 | 0.101 | 1.552 |

celerations is therefore negligible except within short periods of time when the aircraft is changes its speed and/or flight level. During this phase the flight path angle ($\gamma$) is equal to zero due to the fact that the aircraft is flying at a constant altitude, and so the pitch angle ($\theta$) is equal to the angle of attack ($\alpha$). Although, the angle of attack does not remain constant during the whole flight, the mean of the difference between the aircraft TS and the FDR pitches at the cruise phase for A340-600, A319-111 or A321 shows a small error of 2.45, 1.86 and 1.98 degrees respectively.

As was mentioned earlier, aircraft nominal fuel flow showed similar large errors at the cruise phase of the flight as in the departure phase. A correction is proposed in later section to correct this error.

Characteristics of the performance variables for 1628303 FDR cruise phase of flight are shown in Figure 40 and 41.

### Approach and landing phase of flight

Finally, in the approach and landing phase of flight, the aircraft engines remains close to idle thrust. Figure 42 and 43 show the representation of 1628303 FDR approach and landing phase of the flight. During this phase of flight the aircraft has to land reaching the

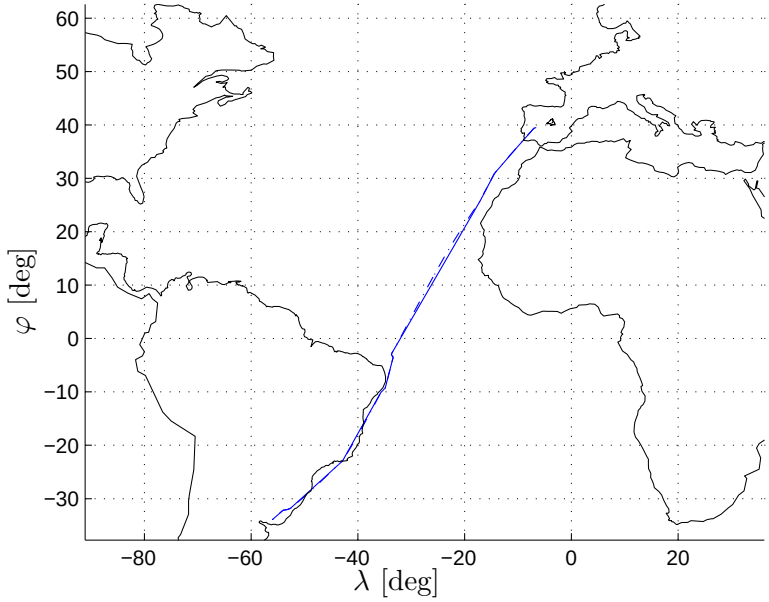


(a) Horizontal profile. FDR values are denoted by doted line and aircraft TS values by the solid line.

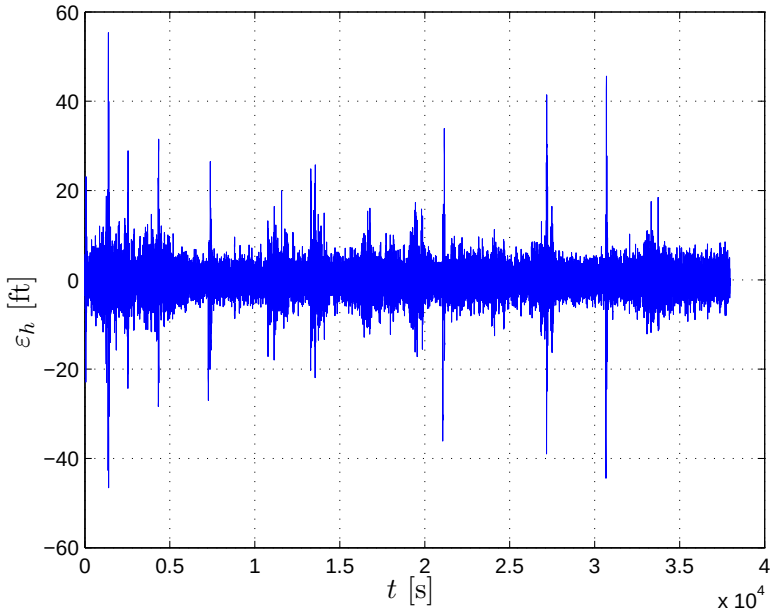


(b) Aircraft TS altitude - FDR altitude vs time

Figure 40: Cruise phase of flight representation for 1628303 FDR

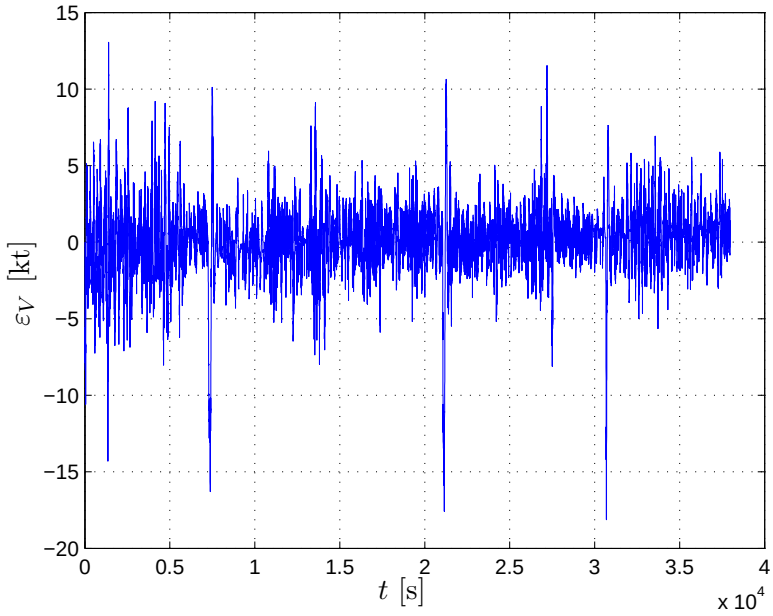


(a) Horizontal profile

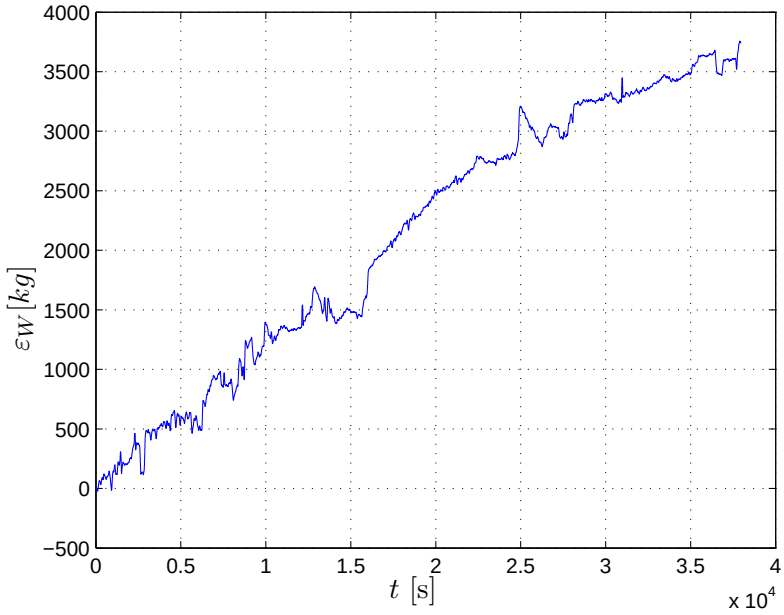


(b) Aircraft TS weight - FDR weight vs time

Figure 41: Cruise phase of flight representation for 1628303 FDR

Table 10: Mean ($\mu$) and Variance ($\sigma$) of the Aircraft Trajectory simulator validation variables errors (pitch $\theta$, bank angle $\phi$, fuel consumption $\dot{m}$ and final mass) and the Flight Control System variables errors (altitude and TAS) for landing phase of flight

| FDR N$^o$ | n | $\varepsilon_\theta$[deg] | | $\varepsilon_\phi$[deg] | | $\varepsilon_{\dot{m}}$[kg/s] | | $\frac{\varepsilon_m\|_{t_f}}{fuel_{used}}$[%] | $\varepsilon_h$[ft] | | $\varepsilon_{TAS}$[kt] | |
|---|---|---|---|---|---|---|---|---|---|---|---|---|
| | | $\mu$ | $\sigma$ | $\mu$ | $\sigma$ | $\mu$ | $\sigma$ | | $\mu$ | $\sigma$ | $\mu$ | $\sigma$ |
| 1628303 | 1661 | -3.900 | 2.276 | 0.250 | 6.520 | 0.152 | 0.608 | 17.264 | 0.066 | 5.376 | 3.934 | 3.659 |
| 1628336 | 1401 | -2.967 | 1.637 | 0.054 | 8.829 | -0.055 | 0.312 | -11.795 | 0.008 | 1.519 | 7.012 | 7.753 |
| 1629008 | 1733 | -2.432 | 1.891 | 0.220 | 6.006 | 0.182 | 0.997 | 19.862 | 0.020 | 7.082 | 4.243 | 5.385 |
| 1629399 | 1919 | -2.641 | 1.079 | 0.285 | 4.767 | 0.157 | 0.923 | 13.598 | 0.029 | 3.919 | 3.386 | 1.811 |
| 1631203 | 1275 | -2.301 | 1.297 | -0.114 | 4.500 | -0.065 | 0.186 | -24.997 | 0.052 | 5.566 | 2.375 | 5.477 |
| 1629858 | 1516 | -2.179 | 0.987 | -0.118 | 5.417 | 0.043 | 0.165 | 11.958 | 0.029 | 3.970 | 3.025 | 4.107 |
| 1629874 | 1184 | -2.219 | 1.691 | -0.118 | 4.780 | 0.067 | 0.155 | 20.184 | 0.014 | 7.244 | 2.613 | 7.194 |
| 1630306 | 1341 | -2.011 | 1.256 | 0.108 | 2.803 | 0.038 | 0.156 | 12.637 | 0.040 | 3.853 | 3.128 | 1.396 |
| 1633358 | 1328 | -2.097 | 1.550 | -0.824 | 2.718 | 0.043 | 0.114 | 14.181 | 0.022 | 5.132 | 2.852 | 2.810 |
| 1633400 | 1204 | -2.188 | 1.406 | 0.051 | 3.765 | 0.011 | 0.229 | 5.096 | 0.050 | 3.943 | 2.710 | 4.133 |
| 1633476 | 1475 | -1.955 | 1.482 | -0.116 | 3.868 | 0.024 | 0.126 | 7.284 | 0.023 | 4.164 | 2.655 | 2.626 |
| 1629850 | 1015 | -2.176 | 1.441 | -0.354 | 5.606 | 0.083 | 0.166 | 25.250 | 0.045 | 4.084 | 5.278 | 5.921 |
| 1633449 | 1680 | -1.633 | 0.899 | -0.067 | 4.370 | 0.047 | 0.149 | 12.131 | 0.029 | 2.925 | 2.431 | 2.392 |
| A346 FDRs | 6714 | -2.966 | 1.848 | 0.211 | 6.525 | 0.118 | 0.787 | 9.732 | 0.032 | 4.996 | 4.500 | 5.102 |
| A319 FDRs | 10743 | -2.037 | 1.352 | -0.172 | 4.268 | 0.043 | 0.160 | 13.590 | 0.031 | 4.488 | 3.005 | 4.117 |
| All FDRs | 18732 | -2.388 | 1.606 | -0.031 | 5.207 | 0.063 | 0.491 | 9.435 | 0.032 | 4.754 | 3.498 | 4.655 |

runway, and therefore the flight has to lose altitude and speed. Aircraft flaps configuration is modified as in the case of departure to avoid the stall situation.

The errors in the aircraft TS variables are insignificant in terms of both mean altitude error and mean TAS error (around 4 kt). Only aircraft exhibiting a high descent or deceleration rates produced mean mass error above 20% of the fuel used in this phase of flight. For instance, FDR 1631203 exhibits a deviation of -25% and FDR 1629850 25.25%, as shown in Table 10. With respect to the performance of the different types of aircrafts, the final mass is better modeled in the A340-600 which produced a mean error of 9% than in the A319-111 which gave a mean error of 13%. The bank angle ($\phi$) is well approximated, but the mean pitch angle error is large due to the assumption in the TS model that angle of attack is equal to zero.

### 3.3.2 Specific manoeuvres analysis

The purpose of this analysis is to determine the aircraft TS behavior when following specific manoeuvres, where the time of simulation is small and the aircraft configuration and performance remains constant. The cruise phase of flight has been selected for this purpose considering that the TS model hypothesis, cited in section 3.1, are better satisfied in this

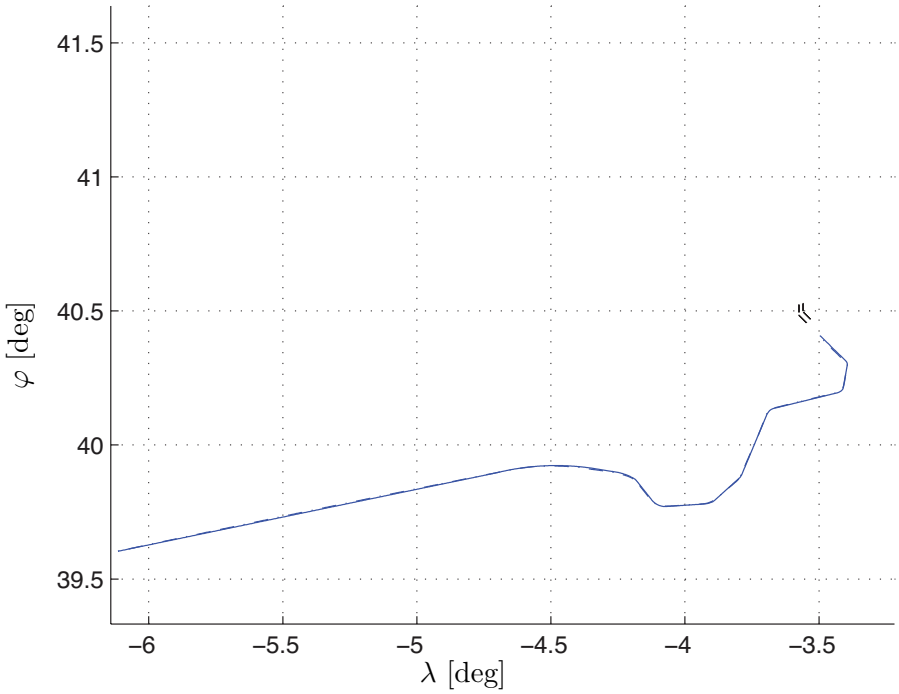


(a) Horizontal profile. FDR values are denoted by doted line and aircraft TS values by the solid line.

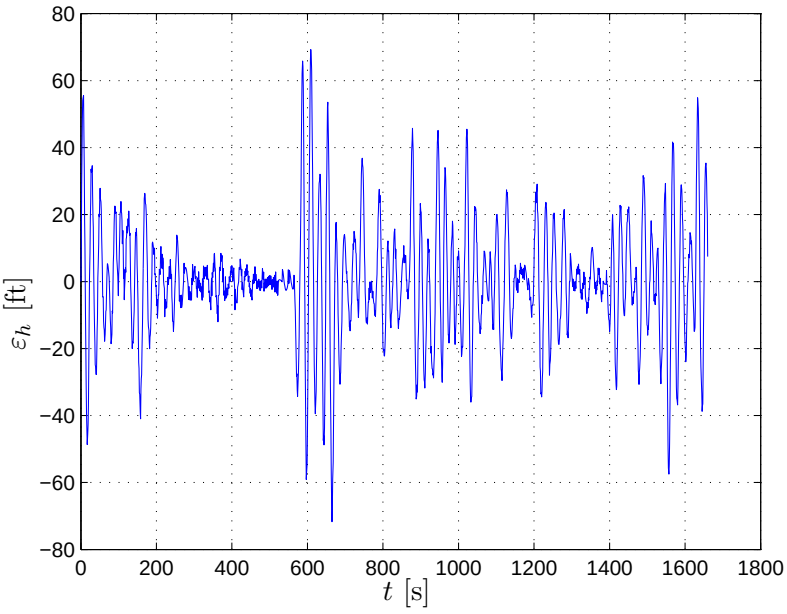


(b) Aircraft TS altitude - FDR altitude vs time

Figure 42: Approach and landing phase of flight representation for 1628303 FDR

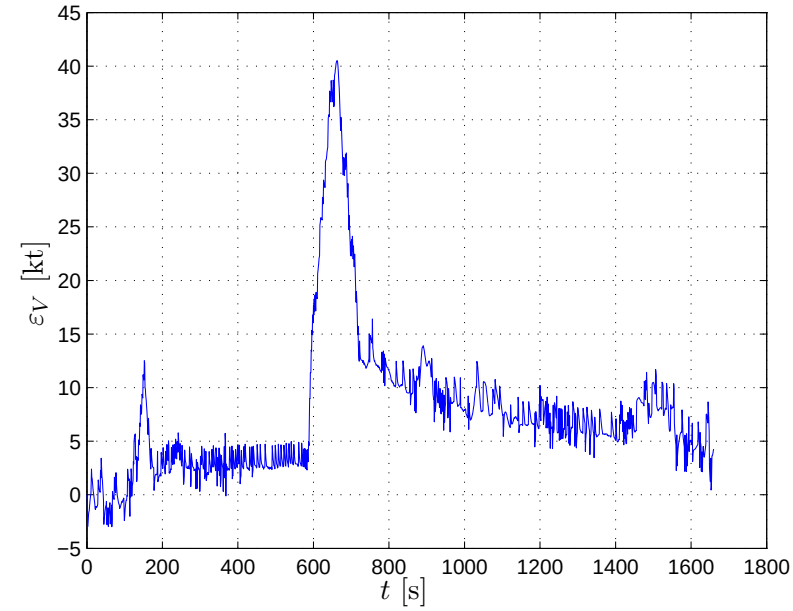


(a) Aircraft TS TAS - FDR TAS vs time

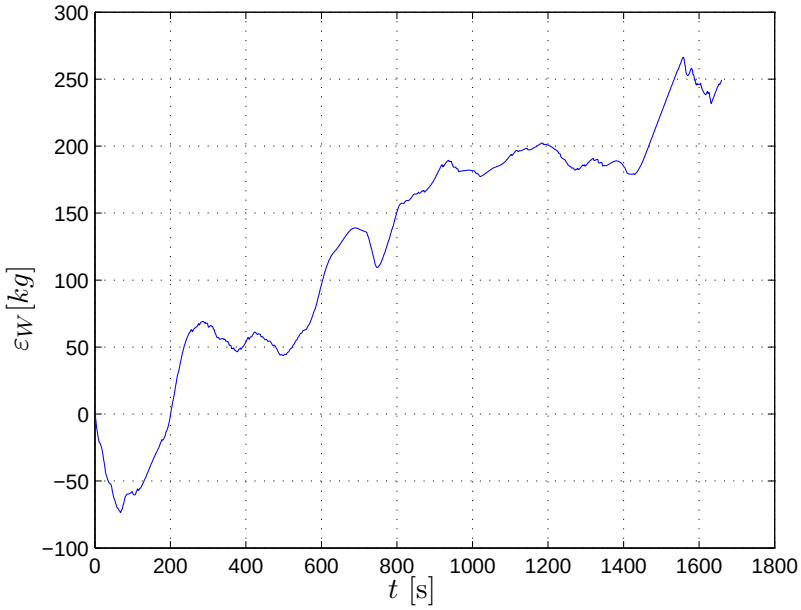


(b) Aircraft TS weight - FDR weight vs time

Figure 43: Approach and landing phase of flight representation for 1628303 FDR

Table 11: Mean ($\mu$) and Variance ($\sigma$) of the Aircraft Trajectory simulator validation variables errors (pitch $\theta$, bank angle $\phi$, fuel consumption $\dot{m}$ and final mass) and the Flight Control System variables errors (altitude and TAS) for straight line manoeuvre

| FDR N$^o$ | n | $\varepsilon_\theta$[deg] | | $\varepsilon_\phi$[deg] | | $\varepsilon_{\dot{m}}$[kg/s] | | $\frac{\varepsilon_m\|_{t_f}}{fuel_{used}}$[%] | $\varepsilon_h$[ft] | | $\varepsilon_{TAS}$[kt] | |
|---|---|---|---|---|---|---|---|---|---|---|---|---|
| | | $\mu$ | $\sigma$ | $\mu$ | $\sigma$ | $\mu$ | $\sigma$ | | $\mu$ | $\sigma$ | $\mu$ | $\sigma$ |
| 1628303 | 922 | -2.338 | 0.306 | -0.052 | 1.241 | -0.016 | 0.741 | -0.605 | -0.001 | 1.356 | 0.257 | 1.459 |
| 1628336 | 701 | -2.275 | 0.095 | 0.195 | 0.841 | 0.133 | 0.989 | 6.581 | 0.007 | 0.693 | 0.021 | 0.692 |
| 1629008 | 1783 | -2.458 | 0.191 | -0.053 | 1.811 | 0.289 | 0.803 | 9.968 | 0.002 | 0.982 | 0.045 | 0.857 |
| 1629399 | 412 | -2.771 | 0.109 | 0.337 | 0.906 | 0.110 | 0.348 | 4.819 | 0.010 | 0.712 | 0.225 | 0.617 |
| 1631203 | 1416 | -2.100 | 0.062 | 0.305 | 1.187 | 0.036 | 0.121 | 3.838 | 0.001 | 1.083 | 0.106 | 0.588 |
| 1629858 | 1263 | -2.098 | 0.059 | 0.330 | 1.358 | 0.065 | 0.091 | 9.478 | 0.017 | 0.767 | -0.305 | 0.554 |
| 1629874 | 1238 | -2.009 | 0.139 | 0.544 | 3.005 | 0.082 | 0.094 | 11.672 | -0.002 | 1.038 | -0.251 | 0.783 |
| 1630306 | 1278 | -2.059 | 0.134 | 0.622 | 3.411 | 0.148 | 0.105 | 19.543 | -0.003 | 1.482 | -0.149 | 1.220 |
| 1633358 | 1338 | -2.096 | 0.084 | -0.007 | 2.430 | 0.042 | 0.083 | 6.463 | 0.010 | 1.043 | -0.261 | 0.941 |
| 1633400 | 1455 | -2.097 | 0.084 | 0.522 | 3.016 | 0.096 | 0.108 | 13.721 | 0.012 | 0.979 | -0.071 | 0.964 |
| 1633476 | 1025 | -1.837 | 0.116 | 0.324 | 2.732 | 0.082 | 0.080 | 11.251 | -0.002 | 1.200 | -0.651 | 0.520 |
| 1629850 | 2910 | -2.124 | 0.122 | 0.288 | 1.244 | 0.096 | 0.091 | 13.155 | 0.007 | 1.008 | -0.464 | 0.607 |
| 1633449 | 1778 | -1.407 | 0.138 | 0.207 | 1.088 | 0.031 | 0.086 | 4.221 | 0.006 | 1.550 | 0.415 | 0.841 |
| A346 FDRs | 3818 | -2.429 | 0.249 | 0.035 | 1.463 | 0.167 | 0.801 | 5.191 | 0.003 | 1.018 | 0.111 | 0.998 |
| A319 FDRs | 12285 | -1.969 | 0.269 | 0.340 | 2.285 | 0.080 | 0.098 | 11.188 | 0.006 | 1.156 | -0.213 | 0.871 |
| All FDRs | 17519 | -2.080 | 0.316 | 0.270 | 2.063 | 0.096 | 0.386 | 8.777 | 0.005 | 1.122 | -0.117 | 0.894 |

phase of flight.

Most kinematics variables mean errors are negligible, except the TAS that present a small differences when the aircraft is changing flight level. This was because in this scenario the assumption that climb acceleration angle $\dot{\gamma}$ is not negligible at the transition points. These results can be seen in Table 11-13.

Comparison of the FDR variables to the aircraft TS do not show significant differences. For the the straight flight analysis only the 1630306 FDR produced an error above the 14% of the final mean mass error. For the aircraft turning manoeuver , time associated to aircraft turn were typically around 100 seconds for both TS and FDR simulated trajectories. Lastly, change of flight level manoeuver for the aircraft TS were approximately equal to those of the FDR except in the case of FDR 1628336 which showed some unusual behavior during its first two climb manoeuvers.

Figure 44-49 show results for the simulation of the 1628303 FDR for straight, arc and change of flight level manoeuvres.

Table 12: Mean ($\mu$) and Variance ($\sigma$) of the Aircraft Trajectory simulator validation variables errors (pitch $\theta$, bank angle $\phi$, fuel consumption $\dot{m}$ and final mass) and the Flight Control System variables errors (altitude and TAS) for curved line manoeuvre

| FDR N$^o$ | n | $\varepsilon_\theta$[deg] | | $\varepsilon_\phi$[deg] | | $\varepsilon_{\dot{m}}$[kg/s] | | $\frac{\varepsilon_m\|_{t_f}}{fuel_{used}}$[%] | $\varepsilon_h$[ft] | | $\varepsilon_{TAS}$[kt] | |
|---|---|---|---|---|---|---|---|---|---|---|---|---|
| | | $\mu$ | $\sigma$ | $\mu$ | $\sigma$ | $\mu$ | $\sigma$ | | $\mu$ | $\sigma$ | $\mu$ | $\sigma$ |
| 1628303 | 62 | -2.035 | 0.145 | -0.242 | 7.417 | -0.310 | 1.758 | -21.831 | 0.085 | 1.213 | 0.970 | 0.585 |
| 1628336 | 101 | -2.407 | 0.040 | 1.043 | 4.322 | -0.315 | 0.367 | -22.872 | -0.011 | 0.458 | -0.644 | 0.396 |
| 1629008 | 144 | -2.680 | 0.161 | -2.097 | 11.640 | -0.045 | 0.231 | -1.999 | 0.005 | 1.029 | -0.612 | 0.928 |
| 1629399 | 70 | -2.801 | 0.032 | -3.124 | 10.828 | 0.064 | 0.300 | 2.361 | -0.016 | 0.680 | 0.237 | 0.572 |
| 1631203 | 44 | -2.477 | 0.209 | -2.841 | 5.621 | 0.145 | 0.029 | 16.439 | 0.257 | 1.633 | -1.267 | 1.213 |
| 1629858 | 51 | -2.024 | 0.114 | 1.986 | 7.932 | 0.119 | 0.041 | 16.405 | -0.144 | 1.241 | -0.600 | 0.411 |
| 1629874 | 115 | -2.332 | 0.185 | 2.183 | 11.769 | 0.033 | 0.107 | 5.212 | -0.052 | 0.761 | 0.248 | 0.571 |
| 1630306 | 51 | -2.050 | 0.177 | 3.128 | 8.595 | -0.058 | 0.056 | -11.130 | 0.272 | 1.935 | 0.128 | 0.229 |
| 1633358 | 51 | -2.082 | 0.139 | 3.077 | 10.732 | -0.030 | 0.046 | -5.676 | -0.065 | 1.490 | 0.099 | 0.303 |
| 1633400 | 141 | -2.019 | 0.106 | 2.512 | 10.529 | 0.079 | 0.080 | 11.191 | 0.006 | 0.989 | -0.459 | 0.944 |
| 1633476 | 51 | -1.965 | 0.179 | 1.817 | 16.120 | 0.160 | 0.017 | 20.903 | 0.099 | 1.282 | -0.170 | 0.494 |
| 1629850 | 51 | -2.143 | 0.152 | 3.450 | 11.510 | 0.249 | 0.033 | 29.294 | 0.104 | 1.196 | -0.403 | 0.710 |
| 1633449 | 101 | -1.364 | 0.088 | 1.002 | 8.479 | 0.247 | 0.040 | 25.446 | 0.034 | 0.739 | 0.461 | 0.299 |
| A346 FDRs | 377 | -2.523 | 0.284 | -1.141 | 9.457 | -0.140 | 0.773 | -11.085 | 0.010 | 0.885 | -0.203 | 0.929 |
| A319 FDRs | 612 | -1.984 | 0.332 | 2.276 | 10.783 | 0.102 | 0.121 | 11.456 | 0.019 | 1.139 | -0.062 | 0.712 |
| All FDRs | 1033 | -2.202 | 0.407 | 0.811 | 10.294 | 0.015 | 0.491 | 4.903 | 0.026 | 1.080 | -0.165 | 0.857 |

Table 13: Mean ($\mu$) and Variance ($\sigma$) of the Aircraft Trajectory simulator validation variables errors (pitch $\theta$, bank angle $\phi$, fuel consumption $\dot{m}$ and final mass) and the Flight Control System variables errors (altitude and TAS) for change flight level manoeuvre

| FDR N$^o$ | n | $\varepsilon_\theta$[deg] | | $\varepsilon_\phi$[deg] | | $\varepsilon_{\dot{m}}$[kg/s] | | $\frac{\varepsilon_m\|_{t_f}}{fuel_{used}}$[%] | $\varepsilon_h$[ft] | | $\varepsilon_{TAS}$[kt] | |
|---|---|---|---|---|---|---|---|---|---|---|---|---|
| | | $\mu$ | $\sigma$ | $\mu$ | $\sigma$ | $\mu$ | $\sigma$ | | $\mu$ | $\sigma$ | $\mu$ | $\sigma$ |
| 1628303 | 331 | -2.709 | 0.196 | -1.231 | 6.995 | -0.285 | 0.836 | -11.555 | -0.000 | 2.331 | -3.162 | 3.252 |
| | 331 | -2.236 | 0.271 | -0.698 | 5.819 | -0.160 | 0.645 | -6.519 | 0.002 | 2.661 | -1.815 | 3.805 |
| | 280 | -2.089 | 0.325 | 0.695 | 4.033 | -0.047 | 0.303 | -2.233 | -0.000 | 3.694 | -0.104 | 3.275 |
| 1628336 | 330 | -2.235 | 0.173 | 0.631 | 4.087 | -0.399 | 2.317 | -26.187 | -0.004 | 1.492 | -4.728 | 4.155 |
| | 400 | -2.503 | 0.175 | 0.558 | 6.526 | 0.850 | 1.287 | 31.590 | -0.003 | 1.261 | -3.210 | 2.271 |
| | 318 | -2.061 | 0.157 | 0.674 | 4.080 | -0.060 | 0.315 | -4.478 | 0.012 | 2.037 | 0.420 | 2.233 |
| 1629008 | 316 | -2.153 | 0.240 | -1.401 | 7.634 | 0.011 | 1.138 | 0.587 | 0.004 | 2.688 | -1.565 | 3.870 |
| | 362 | -2.577 | 0.366 | -0.935 | 6.414 | 0.023 | 1.447 | 0.931 | 0.009 | 3.510 | -2.299 | 3.466 |
| | 280 | -2.128 | 0.383 | 0.736 | 4.941 | 0.203 | 0.450 | 8.480 | 0.002 | 4.725 | -0.070 | 2.960 |
| 1629399 | 643 | -3.093 | 0.537 | 0.377 | 6.425 | 0.410 | 0.881 | 11.105 | -0.004 | 3.641 | -1.255 | 2.970 |
| | 463 | -3.039 | 0.239 | 1.340 | 4.635 | 0.366 | 0.576 | 10.866 | 0.006 | 2.102 | -1.802 | 3.268 |
| | 295 | -2.799 | 0.299 | 0.086 | 11.580 | 0.007 | 0.863 | 0.256 | 0.007 | 3.141 | -2.593 | 3.130 |
| | 468 | -2.686 | 0.291 | 0.290 | 0.707 | 0.024 | 0.372 | 1.111 | -0.016 | 1.721 | -0.341 | 1.572 |
| | 422 | -2.880 | 0.244 | 0.966 | 5.342 | 0.156 | 0.457 | 6.687 | 0.004 | 2.425 | -0.444 | 2.896 |
| 1631203 | 641 | -2.208 | 0.269 | -0.017 | 3.766 | 0.033 | 0.098 | 3.510 | 0.004 | 1.938 | -6.507 | 5.049 |
| 1633476 | 447 | -2.087 | 0.197 | 0.101 | 0.467 | 0.066 | 0.080 | 9.788 | 0.018 | 1.384 | -1.107 | 1.466 |
| | 703 | -1.902 | 0.255 | 0.163 | 1.271 | 0.047 | 0.078 | 8.192 | 0.006 | 1.674 | 1.577 | 0.960 |
| A346 FDRs | 5239 | -2.580 | 0.476 | 0.202 | 6.041 | 0.116 | 1.033 | 1.474 | 0.001 | 2.794 | -1.620 | 3.378 |
| A319 FDRs | 1150 | -1.974 | 0.251 | 0.139 | 1.036 | 0.054 | 0.079 | 8.990 | 0.011 | 1.567 | 0.534 | 1.764 |
| All FDRs | 7030 | -2.447 | 0.490 | 0.172 | 5.354 | 0.099 | 0.894 | 2.478 | 0.003 | 2.561 | -1.713 | 3.777 |

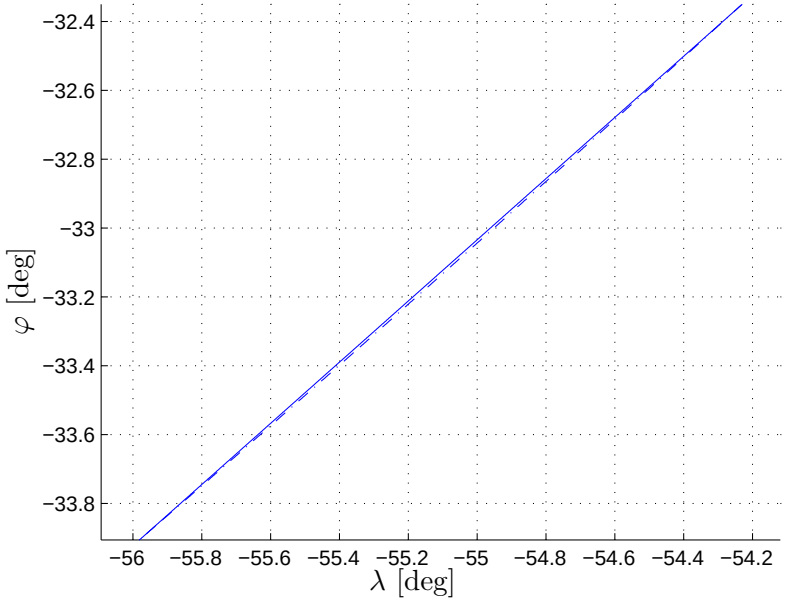


(a) Horizontal profile. FDR values are denoted by doted line and aircraft TS values by the solid line.

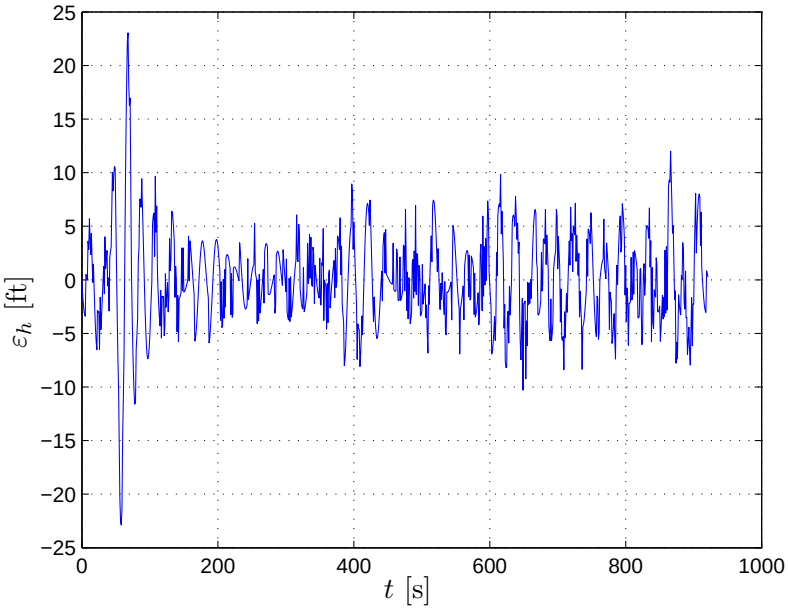


(b) Aircraft TS altitude - FDR altitude vs time

Figure 44: Straight line manoeuvre representation for 1628303 FDR

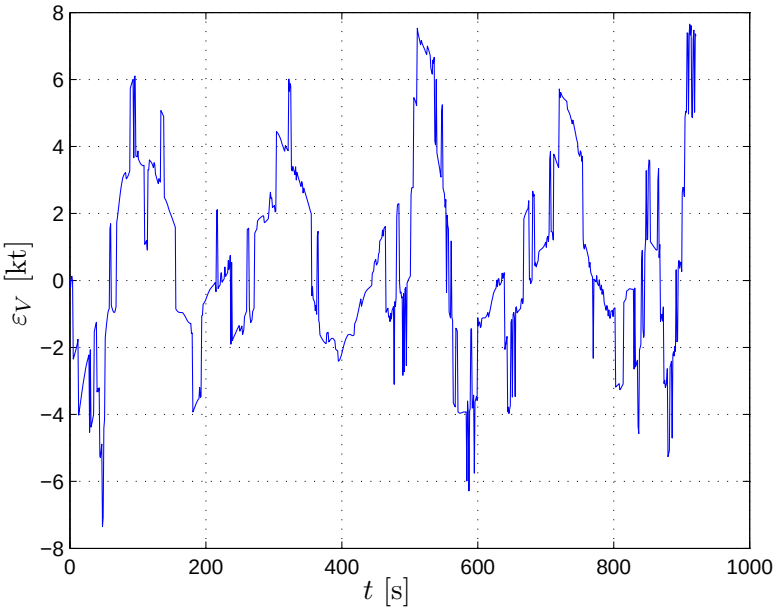


(a) Aircraft TS TAS - FDR TAS vs time

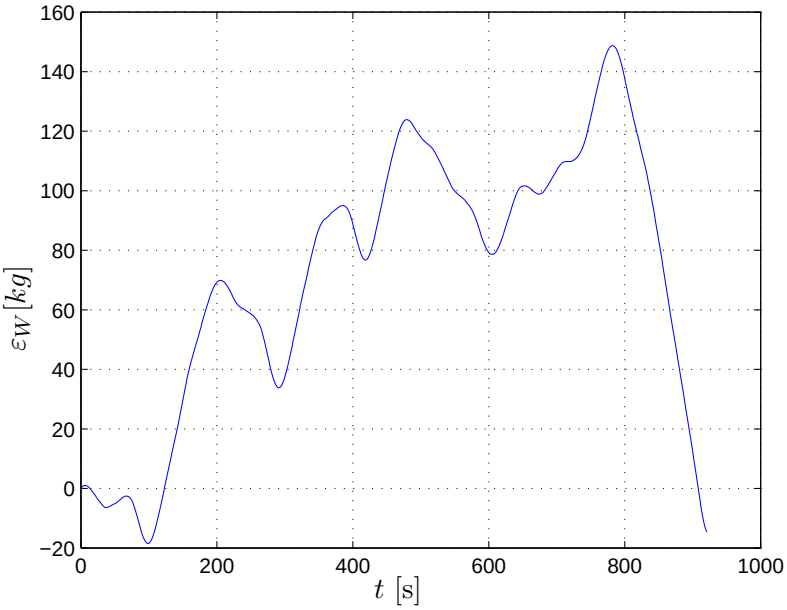


(b) Aircraft TS weight - FDR weight vs time

Figure 45: Straight line manoeuvre representation for 1628303 FDR

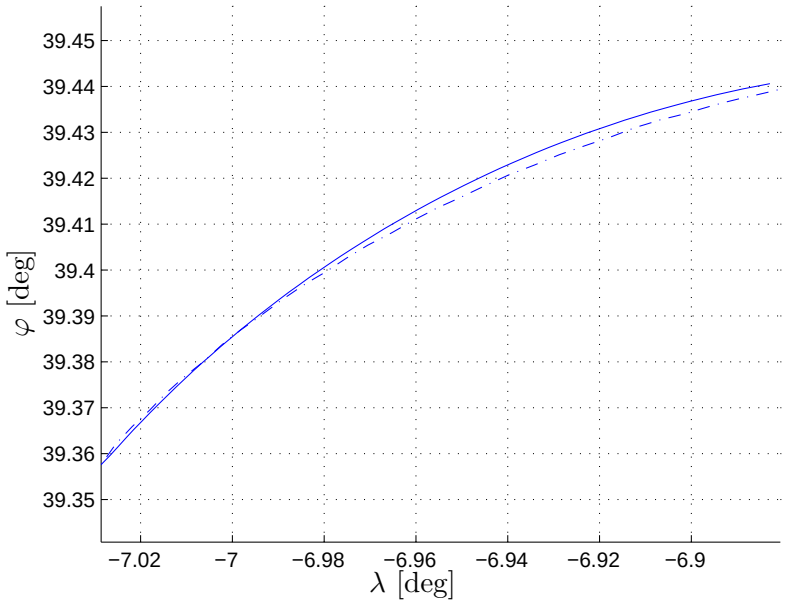


(a) Horizontal profile. FDR values are denoted by doted line and aircraft TS values by the solid line.

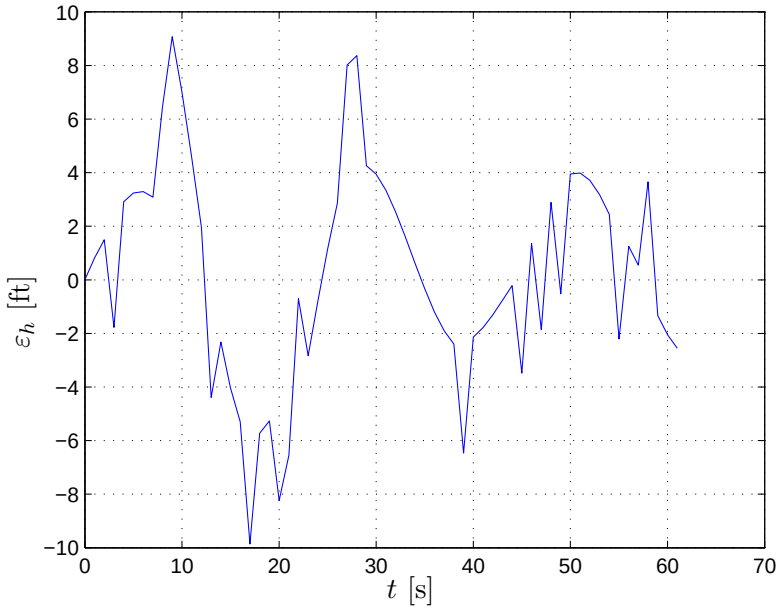


(b) Aircraft TS altitude - FDR altitude vs time

Figure 46: Curve line manoeuvre representation for 1628303 FDR

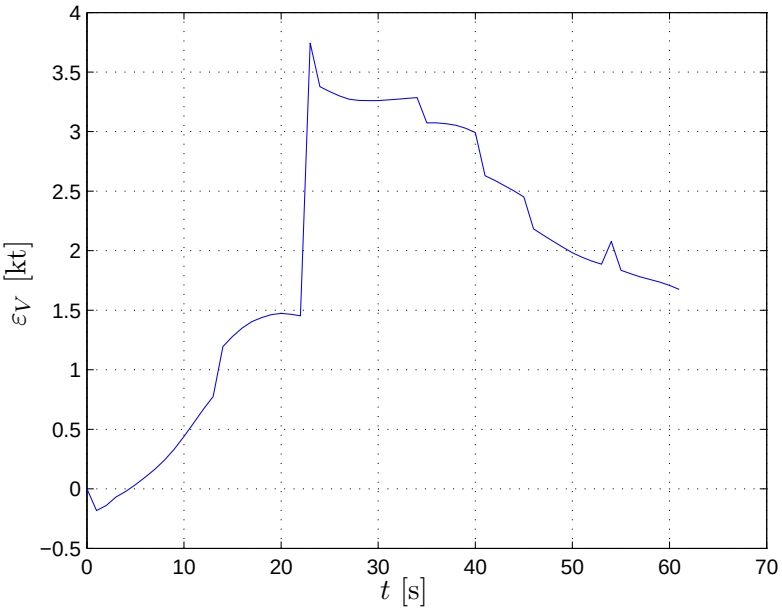


(a) Aircraft TS TAS - FDR TAS vs time

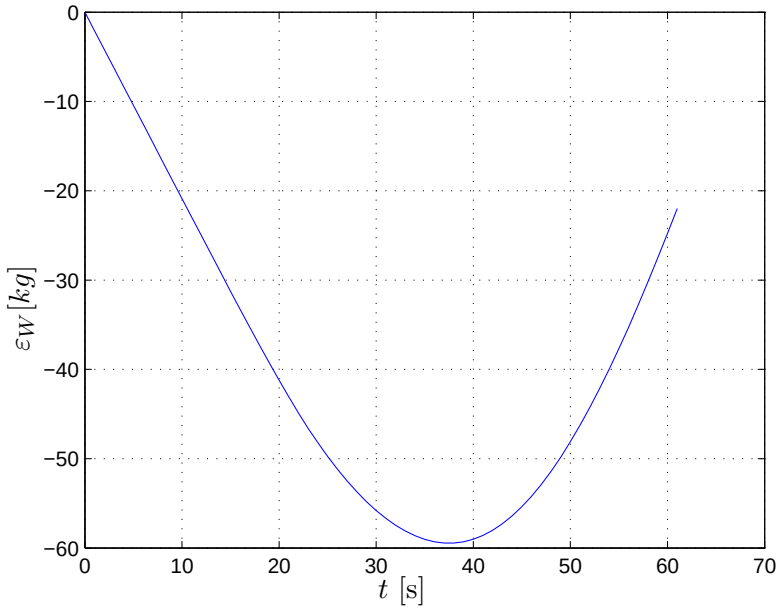


(b) Aircraft TS weight - FDR weight vs time

Figure 47: Curve line manoeuvre representation for 1628303 FDR

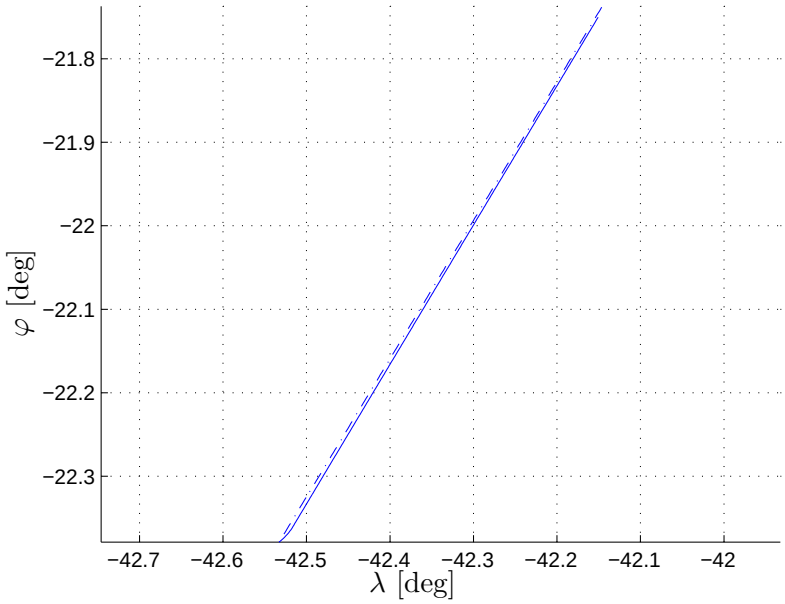


(a) Horizontal profile. FDR values are denoted by doted line and aircraft TS values by the solid line.

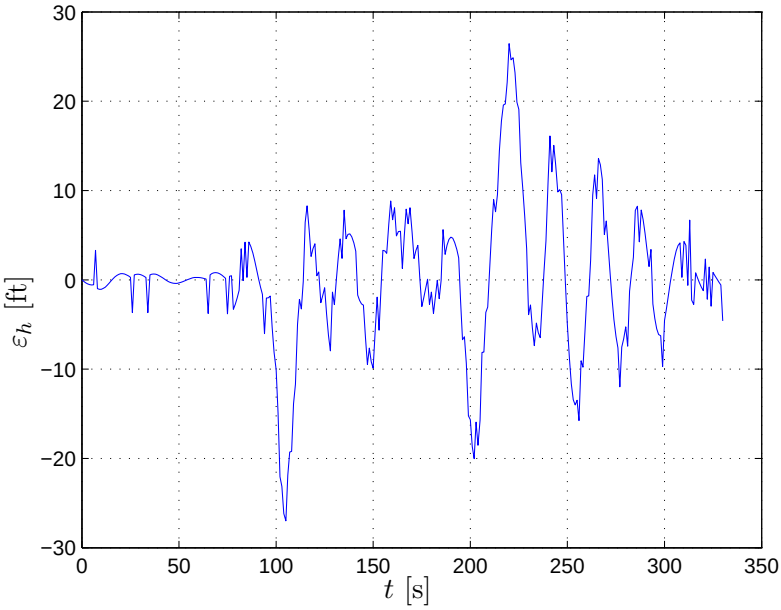


(b) Aircraft TS altitude - FDR altitude vs time

Figure 48: Change of flight level manoeuvre representation for 1628303 FDR

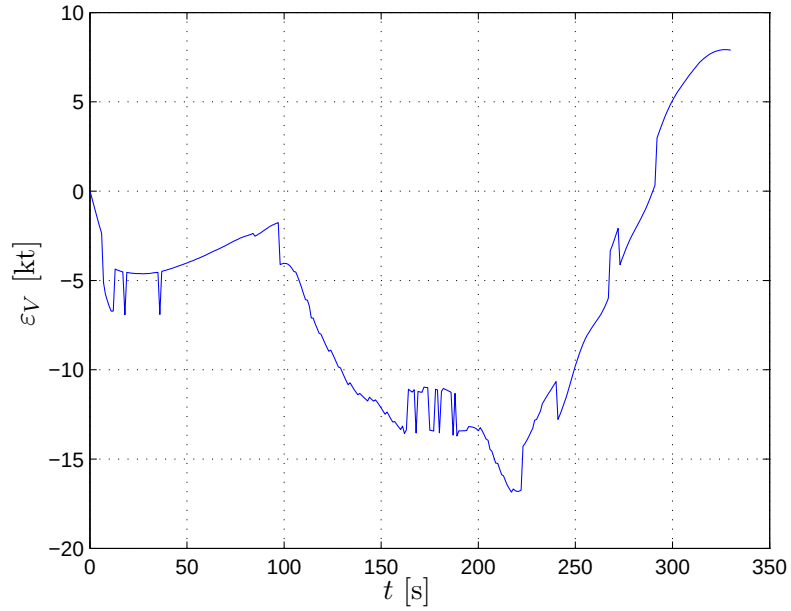


(a) Aircraft TS TAS - FDR TAS vs time

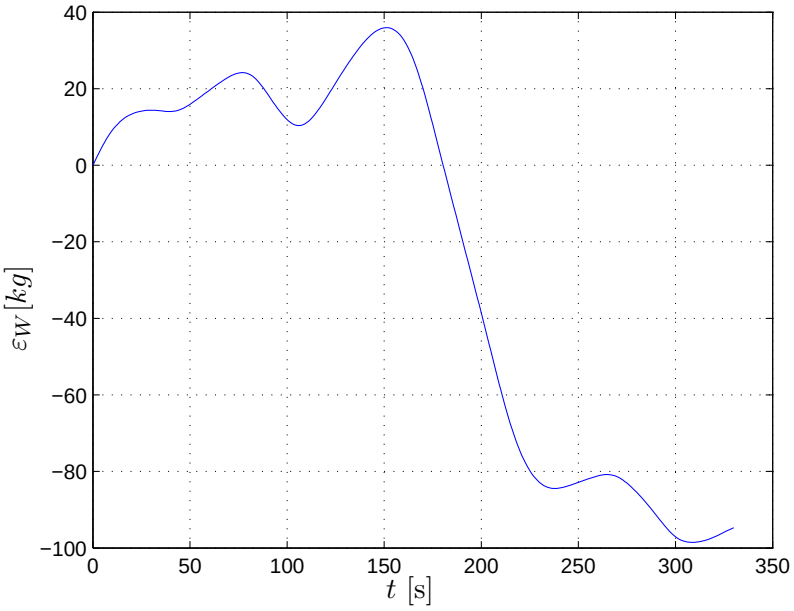


(b) Aircraft TS weight - FDR weight vs time

Figure 49: Change of flight level manoeuvre representation for 1628303 FDR

### 3.3.3 Corrections to be applied to the aircraft Trajectory Simulator

It was observed that the fuel consumption for the aircraft TS showed a constant deviation from that of the FDR. Therefore, a correction factor ($CF$) should be added to the $\dot{m}$ equation with respect to flight level and initial weight:

$$\dot{m}_c = \dot{m} + CF \tag{58}$$

where $\dot{m}_c$ is the weight after correction.

Figure 50 represents distribution of the mean mass error with respect to flight levels for A319-111 and A340-600. The available sample of FDR makes it infeasible to obtain an analytical dependence on altitude and initial mass. Therefore, the correction factor is obtained as the mean value of all measured differences, see Figure 51. The following results have been obtained: $4.8438e^{-2}$, $-7.9975e^{-3}$ and $9.3652e^{-2}$ kg/s to an A319-111, A321 and A340-600 respectively. After introducing the above correction factors, a relevant reduction of the mass errors was obtained for the different flights as shown in Table 14 and Table 15.

## 3.4 Discussion on the results

This chapter presents a simplified aircraft TS based on a 3DoF PMM and makes a comparison of its performance with actually flown trajectories obtained from FDR. The aircraft TS can be considered as a good aircraft trajectory predictor of a variety of aircraft since it reproduces an acceptable real trajectory and the trajectory produced is sufficiently accurate to be used in the strategic and pre-tactical ATM planning layers. The TS was designed to easily incorporate aircraft data from BADA universal performance database.

This aircraft TS is modeled in a user-friendly Simulink® tool, where all possible scenarios can be simulated, and the atmosphere and aircraft type information can be introduced as user preference. The atmosphere is one of the most important sources of uncertainty in trajectory modeling. Aircraft performance are greatly affected by its behavior so it is important to accurately estimate its characteristic values to avoid large deviation in planned and flown

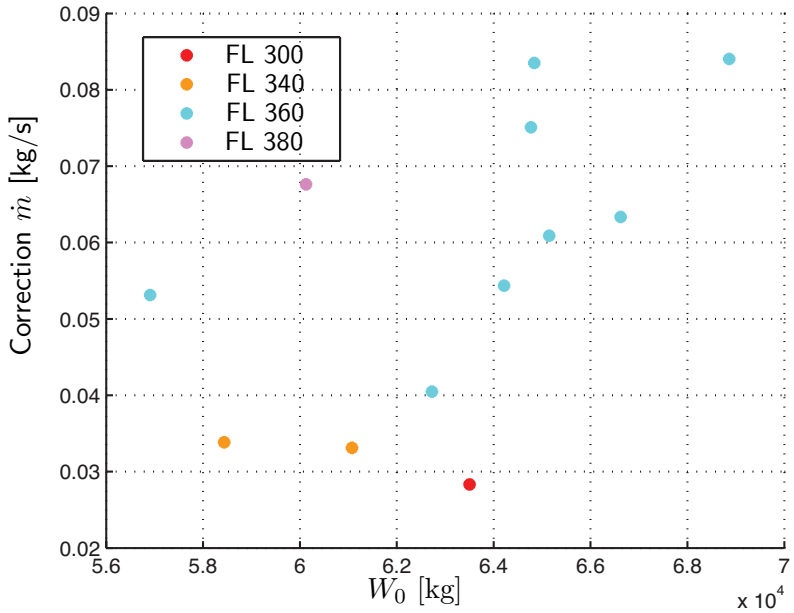


(a) Fuel Consumption correction factor vs initial weight for an A319

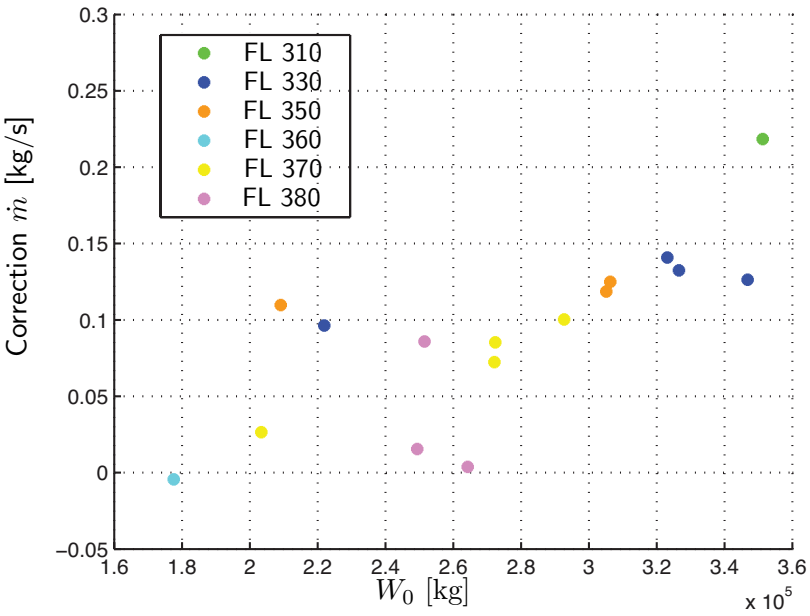


(b) Fuel Consumption correction factor vs initial weight for an A346

Figure 50: Fuel Consumption correction factor representations

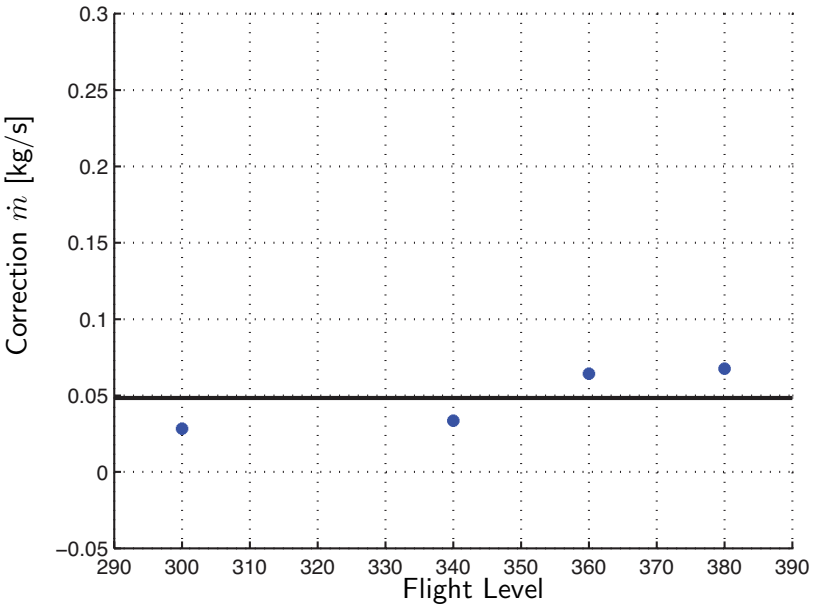


(a) Fuel Consumption correction factor vs flight level for an A319

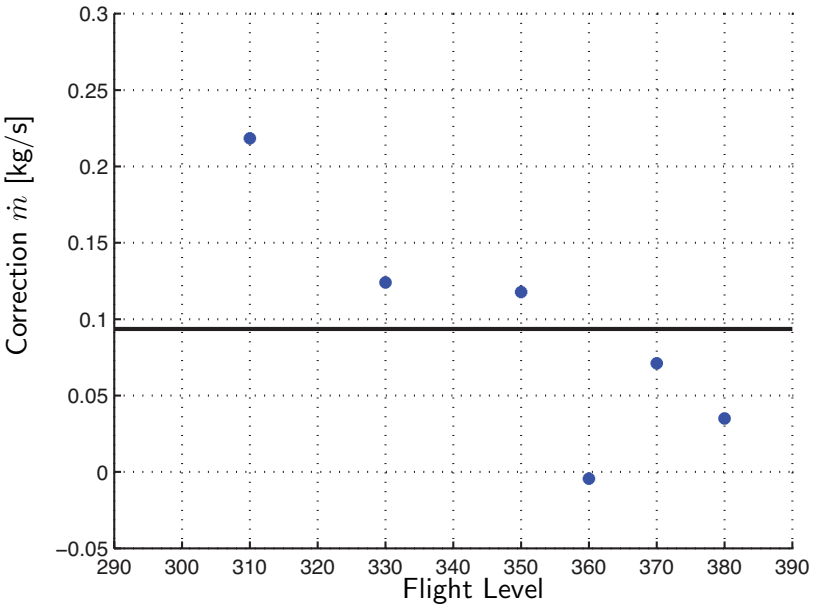


(b) Fuel Consumption correction factor vs flight level for an A346

Figure 51: Fuel Consumption correction factor representations

Table 14: Fuel consumption correction factor

| FDR number | n | FL [ft/100] | $m_0$ [kg] | $\frac{\varepsilon_m\|_{t_f}}{fuel_{used}}$ [%] | $\varepsilon_{\dot{m}}$[kg/s] | |
|---|---|---|---|---|---|---|
| | | | | | $\mu$ | $\sigma$ |
| 1628303 | 7260 | 330 | 326554.545 | 4.928 | 0.132 | 1.146 |
| | 13520 | 350 | 306313.605 | 5.061 | 0.125 | 0.931 |
| | 9389 | 370 | 272404.306 | 3.883 | 0.085 | 0.581 |
| | 7218 | 380 | 251526.667 | 4.152 | 0.086 | 0.721 |
| 1628336 | 6575 | 330 | 221977.558 | 4.920 | 0.096 | 1.003 |
| | 2799 | 350 | 209134.762 | 5.994 | 0.110 | 1.349 |
| | 16104 | 370 | 203402.121 | 1.659 | 0.026 | 0.460 |
| | 9015 | 360 | 177550.247 | -0.297 | -0.004 | 0.709 |
| 1629008 | 10798 | 330 | 323170.725 | 5.271 | 0.141 | 1.020 |
| | 18774 | 370 | 292735.174 | 4.407 | 0.100 | 0.676 |
| | 6624 | 380 | 249391.087 | 0.778 | 0.015 | 0.789 |
| 1629399 | 1179 | 310 | 351287.138 | 7.161 | 0.218 | 1.369 |
| | 14784 | 330 | 346817.328 | 4.566 | 0.126 | 1.561 |
| | 13051 | 350 | 305132.906 | 4.798 | 0.119 | 0.843 |
| | 3372 | 370 | 272146.957 | 3.251 | 0.072 | 0.602 |
| | 4300 | 380 | 264275.626 | 0.180 | 0.004 | 0.414 |
| 1631203 | 4817 | 330 | 83065.973 | 0.214 | 0.002 | 0.103 |
| | 4685 | 360 | 78496.996 | -2.251 | -0.018 | 0.101 |
| 1629858 | 14762 | 360 | 65147.324 | 9.283 | 0.061 | 0.094 |
| 1629874 | 14476 | 360 | 64770.889 | 11.146 | 0.075 | 0.097 |
| 1630306 | 5353 | 360 | 64839.410 | 12.287 | 0.084 | 0.111 |
| | 8247 | 340 | 61074.947 | 5.047 | 0.033 | 0.081 |
| 1633358 | 14004 | 360 | 62725.292 | 6.466 | 0.040 | 0.081 |
| 1633400 | 14317 | 360 | 64215.561 | 8.447 | 0.054 | 0.093 |
| 1633476 | 9485 | 360 | 66623.446 | 9.496 | 0.063 | 0.093 |
| | 2291 | 380 | 60126.155 | 11.043 | 0.068 | 0.080 |
| | 1494 | 340 | 58434.983 | 5.227 | 0.034 | 0.071 |
| 1629850 | 15415 | 360 | 68863.140 | 11.985 | 0.084 | 0.095 |
| 1633449 | 8786 | 300 | 63502.633 | 3.909 | 0.028 | 0.097 |
| | 5841 | 360 | 56906.255 | 8.467 | 0.053 | 0.089 |

Table 15: Fuel consumption correction factor after including the correction factor

| FDR number | n | FL [ft/100] | $m_0$ [kg] | $\frac{\varepsilon_m\|_{t_f}}{fuel_{used}}$ [%] | $\varepsilon_{\dot{m}}$[kg/s] | |
|---|---|---|---|---|---|---|
| | | | | | $\mu$ | $\sigma$ |
| 1628303 | 7260 | 330 | 326554.545 | 1.517 | 0.041 | 1.146 |
| | 13520 | 350 | 306313.605 | 1.409 | 0.035 | 0.931 |
| | 9389 | 370 | 272404.306 | -0.266 | -0.006 | 0.581 |
| | 7218 | 380 | 251526.667 | -0.281 | -0.006 | 0.721 |
| 1628336 | 6575 | 330 | 221977.558 | 0.206 | 0.004 | 1.003 |
| | 2799 | 350 | 209134.762 | 0.891 | 0.017 | 1.349 |
| | 16104 | 370 | 203402.121 | -3.995 | -0.064 | 0.460 |
| | 9015 | 360 | 177550.247 | -6.528 | -0.096 | 0.709 |
| 1629008 | 10798 | 330 | 323170.725 | 1.868 | 0.050 | 1.020 |
| | 18774 | 370 | 292735.174 | 0.507 | 0.012 | 0.676 |
| | 6624 | 380 | 249391.087 | -3.837 | -0.077 | 0.789 |
| 1629399 | 1179 | 310 | 351287.138 | 4.112 | 0.125 | 1.369 |
| | 14784 | 330 | 346817.328 | 1.320 | 0.037 | 1.561 |
| | 13051 | 350 | 305132.906 | 1.144 | 0.028 | 0.842 |
| | 3372 | 370 | 272146.957 | -0.916 | -0.020 | 0.602 |
| | 4300 | 380 | 264275.626 | -4.254 | -0.089 | 0.414 |
| 1631203 | 4817 | 330 | 83065.973 | 1.107 | 0.010 | 0.103 |
| | 4685 | 360 | 78496.996 | -1.256 | -0.010 | 0.101 |
| 1629858 | 14762 | 360 | 65147.324 | 2.087 | 0.014 | 0.094 |
| 1629874 | 14475 | 360 | 64770.889 | 4.132 | 0.028 | 0.096 |
| 1630306 | 5353 | 360 | 64839.410 | 5.232 | 0.036 | 0.111 |
| | 8246 | 340 | 61074.947 | -2.228 | -0.015 | 0.081 |
| 1633358 | 14004 | 360 | 62725.292 | -1.092 | -0.007 | 0.081 |
| 1633400 | 14317 | 360 | 64215.561 | 1.103 | 0.007 | 0.093 |
| 1633476 | 9485 | 360 | 66623.446 | 2.361 | 0.016 | 0.093 |
| | 2291 | 380 | 60126.155 | 3.169 | 0.019 | 0.080 |
| | 1494 | 340 | 58434.983 | -2.242 | -0.014 | 0.071 |
| 1629850 | 15415 | 360 | 68863.140 | 5.267 | 0.037 | 0.095 |
| 1633449 | 8786 | 300 | 63502.633 | -2.697 | -0.020 | 0.097 |
| | 5841 | 360 | 56906.255 | 0.822 | 0.005 | 0.089 |

trajectories. More accurate and atmosphere models will further improve the performance of the aircraft TS.

The tool was evaluated in order to measure its deviation from the real aircraft performance. As a result of that validation process, a nominal fuel consumption correction per aircraft type was determined. The evaluation provides relevant performance behaviour for long and short haul flight as well as those related to specific manoeuvers. Furthermore, the aircraft nominal fuel consumption correction showed a varying factor for for different aircraft types.

The quasi-stationary assumption of $\dot{\gamma}$ being negligible was a good approximation and sufficient in modeling most part of the trajectory except at the take off and landing phases of the flight.

The aircraft TS kinematics variables, for both long and short range trajectory, as well as for different types of aircraft were precise. A good roll angle ($\phi$) is well reproduced. However, a slightly higher mean difference for the aircraft TS and the FDR pitch angle ($\theta$) was identified. This was due to the assumption that the angle of attack ($\alpha$) was equated to zero instead of a small value. The result also indicates that the TAS accuracy decreases when the aircraft TS negotiate a change of flight level. This is because in real situations aircraft speed remains almost constant the TS lightly decrease or increase aircraft speed in climbs or descents, respectively.

**List of References**


[1] Nuic A., *User Manual for the base of Aircraft Data (BADA) Revision 3.9*, Eurocontrol Experimental Cente, 2008.

[2] M. Soler, A. Olivares, and E. Staffetti, "Hybrid Optimal Control Approach to Commercial Aircraft Trajectory Planning," *Journal of Guidance Control and Dynamics*, vol. 33, pp. 985–991, 2010.

[3] D. Rivas, A. Valenzuela, and J. L. de Augusto, "Computation of global trajectories of commercial transport aircraft," *Proceedings of the Institution of Mechanical*

*Engineers, Part G: Journal of Aerospace Engineering*, 2012. [Online]. Available: http://pig.sagepub.com/content/early/2012/01/11/0954410011427107.abstract

[4] A. V. Romero, "Aircraft trajectory optimization using parametric optimization theory," Ph.D. dissertation, University of Seville, Seville, Spain, 2012.

[5] S. Khardi, "Aircraft flight path optimization. the hamilton-jacobi-bellman considerations," *Applied Mathematical Sciences*, vol. 6, no. 25, pp. 1221–1249, 2012.

[6] R. Howe-Veenstra, "Commercial aircraft trajectory optimization and efficiency of air traffic control procedures," Master's thesis, University of Minnesota, 2011.

[7] D. G. Hull, *Fundamentals of Airplane Flight Mechanics, 1st. edn.* New York, United States of America: Springer-Verlag Berlin and Heidelberg GmbH & Co. K, 2007.

[8] M. Soler, "Commercial aircraft trajectory planning based on multiphase mixed-integer optimal control," Ph.D. dissertation, Universidad Rey Juan Carlos, 2013. [Online]. Available: http://www.aerospaceengineering.es/publications/phd-thesis/

[9] MATLAB, *version 7.10.0 (R2010a)*. Natick, Massachusetts: The MathWorks Inc., 2010.

[10] ICAO, *Operation of Aircraft*, Montreal, Canada, 2010.

[11] B. L. Stevens and F. L. Lewis, *Aircraft Control and Simulation*. Wiley-Interscience, Oct. 2003. [Online]. Available: http://www.amazon.com/exec/obidos/redirect?tag=citeulike07-20&path=ASIN/0471371459

[12] National Imagery and Mapping Agency (NIMA), *Department of Defense World Geodetic System 1984, Its Definition and Relationships With Local Geodetic Systems. Report TR8350.2*, Virginia, 22150-7500.

[13] Office of Research and Engineering Natinal Transportation Sagety Board, *Flight Data Recorder Handbook for Aviation Accident Investigations*, Washington, DC 20594, 2002.

[14] Ministère des Transports, de L'Équipement, du Tourisme et de la mer Bureau D'Enquetes et D'Analyses Pour la Securite de L'Aviation Civile, *Flight Data Recorder Read-Out Technical and Regulatory Aspects*, France, 2005.

# CHAPTER 4

## Optimization Assessment

In the future ATM system, the trajectory becomes the fundamental element of a new set of operating procedures collectively referred to as TBO [1]. The underlying idea behind TBO is the concept of business trajectory. The business trajectory is the trajectory that will meet best airline business interests. This business interests may be, for instance, minimum duration, minimum consumption, or minimum operational cost. The TBO concept of operations and the notion of business trajectory will result in more efficient 4D trajectories, that will be necessarily flown under the presence of constraints due to, for instance, airport operations or ATC intervention. Any modification in that trajectory will result in a change in the cost effectiveness of the operation. Thus, the future ATM system should modify the business trajectory as little as possible. Furthermore, the necessary tactical intervention will be limited to exceptions, so the development of techniques for strategic planning of business 4D trajectories will be key, resulting in significant fuel savings for airlines. Effective flight planning can not only reduce fuel costs, but also time-based costs and lost revenue from payload that can not be carried, simply by choosing efficient routes and altitudes, speed, and the optimal amount of departure fuel.

The flight planning problem can be regarded as a trajectory optimisation problem. The trajectory optimisation problem can be studied as an optimal control problem of a dynamic system in which the goal is to find the trajectory and the corresponding control inputs that steer the state of the system between two configurations satisfying a set of constraints on the state and/or control variables while minimising an objective functional.

Therefore, the main contribution of this chapter is to present a comparison between HLGL and pseudospectral collocation methods in a classical type of problem arising in ATM, i.e., those of finding the minimum fuel trajectory with a required time of arrival. First we

analyze a benchmark problem: the minimum fuel cruise at constant altitude with fixed arrival time that was solved as a singular arc in [2]. In this manner, a comparison between the singular arc solution and different direct solutions can be also drawn. Second, in order to scale the obtained results to more realistic examples, a real trajectory through Flight Data Recorder (FDR) information of an El Cairo-Madrid flight has been tackled considering its cruise, approach, and descent phases. FDR based trajectory (information extracted from FDR data of regular flights) has been fairly compared to the minimum fuel trajectory with required time of arrival (resulting to the solution of the corresponding optimal control problem). Results show the substantial reduction in fuel burnt and $CO_2$ emissions that could be achieved by substituting current operations by continuous operations. Moreover, it is shown that pseudospectral methods are much more accurate and computationally more efficient that HLGL methods.

The chapter is structured as follows. First, in section 4.1, we state the optimal control problem and present the optimality conditions. In section 4.2, the most common numerical methods to solve such problem are described. A more detailed description of the pseudospectral collocation methods are presented in section 4.3. The two cases study are discussed in section 4.4. Finally, some conclusions are drawn in section 4.5.

## 4.1 Optimal Control Problem

Optimal control has been used in very different areas [3], from agriculture or biology to engineer, including economist or mathematicians.

Optimal control was born in 1697 with the works of Johann Bernoulli, the *brachistrochrone problem* [4]. The *brachistrochrone problem* is to find the trajectory described for the shortest time by a particle of mass $m$ without friction [5]. Also, this problem has been solved by many authors in different ways and methods [6, 7, 8]. In 1744, Euler developed the basic of the *Calculus of Variation* [9, 10]. For fundamental background in the associated calculus of variations, the reader should refer to Bliss [11, 12]. But is not until the 1940 decade

with the development of computers when computer programming begins and the *Numerical Methods* are more deeply used and analysed.

The goal of optimal control theory is to determine the control input that will cause a dynamical system (typically characterised by a set of differential-algebraic equations) to be steered from an initial state configuration to a final one, satisfying a set of path constraints, and at the same time optimise some performance criterion. Figure 52 illustrates it schematically.

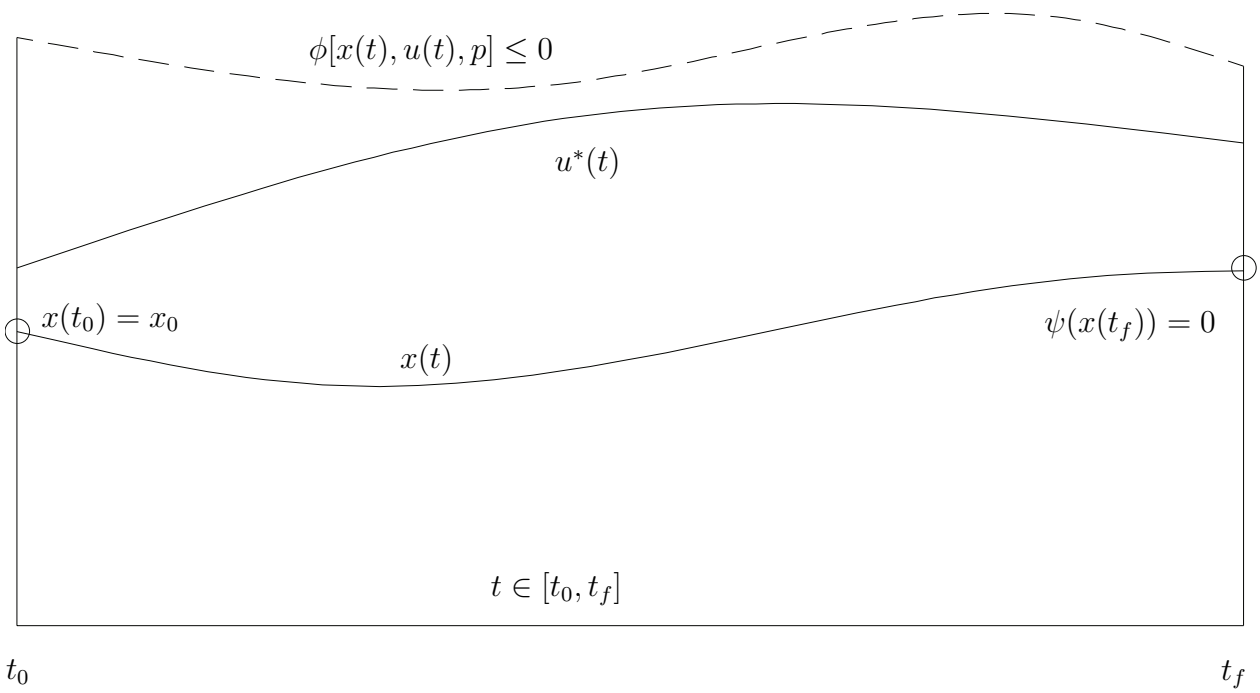


Figure 52: Optimal control problem

The optimal control problem can be stated as follows [13]:

**Problem 1** (***Optimal Control Problem***)**.**

$$
\begin{aligned}
&min\ J(t, x(t), u(t), l) = E(t_f, x(t_f)) + \int_{t_0}^{t_f} L(x(t), u(t), l)dt; \\
&subject\ to: \\
&\dot{x}(t) = f(x(t), u(t), l),\ dynamic\ equations; \\
&0 = g(x(t), u(t), l),\ algebraic\ equations; \\
&x(t^I) = x^I,\ initial\ boundary\ conditions; \\
&\psi(x(t^F)) = 0,\ terminal\ boundary\ conditions; \\
&\phi_l \leq \phi[x(t), u(t), p] \leq \phi_u,\ path\ constraints.
\end{aligned}
\tag{OCP}
$$

*Variable* $t \in [t^I, t^F] \subset \mathbb{R}$ *represents time and* $l \in \mathbb{R}^{n_l}$ *is a vector of parameters. Notice that the initial time* $t^I$ *is fixed and the final time* $t^F$ *might be fixed or left undetermined.* $x(t) : [t^I, t^F] \mapsto \mathbb{R}^{n_x}$ *represents the state variables.* $u(t) : [t^I, t^F] \mapsto \mathbb{R}^{n_u}$ *represents the control functions, also referred to as control inputs, assumed to be measurable. The objective function* $J : [t^I, t^F] \times \mathbb{R}^{n_x} \times \mathbb{R}^{n_u} \times \mathbb{R}^{n_l} \to \mathbb{R}$ *is given in Bolza form. It is expressed as the sum of the Mayer term* $E(t^F, x(t^F))$ *and the Lagrange term* $\int_{t^I}^{t^F} L(x(t), u(t), l)dt$*. Functions* $E : [t^I, t^F] \times \mathbb{R}^{n_x} \to \mathbb{R}$ *and* $L : \mathbb{R}^{n_x} \times \mathbb{R}^{n_u} \times \mathbb{R}^{n_l} \to \mathbb{R}$ *are assumed to be twice differentiable. The system is a DAE system in which the right hand side function of the differential set of equations* $f : \mathbb{R}^{n_x} \times \mathbb{R}^{n_u} \times \mathbb{R}^{n_l} \to \mathbb{R}^{n_x}$ *is assumed to be piecewise Lipschitz continuous, and the derivative of the algebraic right hand side function* $g : \mathbb{R}^{n_x} \times \mathbb{R}^{n_u} \times \mathbb{R}^{n_l} \to \mathbb{R}^{n_z}$ *with respect to* $z$ *is assumed to be regular.* $x^I \in \mathbb{R}^{n_x}$ *represents the vector of initial conditions given at the initial time* $t^I$ *and the function* $\psi : \mathbb{R}^{n_x} \to \mathbb{R}^{n_q}$ *provides the terminal conditions at the final time and it is assumed to be twice differentiable. The system must satisfy algebraic path constraints given by the function* $\phi : \mathbb{R}^{n_x} \times \mathbb{R}^{n_u} \times \mathbb{R}^{n_l} \to \mathbb{R}^{n_\phi}$ *with lower bound* $\phi_l \in \mathbb{R}^{n_\phi}$ *and upper bound* $\phi_u \in \mathbb{R}^{n_\phi}$*. Function* $\phi$ *is assumed to be twice differentiable.*

## 4.2 Numerical methods

Optimal control problem in commonly used to solve the flight planing problem into the strategic perspective. Problem number of variables and its highly non-linearity make the numerical methods the typically used. There are three main approaches to numerically solve continuos time optimal control problems such as problem (OCP):

- **Dynamic Programming (DP) methods:** It is introduced by Bellman in the 1050s [14]. It transform a complex problem into a sequence of simpler problems called stages and this subproblem are linked together by a recurrence relation. Unfortunately, its application is severely restricted in the case of continuous states systems because of the exponential increase in size of the state space. Therefore, for solving nonlinear, continuous optimal control problems with a large number of variables, e.g., the aircraft trajectory planning problem, DP is clearly not adequate.

- **Indirect methods**: Indirect methods rely on Pontryagin's Maximum Principle [15]. Typically, the optimal control problem is turned into a two point boundary value problem containing the same mathematical information as the original one by means of necessary conditions of optimality. Then, the boundary value problem is discretised by some numerical technique to get a solution. Thus, Indirect methods follow a "first optimise, then discretise" scheme. Numerical techniques for solving this two point boundary value problem can be classified as gradient methods [16], indirect shooting and indirect multiple shooting [17, 18], and indirect collocation [19].

- **Direct methods:** The so called direct methods do not use the first-order necessary conditions of the continuous optimal control problem. They convert the infinite dimensional problem into a problem with a finite set of variables, and then solve the finite dimensional problem using optimisation methods. Direct methods thus follow a "first discretise, then optimise" approach. A typical strategy is to convert the infinite problem into a NLP problem which is solved using mathematical programming techniques

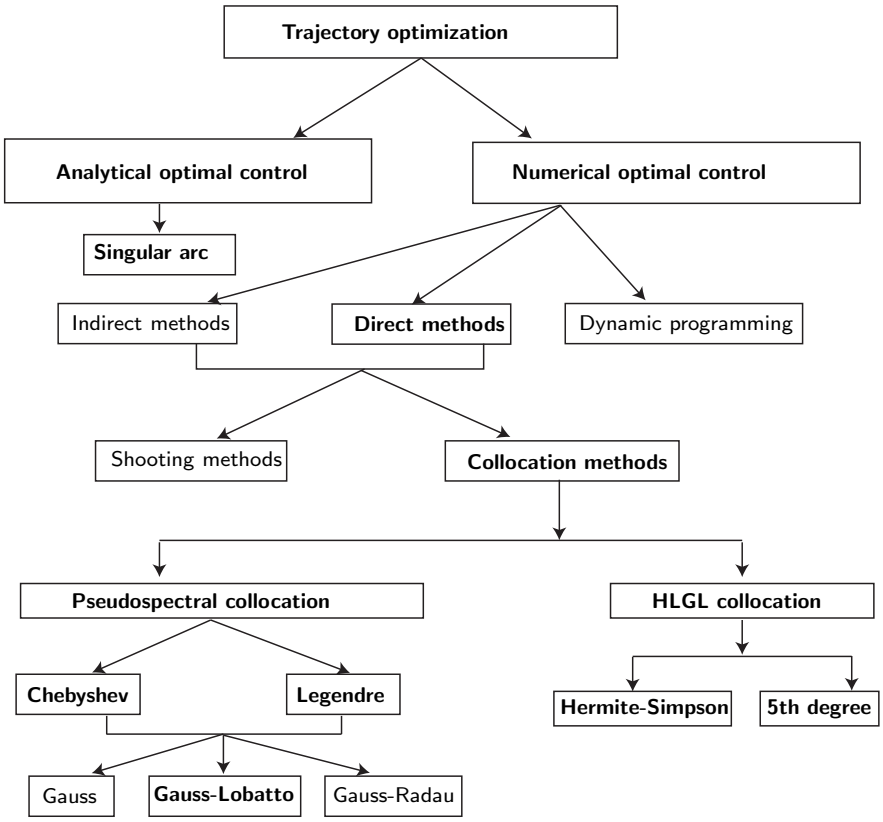


Figure 53: Taxonomy of trajectory optimization methods using optimal control.

[20, 21].The direct numerical methods can be classified as: direct shooting [22], direct multiple shooting [23] and direct collocation [24].

A taxonomy of optimal control methods for trajectory optimization is given in Figure 53. Notice that this taxonomy is not necessarily exhaustive. The reader is referred to [13, chapter 2.3.1] for all the detailed information about the **direct collocation using HLGL polynomials** used in the present chapter.

## 4.3 Pseudospectral collocation methods

Pseudospectral collocation methods approximate state and control variables through a sequence of global orthogonal polynomials. These polynomials are typically defined over the interval [-1,1]; they are the eigenfunctions of a suitable Sturm-Luiouville problem [25]. The two most frequently used are the Legendre and Chebyshev polynomials.

The Optimal Control Problem (OCP) has to be reformulated using a time affine transformation mapping $t \in [t_0, t_f]$ to $\tau \in [-1, 1]$. For instance, for a finite time horizon optimal control problem the mapping function is as follows:

$$t = \frac{t_f + t_0}{2} + \frac{t_f - t_0}{2}\tau. \tag{59}$$

In such a form the Optimal Control Problem (OCP) can now be rewritten taking into consideration that:

- The initial time and the final time are $\tau = -1$ and $\tau = 1$, respectively.
- The dynamic equations in OCP are: $\dot{x}(\tau) = \frac{t_f - t_0}{2} f(x(\tau), u(\tau), p)$.
- The path constraint and algebraic equations in OCP are: $\boldsymbol{\phi}[x(\tau), u(\tau), p] \leq 0$ and $0 = g(x(\tau), u(\tau), p)$, respectively.

### 4.3.1 Collocation points determination

Let us approximate each of the state variables (same approximation applies to control variables) as:

$$x(\tau) = \sum_{k=0}^{N} \frac{W(\tau)}{W(\tau_k)} x_k \phi_k(\tau), \tag{60}$$

where $k$ is an index denoting the node for the global Lagrange interpolating polynomial of order $N$, $W$ denotes a positive weight function, $x_k$ denotes the state value for node $k$, and $\phi_k(\tau)$ denotes the general expression for a Lagrange interpolation polynomial of degree N that satisfies $\phi_k(\tau_i) = 0, i \neq k$ and $\phi_k(\tau_k) = 1$, i.e.,

$$\phi_k(\tau) = \prod_{i=0, i\neq k}^{N} \frac{\tau - \tau_i}{\tau_k - \tau_i}. \tag{61}$$

Notice that $i$ is another index denoting the node for the global Lagrange interpolating polynomial of order $N$.

Collocation points in pseudospectral methods differ depending on the polynomial approximation used. In the Legendre pseudospectral methods they correspond to the zeros

of a specific Lagrange polynomials expression, otherwise in the Chebyschev pseudospectral methods the collocation points have a explicit formula.

**Legendre polynomials:** The Legendre polynomials $L_k(x)$, $k = 0, 1, ..., N$ are the eigenfunctions of the singular Sturm-Liouville problem denoted by

$$((1-\tau^2)L_k'(\tau))' + k(k+1)L_k(\tau) = 0, \tag{62}$$

which solution satisfies the following relation:

$$L_{k+1}(\tau) = \frac{2k+1}{k+1}\tau L_k(\tau) - \frac{k}{k+1}L_{k-1}(\tau), \tag{63}$$

with $L_0(\tau) = 1$ and $L_1(\tau) = \tau$.

Legendre pseudospectral methods utilize three different types of collocation points among those in the family of the Legendre-Gauss points [25], namely:

- The Legendre-Gauss (LG), where the collocation points $\tau_k(k = 0, \cdots, N)$ are the roots obtained from $L_{N+1}(\tau)$. In this group neither the initial point ($\tau = -1$) nor the endpoint ($\tau = 1$) are part of the collocation points.

- The Legendre-Gauss-Radau (LGR), where the collocation points $\tau_k(k = 0, ..., N)$ are the roots obtained from $L_N(\tau) + L_{N+1}(\tau)$, in these points only the origin ($\tau = -1$) is included.

- The Legendre-Gauss-Lobatto (LGL), where the collocation points $\tau_0 = -1, \tau_N = 1, \tau_k(k = 1, ..., N-1)$ are the roots obtained from $\dot{L}_N(\tau)$ and also is considered as collocation points the boundaries $\tau = -1$ and $\tau = 1$.

**Chebyshev polynomials:** The Chebyshev polynomials $T_k(\tau), k = 0, 1, \cdots, N$ are the eigenfunction of the singuar Sturm-Liouville problem denoted by:

$$(\sqrt{1-\tau^2}T_k'(\tau))' + \frac{k^2}{\sqrt{1-\tau^2}}T_k(\tau) = 0. \tag{64}$$

The solution to this problem satisfies the following relation:

$$T_k = cos(k\theta); \quad \theta = arccos(\tau). \tag{65}$$

Applying the trigonometric relation $\cos(k+1)\theta + \cos(k-1)\theta = 2\cos\theta\cos(k\theta)$, the solution to the problem result in the following recursive relation:

$$T_{k+1}(\tau) = 2\tau T_k(\tau) - T_{k-1}(\tau), \tag{66}$$

with $T_0 = 1$ and $T_1 = \tau$.

As in the previous case, Chebyshev pseudospectral methods utilize three different types of collocation points among those in the family of the Chebyshev-Gauss points [25], namely:

- Chebyshev-Gauss (CG): neither the initial point ($\tau = -1$) nor the endpoint ($\tau = 1$) are part of the collocation points.

$$\tau_k = cos\frac{(2k+1)\pi}{2N+2}, \quad k = 0, ..., N. \tag{67}$$

- Chebyshev-Gauss-Radau (CGR): only the endpoint ($\tau = 1$) is included.

$$\tau_k = cos\frac{2\pi k}{2N+1}, \quad k = 0, ..., N. \tag{68}$$

- Chebyshev-Gauss-Lobatto (CGL): both boundaries $\tau = -1$ and $\tau = 1$ are considered as collocation points.

$$\tau_k = cos\frac{\pi k}{N}, \quad k = 0, ..., N. \tag{69}$$

Figure 54 illustrates the non uniform grids of collocation points with eight samples for the aforementioned pseudospectral collocation methods.

The success or failure of a pseudospectral method depends on the type of optimal control problem, e.g., type of boundary conditions, the appropriate selection of time affine transformation and weight function, and the selection of the collocation points. This fact has been deeply studied by Fahroo and Ross in [26, 27, 28]. Table 16 summarizes the suitable choices

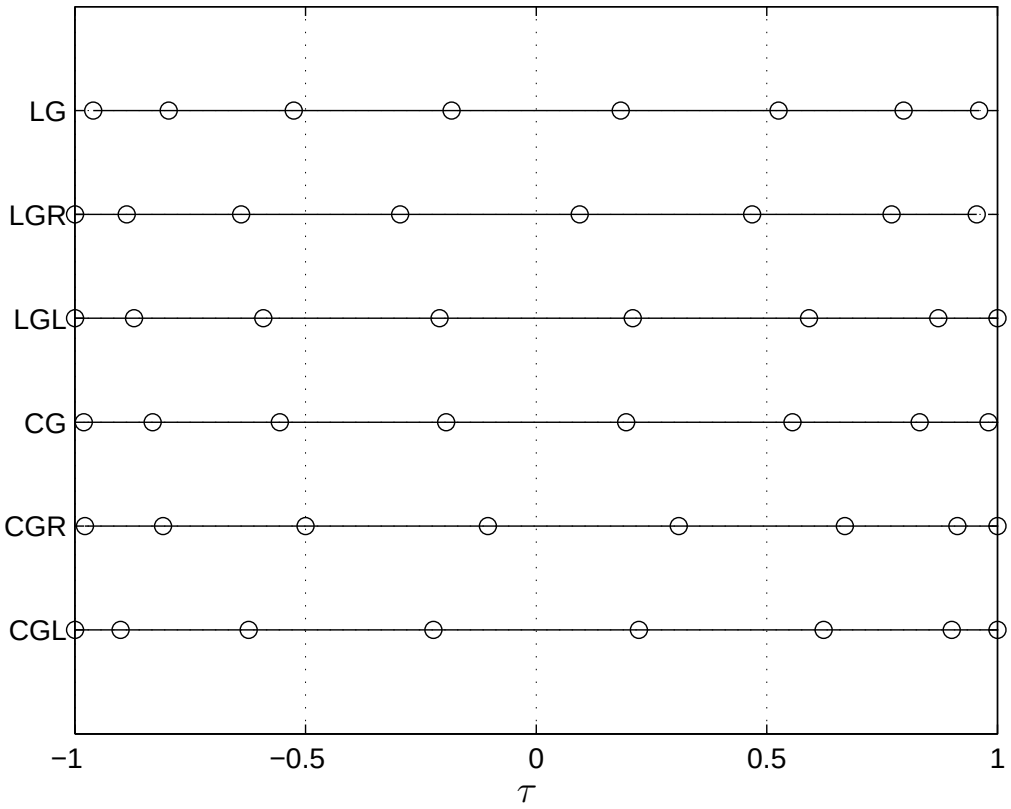


Figure 54: Pseudospectral methods collocation points (N=8).

within the above listed items. According to the type of problems arising in the scope of commercial aircraft trajectory optimization, i.e., optimal control problems with any kind of initial and final boundary conditions (fixed or free) and finite time horizon, the sequel will focus on both Legendre and Chebyschev pseudospectral methods based on Gauss-Lobatto collocation points.

Table 16: Pseudospectral methods' choices in optimal control problems.

| Weight functions | Collocation points | Boundary conditions | Typical horizon | Time transformation |
|---|---|---|---|---|
| $1-\tau^2$ | Gauss | Free-free | NA | NA |
| $1-\tau$ | Gauss-Radau | Fixed-free | Infinite | Bi-linear |
| 1 | Gauss-Lobatto | Any | Finite | Linear |

### 4.3.2 Application to differential equations

The first derivative of each of the state variables $\dot{x}(\tau(t))$ is approximated by the following equation:

$$\dot{x}(\tau_j) = \dot{x}(t_j)\frac{dt}{d\tau} \approx \sum_{k=0}^{N} x_k \dot{\phi}_k(\tau_j) = \sum_{k=0}^{N} D_{jk} x_k. \tag{70}$$

where $D_{jk}$ denotes the first derivative matrix of a Lagrange polynomial interpolation of order N ($\dot{\phi}_k(\tau(t))$).

In the case of Legendre-Gauss-Lobatto points (LGL), the Lagrange polynomial interpolation of order N is given by

$$\phi_k(\tau(t)) = \frac{1}{N(N+1)L_N(\tau_k)} \frac{(\tau^2-1)\dot{L}_N(\tau)}{\tau - \tau_k}. \tag{71}$$

and its first derivative matrix yields [29]:

$$D_{jk} = \begin{cases} \frac{L_N(\tau_j)}{L_N(\tau_k)} \frac{1}{\tau_j - \tau_k}, & j \neq k, \\ -\frac{(N+1)N}{4}, & j = k = 0, \\ \frac{(N+1)N}{4}, & j = k = N, \\ 0, & otherwise. \end{cases} \tag{72}$$

In the case of Chebyshev-Gauss-Lobatto points (CGL), the Lagrange polynomial interpolation of order N is given by

$$\phi_k(\tau(t)) = \frac{(-1)^{k+1}}{N^2 c_k} \frac{(1-\tau^2)\dot{T}_N(\tau)}{\tau - \tau_k}, \tag{73}$$

where

$$c_k = \begin{cases} 2, & k = 0, N, \\ 1, & k = 1, ..., N-1. \end{cases} \tag{74}$$

and its first derivative matrix yields [30]:

$$D_{jk} = \begin{cases} \frac{c_j}{c_k}\frac{(-1)^{j+k}}{\tau_j - \tau_k}, & j \neq k, \\ -\frac{\tau_k}{2(1-\tau_k^2)}, & 1 \leq j = k \leq N-1, \\ \frac{2N^2+1}{6}, & j = k = 0, \\ -\frac{2N^2+1}{6}, & j = k = N. \end{cases} \tag{75}$$

As mentioned before, the CGL collocation nodes are defined from 1 to $-1$. Therefore, a symmetric transformation is needed to make the initial point $-1$ and the final point 1. As a result both collocation nodes and the first derivative matrix have opposite sign after such transformation, i.e., $\hat{\tau} = -\tau$ and $\hat{D}_{jk} = -D_{jk}$.

### 4.4 Cases study

Aircraft fly following air routes that are composed of airways connected by waypoints. Typically, due to ATM requirements aircraft should accomplish with a Required Time of Arrival (RTA) over a prescribed waypoint. The optimal control problem (OCP) under analysis in this forthcoming cases study is that of finding the control inputs that steer an aircraft form a given initial condition towards reaching a particular waypoint at a prescribed RTA, fulfilling certain operational constraints, and at the same time minimizing the amount of fuel burnt in the process. A sketch of such problem is provided in Figure 55. The solution to the problem entails the optimal control inputs, yet the optimal four dimensional trajectory, i.e., the evolution of both control and state variables over time.

For trajectory planning purposes it is common to consider a 3 degree of freedom (3DoF) dynamic model that describes the point variable-mass motion of the aircraft over a spherical flat-earth model. We consider a symmetric flight, that is, we assume there is no sideslip and all forces lie in the plane of symmetry of aircraft. The resulting set of differential equations that govern the motion of the aircraft are as shown Equation 37.

The states are: the true airspeed, the heading angle, the flight-path angle, the longitu-

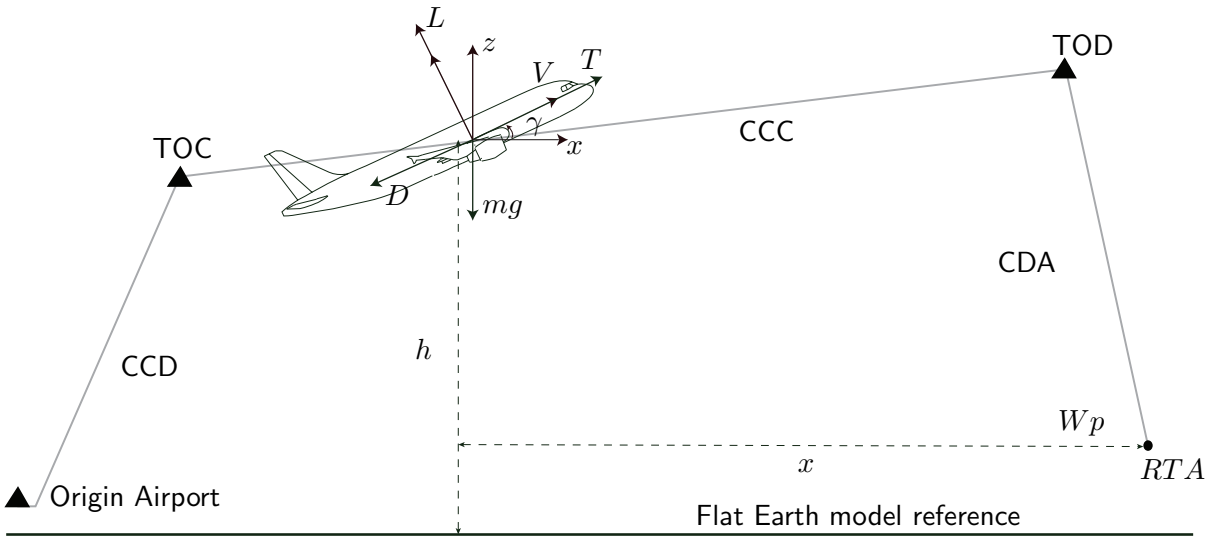


Figure 55: Sketch of the aircraft trajectory optimization problem. CCD is the continuous climb departure, CCC is the continuous cruise climb, CDA is the continuous descent appoarch, TOC is the top of climb, and TOD is the top of descent.

dinal position, the lateral position, the altitude, and the mass of the aircraft. A parabolic drag polar and an International Standard Atmosphere (ISA) model are assumed. Coefficient of lift is a known function of the angle of attack and the Mach number. The engine thrust, the coefficient of lift, and the bank angle, are the inputs of the 3DoF aircraft model. For further details on aircraft dynamics, please refer to [31].

The flight envelope constraints are derived from the geometry of the aircraft, structural limitations, engine power, and aerodynamic characteristics. We use the BADA performance limitations model and parameters [32]. For this particular problem, we have:

$$
\begin{array}{ll}
0 \leq h(t) \leq \min[h_{M0}, h_u(t)], & \gamma_{min} \leq \gamma(t) \leq \gamma_{max}, \\
M(t) \leq M_{M0}, & m_{min} \leq m(t) \leq m_{max}, \\
\dot{V}(t) \leq \bar{a}_l, & C_v V_s(t) \leq V(t) \leq V_{Mo}, \\
T_{min}(t) \leq T(t) \leq T_{max}(t), & 0 \leq C_L(t) \leq C_{L_{max}} \\
\dot{\gamma}(t) V(t) \leq \bar{a}_n, & \mu_{min} \leq \mu(t) \leq \mu_{max}.
\end{array}
$$

Note that the maximum dynamic altitude increases as fuel is burned, and also that several flight envelop constraints are nonconvex.

The previously described trajectory optimization problem is solved using four different collocation methods: Hermite-Simpson, 5th degree Gauss-Lobatto, Chebyshev-Gauss-

Lobatto and Legendre-Gauss-Lobatto. These methods have been hand-tailored and implemented in AMPL modeling language according to what has been exposed in section 4.2 and section 4.3 and using IPOPT as NLP solver.

Additionally, notice that since very recently there exist commercial-of-the-self softwares that implement pseudospectral collocation methods for solving optimal control problems. Two of the most well-known are DIDO and GPOPS [33, 34]. They run in an extensively used, user friendly software package as it is Matlab. The problems to be presented in the sequel of this manuscript have also been formulated and solved using these software tools. When compared to AMPL hand-tailored implementation and given that the same optimal solution is obtained, the former can be achieved at a much lower manpower employed. In other words, is much easier and straight forward to use DIDO and GPOPS than proceed on with a self-implementation from scratch. However, when it comes to analyzing the performances of the different methods, Matlab computation is much more involved.[1]

### 4.4.1 Unidimensional motion with Required Time of Arrival

The focus herein is on analysing a classical problem arising in ATM, i.e., the minimum fuel trajectory planning problem for an aircraft in cruise phase flying at constant flight level and following an airway from a starting waypoint towards achieving a pre-established RTA at the final waypoint. ISA atmosphere and calm conditions (no wind) are considered into the defined scenario.

#### Aircraft data, boundary conditions, and objective function

An Airbus 320 BADA 3.9 model has beed selected. Moreover, aircraft maximum thrust and specific fuel consumption are evaluated following BADA recommendations. The aerodynamic parameters are those for cruise flap configuration. All these parameters and specifications are available consulting [32].

[1] the authors acknowledge that computational time in Matlab depends strongly on the expertise of the user.

Table 17 shows the initial and final boundary conditions. The final mass and velocity are assumed to be free, nevertheless, final time is considered fixed due to the aircraft should accomplished the RTA. The objective functional is to minimize the total amount of fuel consumption.

Table 17: Boundary conditions.

| States and control variables | Initial conditions | Final conditions |
|---|---|---|
| Time $t[s]$ | 0 | 4,751 |
| Distance $x(t)[m]$ | 0 | 1,000,000 |
| Velocity $V(t)[kts]$ | 420 | Free |
| Mass $m(t)[kg]$ | 51,200 | Free |
| Thrust $T(t)[N]$ | Free | Free |

**Numerical results**

It has been proved that the KKT NLP necessary conditions approach the optimal control necessary conditions of optimality as the number of variables grows. Indeed, at the solution of the NLP problem, the Lagrange multipliers can be interpreted as discrete approximations to the optimal control adjoint variables [35]. Therefore, we first solve the trajectory optimization problem using the above mentioned direct collocation methods for an increasing number of sample points. Results for the Hermite-Simpson, the 5th degree, the LGL pseudospectral, and the CGL pseudospectral are presented in Table 18, Table 19, Table 20, and Table 21, respectively. Figure 60 and Figure 61 illustrate the different solutions for the true airspeed and the thrust of the aircraft.

Table 18: Numerical results Hermite-Simpson.

| Samples (N) | 25 | 50 | 100 | 200 | 400 | 800 |
|---|---|---|---|---|---|---|
| Fuel Consumption [kg] | 2521.89 | 2493.92 | 2483.93 | 2479.69 | 2477.74 | 2476.81 |
| CPU time in IPOPT (w/o function evaluation) [s] | 0.062 | 0.077 | 0.203 | 0.406 | 1.721 | 25.639 |
| CPU time in IPOPT NLP function evaluation [s] | 0.000 | 0.079 | 0.109 | 0.359 | 0.732 | 1.377 |
| Iterations | 19 | 21 | 18 | 23 | 20 | 21 |
| Total number of variables | 120 | 245 | 495 | 995 | 1995 | 3995 |
| Total number of eq. constraints | 96 | 196 | 396 | 796 | 1596 | 3196 |
| Total number of ineq. constraints | 72 | 147 | 297 | 597 | 1197 | 2397 |

Table 19: Numerical results 5th degree.

| Samples (N) | 25 | 50 | 100 | 200 | 400 | 800 |
|---|---|---|---|---|---|---|
| Fuel Consumption [kg] | 2509.53 | 2488.35 | 2479.85 | 2475.97 | 2474.11 | 2473.2 |
| CPU time in IPOPT (w/o function evaluation) [s] | 0.468 | 0.828 | 2.154 | 5.459 | 15.404 | 34.844 |
| CPU time in IPOPT NLP function evaluation [s] | 0.313 | 0.703 | 1.784 | 3.962 | 8.268 | 28.500 |
| Iterations | 33 | 34 | 39 | 41 | 42 | 70 |
| Total number of variables | 433 | 883 | 1783 | 3583 | 7183 | 14383 |
| Total number of eq. constraints | 336 | 686 | 1386 | 2786 | 5586 | 11186 |
| Total number of ineq. constraints | 288 | 588 | 1188 | 2388 | 4788 | 9588 |

Table 20: Numerical results Legendre-Gauss-Lobatto.

| Samples (N) | 5 | 10 | 20 | 40 | 80 | 160 | 200 |
|---|---|---|---|---|---|---|---|
| Fuel Consumption [kg] | 2508.1 | 2485.46 | 2473.06 | 2472.44 | 2472.3 | 2472.3 | 2472.3 |
| CPU time in IPOPT (w/o function evaluation) [s] | 0.046 | 0.110 | 0.251 | 0.235 | 0.734 | 9.842 | 11.545 |
| CPU time in IPOPT NLP function evaluation [s] | 0.000 | 0.000 | 0.015 | 0.015 | 0.079 | 0.173 | 0.174 |
| Iterations | 22 | 45 | 50 | 23 | 26 | 46 | 34 |
| Total number of variables | 20 | 40 | 80 | 160 | 320 | 640 | 800 |
| Total number of eq. constraints | 18 | 33 | 63 | 123 | 243 | 483 | 603 |
| Total number of ineq. constraints | 30 | 60 | 120 | 240 | 480 | 960 | 1200 |

Table 21: Numerical results Chebychev-Gauss-Lobatto.

| Samples (N) | 5 | 10 | 20 | 40 | 80 | 160 | 200 |
|---|---|---|---|---|---|---|---|
| Fuel Consumption [kg] | 2505.45 | 2483.78 | 2473.3 | 2472.41 | 2472.3 | 2472.3 | 2472.3 |
| CPU time in IPOPT (w/o function evaluation) [s] | 0.125 | 0.203 | 0.155 | 0.141 | 0.765 | 3.701 | 8.079 |
| CPU time in IPOPT NLP function evaluation [s] | 0.000 | 0.000 | 0.032 | 0.047 | 0.032 | 0.143 | 0.171 |
| Iterations | 82 | 65 | 40 | 21 | 25 | 30 | 32 |
| Total number of variables | 20 | 40 | 80 | 160 | 320 | 640 | 800 |
| Total number of eq. constraints | 18 | 33 | 63 | 123 | 243 | 483 | 603 |
| Total number of ineq. constraints | 30 | 60 | 120 | 240 | 480 | 960 | 1200 |

For the HLGL collocation methods, i.e., Hermite-Simpson and 5th degree, it can be observed that the objective function is very sensitive to the number of samples. This is specially noticeable for a low number of samples. Notice that by increasing the number of samples, the solution converges to a value of minimum fuel consumption (objective function) and so do velocity and thrust. Moreover, the instabilities due to the boundary conditions are soften as illustrated in Figure 60. These methods need a considerable amount of sample points to achieve the optimal solution, and thus the employed computational time is higher than in pseudospectral methods. This is because the grid of samples is uniformly distributed, and thus near the bounds of the interval the function approximation error is remarkably greater than in the center points of the interval. This is called the Ruge phenomenon[36].

On the contrary, the pseudospectral collocation methods, i.e., LGL and CGL, do not show much sensitivity to the number of samples, neither instabilities near the boundaries. This is due to the fact that pseudospectral methods employ a non-homogeneous grid of sample points, locating more sample points near the boundaries (where typically high frequency dynamics are found). See Figure 61.

We turn now the discussion to compare the performances in terms of accuracy and computational time of the different direct collocation methods. The solution to the different methods seems to converge towards a fuel consumption value of 2472.2 [kg]. Let us assume that value as the baseline for comparison. Notice that the accuracy value has been calculated through the following equation:

$$\varepsilon = \frac{(m_0 - m_f) - (m_0 - m_f)_{baseline}}{(m_0 - m_f)_{baseline}} \tag{76}$$

Table 22 presents the performances of the different collocation methods for a particular number of samples (40-50 samples). We observe a much higher accuracy for the pseudospectral methods at a similar computational time (ten times better when compared to the 5th degree collocation method). If one requires to achieve a particular accuracy, for instance of order $10^{-4}$, the amount of fuel burnt has to be lower or equal than 2474.6 [kg]. Table 23 presents the results in this case. Notice that the Hermite-Simpson method would not achieve such a degree of accuracy, whereas the 5th degree would need 400 samples and 23 seconds of computational time.

Table 22: Accuracy and computational time for the different collocation methods.

| | Samples (N) | Number of variables | Accuracy | CPU time [s] |
|---|---|---|---|---|
| Hermite-Simpson | 50 | 245 | $8.8 \cdot 10^{-3}$ | 0.1560 |
| 5th-Degree | 50 | 883 | $6.5 \cdot 10^{-3}$ | 1.5310 |
| LGL | 40 | 160 | $9.7080 \cdot 10^{-5}$ | 0.25 |
| CGL | 40 | 160 | $8.4945 \cdot 10^{-5}$ | 0.189 |

Table 23: Performances of the different collocation methods for an accuracy of order $10^{-4}$.

| | Samples (N) | Number of variables | Accuracy | CPU time [s] |
|---|---|---|---|---|
| Hermite-Simpson | - | - | - | - |
| 5th-Degree | 400 | 7183 | $7.7259 \cdot 10^{-4}$ | 23.672 |
| LGL | 20 | 80 | $3.4787 \cdot 10^{-4}$ | 0.267 |
| CGL | 20 | 80 | $4.4495 \cdot 10^{-4}$ | 0.187 |

All methods' solutions (based on the solutions with appropriate number of samples) are depicted together in Figure 56 for the sake of comparison. A singular arc solution, which is that by [2] and has been implemented and solve using the ODE 45 function in Matlab, has been also included. The first thing that can be observed is that all four direct collocation methods follow very similar patterns in terms of speed and TLP profile. In terms of performances, aircraft weight decreases with time since fuel is burned. Therefore, according to aircraft dynamics in Equation 37, velocity also decreases, and so does the throttle level position (the control input to speed up/slow down). It is important to observe that near the final fix, the throttle level goes down to stall the aircraft and thus save fuel. The behavior for the singular arc solution is slightly different. Singular arc solution provides 2507.7 [kg] of fuel consumption, around 4-5% more than direct solutions. This solution, even though is smoother and thus nice from an operational perspective, results less efficient than any of the ones provided by the different direct methods. This is because the singular arc solution does not consider constrained arcs. Indeed, as commented above, direct methods suggest that the optimal performance is to stall the aircraft (where the stall speed constraint implies a constrained arc) before reaching the final waypoint at the RTA. This is obviously unrealistic. Notice however that a similar behavior can be observed in Flight Data Records (FDRs) since the aircraft typically decelerates sharply in order to intercept the top of descent fix at the optimal (or required) descent speed. Therefore, the singular arc solution must be at some point complemented with another type of solution, for instance a minimum thrust one.

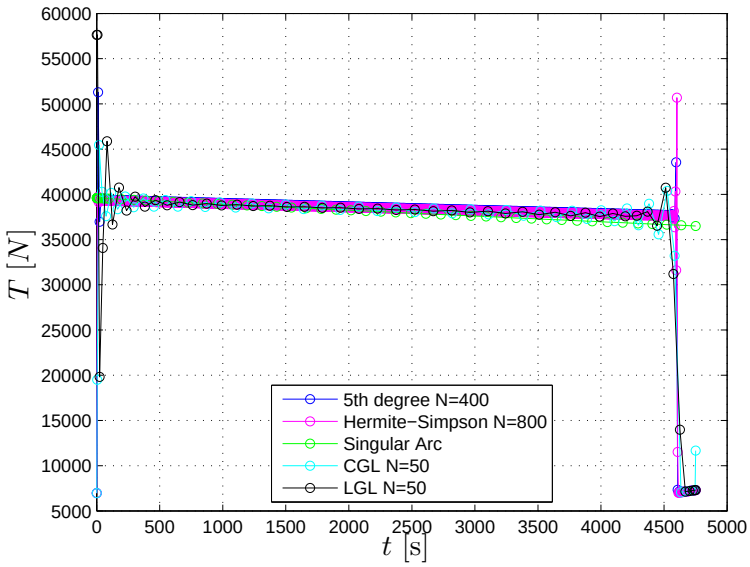


(a) Thrust vs time.

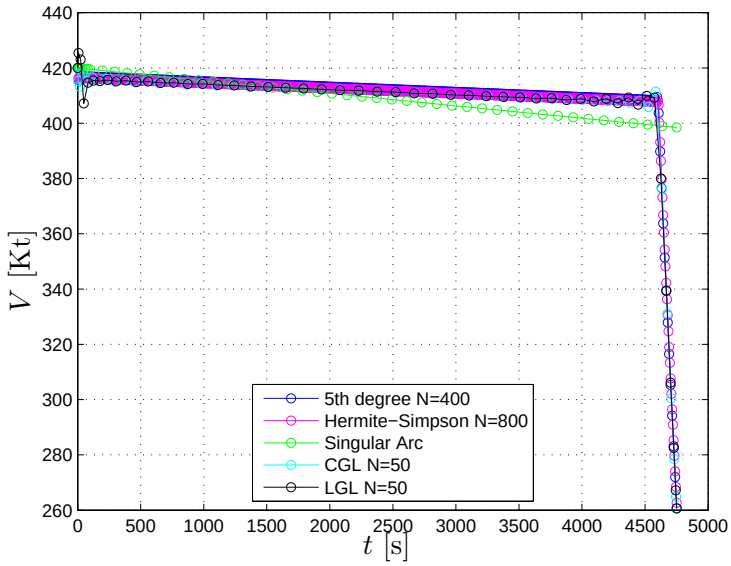


(b) Velocity vs time.

Figure 56: State variable $V(t)$ and control input $T(t)$ for Singular arc, Hermite-Simpson, 5th degree, Chebychev-Gauss-Lobatto (CGL) and Legendre-Gauss-Lobatto (LGL) simulations. N is the number of sample points.

### 4.4.2 Real trajectory (cruise, descent and landing) with Required Time of Arrival

With the aim at comparing current procedures with future, optimised aircraft performances, we analyse a 4D trajectory with RTA at a given final fix based on FDR data of an Airbus 319 real flight flying form El Cairo-Madrid. See Figure 57.

According to the previously presented analysis on the different numerical methods in subsection 4.4.1, both LGL and CGL pseudoespectral collocation methods are selected for solving the optimal control problem (OCP).

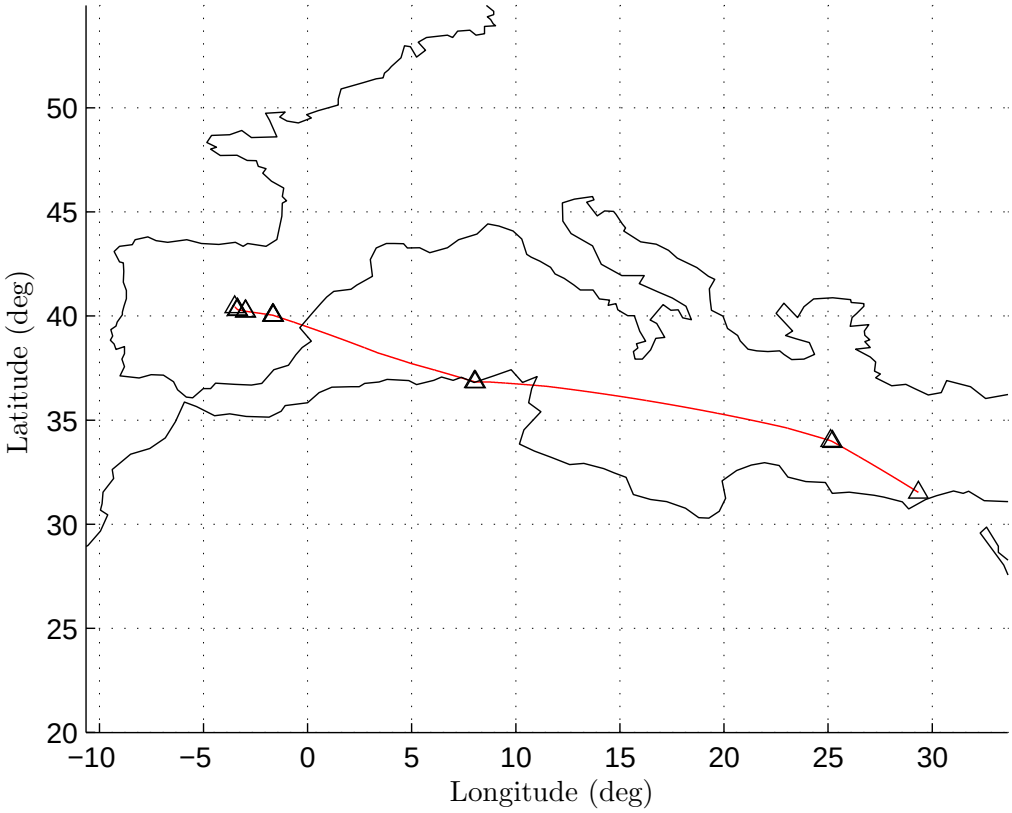


Figure 57: Aircraft horizontal profile. Triangles correspond to waypoints and the read line to the horizontal path.

In sum, the goal herein is to fairly compare current procedures, i.e., those read from the FDR, with optimised aircraft performances. For the sake of achieving a fair comparison,

an aircraft Trajectory Simulator (herein termed as aircraft TS) has been built using Matlab and Simulink so that both trajectories can be simulated with exactly the same models and parameters, i.e., aircraft model, atmosphere, wind conditions, etc.

As sketched in Figure 59, the process followed to compare both trajectories can be divided into three consecutive steps, namely, calibration, simulation, and comparison.

FDR information records real flight conditions, e.g., aircraft state and control variables, real atmosphere relevant variables, etc.; the optimal control problem (OCP) (which solution results in optimal performances) is formulated using BADA aircraft performance models, ISA, and wind as a function of the distance covered by the aircraft. It is straightforward to see that the optimal control problem modelling does not capture the FDR real behaviour. Thus in order the aircraft TS to perfectly reproduce the FDR trajectory, the former needs to be calibrated. In particular, specific fuel consumption has been corrected due to discrepancies between real consumption recorded in FDR and BADA models. Real wind has been approximated fitting the obtained from FDR by using the following polynomial:

$$\begin{aligned}\hat{w} = 6.798 \cdot 10^{-56} \cdot s^9 + 4.394 \cdot 10^{-48} \cdot s^8 - 5.164 \cdot 10^{-41} \cdot s^7 + 2.194 \cdot 10^{-34} \cdot s^6 \\ -4.435 \cdot 10^{-28} \cdot s^5 + 4.343 \cdot 10^{-22} \cdot s^4 - 1.653 \cdot 10^{-16} \cdot s^3 \\ -1.691 \cdot 10^{-11} \cdot s^2 + 1.547 \cdot 10^{-5} \cdot s - 35.28;\end{aligned} \tag{77}$$

where $s$ is the distance covered by the aircraft in meters.

Then, all the observed differences between FDR trajectory and aircraft TS variables are corrected as it can be observed in Figure 62. The result of this calibration process gives the calibrated aircraft TS. For more information on this regards the reader is referred to chapter 3.

For the simulation step, one just needs to independently (for both FDR data and optimal solution to Problem (OCP)) introduce the reference inputs to the calibrated aircraft TS. Finally, both trajectories can be compared as it will follow in Section 4.4.2.

### Aircraft data, boundary conditions, and objective function

Airbus 319 BADA 3.9 model has been used [32]. We just analyze the portion of the flight in which the aircraft flies in clean configuration. Table 24 present initial and final boundary conditions. The objective functional is to minimize the total amount of fuel consumption.

Table 24: Boundary conditions.

| States and control variables | Initial conditions | Final conditions |
|---|---|---|
| Time $t[s]$ | 0 | 16,306 |
| Distance $s(t)[m]$ | 0 | 3,148,981.97 |
| Altitude $h(t)[m]$ | 10,972.80 | 893.69 |
| Velocity $V(t)[kts]$ | 456.15 | Free |
| Mass $m(t)[kg]$ | 65,147 | Free |
| Thrust $T(t)[N]$ | Free | Free |

### Numerical results

We first solve the optimal control problem (OCP) using CGL and LGL pseudoespectral methods. Results are presented in Table 25. Notice that very similar results have been obtained using Hermite-Simpson and 5th-degree collocation methods. The already exposed in the previous case study in terms of accuracy and computational cost holds herein. Horizontal route, altitude profile, velocity profile, mass profile, throttle, and gamma are presented in Figure 58. The solution to the problem results precisely in a continuous climb cruise followed by continuous descent approach. In order to compare them, Figure 58 also presents its FDR counterpart.

Table 25: Numerical results pseudospectral methods.

| | Legendre-Gauss-Lobatto | | Chebyshev-Gauss-Lobatto | |
|---|---|---|---|---|
| Samples (N) | Fuel consumption [kg] | Computational time [s] | Fuel consumption [kg] | Computational time [s] |
| 5 | 8627.55 | 0.062 | 8597.86 | 0.062 |
| 10 | 8436.59 | 0.125 | 8422.73 | 0.125 |
| 20 | 8395.79 | 0.594 | 8391.02 | 0.515 |
| 40 | 8389.44 | 5.438 | 8390.19 | 3.641 |
| 80 | 8387.03 | 52.984 | 8386.87 | 26.797 |
| 160 | 8386.97 | 402.859 | 8387.01 | 352.328 |
| 320 | 8387.06 | 4,596.16 | 8387.07 | 4,704.98 |

Analyzing FDR data in Figure 58, it can be observed that the aircraft cruises at constant altitude and nearly at constant true airspeed. Nevertheless, true airspeed presents a step down, probably due to ATC advisories to avoid a potential hazard.

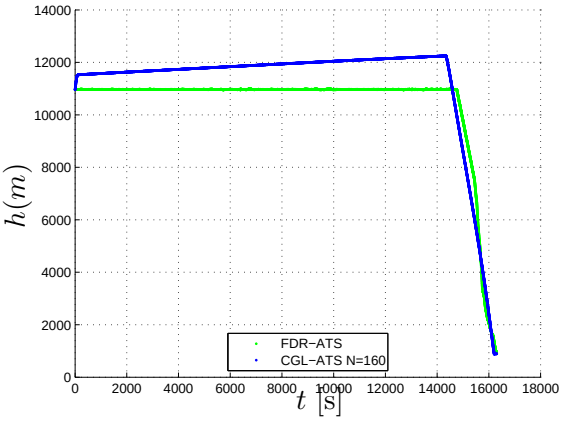


(a) Aircraft vertical profile.

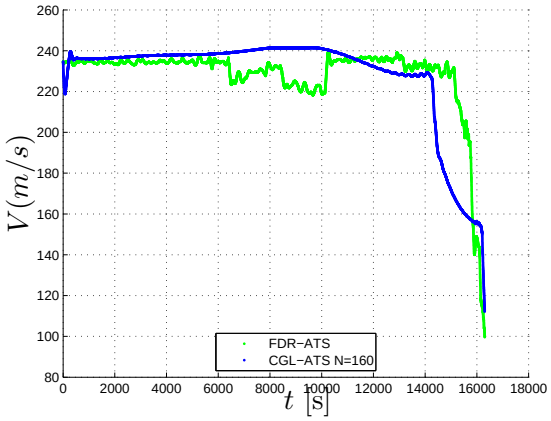


(b) TAS vs. time.

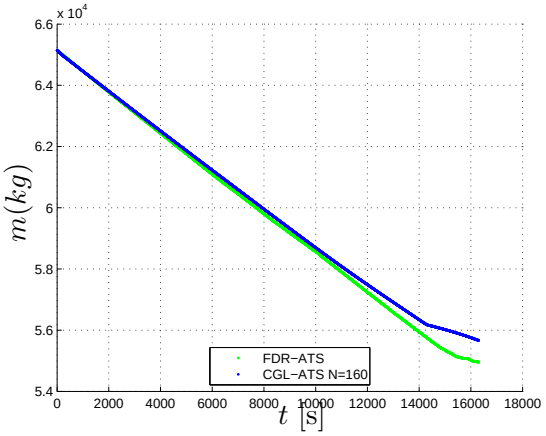


(c) Weight vs time.

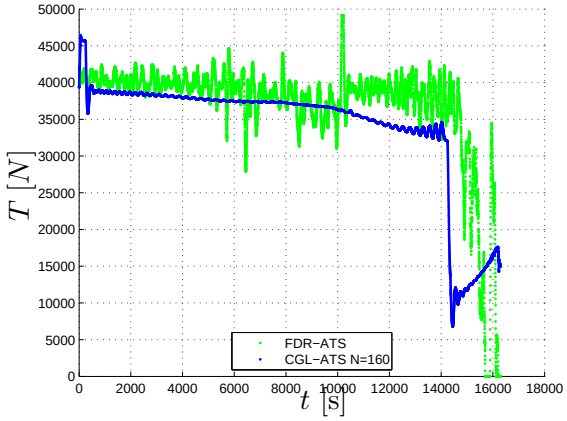


(d) Thrust vs time.

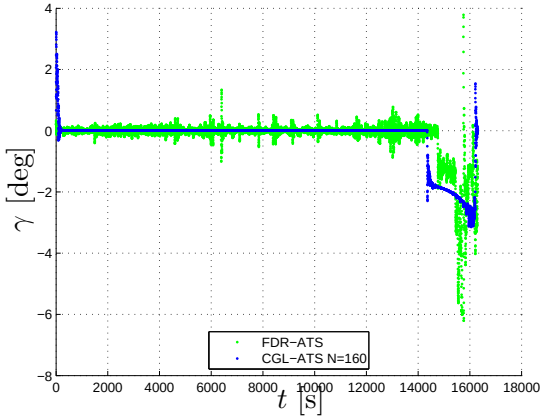


(e) Flight path angle vs time.

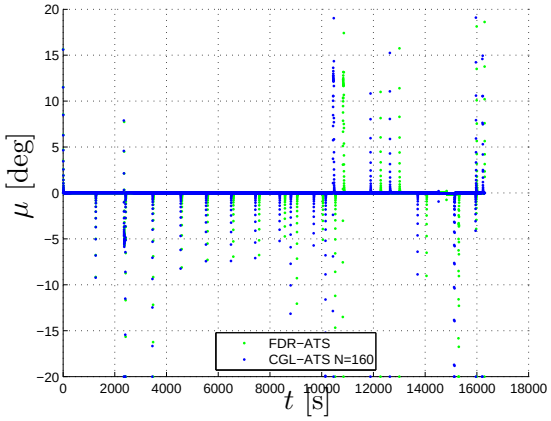


(f) Bank angle vs time.

Figure 58: Minimum fuel trajectory problem of a cruise, approach, and descent phase of flight with fixed arrival time. FDR-ATS corresponds to the FDR data simulated using the calibrated aircraft TS. CGL-ATS corresponds to the solution the Problem (OCP) using a CGL collocation method and simulated using the calibrated aircraft TS.

The optimal trajectory shows that aircraft best interest for saving fuel is to fly at the maximum operational altitude $h_u(t)$, which increases as fuel is burnt and which expression can be consulted in BADA manual. This is indeed a continuous climb cruise. Moreover, the Top of Descent (TOD) is located 300 [s] before the one for the FDR trajectory, and therefore the optimal strategy is to start descent earlier at a reduced speed and typically with idle thrust. The continuous descent from TOD towards runway head (or any intermediate waypoint before final approach) is referred to as continuous descent approach.

FDR trajectory's total fuel consumption (including cruise, descent and landing portions of the flight) amounts 10,177.32 [kg]. On the contrary, the solution to (OCP) provides 9,474.60 [kg] of fuel consumption, resulting in 702.73 [kg] less of fuel burnt than FDR's trajectory. If we restrict ourselves to analyzing the cruise phase of the real flight, FDR trajectory consumption is 9,666.75 [kg] whereas the optimal trajectory consumption is 9,061.35 [kg]. Savings for this flight portion would be 605.39 [kg]. Focusing on descent and approach, FDR trajectory burned 510.58 [kg] of fuel and the optimal trajectory based on a CDA procedure burned 413.24 [kg] of fuel, resulting in 97.33 [kg] of fuel savings only during descent. Please refer to Figure 58.

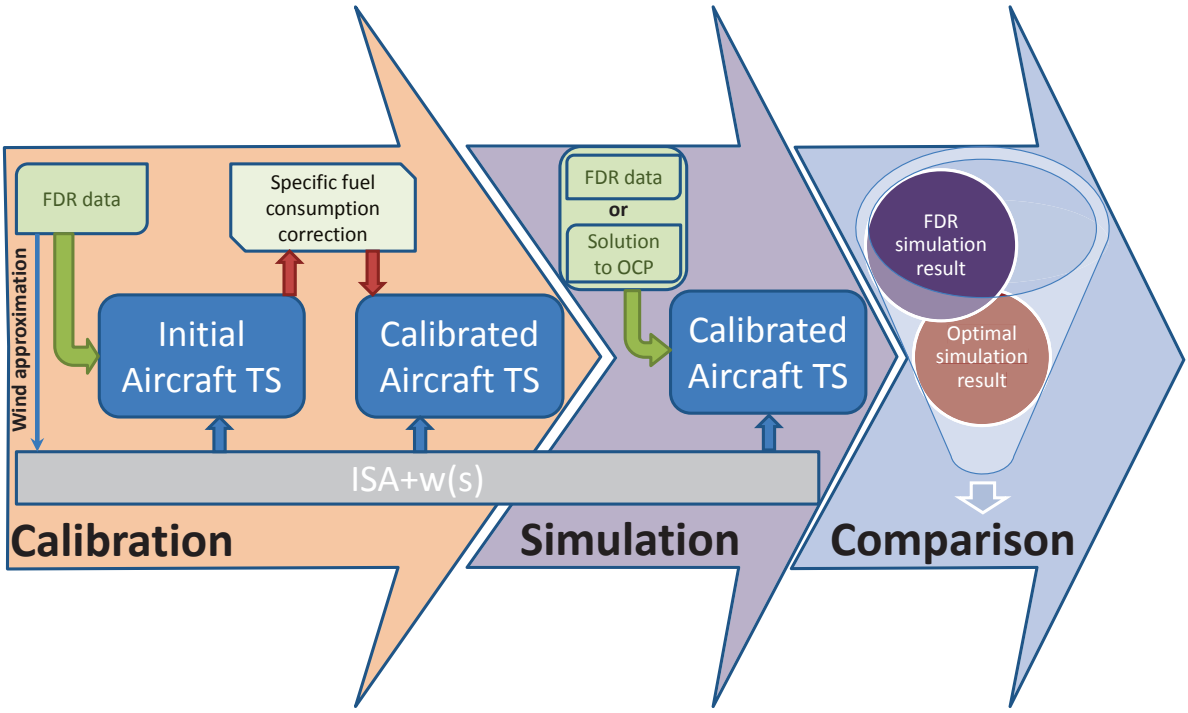


Figure 59: Simulation process.

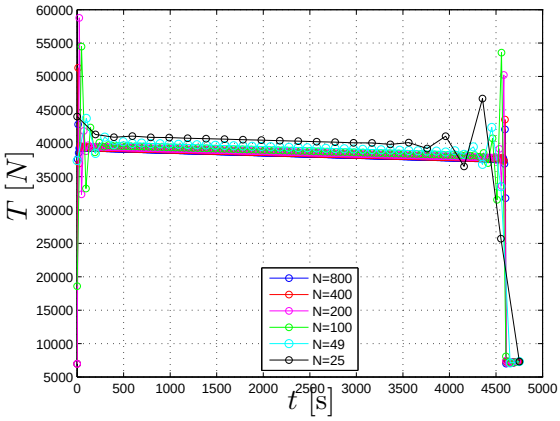


(a) 5th degree.

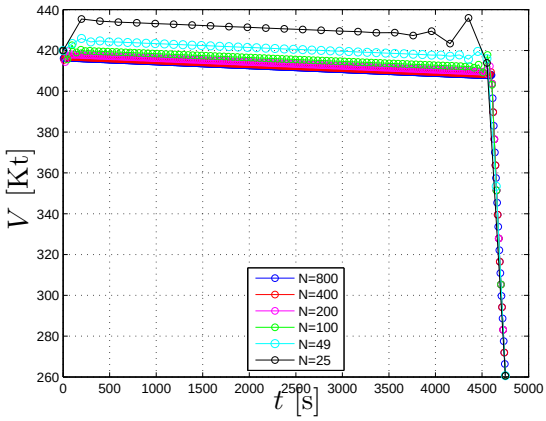


(b) 5th degree.

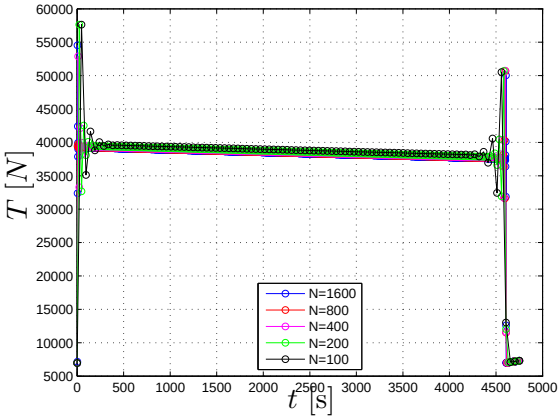


(c) Hermite-Simpson.

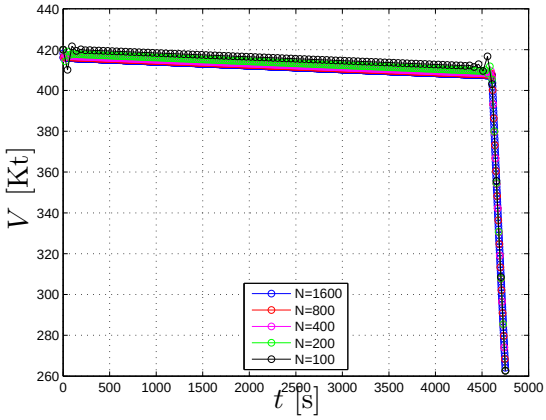


(d) Hermite-Simpson.

Figure 60: State variable $V(t)$ and control input $T(t)$ for different number of sample points.

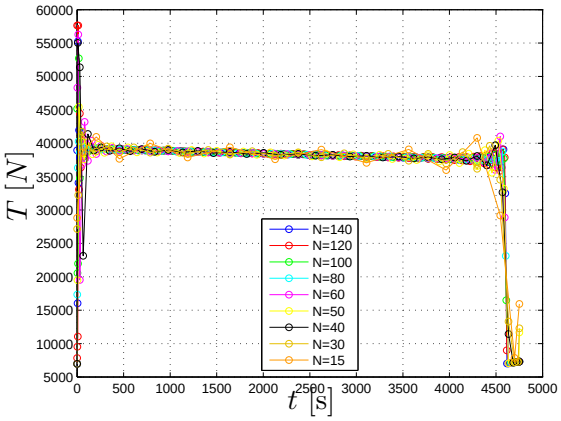


(a) Chebychev-Gauss-Lobatto.

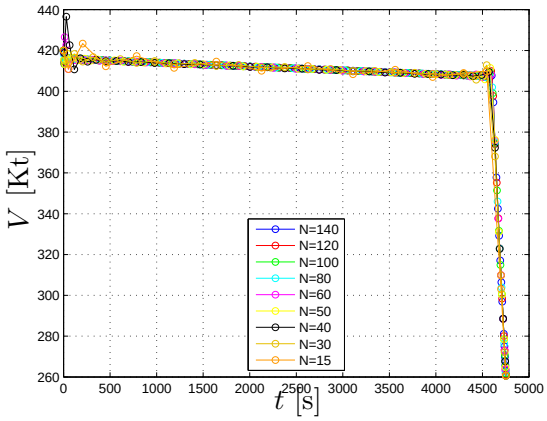


(b) Chebychev-Gauss-Lobatto.

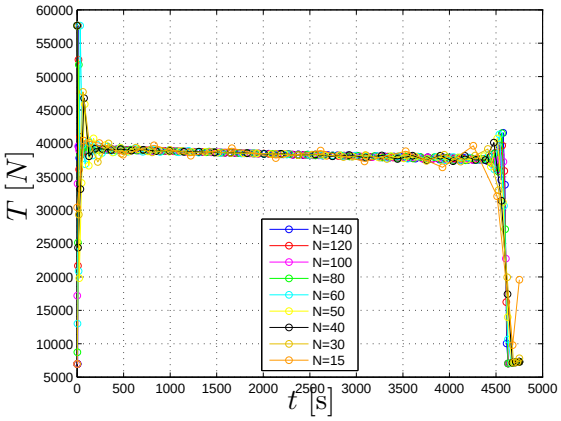


(c) Legendre-Gauss-Lobatto.

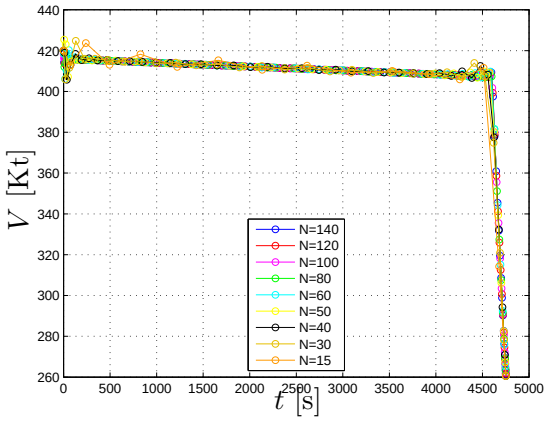


(d) Legendre-Gauss-Lobatto.

Figure 61: State variable $V(t)$ and control input $T(t)$ for different number of sample points.

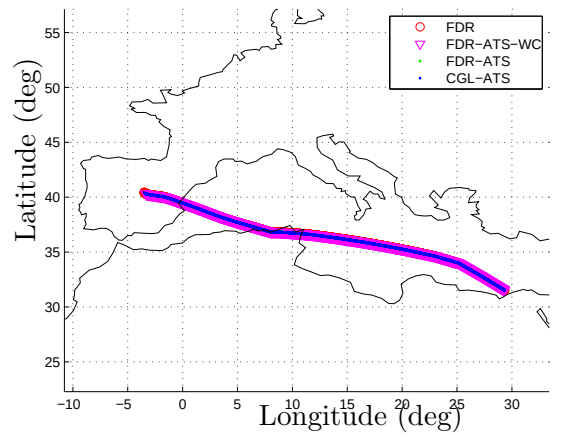


(a) Aircraft horizontal profile.

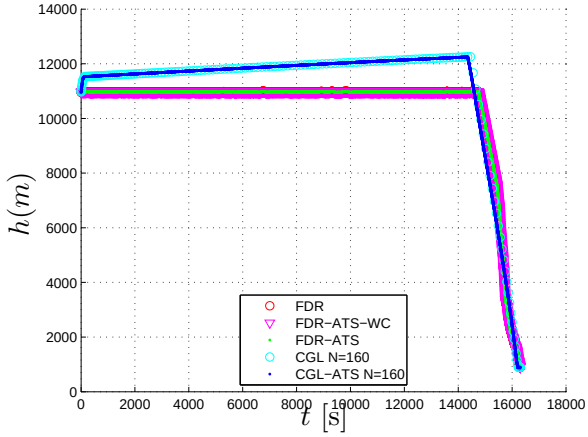


(b) Aircraft vertical profile.

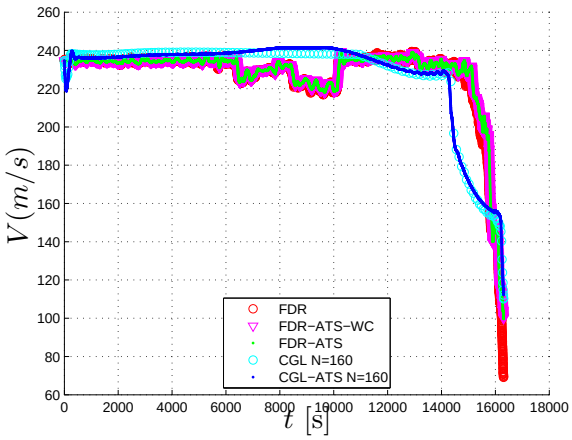


(c) TAS vs. time.

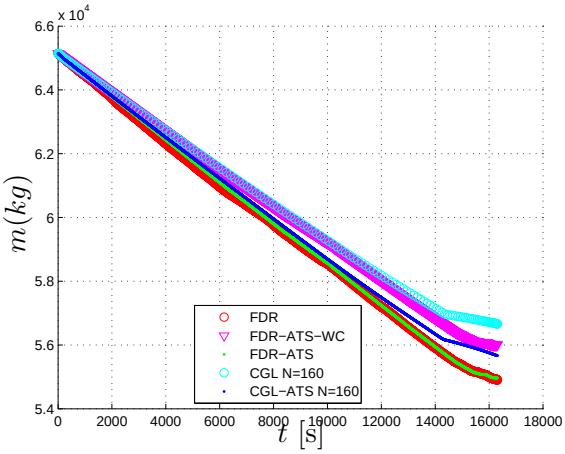


(d) Weight vs time.

Figure 62: Minimum fuel trajectory problem of a cruise, approach and descent phase of flight with fixed arrival time. FDR denotes the real FDR data. FDR-ATS-WC corresponds to the FDR data simulated using the initial aircraft TS. FDR-ATS corresponds to the FDR data simulated using the calibrated aircraft TS. CGL-ATS corresponds to the solution the Problem (OCP) using a CGL collocation method and simulated using the calibrated aircraft TS.

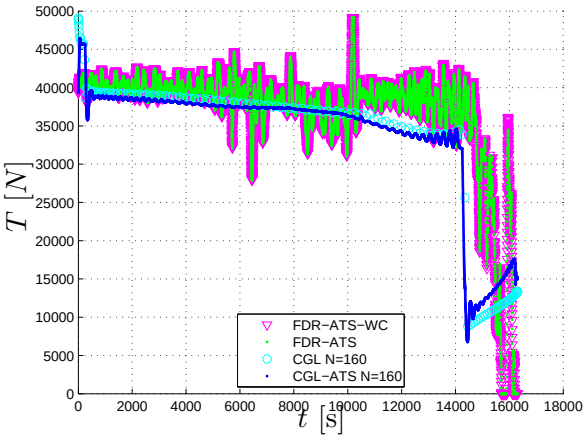


(a) Thrust vs time.

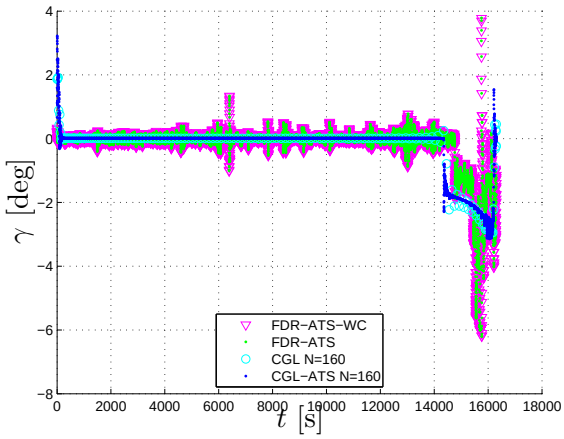


(b) Flight path angle vs time.

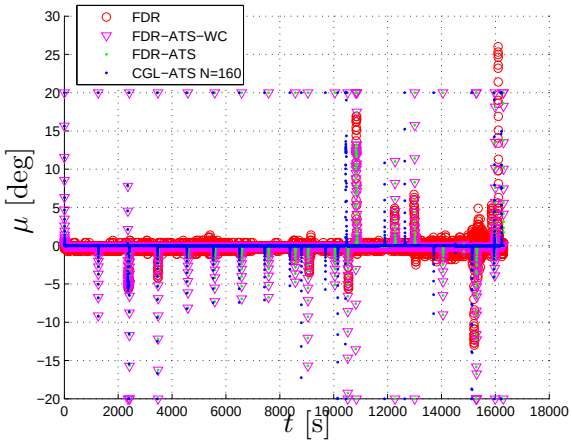


(c) Bank angle vs time.

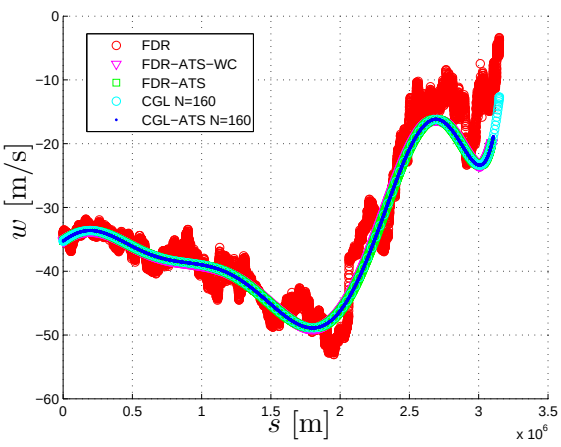


(d) Wind speed vs distance.

Figure 63: Minimum fuel trajectory problem of a cruise, approach and descent phase of flight with fixed arrival time. FDR denotes the real FDR data. FDR-ATS-WC corresponds to the FDR data simulated using the initial aircraft TS. FDR-ATS corresponds to the FDR data simulated using the calibrated aircraft TS. CGL-ATS corresponds to the solution the Problem (OCP) using a CGL collocation method and simulated using the calibrated aircraft TS.

### 4.5 Discussion on the results

The present chapter studies minimum fuel aircraft trajectory optimisation problems with fixed arrival time within Air Traffic Management constraints. Different direct collocation methods have been compared solving a classical type of problem arising in ATM, looking at a compromise between accuracy and computational time. On this regard, pseudospectral collocation methods seem to be the most suitable due to its fast and exponential convergence.

CGL method is slightly faster than LGL due to the fact that Legendre collocation points must be numerically calculated as the zeros of the appropriate polynomials.

A realistic aircraft trajectory optimisation problem under ATM constraints has been successfully solved using both CGL and LGL at a relatively low computational time and good accuracy. Real flight data based on FDR have been compared with optimal performances. Considering only cruise and descent portions of the flight, fuel savings in this case could reach up to 7% (702 [kg] of fuel, with the corresponding $CO_2$ emissions savings).

Unfortunately, the implementation of optimal profiles under the current ATM paradigm is still far from practical due to a set of issues that should be overcome: the heritage on flying based on pressure altitudes, the lack of automation and human decision support tools, uncertainty in the vertical trajectories during climbing/descent, etc. Fast and accurate optimal trajectory computation tools could support tactical modifications on the trajectory facilitating synchronisation between aircraft and ground systems trajectories.

### List of References


[1] Sesar Consortium, "The ATM target concept, SESAR definition phase milestone deliverable 3," September 2007.

[2] A. Franco, D. Rivas, and A. Valenzuela, "Minimum-fuel cruise at constant altitude with fixed arrival time," *Journal of Guidance, Control, and Dynamics*, vol. 33, no. 1, pp. 280–285, 2010.

[3] M. Davidsson, "Optimal Control for Dummies," *Current Research Journal of Economic Theory*, vol. 4, pp. 88–94, 2012. [Online]. Available: http://ssrn.com/abstract=2248368

[4] H. Sussmann and J. Willems, "300 years of optimal control: from the brachystochrone to the maximum principle," *Control Systems, IEEE*, vol. 17, no. 3, pp. 32–44, Jun.

[5] H. J. Sussmann and J. C. Willems, "The Brachistochrone Problem and Modern Control Theory," *Contemporary trends in non-linear geometric control theory and its applications*, pp. 113–165, 2002. [Online]. Available: http://math.rutgers.edu/~sussmann/papers/brachistochrone-mex.pdf

[6] J. C. Hayen, "Brachistochrone with coulomb friction," *International Journal of Non-Linear Mechanics*, vol. 40, no. 8, pp. 1057 – 1075, 2005. [Online]. Available: http://www.sciencedirect.com/science/article/pii/S0020746205000284

[7] R. Bhattacharya, "Optragen: A matlab toolbox for optimal trajectory generation," in *Decision and Control, 2006 45th IEEE Conference on*, 2006, pp. 6832–6836.

[8] S. Gómez-Aíza, R. W. Gómez, and V. Marquina, "A simplified approach to the brachistochrone problem," *European Journal of Physics*, vol. 27, no. 5, p. 1091, 2006. [Online]. Available: http://stacks.iop.org/0143-0807/27/i=5/a=008

[9] I. M. Gelfand and S. V. Fomin, *Calculus of Variations*. Dover Publications, Oct. 2000. [Online]. Available: http://www.amazon.com/exec/obidos/redirect?tag=citeulike07-20&path=ASIN/0486414485

[10] E. Pinch, *Optimal Control and the Calculus of Variations*. Oxford University Press, UK, 1993.

[11] O. Bolza, *Lectures on the Calculus of Variations*. Chelsea Publisher Company, New York, 1904. [Online]. Available: http://hdl.handle.net/2027/uc1.b4359558

[12] G. Bliss, *Lectures on the calculus of variations*, ser. Phoenix science series. University of Chicago Press, 1963.

[13] M. Soler, "Commercial aircraft trajectory planning based on multiphase mixed-integer optimal control," Ph.D. dissertation, Universidad Rey Juan Carlos, 2013. [Online]. Available: http://www.aerospaceengineering.es/publications/phd-thesis/

[14] R. Bellman, *Dynamic Programming*. Princeton UP, 1957.

[15] L. Pontryagin, V. Boltyanskii, R. Gamkrelidze, and E. Mishchenko, *The mathematical theory of optimal processes*. Interscience Publisher, 1962.

[16] H. Kelley, "Gradient theory of optimal flight paths," *AIAA Journal*, vol. 30, no. 10, pp. 947–954, 1960.

[17] U. Ascher, R. Mattheij, and R. Russell, *Numerical solution of boundary value Problems for Ordinary Differential Equations*. Society for Industrial and Applied Mathematics, 1995.

[18] J. Stoer and R. Bulirsch, *Introduction to Numerical Analysis*. Springer Verlag, 2002.

[19] U. Ascher, J. Christiansen, and R. Russell, "A collocation solver for mixed order systems of boundary value problems," *Mathematics of Computation*, vol. 33, no. 146, pp. 659–679, 1979.

[20] J. Nocedal and S. Wright, *Numerical Optimization*. Springer Verlag, 1999.

[21] P. Gill, W. Murray, and M. Wright, *Practical Optimization*. Academic Press, 1981.

[22] D. Kraft, "On converting optimal control problems into nonlinear programming problems," *Computational Mathematical Programming*, vol. 15, pp. 261–280, 1985.

[23] H. G. Bock and K. J. Plitt, "A multiple shooting algorithm for direct solution of optimal control problems," in *In Proceedings of the 9th International Federation of Automatic Control World Congress*, Budapest, Hungary. Pergamon Press, 1984, pp. 242–247.

[24] T. Tsang, D. Himmelblau, and T. Edgar, "Optimal control via collocation and non-linear programming," *International Journal of Control*, vol. 21, no. 5, pp. 763–768, 1975.

[25] C. Canuto, *Spectral methods: Fundamentals in single domains*. Springer Verlag, 2006.

[26] F. Fahroo and I. Ross, "On discrete-time optimality conditions for pseudospectral methods," in *AIAA/AAS Astrodynamics Specialist Conference and Exhibit*, 2006, pp. 21–24.

[27] F. Fahroo and I. M. Ross, "Pseudospectral methods for infinite-horizon nonlinear optimal control problems," *Journal of Guidance, Control, and Dynamics*, vol. 31, no. 4, pp. 927–936, 2014/04/15 2008. [Online]. Available: http://dx.doi.org/10.2514/1.33117

[28] F. Fahroo and I. M. Ross, *Advances in Pseudospectral Methods for Optimal Control*. American Institute of Aeronautics and Astronautics, 2014/04/15 2008. [Online]. Available: http://dx.doi.org/10.2514/6.2008-7309

[29] I. Ross and F. Fahroo, "Legendre pseudospectral approximations of optimal control problems," in *New Trends in Nonlinear Dynamics and Control and their Applications*, ser. Lecture Notes in Control and Information Science, W. Kang, C. Borges, and M. Xiao, Eds. Springer Berlin Heidelberg, 2003, vol. 295, pp. 327–342. [Online]. Available: http://dx.doi.org/10.1007/978-3-540-45056-6_21

[30] F. Fahroo and I. Ross, "Direct trajectory optimization by a Chebyshev pseudospectral method," *Journal of Guidance, Control, and Dynamics*, vol. 25, no. 1, pp. 160–166, 2002.

[31] D. G. Hull, *Fundamentals of Airplane Flight Mechanics, 1st. edn.* New York, United States of America: Springer-Verlag Berlin and Heidelberg GmbH & Co. K, 2007.

[32] Nuic A., *User Manual for the base of Aircraft Data (BADA) Revision 3.9*, Eurocontrol Experimental Cente, 2008.

[33] I. M. Ross, *A Beginner's Guide to DIDO. A MATLAB Application Package for Solving Optimal Control Problems*, September 2010.

[34] A. V. Rao, D. A. Benson, C. Darby, M. A. Patterson, C. Francolin, I. Sanders, and G. T. Huntington, "Algorithm 902: Gpops, a matlab software for solving multiple-phase optimal control problems using the gauss pseudospectral method," *ACM Transactions on Mathematical Software (TOMS)*, vol. 37, no. 2, p. 22, 2010.

[35] J. T. Betts, *Practical Methods for Optimal Control and Estimation using Nonlinear Programming*. Advances in Design and Control. Society for Industrial and Applied Mathematics, 2010.

[36] D. Garg, "Advances in global pseudospectral methods for optimal control," Ph.D. dissertation, University of Florida, 2011.

# CHAPTER 5

## Effects of atmospheric characteristics on the aircraft optimal trajectory

Atmospheric characteristics such as: pressure, density, temperature, and humidity play a crucial role in altering the efficacy of the airplane engine and/or the aerodynamic capability of the aircraft to fly, thus affecting the aircraft performance. In this section, a study of the effect that variation in the atmosphere variables have into the minimum fuel trajectory problem using a Chebyshev-Gauss-Lobatto (CGL) pseudospectral collocation method has been developed. To accomplish this, the case study of the subsection 4.4.2 is used to reproduce the different aircraft trajectories and it is previously calibrated at the ISA atmosphere conditions, as is denoted by Figure 59. After this process, the aircraft TS has been corrected with: -0.0655 [kg/s] term in the $\dot{m}$ equation (as shown Equation 58) when a real atmosphere is introduced, and -0.065 [kg/s] when the wind is approximated according to Equation 77 and ISA model.

All simulations performed have followed the same horizontal trajectory profile from the initial point to the final WP (denoted as a black triangle), which is located at 3 [NM] (5556 [m]) from the Madrid-Barajas airport, as shown Figure 57.

In the presented final WP the following information is analyzed:

- **Cost index**: time and the fuel consumption relatives to the real trajectory $\left(\frac{t_f}{t_{f_{rel}}}, \frac{f_f}{f_{f_{rel}}}\right)$ simulated in ISA atmosphere conditions ratio. This variable has four representatives ranges of values: $\frac{t_f}{t_{f_{rel}}}, \frac{f_f}{f_{f_{rel}}} < 1$; $\frac{t_f}{t_{f_{rel}}} < 1 \wedge \frac{f_f}{f_{f_{rel}}} > 1$; $\frac{t_f}{t_{f_{rel}}} > 1 \wedge \frac{f_f}{f_{f_{rel}}} < 1$; $\frac{t_f}{t_{f_{rel}}}, \frac{f_f}{f_{f_{rel}}} > 1$.

  The first area is the most desirable, because aircraft reaches the desired point in less time and fuel consumption. In the following region, the aircraft spend more fuel but with a reduction in the time to reach the final WP. The opposite situation happens in the third region, with less fuel consumption more time is needed to reach the final

point. The fourth one is the most avoidable area due to the fact that is necessary both more time and fuel to arrive in the final WP.

- **Energy index**: potential and kinetic energy relatives to the real trajectory $\left(\frac{PE_f}{PE_{f_{rel}}}, \frac{KE_f}{KE_{f_{rel}}}\right)$simulated in ISA atmosphere conditions. This variable has four representatives ranges of values: $\frac{PE_f}{PE_{f_{rel}}}, \frac{KE_f}{KE_{f_{rel}}} < 1$; $\frac{PE_f}{PE_{f_{rel}}} < 1 \wedge \frac{KE_f}{KE_{f_{rel}}} > 1$; $\frac{PE_f}{PE_{f_{rel}}} > 1 \wedge \frac{KE_f}{KE_{f_{rel}}} < 1$; $\frac{PE_f}{PE_{f_{rel}}}, \frac{KE_f}{KE_{f_{rel}}} > 1$.

  The first area is the most avoidable due to the aircraft has a low level of energy to land and it could have to use engine thrust to reach the airport and therefore fuel consumption will appreciably increase. Nevertheless, if the final WP was close to the airport this situation is the most beneficial to a better energy use. The second and third section have more for one kind of energy potential of kinetic, but is important to note that a energy exceedance should be compatible with the aircraft performances to reach runway. The last section has the opposite behaviour than the fist area, as final WP is located far to the airport is a very good situation to use this extra energy without using the engine thrust. On the contrary, if the final WP was close to the airport, the aircraft would have to use an inefficient aircraft configuration with the corresponding waste of energy.

- **Figure of merit**: is the indicator of the relationship between existing energy in the final WP and its cost index, it is denoted by the following equation:

$$FM = \frac{\sqrt{\left(\frac{PE_f}{PE_{f_{rel}}}\right)^2 + \left(\frac{KE_f}{KE_{f_{rel}}}\right)^2}}{\sqrt{\left(\frac{t_f}{t_{f_{rel}}}\right)^2 + \left(\frac{f_f}{f_{f_{rel}}}\right)^2}} \tag{78}$$

  A greater than one figure of merit value implies that more energy is produced to less operational cost which is the most desirable situation.

In the present section the following different data sources are analyzed:

- **FDR-ATS**: is the result of introducing the real FDR data into the aircraft TS with real atmosphere conditions. Real speed and altitude have been introduced as the inputs reference values of the aircraft TS.

- **FDR-ATS-ISA**: is the result of introducing the real FDR data into the aircraft TS with ISA atmosphere model. Real speed and altitude have been introduced as the inputs reference values of the aircraft TS.

- **CGL-ATS-ISA**: is the result of introducing the solution to the Optimal Control Problem (OCP) using the CGL pseudospectral collocation method with 80 collocation points and ISA atmosphere model, into the aircraft TS with the studied ISA atmosphere model. Optimal speed and altitude values have been introduced as the inputs reference values of the aircraft TS.

- **CGL-ATS-ISA-opt**: is the result of introducing the solution to the OCP using the CGL pseudospectral collocation method with 80 collocation points and the studied ISA atmosphere model, into the aircraft TS with the same ISA atmosphere model. Optimal speed and altitude values have been introduced as the inputs reference values of the aircraft TS.

This section includes five different cases of study: different temperature at MSL altitude, different troposphere temperature lapse rate values, different pressure at MSL altitude, different extreme pressure and temperature at MSL values, and a mesh grid including temperature and pressure variation at MSL.

## 5.1 Different ISA temperature at MSL

At different temperatures for an assigned barometric altitude, aerodynamic forces are different. This fact has a direct relationship with time, fuel consumption and range of the flight. The goal is to establish how current and optimal vertical procedures are affected by

different ISA vertical temperatures distributions from ISA-20° to ISA+20° in intervals of 5°. These atmosphere vertical distribution are represented in Figure 64.

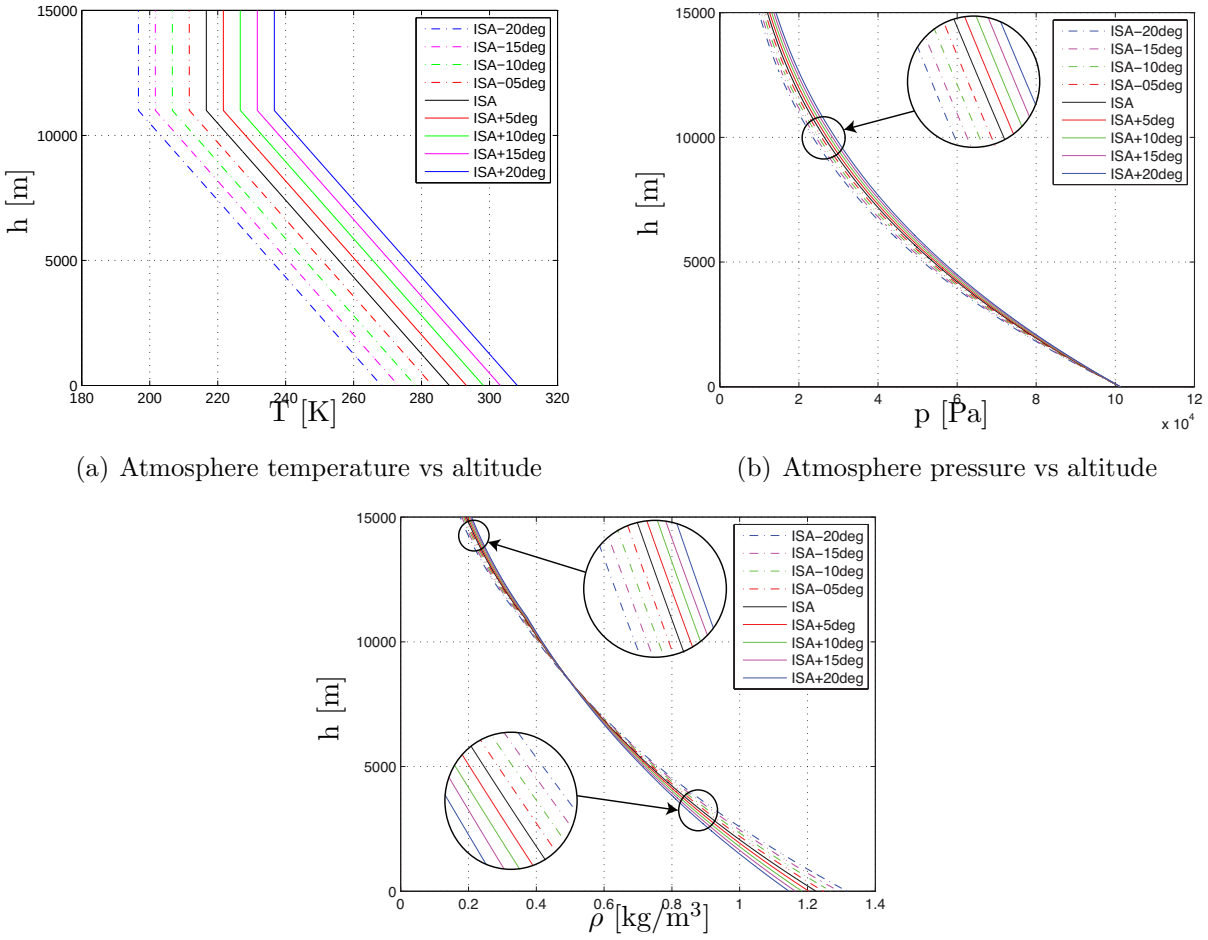


(a) Atmosphere temperature vs altitude

(b) Atmosphere pressure vs altitude

(c) Atmosphere density vs altitude

Figure 64: Atmosphere model temperature variation

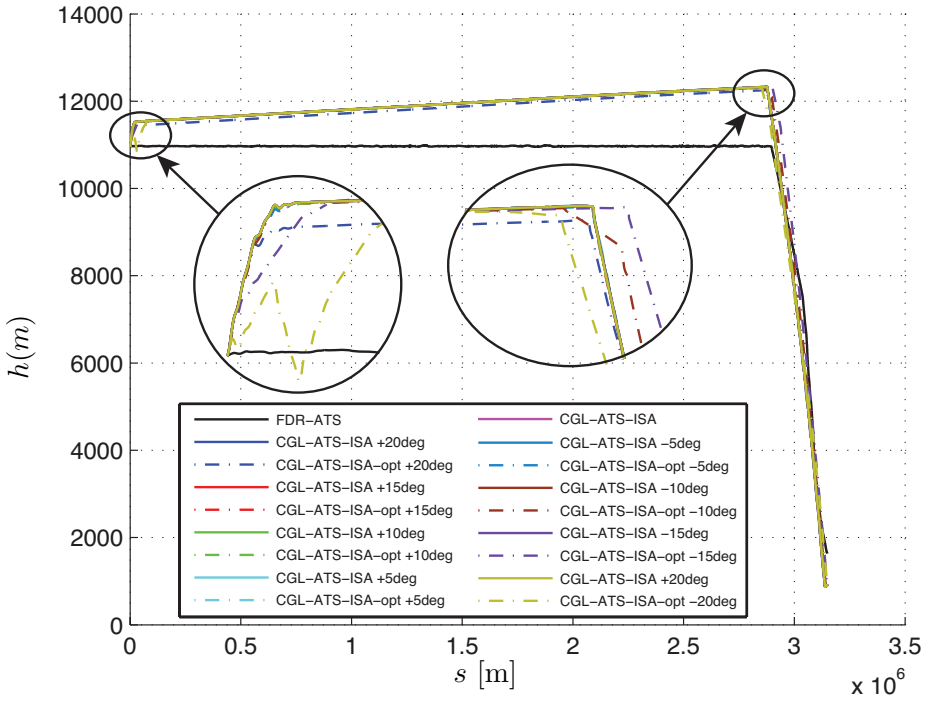


Figure 65: Altitude vs. distance in the temperature variation case of study.

Figure 65 shows that CGL-ATS-ISA different simulation has exactly the same vertical profile since all of them have the same altitude reference value, introduced into the aircraft TS (referred to the ISA). Also, in the CGL-ATS-ISA-opt just in the extreme negative ISA simulation (-15° and -20°), the Top Of Descent (TOD) is located in a different position than in the other simulation results.

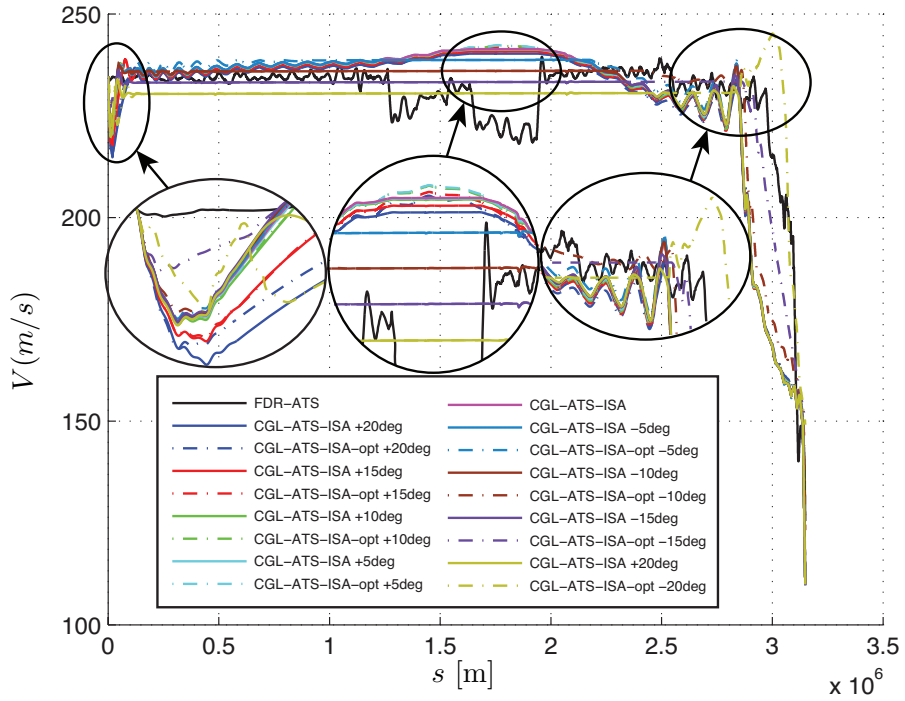


Figure 66: True Air Speed vs. distance in the temperature variation case of study.

In relation to the TAS representation in Figure 66, there are three areas that should be analysed: the origin, the middle and the final area. The first area is characterised by a decreasing in the velocity values for the all simulations. This effect is because the aircraft is increasing highly in altitude until the operational ceiling is reached. Then, in the middle area, TAS reaches a maximum value which has certain differences between the CGL-ATS-ISA and the CGL-ATS-ISA-opt. The CGL-ATS-ISA-opt and the CGL-ATS-ISA as higher ISA temperature is decreasing from the ISA lower and constant TAS values are resulting. This constant value under these circumstances responds to the maximum possible Mach value according to the BADA 3.9 in this kind of aircraft (0.82 in the A319) [1]. Nevertheless, in CGL-ATS-ISA-opt at ISA+5° presents the maximum TAS value in comparison with the other atmosphere condition. TAS is slightly decreasing when ISA temperature is increased. The same effect is happening in the CGL-ATS-ISA but all their TAS values are bellow the

CGL-ATS-ISA at ISA atmosphere conditions simulation. Therefore, in the middle section, only when temperature increases from ISA, differences appear between CGL-ATS-ISA and CGL-ATS-ISA-opt being higher speed the CGL-ATS-ISA-opt correspondent. Besides, when the ISA reference is introduced into the FCS (CGL-ATS-ISA), TAS has lower values in all the atmosphere scenarios than the ISA. This is different to the altitude representation when all the values are coincident. This is because velocity is more thrust dependent and thrust is highly density dependent.

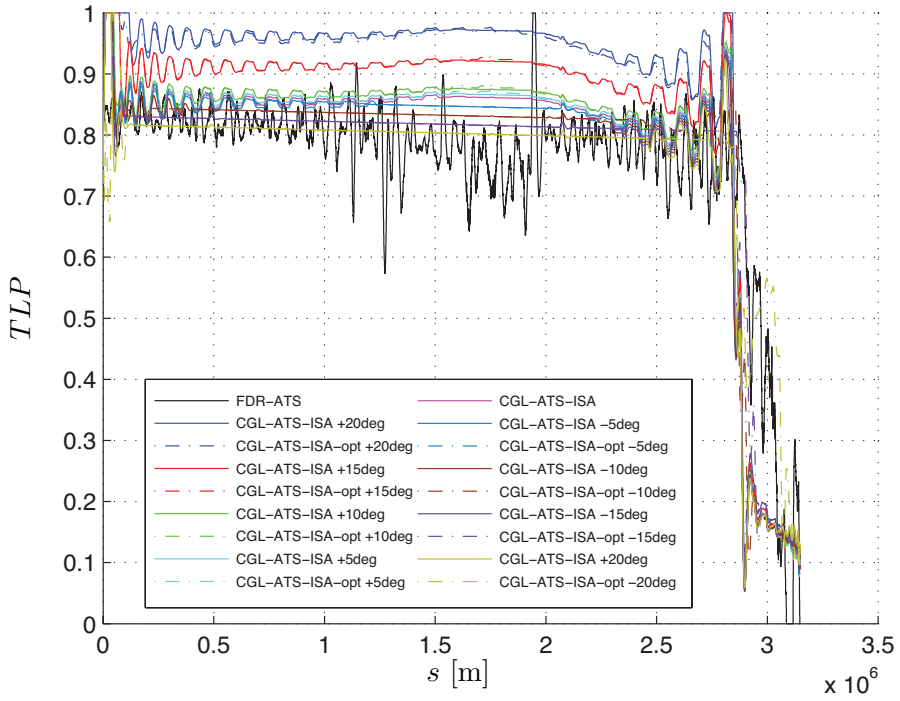


Figure 67: Throttle Lever Percentage vs. distance in the temperature variation case of study.

Finally the TLP in Figure 67 shows as higher temperature aircraft has to use more thrust. Moreover, CGL-ATS-ISA and CGL-ATS-ISA present similar results in TLP values at the same atmosphere condition.

### 5.1.1 Cost index analysis

Figure 68 shows final simulation time and fuel consumption when ISA temperature is modified referred to the FDR-ATS-ISA at ISA conditions. Three different simulations are presented: FDR-ATS-ISA, CGL-ATS-ISA and CGL-ATS-ISA-opt. The three kind of simulations have a fuel consumption reduction when ISA temperature decreases being this an almost linear tendency. As an exception to this fact, CGL-ATS-ISA-opt simulation at ISA-20° has a higher fuel consumption because in the optimal solution the Mach value saturation produced that when aircraft is losing altitude (at the end of the trajectory) the aircraft have to reach higher speed producing an increase in fuel consumption in comparison with the others. In addition, optimal trajectories have between 5 and 9% fuel consumption savings (575-920 [kg]) with respect to current vertical trajectories.

Otherwise, in the final time, the minimum value is always presented in the ISA simulation, increasing this final time value in both situations when the temperature increases or decreases from ISA. Also, it is observed that in lower temperature the final time has an enormous growth. This effect is produced since lower temperatures make higher Mach values, and therefore, TAS should be lower thus more time is needed to reach the final WP. Moreover, CGL-ATS-ISA and CGL-ATS-ISA-opt trajectories show the same values in final time and fuel consumption in hotter ISA temperatures. However, when temperature is lower than ISA conditions CGL-ATS-ISA spends more time to reach the final point because the ISA speed reference value produces a saturation Mach behaviour. For instance, at ISA-20 CGL-ATS-opt saves 720 [kg] more than in FDR-ATS-ISA ISA conditions, by contrast FDR-ATS-ISA 171 [kg] and CGL-ATS-ISA 920 [kg], the last one even being where more fuel is saved the aircraft needs 7 minutes more than FDR-ATS-ISA at ISA conditions, however FDR-ATS-ISA 3.4 minutes and CGL-ATS-ISA-opt near 1 minute before FDR-ATS-ISA at ISA conditions.

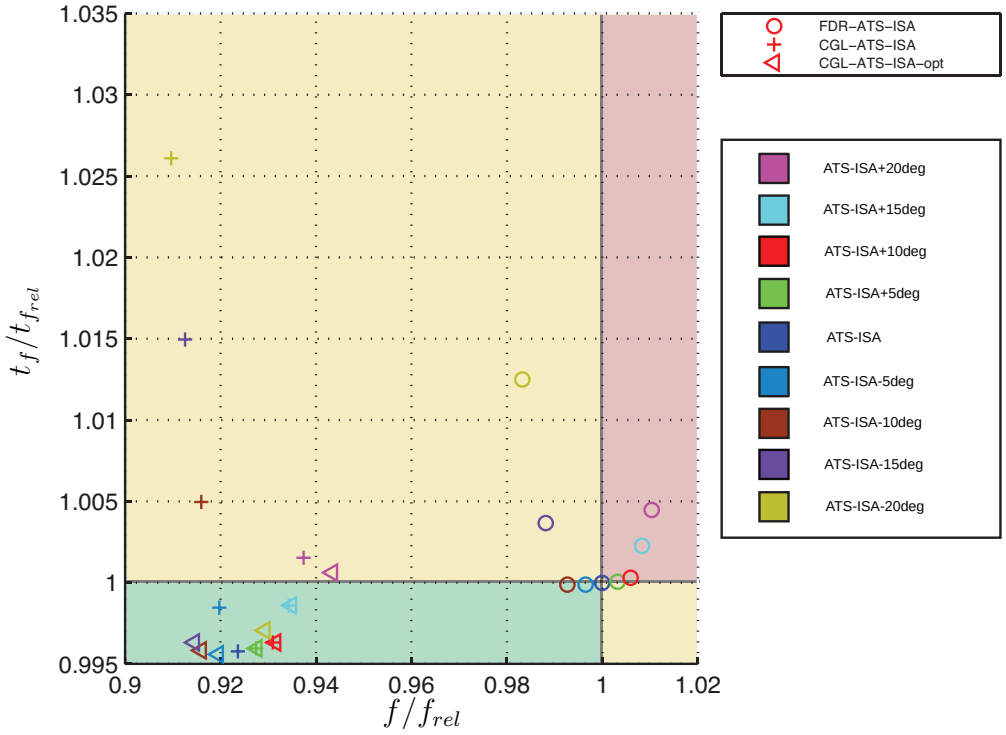


(a) Cost index.

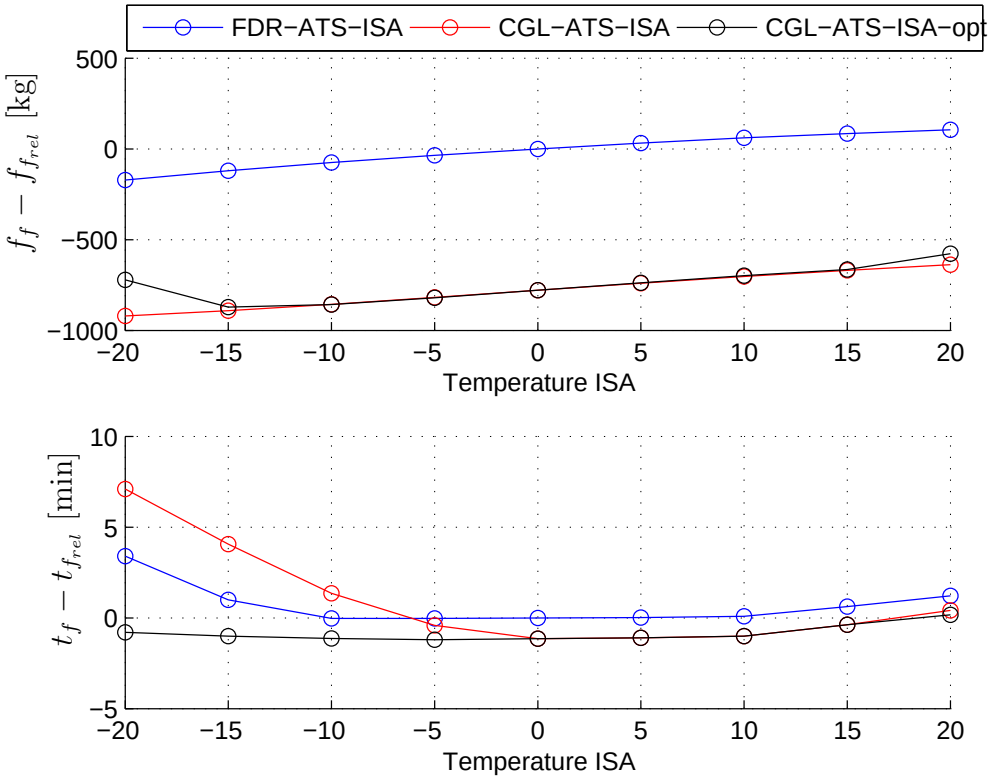


(b) Final time and fuel consumption vs different ISA MSL temperature.

Figure 68: Cost Index representations in the temperature variation case of study.

### 5.1.2 Energy index analysis

Figure 77 depicts the potential and kinetic energy that the aircraft has at the final WP modifying the ISA temperature condition referred to the FDR-ATS-ISA at ISA conditions. The CGL simulations potential energy at all atmospheric conditions remains fairly static at approximately 2.5% higher than the FDR-ATS-ISA at ISA conditions and the FDR-ATS-ISA at about the same value than in the ISA conditions.

The kinematics energy has similar tendency than the potential energy, where the CGL-ATS-ISA carries out a slight decrease from 8.3% to 7.2% higher than FDR-ATS-ISA at ISA conditions and the FDR-ATS-ISA from 1.4% lower than FDR-ATS-ISA at ISA conditions to 1.9% higher than FDR-ATS-ISA at ISA conditions. The CGL-ATS-ISA-opt simulation presents certain differences. It grows steadily from 7.4% in ISA-5° to 13.3% in ISA+20° both higher values than the reference FDR-ATS-ISA at ISA conditions, but from ISA-15° to ISA-5° there a considerable fall in the kinematics energy value and from ISA-20° to ISA-15° it roses moderately from 98.4% to 102.6% higher than FDR-ATS-ISA at ISA conditions.

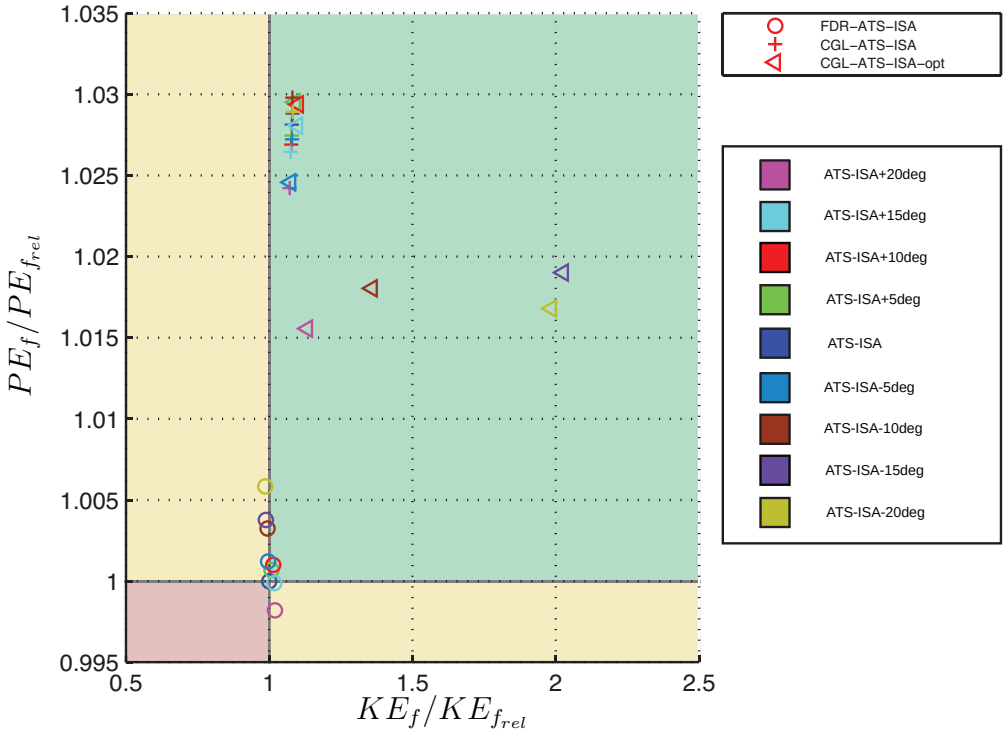


(a) Energy index.

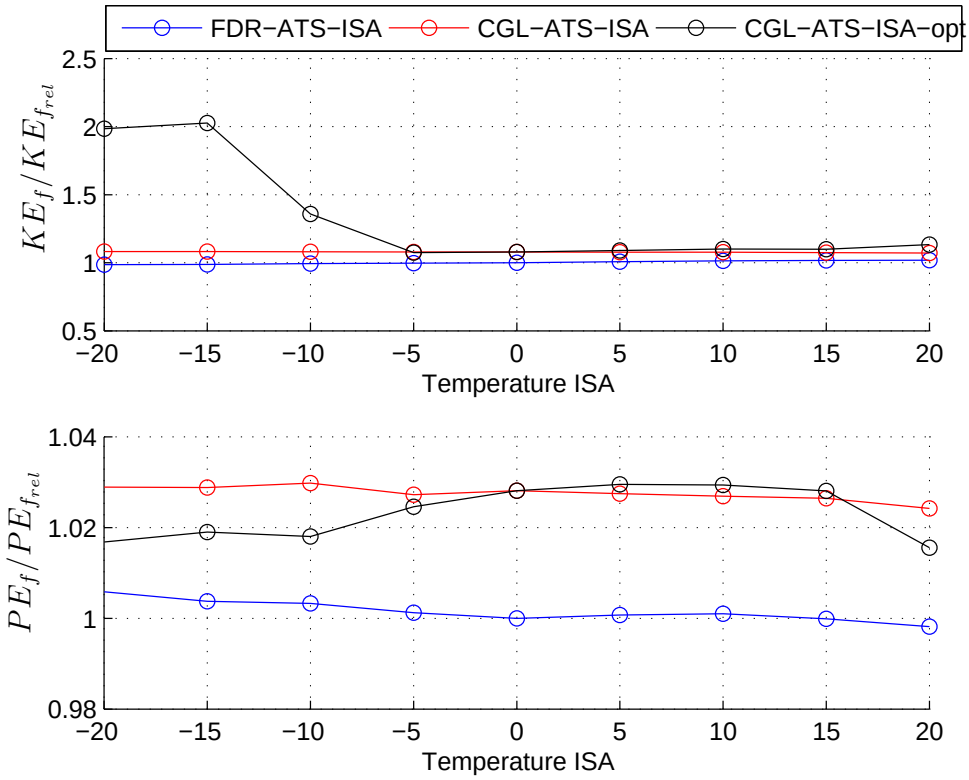


(b) Potential and kinetic energy vs different ISA MSL temperature.

Figure 69: Energy Index representations in the temperature variation case of study.

### 5.1.3 Figure of merit analysis

To conclude in the present section the figure of merit is evaluated following Equation 78. Figure 70 illustrates that in the FDR-ATS-ISA simulations the ratio between energy and cost index remains almost equal to the reference (FDR-ATS-ISA at ISA conditions). In the CGL-ATS-ISA simulations, the value remains close to 1.1 which implies more economics flights since they produce energy with lower cost. In the CGL-ATS-ISA-opt from ISA-5° to ISA+20° the same results than in the previous case is obtained. Meanwhile, from ISA-15° to ISA-5° there is a considerable fall in the Merit value from 1.67 to 1.1 and from ISA-20° to ISA-15° it increase moderately from 1.63% to 1.67%. Those values indicate that these simulations have a high value of energy for reduced cost, which is a very positive indicator. In this respect, the non stabilised landing should be explored, taking into consideration that the final WP is located at 3 [NM] from the airport.

Real FDR data at the final WP (3NM) presents 999.7 [m] (389 [m] height from the airport) and 73.37 [m/s] of altitude and TAS values, respectively. Figure 71 shows similar values in height but higher in TAS. This last issue is because neither flaps configuration change has been considered in the trajectory optimisation nor the conventional procedure simulations. Also, CGL-ATS-ISA-opt simulations under ISA-15° and ISA-20° provides the highest values in TAS thus even good fuel consumption values produces, it produces a non stabilised landing situation.

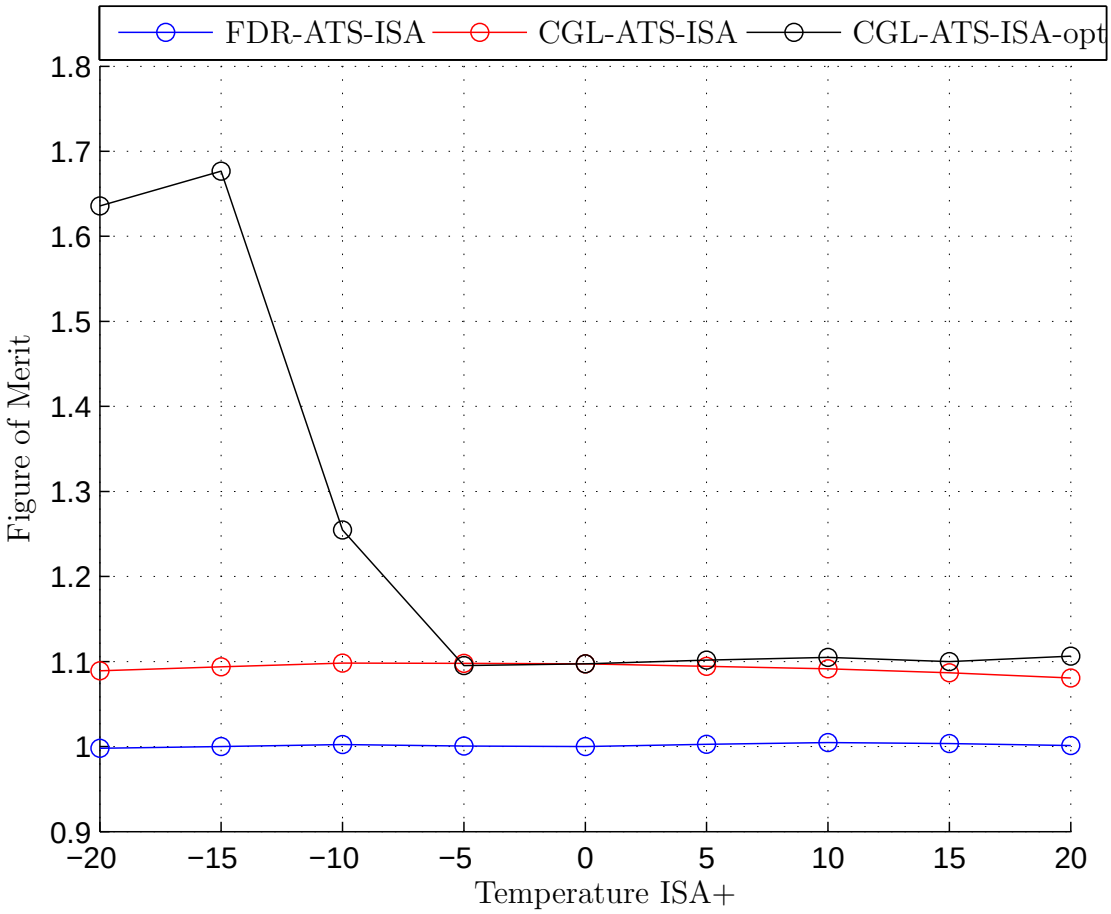


Figure 70: Figure of Merit in the temperature variation case of study.

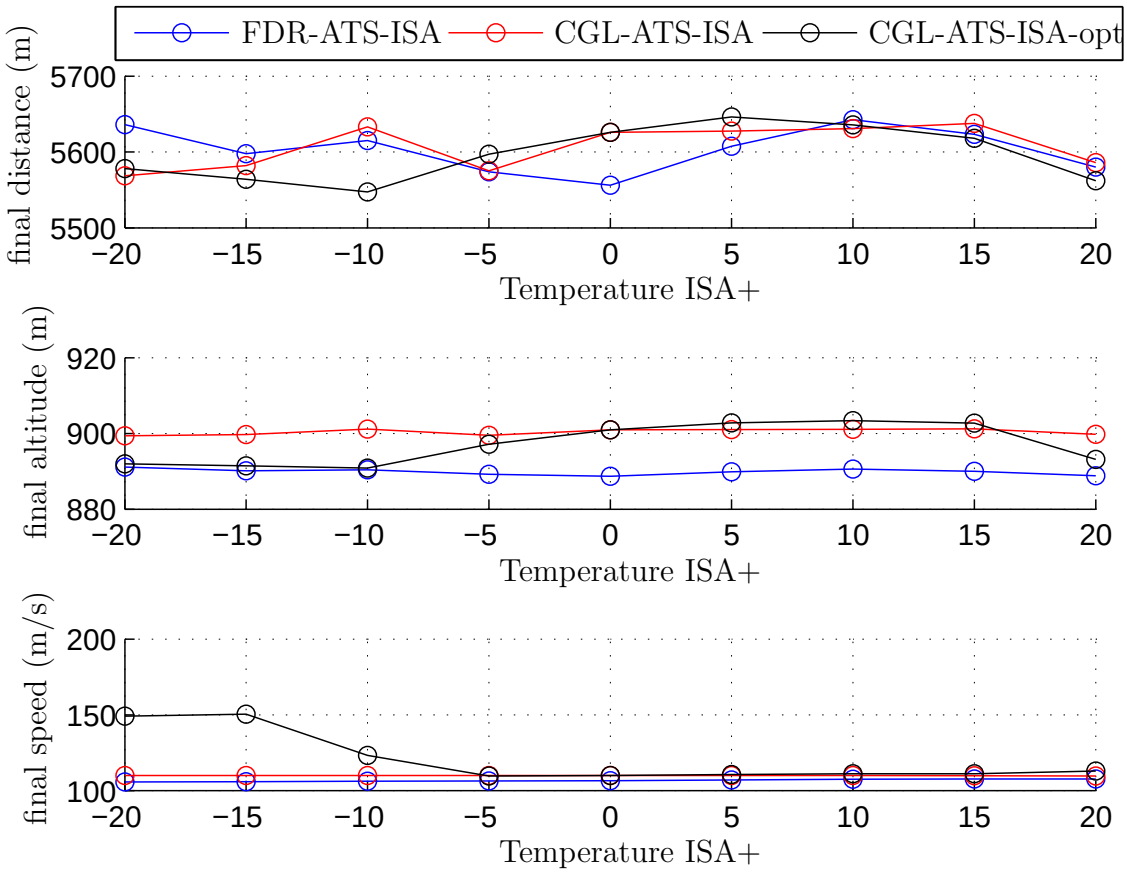


Figure 71: Distance, altitude and altitude from the final waypoint to the airport in the temperature variation case of study.

### 5.2 ISA atmosphere with different Lapse Rate values

As it was shown in the previous section, temperature has a relevant importance in the aircraft performances. Other aspect to readapt a real atmosphere to a modelled one is the lapse rate troposphere refine value. Therefore, the following lapse rate value are analysed: $-5{\cdot}10^{-3}$, $-5.5{\cdot}10^{-3}$, $-6.5{\cdot}10^{-3}$, $-7.5{\cdot}10^{-3}$ and $-8{\cdot}10^{-3}$ [°/m]. The atmosphere main variables are shown in Figure 72.

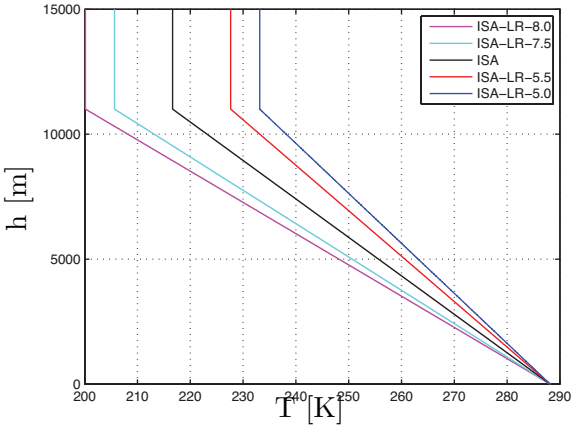


(a) Atmosphere temperature vs altitude

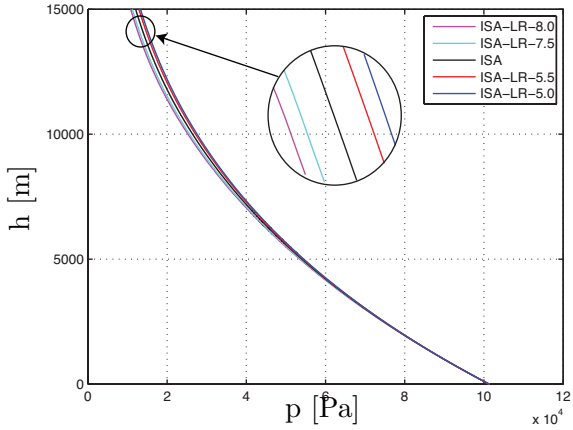


(b) Atmosphere pressure vs altitude

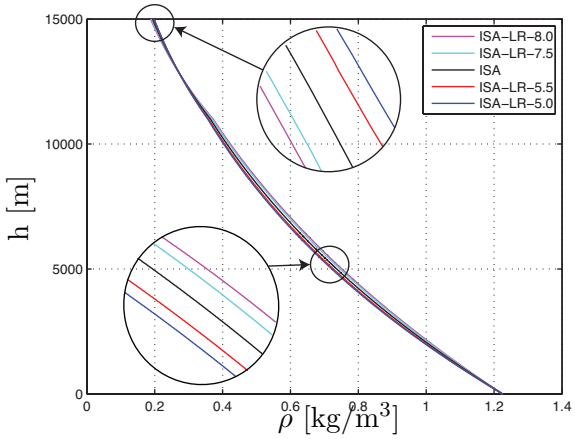


(c) Atmosphere density vs altitude

Figure 72: Atmosphere model in the Lapse Rate temperature variation

From Figure 73, it is shown that at the beginning the optimal altitude value increases from the initial value to the operational celling, with minimal differences between CGL-ATS-ISA-opt and the other simulations. TOD height and distance covered by the aircraft at this point increase with lapse rate temperature value (colder atmosphere conditions) in CGL-ATS-ISA-opt simulations, as shown Figure 73. This effect is because in colder atmosphere, TAS has a lower value since maximum Mach constraint (0.82 in the A319 according to BADA 3.9 [1]) is saturated. CGL-ATS-ISA simulations have exactly the same vertical profile, this is because all of them has the same altitude reference value introduced into the aircraft TS

(referred to the ISA).

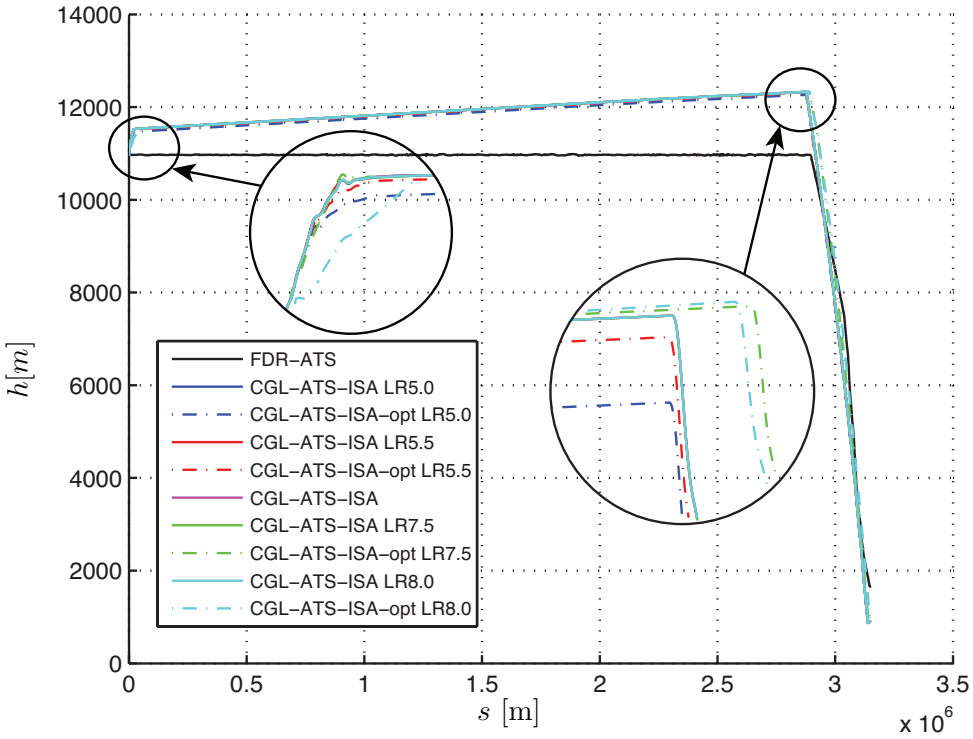


Figure 73: Altitude vs. distance in the Lapse Rate temperature variation case of study.

As in the previous section TAS representation has three representatives areas, as shown Figure 74:

- the initial region where $V$ is decreasing since the aircraft is climbing to the operational celling;
- the middle area is characterised by constant values in the colder atmospheres (lapse rates equal to -7.5·$10^{-3}$ and -8·$10^{-3}$ [°/m]) because it atmosphere produces Mach saturation flight conditions. Otherwise, hotter atmosphere (lapse rates equal to -5.5·$10^{-3}$ and -5·$10^{-3}$ [°/m]) reaches in this region the maximum TAS value, where a small difference between CGL-ATS-ISA-opt and CGL-ATS-ISA is observed since in the last one, temperature is lower and the Mach saturation condition is gotten.

- the final zone depicts that the moment where TAS decreases in the CGL-ATS-ISA and in the CGL-ATS-ISA-opt hotter simulations happen sooner than in the real procedure. Also, in CGL-ATS-ISA-opt hotter simulations the corresponding to lapse rate -8·$10^{-3}$ [°/m].

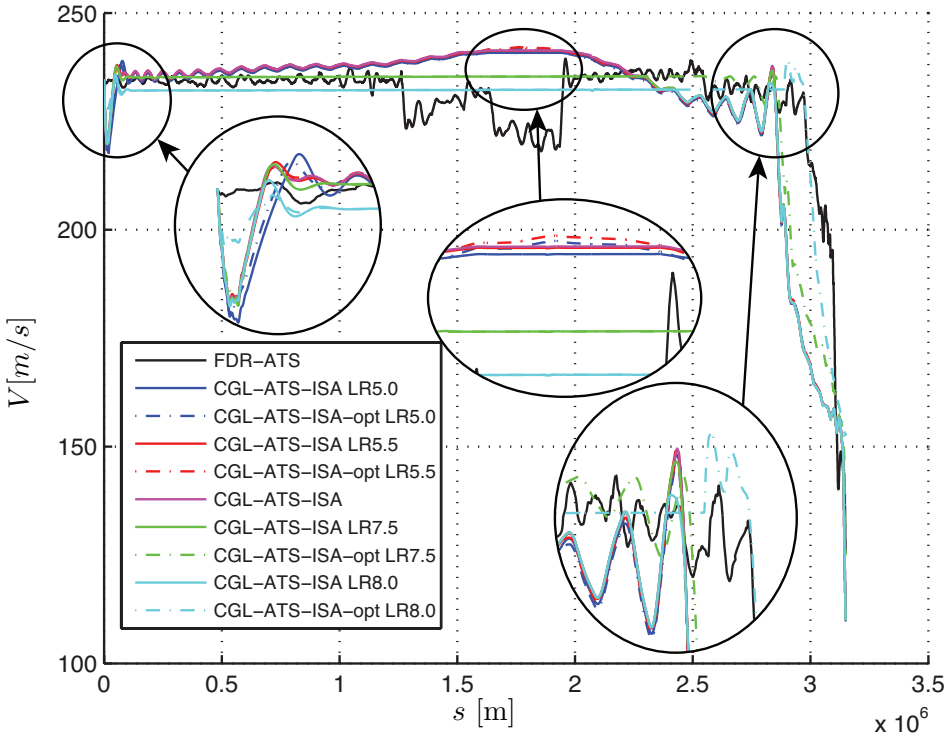


Figure 74: True Air Speed vs. distance in the Lapse Rate temperature variation case of study.

Finally the TLP in Figure 75 shows that higher temperature aircraft uses more thrust, as in the previous section. Moreover, CGL-ATS-ISA and CGL-ATS-ISA present similar results in TLP values at the same atmosphere condition.

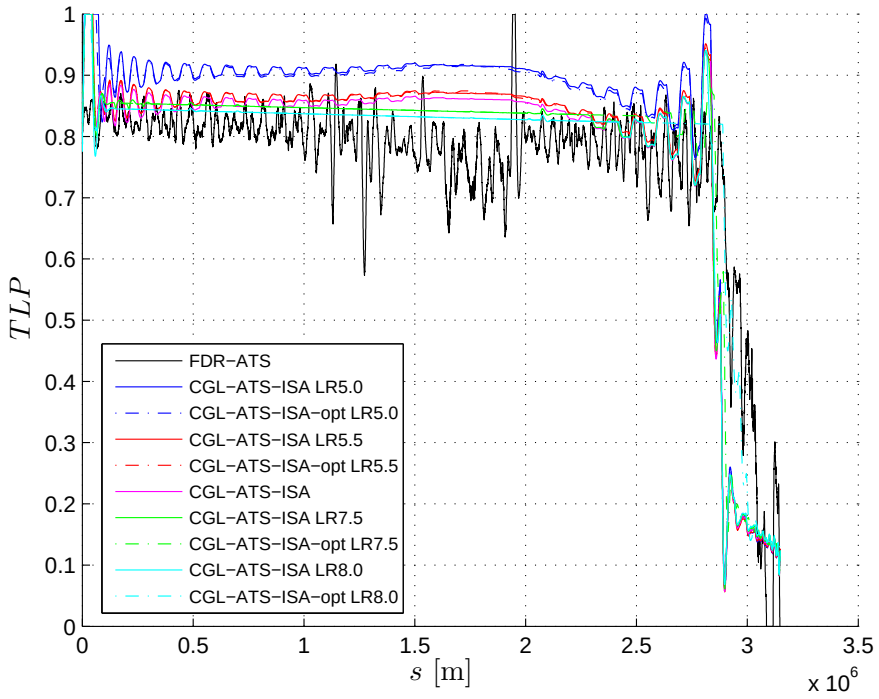


Figure 75: Throttle Lever Percentage vs. distance in the Lapse Rate temperature variation case of study.

### 5.2.1 Cost index analysis

As in the previous case of study, FDR-ATS-ISA, CGL-ATS-ISA and CGL-ATS-ISA-opt in all the temperature lapse rate values previously mentioned are compared with consumption and time at the final WP. Figure 76 denotes that colder atmosphere conditions produces more fuel consumption than in the hotter ones. In FDR-ATS-ISA simulation fuel consumption is moderately decreasing from 120 [kg] (101.2 %) to -125.3 (98.8%) [kg]. Regarding to CGL-ATS-ISA and CGL-ATS-ISA-opt the tendency is similar to the previous simulation, fuel consumption decreases slightly from -714.5 [kg] (93 % relative to the FDR-ATS-ISA at ISA conditions) to -831.7 [kg] (91.8 %) and from -662.5 [kg] (93.5 %) to -791 [kg] (92.24 %), respectively.

According to the time to reach the final WP, the simulations have a minimum final time value in lapse rate atmosphere conditions equal to -6.5·$10^{-3}$ [°/m] where the optimal

trajectory saves 1.15 minutes (99.6 %). In hotter atmospheres the time to reach the final WP grows steadily from 0 to 0.53 minutes (100.2 %) relative to FDR-ATS-ISA at ISA conditions for the FDR-ATS-ISA simulation, from -1.15 (99.6 %) to -0.45 (99.8 %) minutes relative to FDR-ATS-ISA at ISA conditions for CGL-ATS-ISA simulation and from -1.15 (99.6 %) to -0.53 (99.8 %) minutes relative to FDR-ATS-ISA at ISA conditions. On the contrary, in colder atmospheres the delay from the reference condition goes up for all the simulation but with different ratio. CGL-ATS-ISA is the one with the maximum delay value (5.2 minutes [101.9 %]) in the lapse rate -$8{\cdot}10^{-3}$ [°/m] atmosphere condition. The FDR-ATS-ISA presents 1.9 minutes (100.7 %) of delay and the CGL-ATS-ISA-opt with a saving in time of 0.7 minutes (99.7 %) in the same previous mentioned atmosphere conditions.

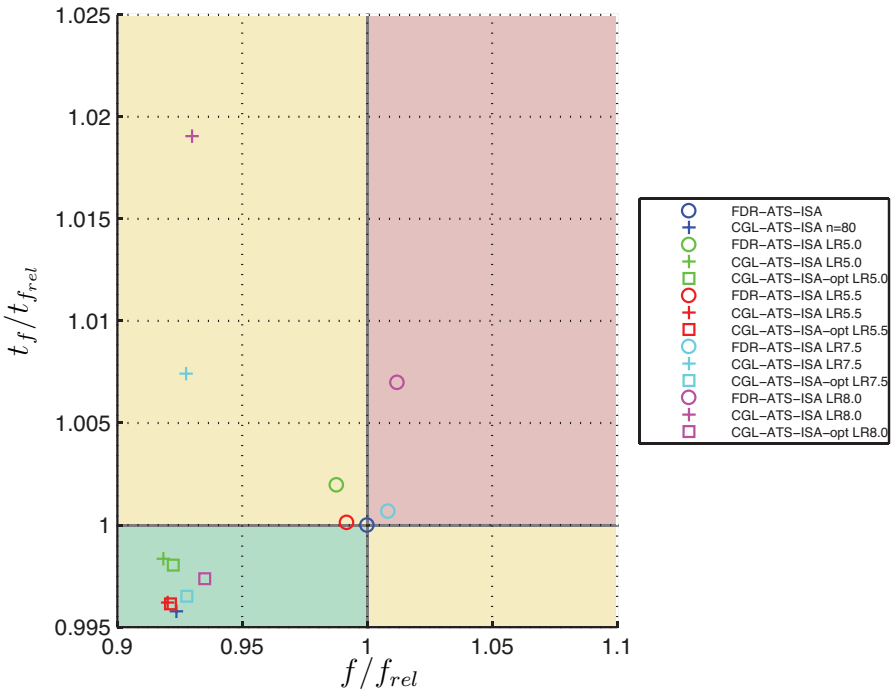


(a) Cost index.

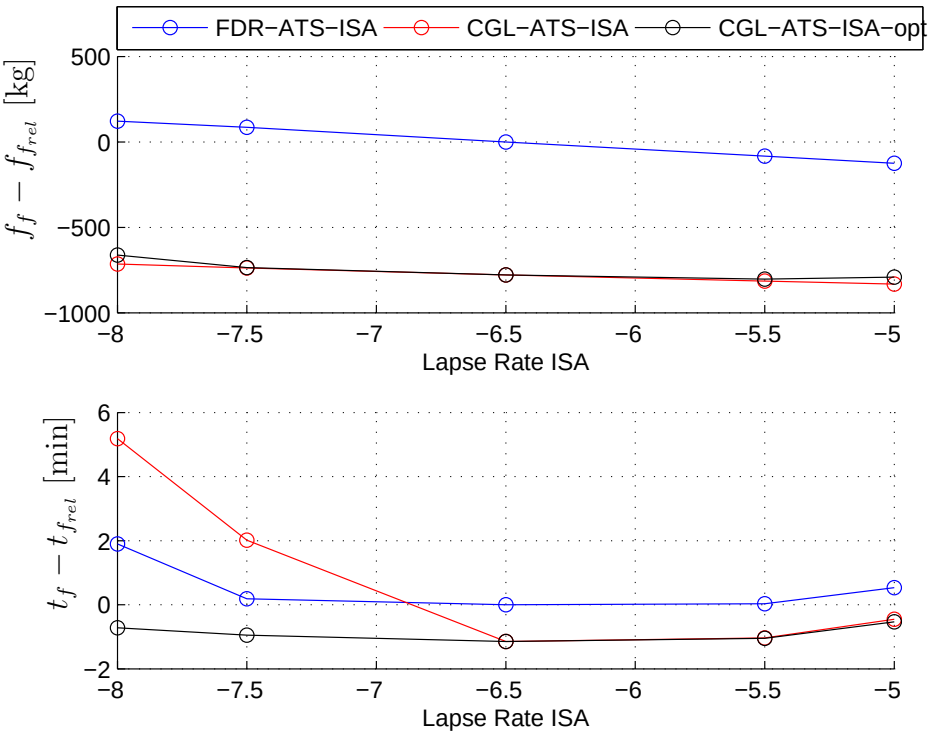


(b) Final time and fuel consumption vs different Lapse Rate temperature.

Figure 76: Cost Index representations in the Lapse Rate temperature variation case of study.

### 5.2.2 Energy index analysis

To modify the lapse rate temperature condition produces into the simulation a increase in the level of kinematic and potential energy, as shown Figure 77.

In the FDR simulations, the potential and kinematic energy at all atmospheric conditions remains almost stable at reference ISA conditions values. Also, CGL-ATS-ISA did not change significantly its final energy status, being this equal to 107.9 % and 102.8 % for the kinematic and potential energy, respectively. Greater differences appear in the CGL-ATS-ISA-opt mainly in colder atmosphere condition, where the kinematic maximum value is 207.2 % and 101.6 % the potential one. Besides, a different effect is observed in hotter atmosphere than colder, because in hotter atmospheres the potential and kinematic energy have an almost constant value, meanwhile in colder atmospheres the kinematic energy is greater but the potential energy is lower, being more important the differences for the kinematic one.

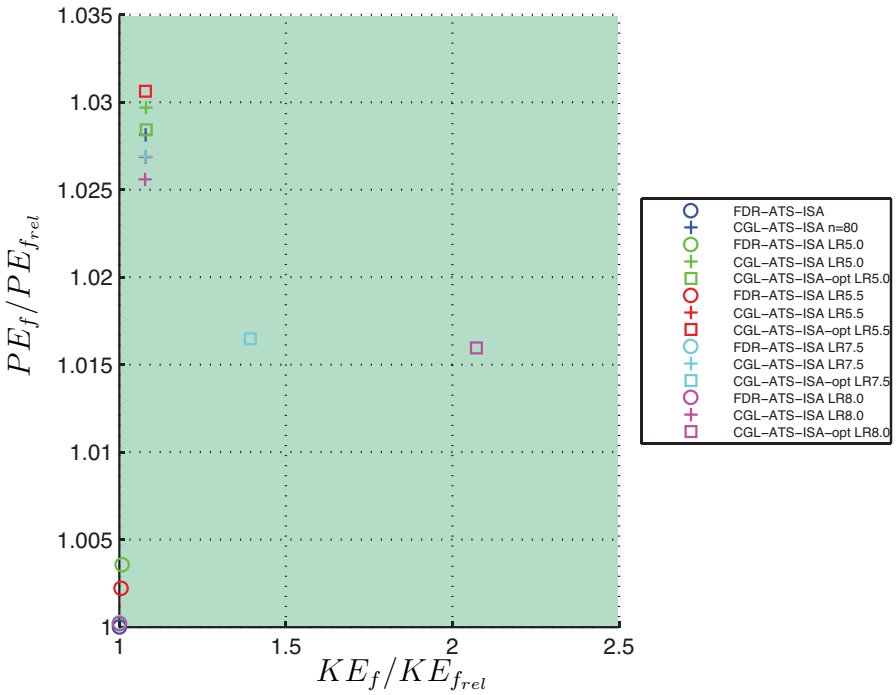


(a) Energy index.

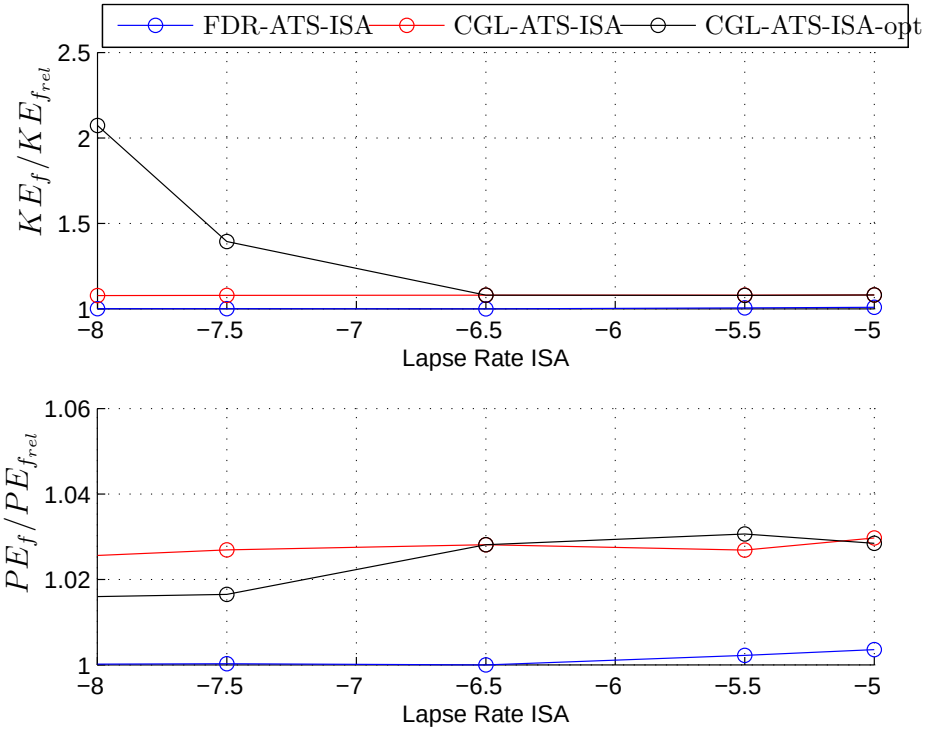


(b) Potential and kinetic energy vs different Lapse Rate temperature.

Figure 77: Energy Index representations in the Lapse Rate temperature variation case of study.

### 5.2.3 Figure of merit analysis

Figure 78 shows the figure of merit value when lapse rate are modified, FDR-ATS-ISA simulations have a steadily growth from 0.9911 to 1.011 therefore better values are obtained in hotter atmospheres. The same result is achieved by CGL-ATS-ISA simulations where the figure of merit roses from 1.078 to 1.1. Nevertheless, CGL-ATS-ISA simulations in colder simulation the figure of merit drops dramatically from 1.688 to 1.097 and in hotter simulations remains steady at approximately 1.097.

Analysing the Figure 79, just the CGL-ATS-ISA-opt simulation in colder atmosphere has a big difference from the stabilised aircraft condition at the final WP (999.7 [m] of altitude (389 [m] height from the airport) and 73.37 [m/s] of TAS value).

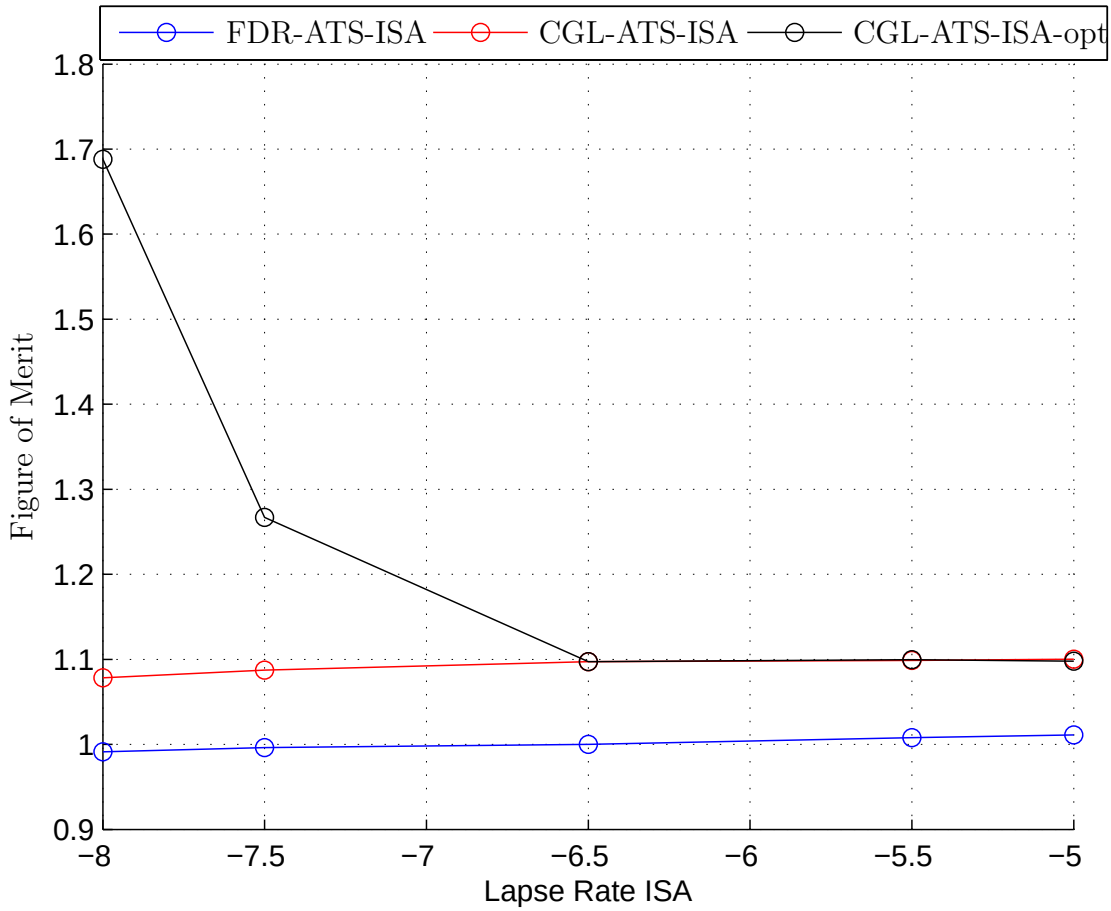


Figure 78: Figure of Merit Lapse Rate in the temperature variation case of study.

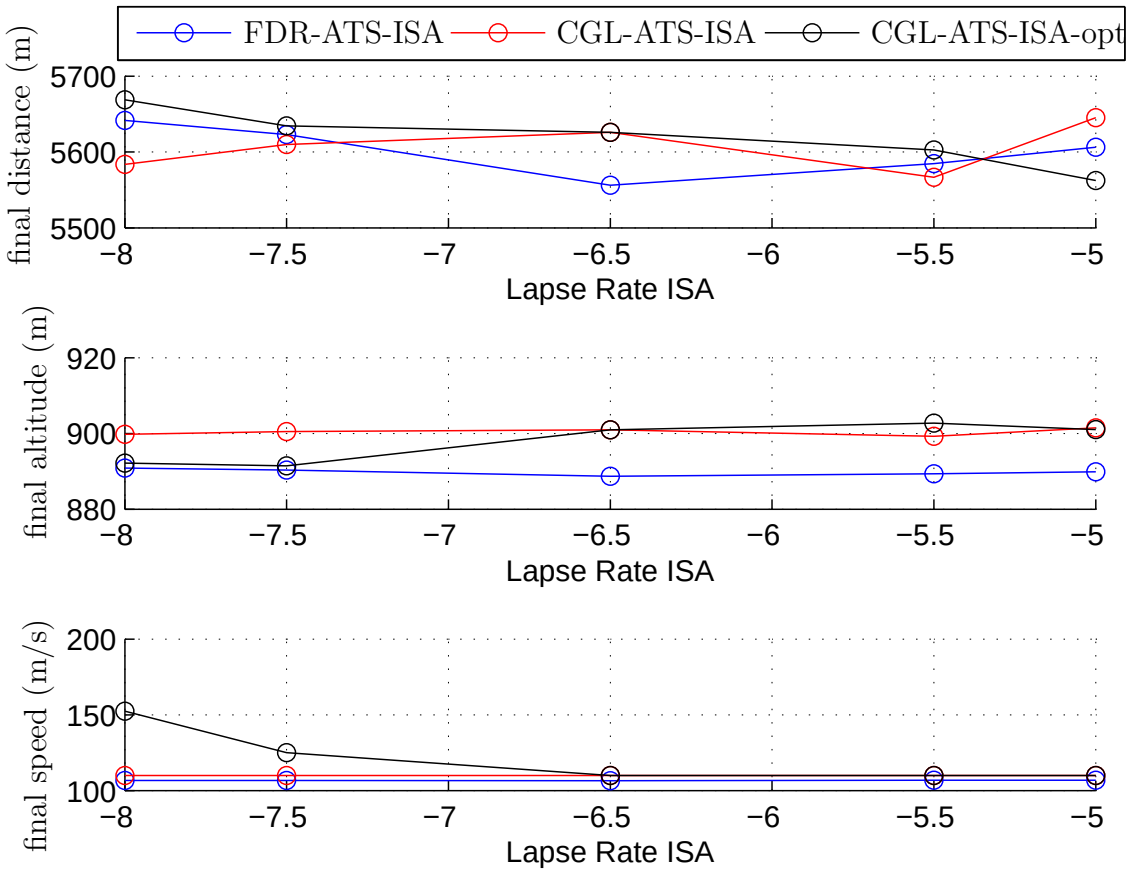


Figure 79: Distance and altitude from the final waypoint to the airport in the Lapse Rate temperature variation case of study.

### 5.3 Different ISA pressure at MSL

Pressure is other atmosphere parameter that can modify the aircraft performances. Thus, in this section real and optimal vertical procedures have been simulated considering a ISA pressure from ISA+2000 [Pa] to ISA-2000 [Pa] in intervals of 500 [Pa]. The atmosphere main variables are shown in Figure 80.

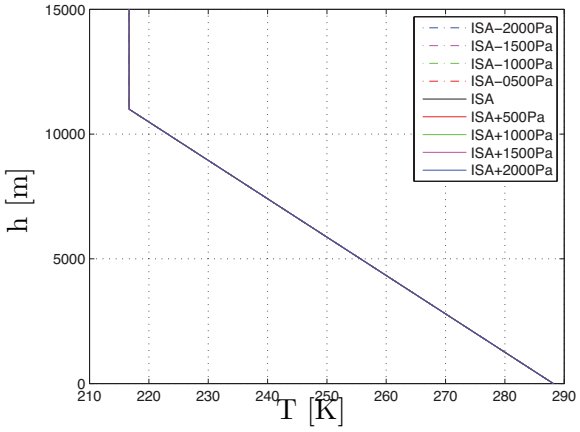


(a) Atmosphere temperature vs altitude

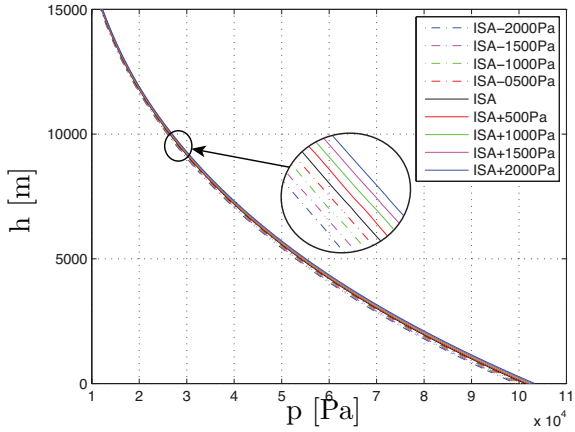


(b) Atmosphere pressure vs altitude

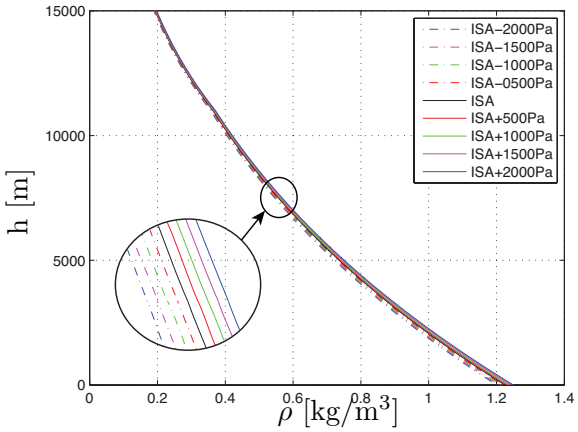


(c) Atmosphere density vs altitude

Figure 80: Atmosphere model pressure variation

This case of study has the particularity that the optimal trajectories are not affected by the Mach saturation condition since temperature is the same for all the simulation of a ISA standard definition value. The vertical profile is shown in Figure 81. The TOD is located at the same point in all the FDR-ATS-ISA and CGL-ATS-ISA, meanwhile for CGL-ATS-ISA-opt as higher pressure further and higher in altitude is located the TOD.

In TAS CGL-ATS-ISA and CGL-ATS-ISA-opt have the same value at the same atmosphere conditions, as illustrated Figure 82. TAS is characterised by a loose of speed at the beginning, then TAS is increasing value until the maximum value is reached in the middle of the route and in the approach and landing phase it has a sharp drop.

It can be seen from Figure 83 that TLP is a bit higher in atmosphere with more pressure value.

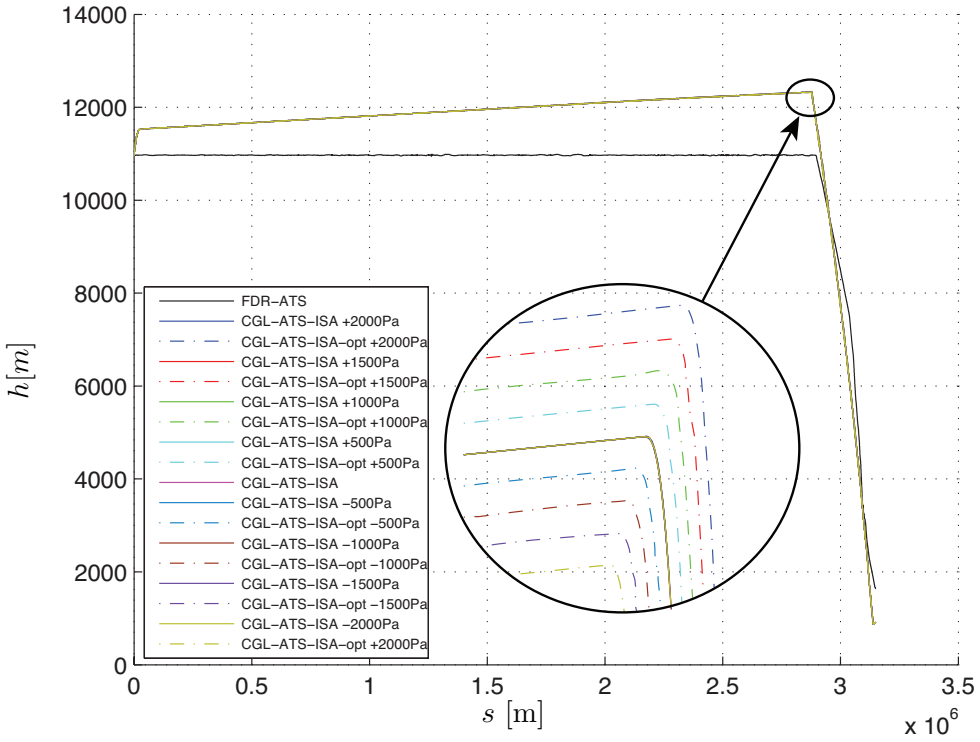


Figure 81: Altitude vs. distance in the pressure variation case of study.

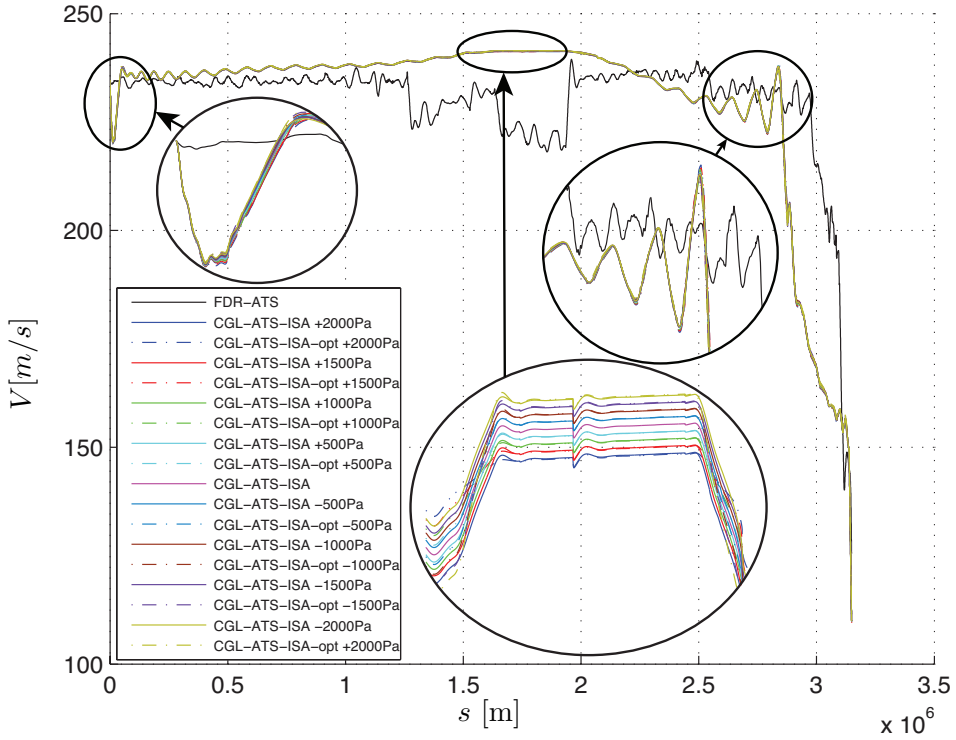


Figure 82: True Air Speed vs. distance in the pressure variation case of study.

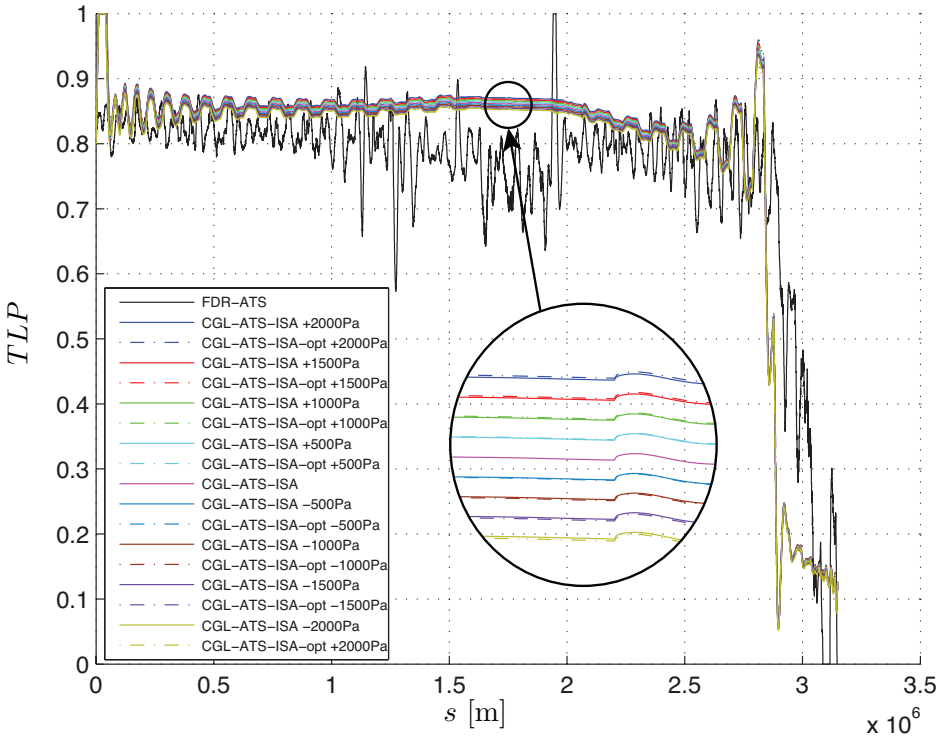


Figure 83: Throttle Lever Percentage vs. distance in the pressure variation case of study.

### 5.3.1 Cost index analysis

Figure 84 shows the cost index value in the FDR and CGL trajectories for the different atmosphere pressure values. Fuel consumption at the final WP in FDR-ATS-ISA simulations grew linearly from -114.8 [kg] (98.87%) in ISA-2000Pa to 116 [kg] (101.10%) in ISA+2000Pa, an increase of 230.8 [kg]. In CGL-ATS-ISA simulation the fuel consumption goes up from -870.3 [kg] (91.46%) to -685 [kg] (99.62%), a rise of 185.3 [kg]. Eventually, in CGL-ATS-ISA-opt it climbs from -862 [kg] (91.54%) to -693.6 [kg] (93.20%), an upward trend of 168.4 [kg].

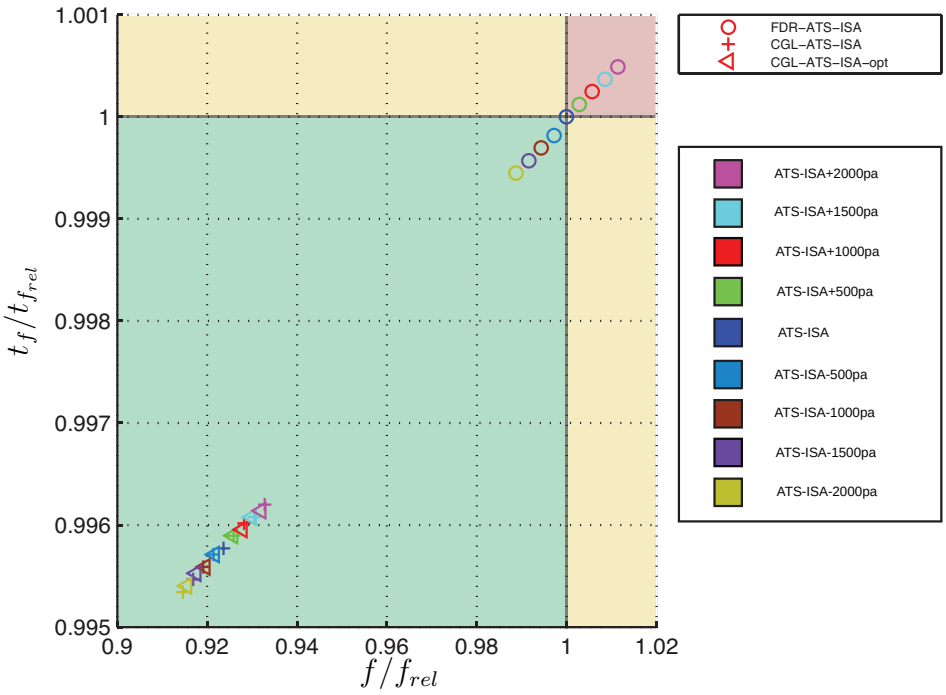


(a) Cost index.

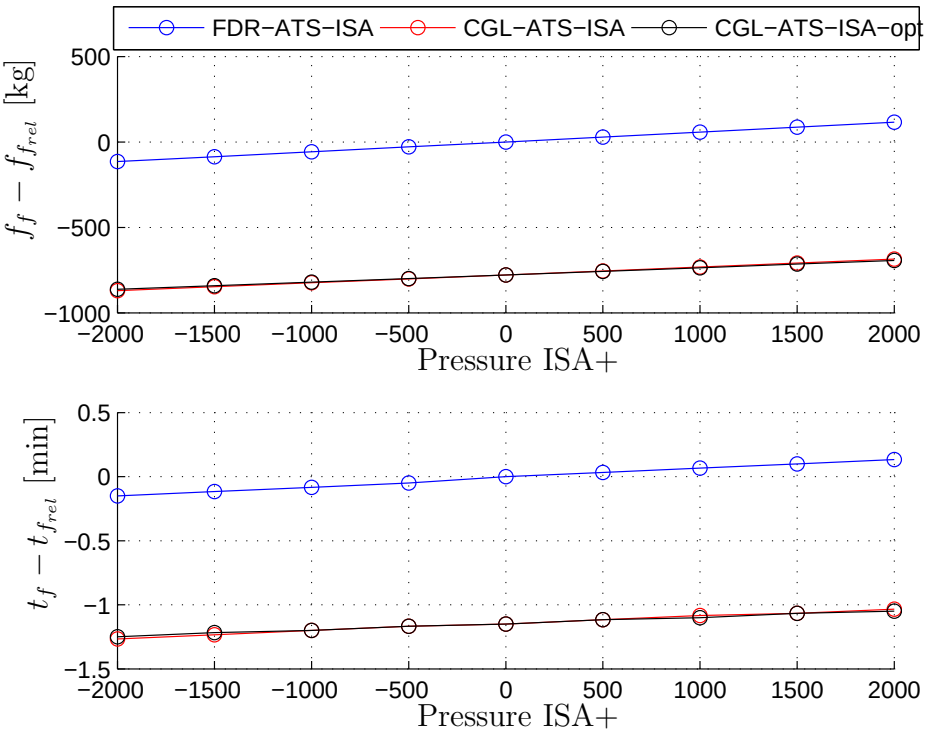


(b) Final time and fuel consumption vs different ISA MSL temperature.

Figure 84: Cost Index representations pressure variation case of study.

Related to the time to reach the final WP the tendency in all the simulation is quite similar they need more time when pressure is increased:

- From -0.15 minutes (99.94%) to 0.13 minutes (100%) in FDR-ATS-ISA simulations,
- From -1.27 minutes (99.53%) to -1.03 minutes (93.28%) in CGL-ATS-ISA simulations, and
- From -1.25 minutes (99.54%) to -1.05 minutes (99.61%) in CGL-ATS-ISA-opt simulations.

### 5.3.2 Energy index analysis

The energy level at the final WP is characterised by simulations have more potential and kinematic energy than the FDR-ATS-ISA at the ISA standard conditions, with the exception of the FDR-ATS-ISA simulations with positive increase in pressure values which have lower values in both kind of energy.

The energy value tendency is not so linear as the observed in the previous analysis of the const index value. All simulation present a fell steadily when the pressure is increased, the kinematic energy:

- From 101.2% to 99.43% in FDR-ATS-ISA simulations,
- From 108.1% to 107.8% in CGL-ATS-ISA simulations, and
- From 109.5% to 107% in CGL-ATS-ISA-opt simulations.

And the potential energy:

- From 100.3% to 99.98% in FDR-ATS-ISA simulations,
- From 103.1% to 102.6% in CGL-ATS-ISA simulations, and
- From 103.3% to 102.1% in CGL-ATS-ISA-opt simulations.

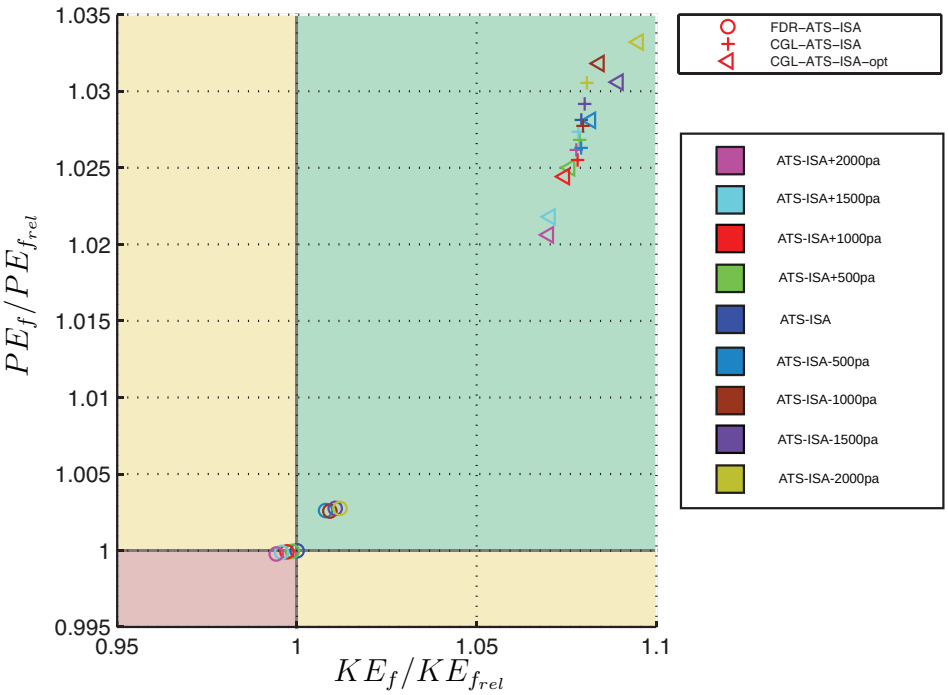


(a) Energy index.

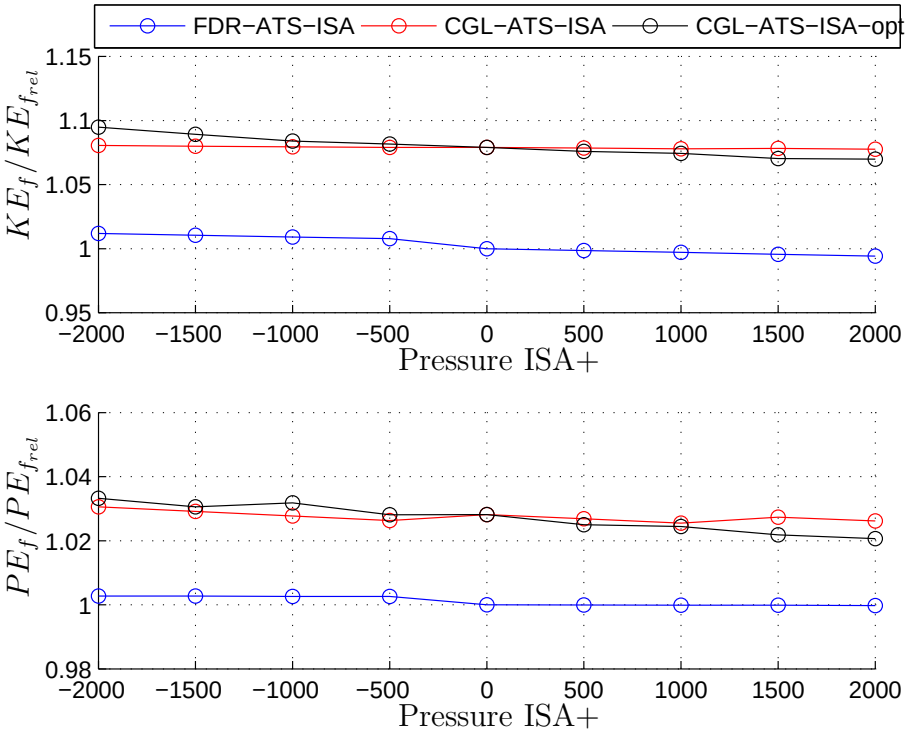


(b) Potential and kinetic energy vs different ISA MSL temperature.

Figure 85: Energy Index representations pressure variation case of study.

### 5.3.3 Figure of merit analysis

Finally, the figure of merit in Figure 86 indicates that the best result are produced in optimal trajectories at lower pressure values since the figure of merit has above one value. Also, Figure 87 shows that all the simulations present final altitude, distance to the airport and TAS values which make possible the aircraft to land.

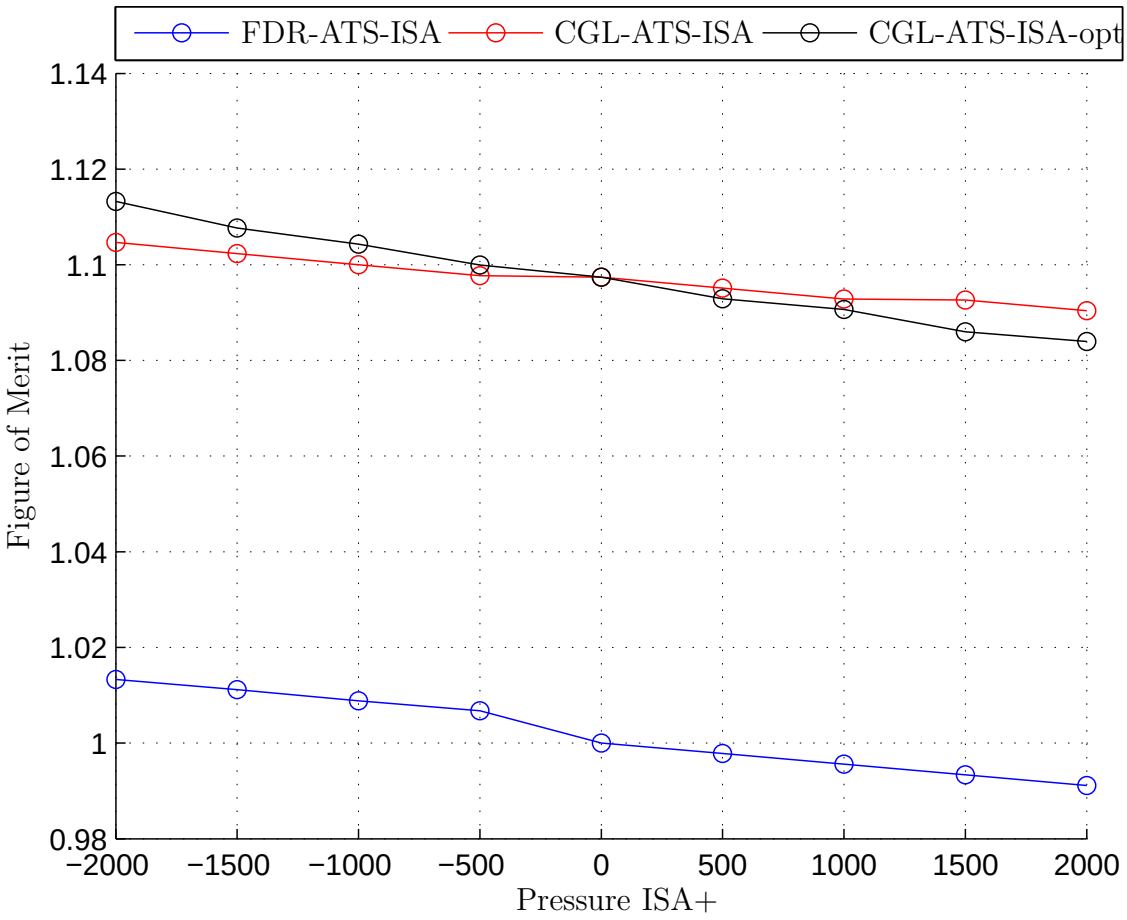


Figure 86: Figure of Merit pressure variation case of study.

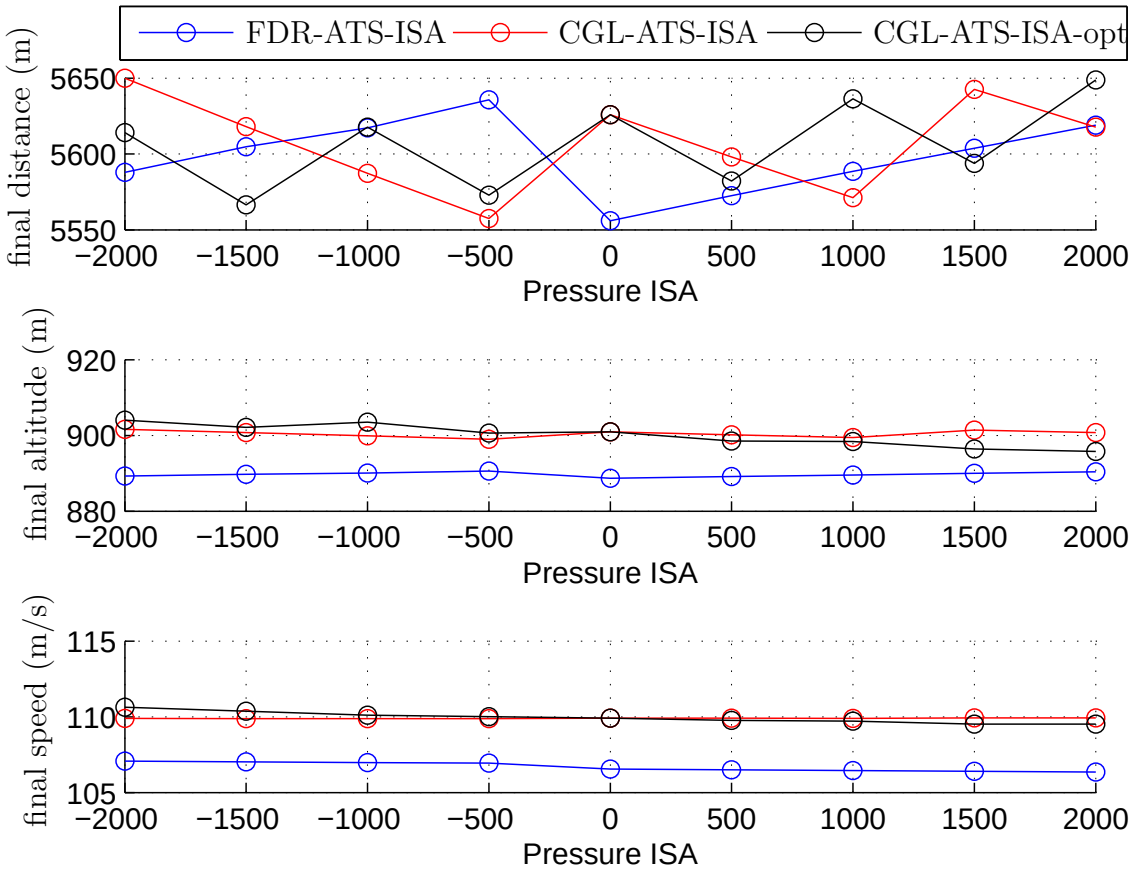


Figure 87: Distance, altitude and altitude from the final waypoint to the airport pressure variation case of study.

### 5.4 Most limitative pressure and temperature at MSL values

In this section, scenarios with a combination of extreme different ISA pressure and temperature are analysed. The normal range of the Earth's air pressure is from 98,000 [Pa] to 105,000 [Pa] and a global maximum temperature deviation from the ISA model of 65 [K] at MSL, then 101,325±2,000–101,325±1,500 [Pa] and 288.15±20–288.15±15 [K] are used, this atmosphere vertical distribution considered are represented in Figure 88.

The previous cited scenarios is to measure how much optimal and current vertical procedure are affected by air pressure and temperature high dropping and rising. It is important to note that a decreasing in air pressure and an increasing in temperature at the aircraft's

location will decrease the aircraft's performance.

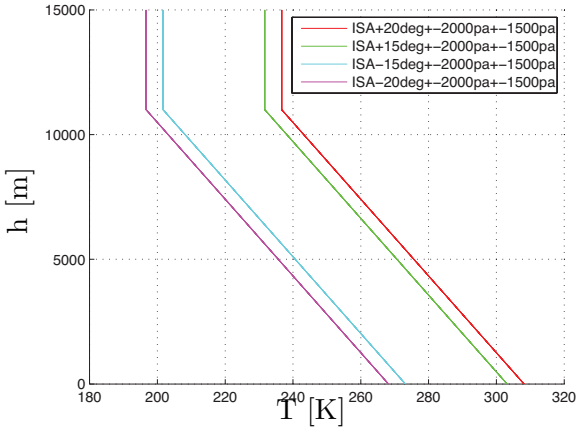


(a) Atmosphere temperature vs altitude

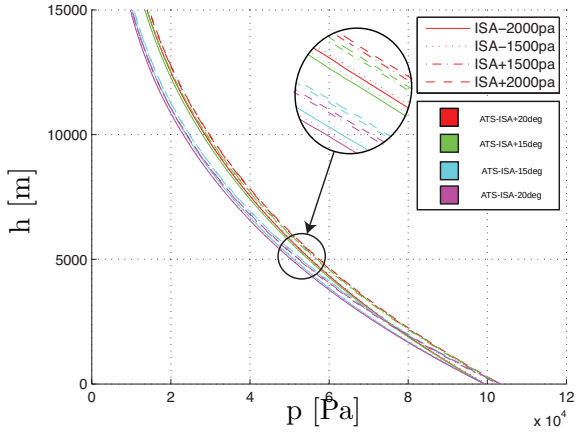


(b) Atmosphere pressure vs altitude

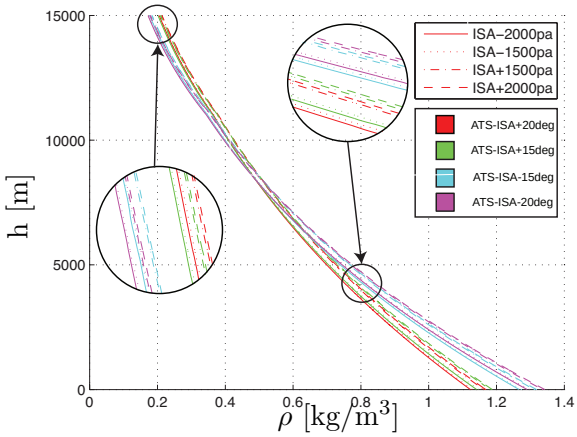


(c) Atmosphere density vs altitude

Figure 88: Atmosphere model temperature and pressure extreme variation

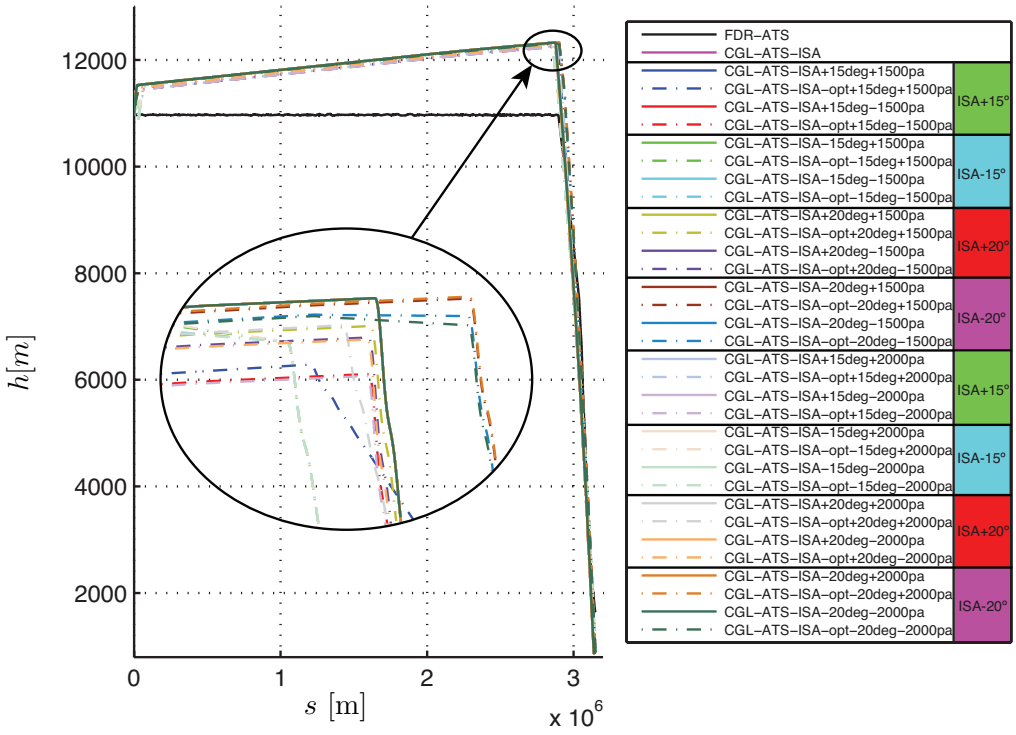


Figure 89: Altitude vs. distance in the extreme temperature and pressure variation case of study.

Figure 90 shows the TAS in function of the distance for all the simulations. As in the previous cases of study, the optimal TAS is characterised by a steady increased in the first part, except for the simulation where the temperature is bellow ISA standard values, because it is constant due to the temperature values make aircraft is flying in the maximum Mach value (0.82 in the A319) [1]. Lower TAS values are found in atmosphere where the temperature is bellow the standard ISA, the lowest is at ISA-15°, followed by ISA-20°, after ISA condition, then ISA+20° and finally ISA+15°. But inside these groups, the minimum value is at ISA+2000Pa, follows by ISA+1500Pa, then ISA-1500Pa and finally ISA-2000Pa, it is important to note that the differences in TAS values among the same temperature simulations are bellow 1 [m/s]. Final TAS representation presents differences among simulations: ISA-15° presents the start point of the descent phase 150 [km] after the ISA-20° making

coincident in this point for the rest of the route except in the CGL-ATS-ISA-opt where some simulation continue until temperature allows a increase in TAS value.

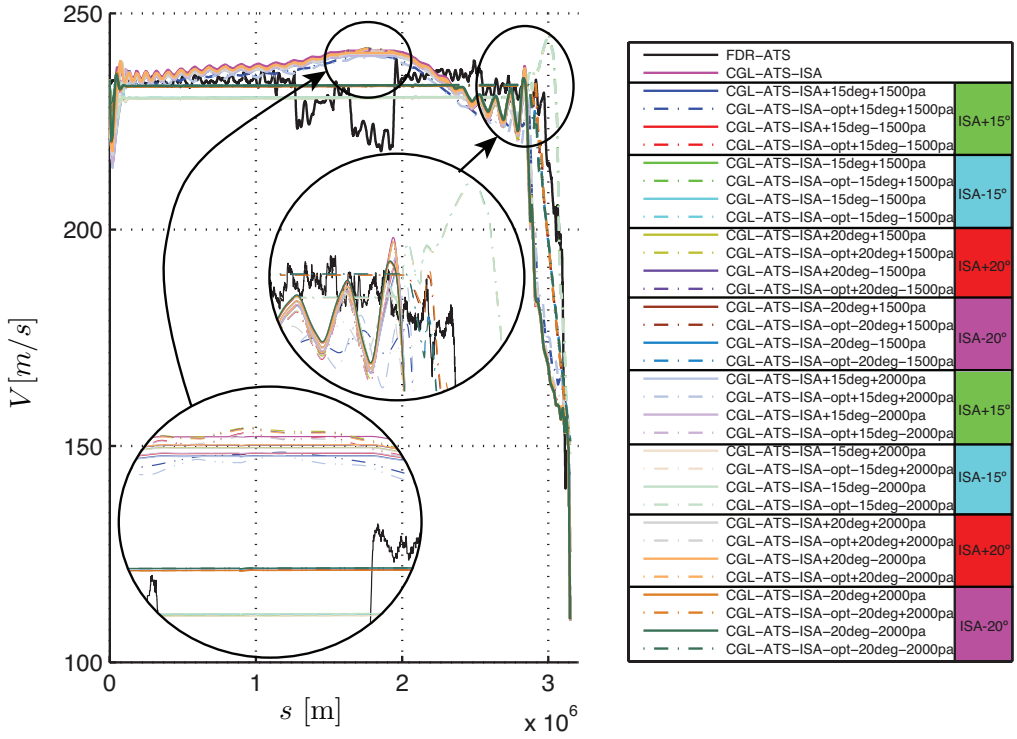


Figure 90: True Air Speed vs. distance in the extreme temperature and pressure variation case of study.

According to Figure 91 simulations at ISA-15° have the minimum TLP values, follows by ISA-20°, after ISA, then ISA+20° and finally ISA+15°. Between ISA temperature simulations previously mentioned the least TLP values are produced in the ISA-2000Pa, follows by ISA-1500Pa, then ISA+1500Pa and finally ISA+2000Pa, in this groups of simulations the different TLP values are negligible.

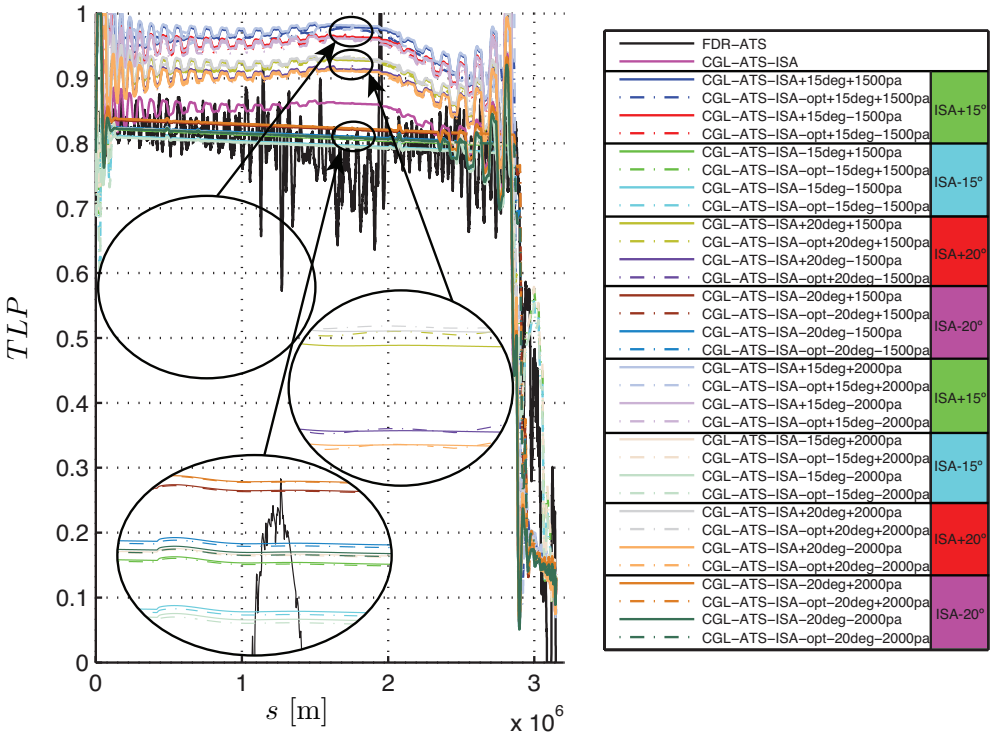


Figure 91: Throttle Lever Percentage vs. distance in the extreme temperature and pressure variation case of study.

### 5.4.1 Cost index analysis

Figure 92 denotes the cost index relative value to FDR-ATS-ISA at ISA standard condition. ISA+2000Pa and ISA+1500Pa have almost the same cost index value for all temperatures analysed, the same happens with ISA-2000Pa and ISA-1500Pa. It is observed that optimal trajectory produce in the most cases more than 5% of fuel savings and almost the same time at the final WP. Besides, very similar CGL-ATS-ISA and CGL-ATS-ISA-opt cost index values are obtained in ISA+20° and ISA+15°.

If the time to reach the final WP is observed, temperatures under standard ISA have worse results with greater differences among FDR and CGL simulations in the less temperatures (ISA-20° and ISA-15°) than in the hotter atmospheres (ISA+15° and ISA+20°). Moreover, hotter atmosphere CGL-ATS-ISA and CGL-ATS-ISA-opt have similar results and

better than FDR-ATS, meanwhile in colder atmosphere high differences are detected between CGL-ATS-ISA and CGL-ATS-ISA-opt, as shown Figure 93. Also, time at the final WP rises up slightly when pressure is modified:

- FDR-ATS-ISA: from 3.27 to 3.53 minutes at ISA-20°. From 0.87 to 1.13 minutes at ISA-15°. From 0.47 to 0.78 minutes at ISA+15°. And from 1.05 to 1.38 minutes at ISA+20°.

- CGL-ATS-ISA: from 7 to 7.2 minutes at ISA-20°. From 3.97 to 4.17 minutes at ISA-15°. From -0.52 to -0.23 minutes at ISA +15°. And form 0.25 to 0.6 minutes at ISA+20°.

- CGL-ATS-ISA-opt: from -0.9 to -0.7 minutes at ISA-20°. From -1.1 to -0.9 minutes at ISA-15°. From -0.57 to -0.28 minutes at ISA+15°. And from 0.03 to 0.4 minutes at ISA+20°.

Fuel consumption at the final WP presents also a steadily increase when pressure is modified but at the same temperature. In this case, fuel consumption shows worst values when ISA temperature is increased, as shown Figure 93.

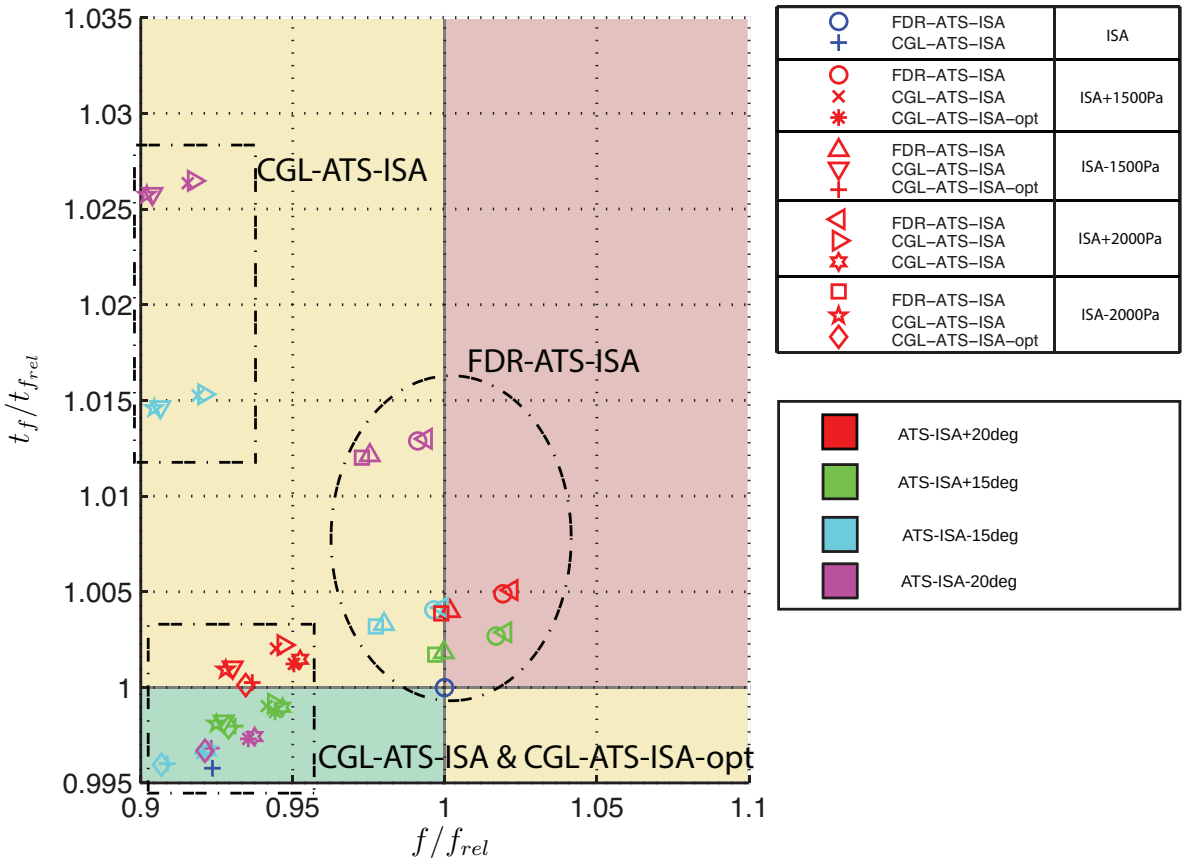


Figure 92: Cost Index in the most extreme atmosphere situations.

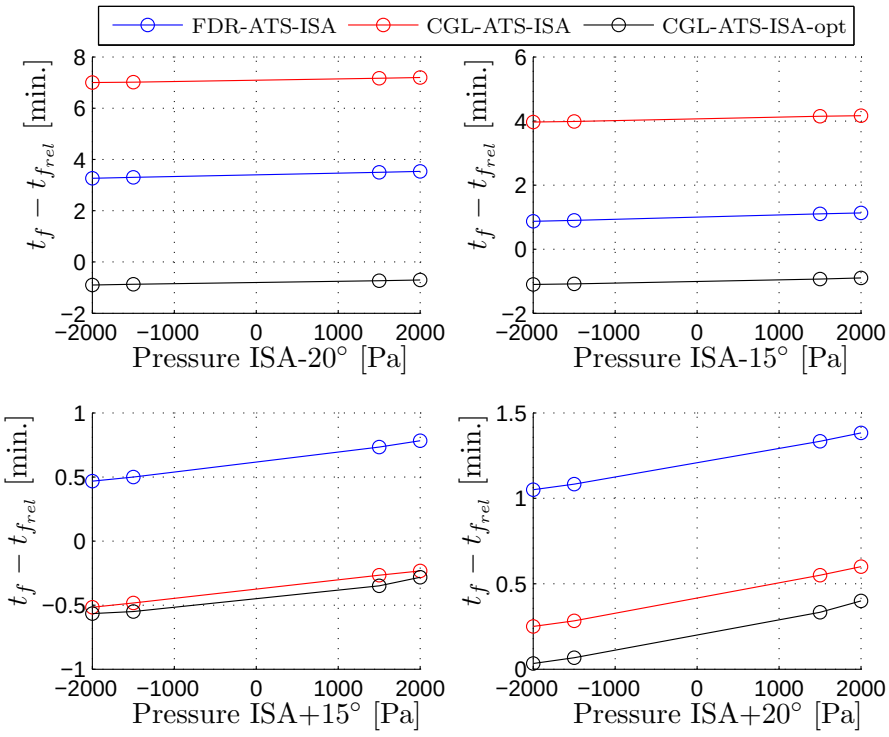


(a) Final time difference.

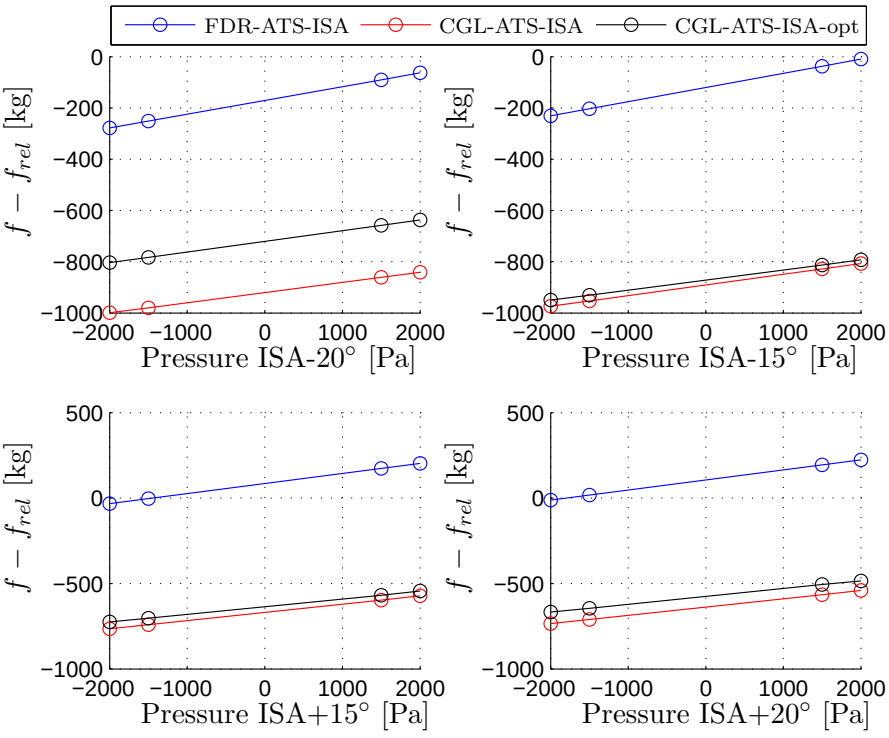


(b) Final fuel consumption difference.

Figure 93: Cost Index differences in the most extreme atmosphere situations.

### 5.4.2 Energy index analysis

In Figure 94 for group with similar energy index are detected. Also, more notable differences in kinetic energy than potential are observed. Figure 95 shows that potential energy has an almost stable value during the all simulations, but kinematic energy presents remarkable differences for the CGL-ATS-ISA-opt simulations at hotter ISA conditions.

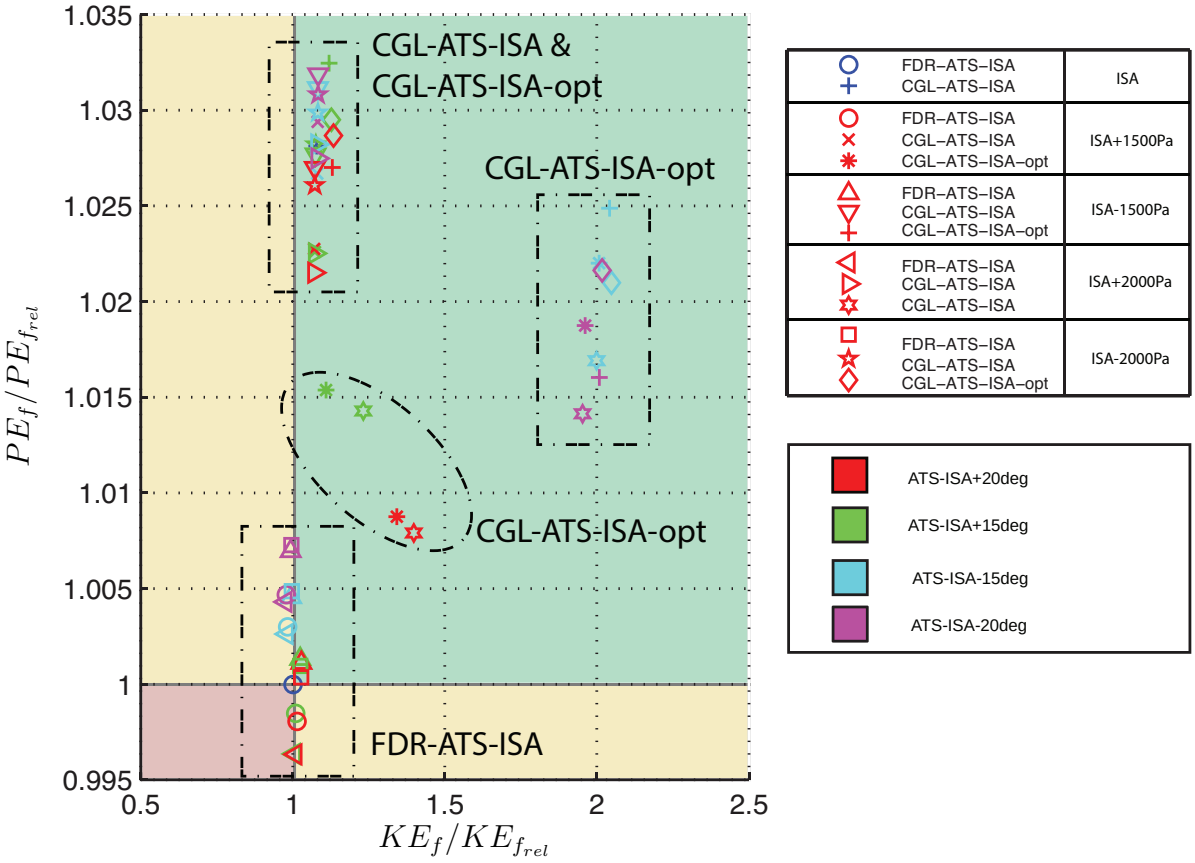


Figure 94: Energy Index in the most extreme atmosphere situations.

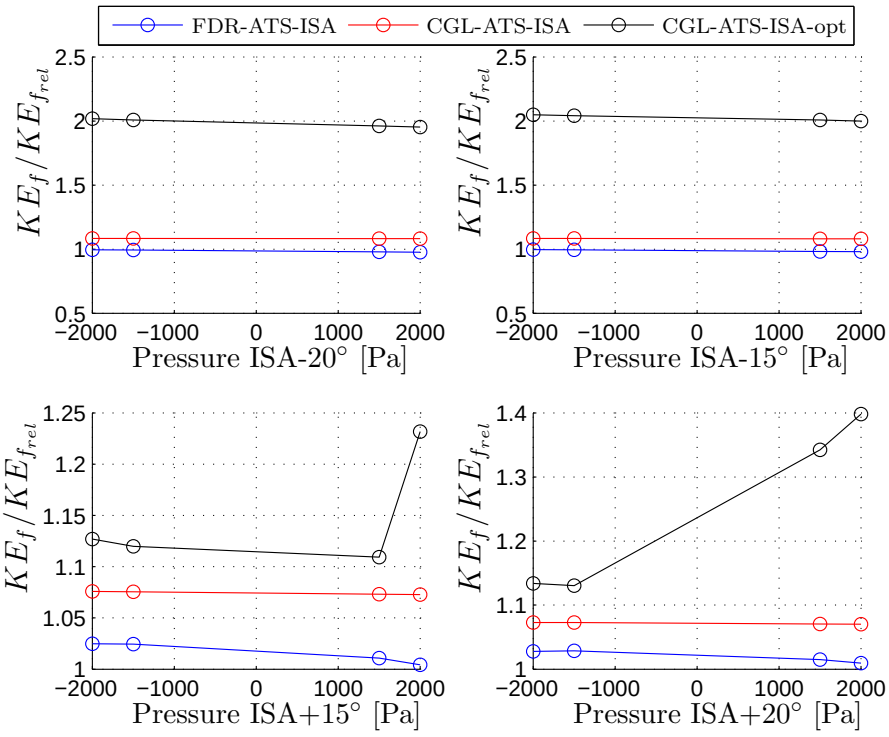


(a) Kinetic Energy Index.

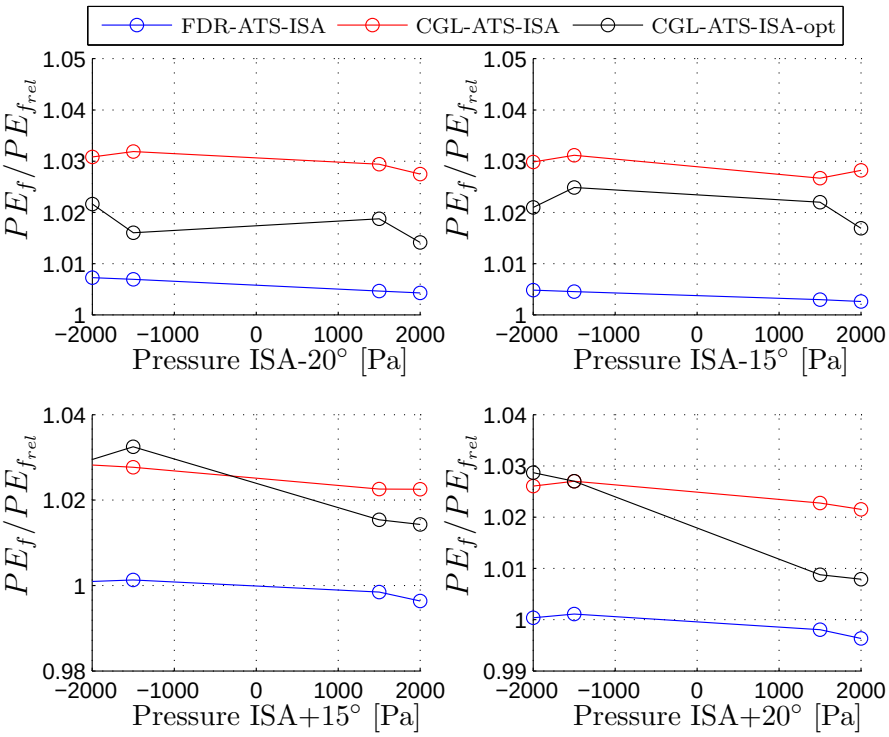


(b) Potential Energy Index.

Figure 95: Energy Index per temperatures in the most extreme atmosphere situations.

### 5.4.3 Figure of merit analysis

The figure of merit observed in Figure 96 denotes that optimal trajectories have a good figure of merit (greater than one), and therefore with a more economical energy status. However, FDR simulations have lower than one figure of merit value in ISA+1500Pa and ISA+2000Pa at all temperatures conditions.

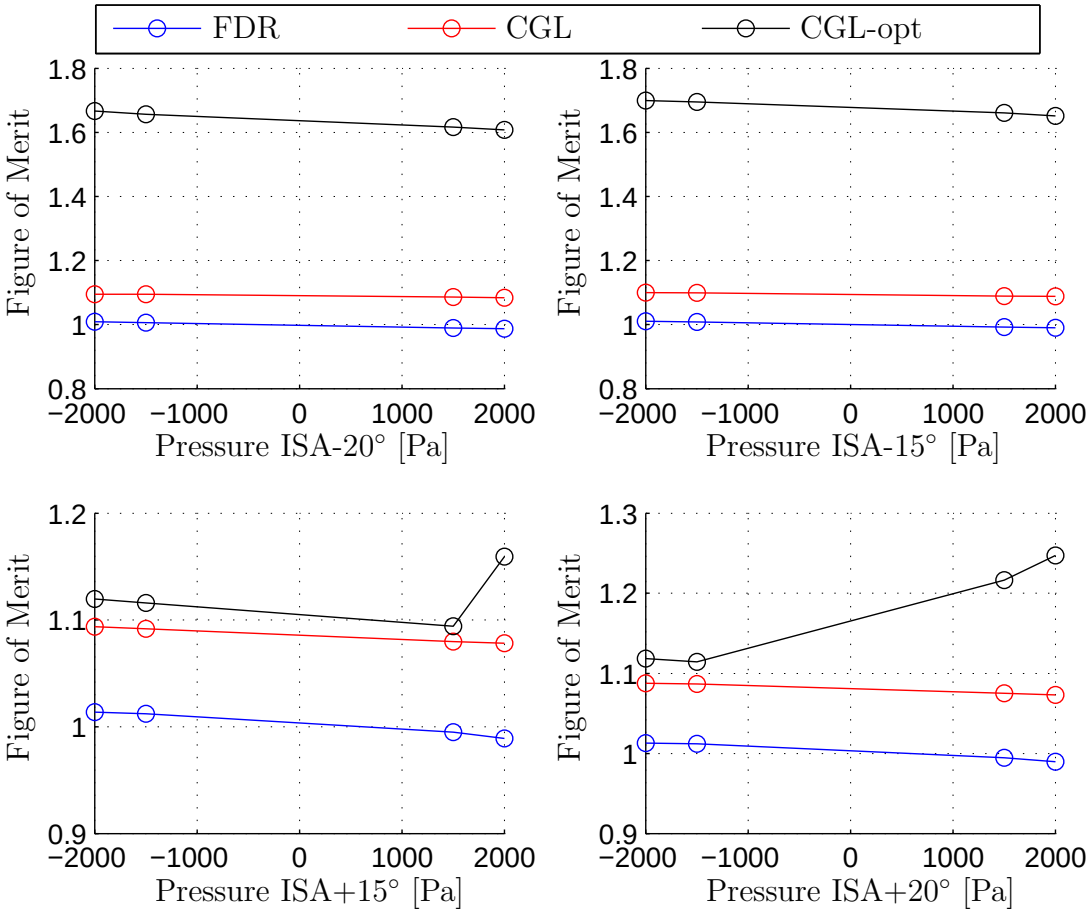


Figure 96: Energy Index in the most extreme atmosphere situations.

From Figure 97 and 98 it is clear that stabilised landing can be accomplished for all simulation and all condition except for CGL-ATS-ISA-opt at ISA-20° and ISA-15° where final TAS has a great value.

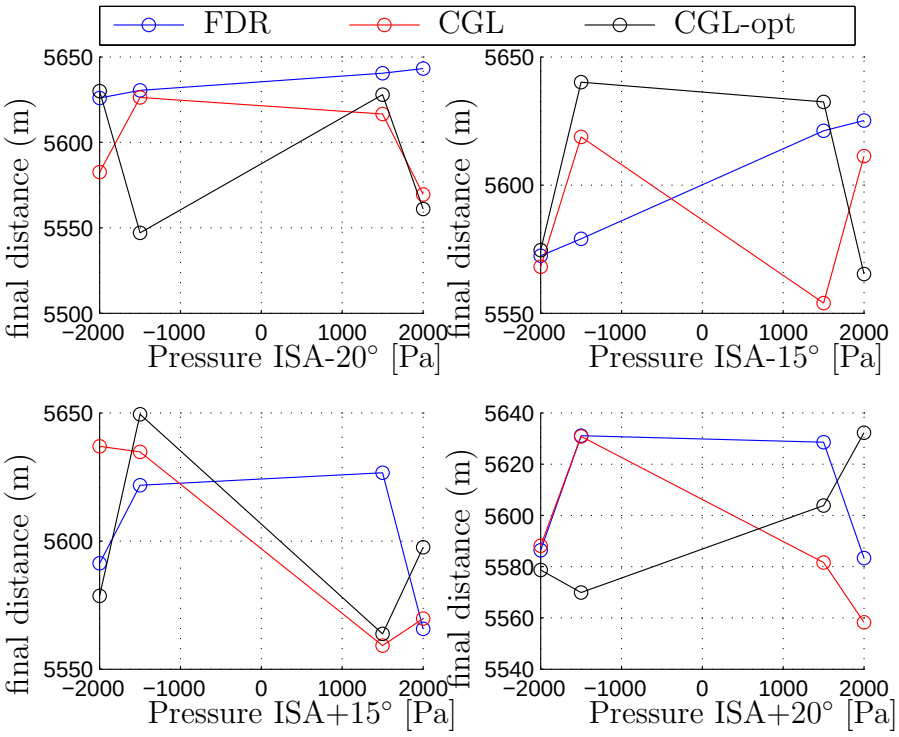


(a) Distance from the final waypoint to the airport.

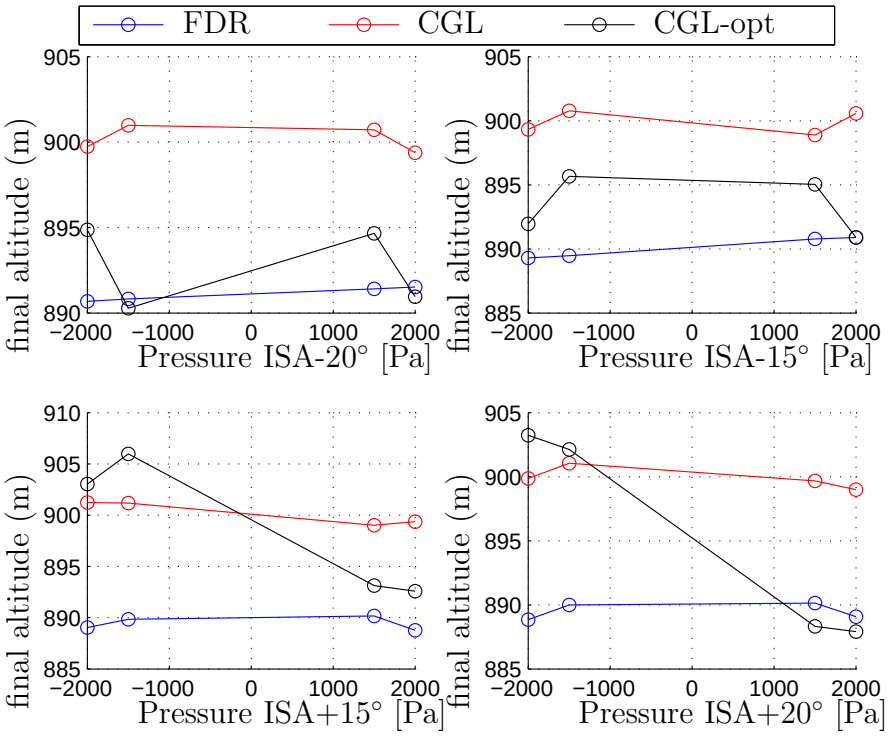


(b) Altitude from the final waypoint to the airport.

Figure 97: Distance and altitude from the final WP to the airport in the most extreme atmosphere situations.

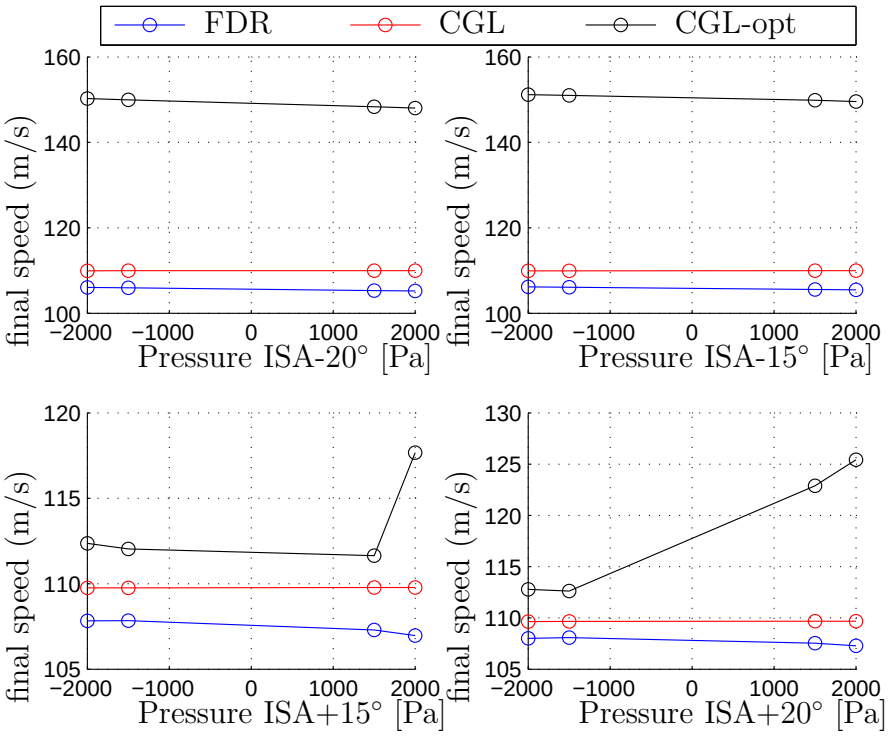


(a) TAS from the final waypoint to the airport.

Figure 98: TAS from the final WP to the airport in the most extreme atmosphere situations.

## 5.5 Different pressure and temperature at MSL values

This section presents real and optimal vertical procedures simulated at ISA pressure from ISA+2000 [Pa] to ISA-2000 [Pa] in intervals of 500 [Pa] and different temperature at MSL from ISA-20° to ISA+20° in intervals of 5°. The goal of this exercise is to establish a relationship between temperature and pressure variation in aircraft trajectories.

### 5.5.1 Cost index analysis

The fuel consumption increases proportionally with temperature and pressure, as shown in Figure 99. CGL-ATS-ISA-opt presents a different tendency in ISA-20° where fuel consumption values are higher in comparison with the other simulations.

The time at the final WP has a less dependency in pressure. FDR-ATS-ISA and CGL-ATS-ISA simulations have the worst values in ISA-15° and ISA-20° being bigger in the

CGL-ATS-ISA ones. Nevertheless, in the CGL-ATS-ISA-opt not greater delays are shown and the big ones are located at ISA+15 and ISA+20, as shown in Figure 99.

### 5.5.2 Energy index analysis

The potential energy does not depicts a particular tendency, it has less potential energy value the simulations at ISA+20°+2000Pa and the maximum at ISA-20°-2000Pa. Also, the existing differences among simulation are reduced, as shown Figure 100.

Regarding to the kinematic energy, in FDR-ATS-ISA simulations as high temperature and low pressure as great kinematic energy index is observed, as shown Figure 100. In CGL-ATS-ISA this effect is produced as high temperature and pressure. And in CGL-ATS-ISA-opt a non appreciable pressure dependence is detected, also in this simulations the kinematic values are remarkable higher than those in the others simulations.

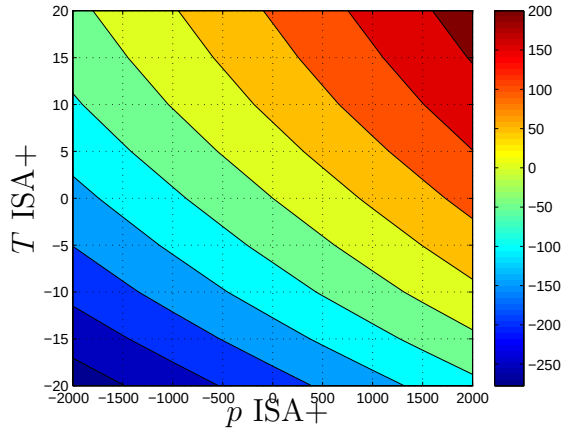


(a) $f - f_{rel}$ (kg) FDR-ATS-ISA.

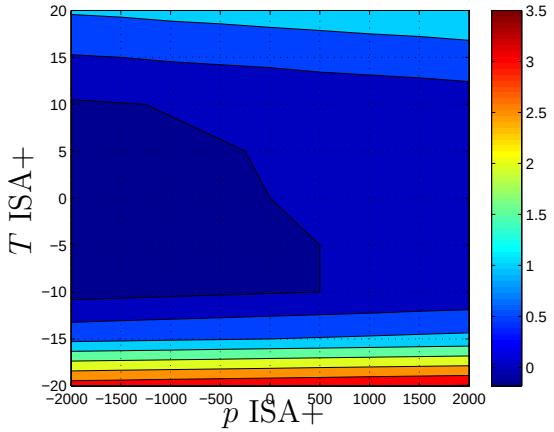


(b) $t_f - t_{f_{rel}}$ (min.) FDR-ATS-ISA.

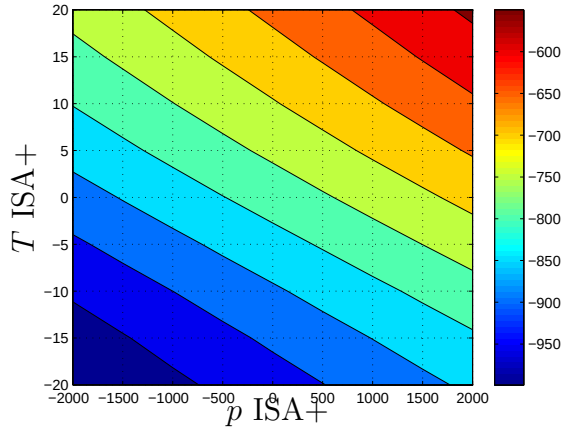


(c) $f - f_{rel}$ (kg) CGL-ATS-ISA

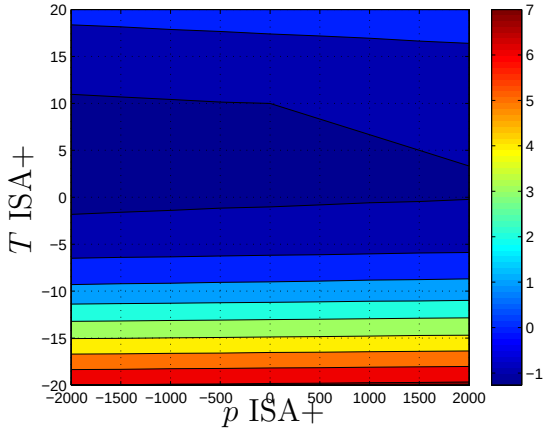


(d) $t_f - t_{f_{rel}}$ (min.) CGL-ATS-ISA

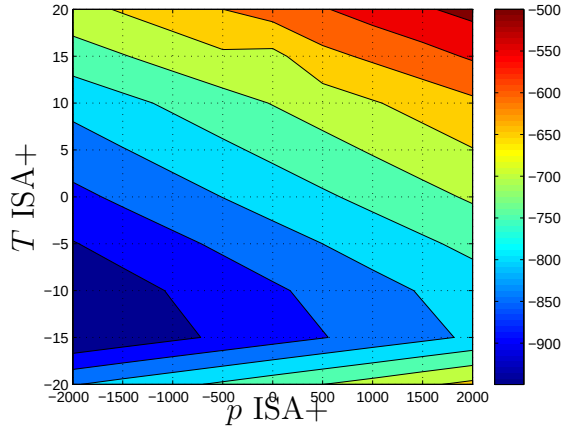


(e) $f - f_{rel}$ (kg) CGL-ATS-ISA-opt

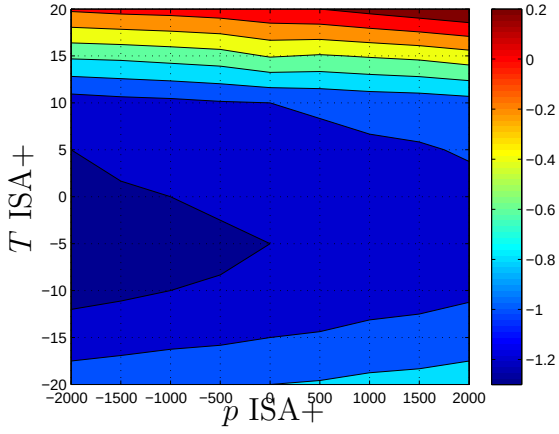


(f) $t_f - t_{f_{rel}}$ (min.) CGL-ATS-ISA-opt

Figure 99: Cost index in different atmosphere pressure and temperature at MSL.

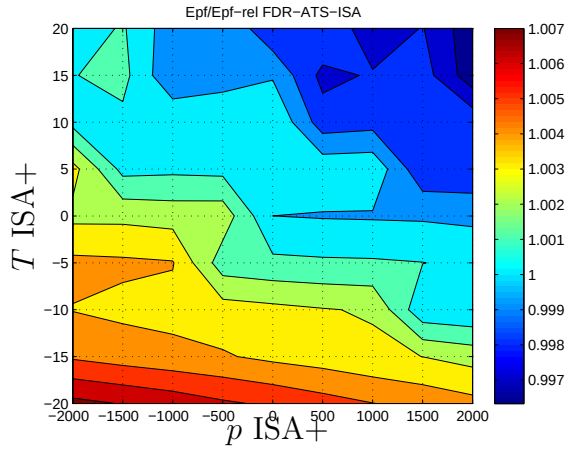


(a) Potential energy at final WP FDR-ATS-ISA.

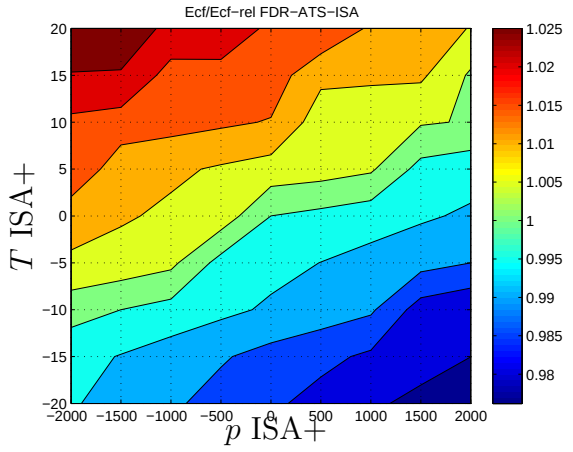


(b) Kinematic energy at final WP FDR-ATS-ISA.

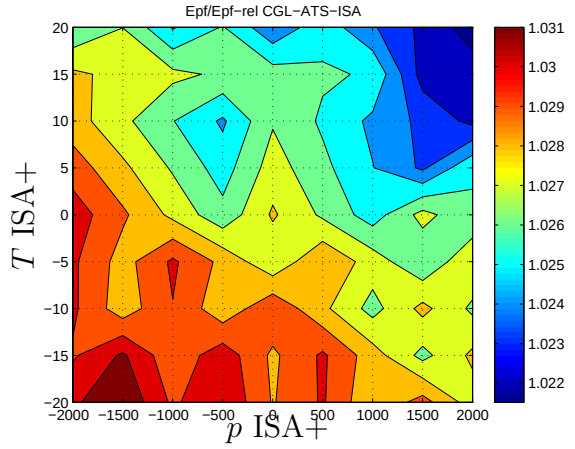


(c) Potential energy at final WP CGL-ATS-ISA

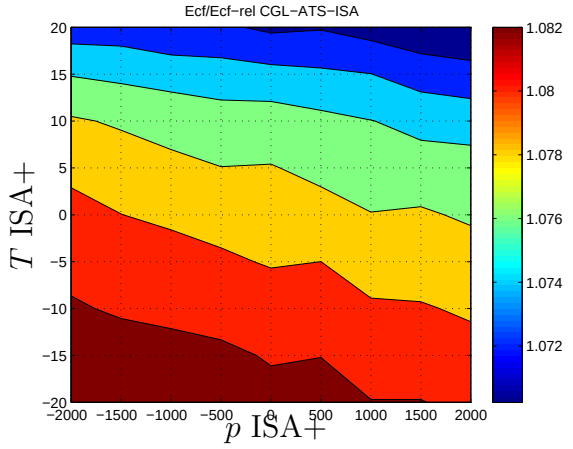


(d) Kinematic energy at final WP CGL-ATS-ISA

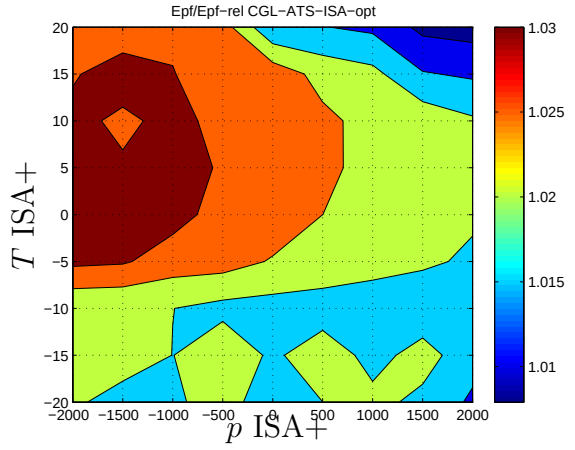


(e) Potential energy at final WP CGL-ATS-ISA-opt

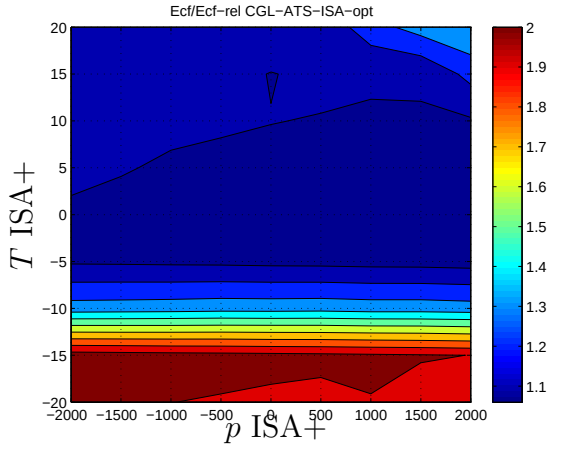


(f) Kinematic energy at final WP CGL-ATS-ISA-opt

Figure 100: Energy index in different atmosphere pressure and temperature at MSL.

### 5.5.3 Figure of merit analysis

All optimal trajectory simulations have positive figure of merit values (greater than one), but with different shapes, as shown in Figure 101; CGL-ATS-ISA has the minimum value at ISA-5°-2000Pa decreasing in value with and increase in pressure and a variation in temperature. CGL-ATS-ISA-opt shows less pressure dependent with the highest values at ISA-15° and ISA-20° and almost constant at higher than ISA-10. Nevertheless, FDR-ATS-ISA has a more pressure dependency with the non beneficial values at ISA+500Pa and above, presenting the biggest values at ISA-2000Pa.

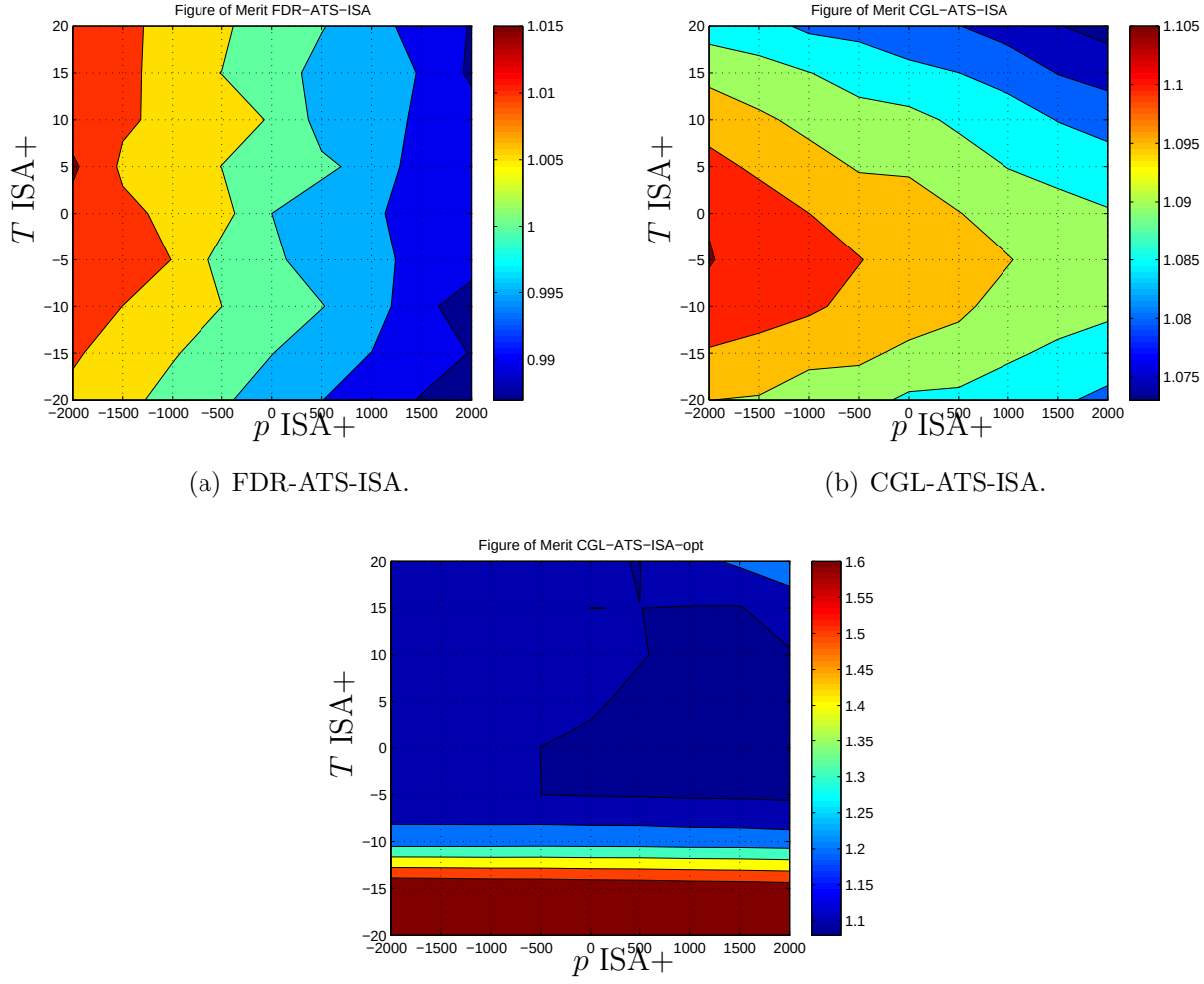


(a) FDR-ATS-ISA.

(b) CGL-ATS-ISA.

(c) CGL-ATS-ISA-opt

Figure 101: Figure of merit in different atmosphere pressure and temperature at MSL.

Figure 102 and 103 show the distance to the airport form the final WP, the altitude and the TAS at the final WP. Only TAS representations have different value among simulations. The FDR-ATS-ISA and CGL-ATS-ISA have values which allow aircraft to land. In CGL-ATS-ISA-opt non stabilised landing are presented in ISA-15° simulations.

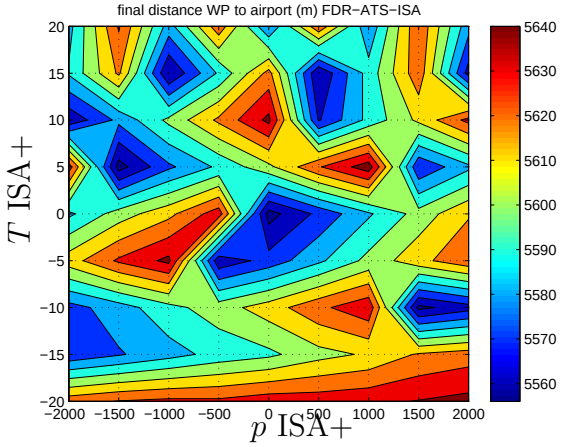


(a) FDR-ATS-ISA.

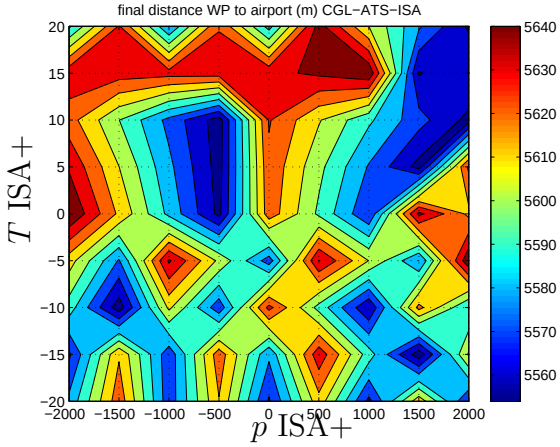


(b) CGL-ATS-ISA.

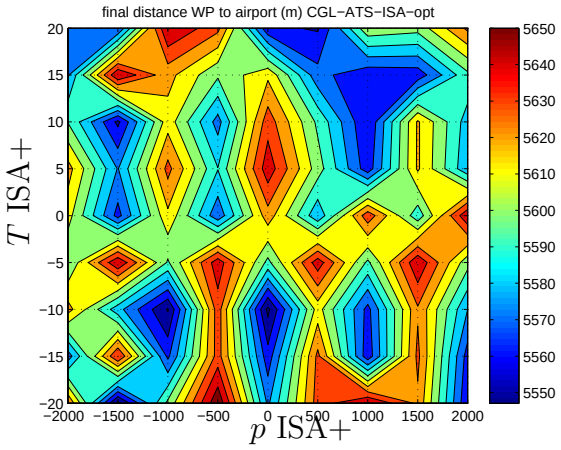


(c) CGL-ATS-ISA-opt

Figure 102: Distance from the final WP in different atmosphere pressure and temperature at MSL.

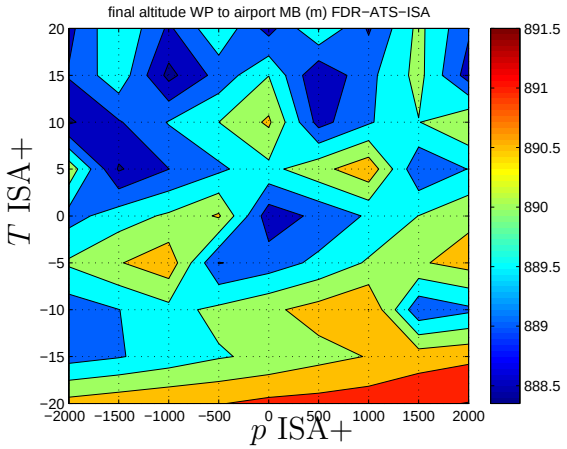


(a) Altitude at final WP FDR-ATS-ISA.

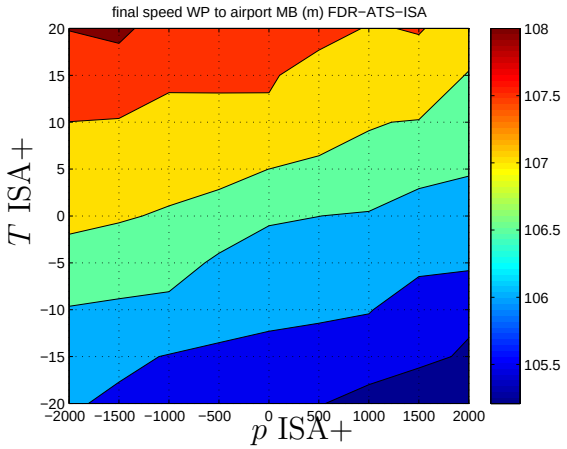


(b) TAS at final WP FDR-ATS-ISA.

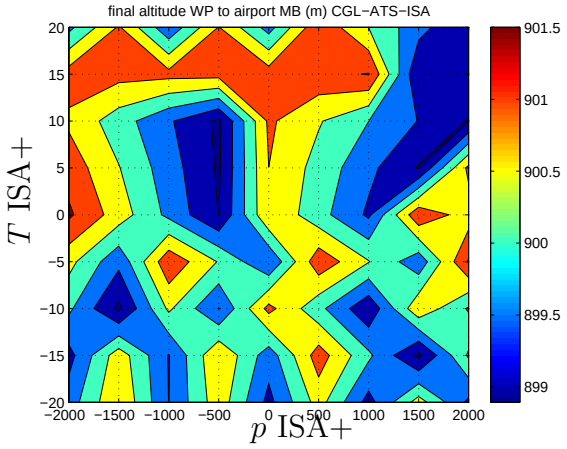


(c) Altitude at final WP CGL-ATS-ISA

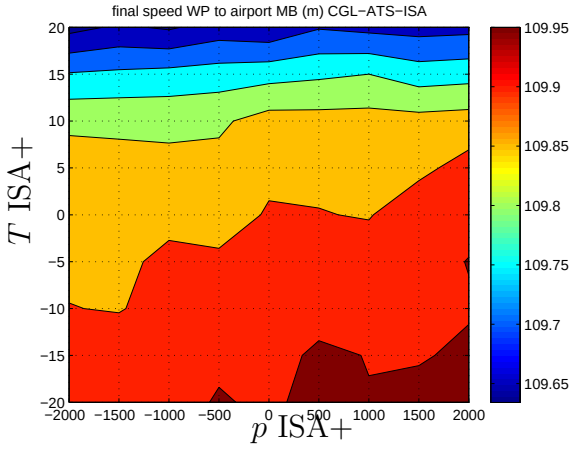


(d) TAS at final WP CGL-ATS-ISA

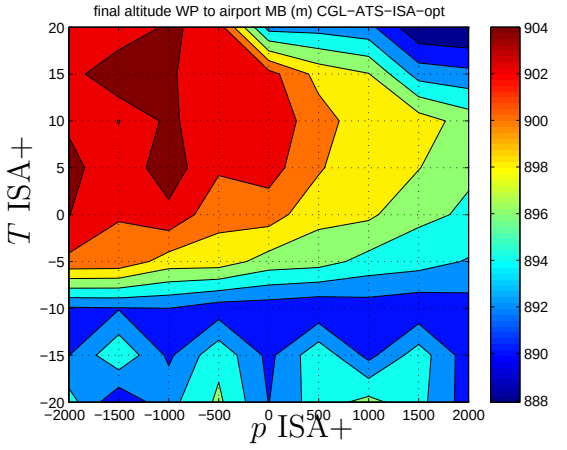


(e) Altitude at final WP CGL-ATS-ISA-opt

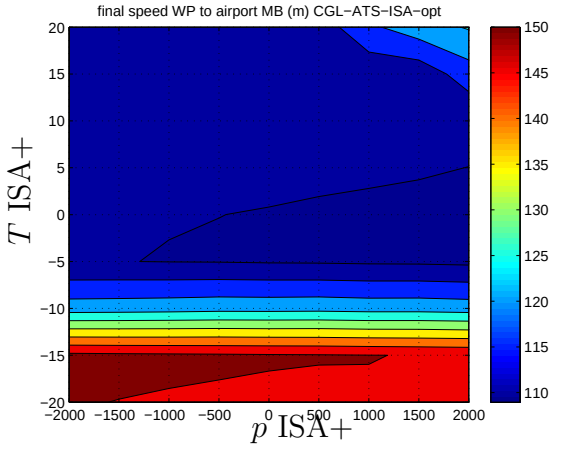


(f) TAS at final WP CGL-ATS-ISA-opt

Figure 103: Altitude and TAS from the final WP in different atmosphere pressure and temperature at MSL.

## 5.6 Discussion on the results

As atmosphere is one of the most important uncertainty source of an aircraft trajectory, this chapter presents a comparison among different atmosphere conditions applied to the optimal and real procedures presented in subsection 4.4.2 which have been introduced previously into the calibrated aircraft TS. Also, in order of analysing what happen when one optimises trajectory in one atmosphere condition at the strategic phase, but when the aircraft is flying this condition can be different optimal procedures have been compared one with ISA standard conditions (CGL-ATS-ISA) and the other optimised to the ISA studied (CGL-ATS-ISA-opt).

To get a good understanding of how atmosphere can affect aircraft performances, five different case of study have been reproduced: temperature at MSL modification, different temperature lapse rates, pressure at MSL variation, most limitative temperature and pressure value and the whole combination of temperature and pressure at MSL.

Optimal profiles presents savings form 500 to 900 [kg] in relation to the consumption at ISA standard condition into the real procedure. But where more fuel is saved and in some of the optimal simulation a delay of 7 minutes is obtained. Most colder atmospheres produces aircraft optimal trajectory is in the Mach maximum value for this kind of aircraft, and therefore TAS optimal value cannot follow the standard optimal values, with more speed at the end of the route fact that produces greater aircraft TAS final values. However, pressure variation produces almost the same vertical and TAS profile with no appreciable differences between the optimal procedures optimised to the analysing atmosphere condition and those under the ISA standard optimised parameters.

To adapt better the landing phase of flight mainly in TAS values, change of flap configuration should be applied. Also, it is interesting to optimise the moment where flap configuration should be changed.

## List of References

[1] Nuic A., *User Manual for the base of Aircraft Data (BADA) Revision 3.9*, Eurocontrol Experimental Cente, 2008.

# CHAPTER 6

## Conclusion and Future work

In this dissertation an aircraft trajectory simulator has been developed to evaluate optimal procedures in a simulated atmosphere in order of measuring the differences between the optimal trajectories and the conventional procedures. As a simplified trajectory simulator which is able to predict aircraft trajectories is required, a three degrees of freedom point mass model with BADA aircraft performance information is used. Also, the trajectory optimisation problem can be solved using optimal control problem. Therefore, a comparison among different optimisation methods was performed choosing the pseudospectral method. This is characterised by its accuracy and low computational time for the problem presented in this dissertation.

After that, through this pseudospectral method, optimal trajectories are evaluated under different atmosphere conditions. The calculated optimal trajectories and the conventional procedures with same specific atmosphere conditions are compared introducing the reference values into the aircraft trajectory simulator tool. Besides, the optimal trajectory at the specific atmosphere condition is compared with the optimal trajectory calculated at the ISA standard condition, then it is simulated at the specific atmosphere to determine how differ the planed optimal trajectory with other atmosphere conditions.

The result shows that optimal trajectory produces al least 500 [kg] of fuel savings if it is compared with the current procedures. Temperatures under standard ISA could make aircraft operates into a Mach saturation condition so slower TAS profile are obtained. For this reason, the optimal trajectory at ISA standard condition simulated in the aircraft TS with a lower atmospheric temperature makes that more time is needed to reach the final WP. However, pressure variation has a lower importance into the fuel consumption and time at the final WP. Moreover, lapse rate temperature variation produces a bit more of fuel

consumption when this variable is lower.

As future works certain research should be done in this area. Firstly, a whole flight has to be analysed under different atmosphere conditions including change of flaps configuration in order of checking if differences with the present dissertation are obtained. Also the full optimal trajectory has to be applied including the longitudinal and the vertical plane. Then, a multi-objective optimal trajectory has to be analysed above all in the take-off and landing phase, taking into consideration for instance noise, and non allowed areas. Moreover, wind has to be included into the optimisation process because it is one of the biggest uncertainties that a current aircraft trajectory has. This has to include how different wind vector affects not only the trajectory profile but also how aircraft performances (mainly fuel consumption) are affected. Finally, aircraft on-board avionic systems studies have to be done to clarify if this optimal trajectory can be implemented under geometric references or however it is unaffordable due to the lack of inputs or the great aircraft variables uncertainties in the aircraft trajectory definition.

## List of Publications

The list of publications resulting from this PhD. work is given in inverse chronological order as follows:

### Journal Papers

J. García-Heras, M. Soler, and F. J. Sáez Nieto, Comparison of Collocation Methods to Aircraft Minimum Fuel Trajectory Problems with Required Time of Arrival, *Chinese Journal of Aeronautics.* [Submitted]

J. García-Heras, F. J. Sáez, L.K. Asante and E. Justel, Validation of an Aircraft Point Mass Model Trajectory Simulator using Flight Data Recorder, *Transportation Research Part C* [Submitted]

J. García-Heras Carretero, M. Soler, and F. J. Sáez, A comparison of optimal control methods for minimum fuel cruise at constant altitude and course with fixed arrival time, in *Symposium on Aircraft Airworthiness.* The Procedia: Procedia Engineering/ELSEVIER Ltd, 2013, p. 14.

J. F. Alonso, F. J. Sáez, and J. García-Heras, Aircraft used as a sensor for atmospheric behaviour determination. practical case: pressure estimation using automatic dependent surveillance-broadcast, *Proceedings of the Institution of Mechanical Engineers, Part G: Journal of Aerospace Engineering*, vol. 227, no. 5, pp. 778-797, 2013. [Online]. Available: http://pig.sagepub.com/content/227/5/778.abstract

### Conference Proceedings

J. García-Heras, M. Soler, and F. J. Sáez, A comparison of optimal control methods for minimum fuel cruise at constant altitude and course with fixed arrival time, in *3rd International Symposium on Aircraft Airworthiness*. Toulouse, France. 2013, pp. 14.

J. García-Heras, F. J. Sáez , and R. Román, Aircraft trajectory simulator using a three degrees of freedom aircraft point mass model, in *Proceedings of the 3rd International Conference on Application and Theory of Automation in Command and Control Systems*. ACM, 2013, pp. 114-117.

J. García-Heras and F. J. Sáez, Analysis of the geometric altimetry to support aircraft optimal profiles within future 4d trajectory management, in *2nd International Conference on Application and Theory of Automation in Command and Control Systems*. ACM, 2012, pp. 196-199.

## Acronyms

**2D** two dimensional. 22

**3D** three dimensional. 22–24

**4D** four dimensional. 20, 22–24

**1090 ES** 1090MHz Extended Squitter. 21, 25, 28, 29

**AOC** Aircraft Operator Company. 2, 64

**ATM** Air traffic Management. v, 2, 9, 10, 20–24, 26, 64, 108, 119, 121

**ATC** Air Traffic Control. 1, 8, 17, 23, 108

**ADS-B** Automatic Dependent Surveillance-Broadcast. 2, 4, 6, 10, 16, 21, 22, 25–28, 35, 37, 38, 40, 46

**ACARS** Aircraft Communications, Addressing, and Reporting System. 24, 25

**ASE** Altimetry System Error. 25

**AGDL** Air/Ground Data Link. 2

**AIRE** Atlantic Interoperability initiative to Reduce Emissions. 7

**ACC** Area Control Center. 7

**AMAN** Arrivals Managers. 8

**BADA** Base of Aircraft Data. 64, 66, 78

**CDA** Continuous Descent Approach. 3, 8

**CCC** Continuous Climb Cruise. 3, 7, 8

**CCD** Continuos Climb Departure. 3, 7

**CAS** Calibrated Air Speed. 81, 82

**CVR** Cockpit Voice Recorder. 82

**CPR** Compact Position Reporting. 28

**CGL** Chebyshev-Gauss-Lobatto. 141

**CCO** Continuous Climb Operation. 6

**CI** Cost Index. 8

**DoF** Degrees of Freedom. 4, 5, 64–66

**DF** Downlink Format. 26, 28

**DEM** Diffuse Element Method. 32

**DOP** Dilution of Precision. 53, 54

**DP** Dynamic Programming. 9

**EFGM** Element-Free Galerkin Method. 32, 33, 37, 38, 46

**FMS** Flight Management System. 3, 5, 67, 68

**FCS** Flight Control System. 5, 67–69, 80, 83, 147

**FDR** Flight Data Recorder. 5, 11, 65, 68, 78, 80–82, 127

**FL** Flight Level. 1, 18

**FEM** Finite Element Method. 33

**GPS** Global Positioning System. 3, 28

**GS** Ground Speed. 80, 82

**HAE** Height Above Ellipsoid. 41

**HLGL** Hermite-Legendre-Gauss-Lobatto. 9, 10, 113

**ISA** International Standard Atmosphere. 1, 5, 6, 11, 17–19, 22, 30, 37, 40, 43, 44, 46, 67, 121, 141, 143, 145, 148, 150, 156, 165, 170, 173, 192

**INS** Inertial Navigation System. 3

**ILS** Instrumental Landing System. 4

**ICAO** International Civil Aviation Organization. 16

**IAS** Indicated Air Speed. 81, 82

**LLS** Local Level System. 80

**LIDAR** Laser Imaging Detection and Ranging. 17

**LMS** Least Mean Square. 18

**LGL** Legendre-Gauss-Lobatto. 10

**MSL** Mean Sea Level. 1, 11, 17–19, 22, 35, 37, 41, 42, 44, 143, 173, 185, 192

**ME** Message. 26

**MSG** Message. 27

**MLS** Moving Least-Squares. 33

**NASA** National Aeronautics and Space Administration. 18

**NOAA** National Oceanic and Atmospheric Administration. 25

**NM** Nautical Miles. 29

**OCP** Optimal Control Problem. 143

**PMM** Point Mass Model. 4, 5, 64, 66

**PBN** Performance Based Navigation. 2, 22

**PID** Proportional-Integral-Derivative. 69

**RNP** Required Navigation Performance. 22

**RVSM** Reduced Vertical Separation Minima. 7, 25

**RTA** Required Time of Arrival. 119, 121, 127

**SWIM** System Wide Information Management. 2

**TLP** Throttle Lever Percentage. 5, 69, 125, 147, 157, 166, 176

**TIMED** Thermosphere Ionosphere Mesosphere Energetics and Dynamics. 17

**TS** Trajectory Simulator. 64–67, 69, 82, 88, 93, 141–143, 145, 155, 192

**TAS** True Air Speed. 68, 78, 80, 83, 146, 148, 152, 155–157, 163, 165, 172, 175, 183, 190

**TBO** Trajectory Based Operation. 2, 64, 108

**TMA** Terminal Management Area. 40

**TOD** Top Of Descent. 145, 155, 165

**UTC** Universal Time Coordinated. 35

**WMO** World Meteorological Organization. 18

**WGS** World Geodetic System. 41, 80

**WP** Waypoint. 68, 69, 141, 142, 148, 150, 152, 158, 163, 168, 170, 177, 185, 190

**WP-8** Work Package number 8. 24

**WP-11** Work Package number 11. 24

## Nomenclature

| | |
|---|---|
| $\alpha$ | angle of attack |
| $\bar{a}_l$ | maximum longitudinal acceleration for civilian aircraft |
| $\bar{a}_n$ | maximum normal acceleration for civilian aircraft |
| $\beta$ | rough land representative value |
| $\epsilon$ | thrust angle of attack |
| $\eta$ | specific fuel consumption |
| $\gamma$ | pitch angle |
| $\gamma_{max}$ | maximum recommended pitch angle |
| $\gamma_{min}$ | minimum recommended pitch angle |
| $\lambda$ | longitude |
| $\mathbf{d}_{mI}$ | influence distance, which is the distance that allows the use of points that are far from the evaluation pressure point |
| $\mathbf{p}$ | base functions vector of the polynomial approximation |
| $\mu$ | roll angle |
| $\mu_{max}$ | maximum recommended roll angle |
| $\mu_{min}$ | minimum recommended roll angle |
| $\nabla p_n$ | air pressure gradient normal to the air velocity vector |
| $\omega_x$ | longitudinal component of the wind vector |

$\omega_y$ lateral component of the wind vector

$\phi$ bank angle

$\psi$ heading angle

$\rho$ atmosphere density

$\theta$ pitch angle

$\varphi$ latitude

$\varphi_c$ latitude of the area in question ($\sim 40°$)

$\vec{a}$ vector director of the current segment

$\vec{b}$ aircraft TS vector referred to the beginning WP of the current segment

$a_{ij}(x, y)$ polynomial approximation parameters

$c_I$ characteristic distance of the area

$C_v$ minimum speed coefficient

$C_{Lmax}$ maximum lift coefficient

$C_L$ lift coefficient

$Cd0$ parasitic drag coefficient of an aircraft

$D$ aircraft drag force

$d_I$ is the distance between the point at which the pressure is estimated $\mathbf{x}$ and the known pressure point (A/C location) $\mathbf{x_I}$

$d_{center}$ the distance from the aircraft TS position to the circle arc centre

$d_{straight}$ minimum distance in the straight line segment

$d_{turn}$ minimum distance in the curved line segment

$f$ Coriolis parameter

$g$ acceleration of gravity

$g_0$ acceleration of gravity at MSL

$h$ altitude

$H_b$ pressure altitude

$h_u$ maximum operative altitude at a given mass

$h_{MO}$ maximum reachable altitude

$k$ induced drag coefficient of an aircraft

$k_f$ faraway points relevance

$L$ aircraft lift force

$l_c$ characteristic distance

$LR$ temperature gradient with altitude between MSL and 11,000 [m]

$M$ mach number

$m$ aircraft mass

$M_{max}$ maximum operating mach number

$m_{max}$ maximum aircraft mass

$m_{min}$ minimum aircraft mass

$p$ pressure

$R_a$ gas constant

$Radius$ Radius value of the circumference centre

$T$ atmosphere temperature

$t_c$ characteristic time

$T_{Dev}$ difference from the ISA atmosphere temperature model to the actual atmosphere temperature

$T_{ISA}$ atmosphere temperature from ISA model

$Thr$ aircraft thrust force

$Thr_{max}$ maximum aircraft thrust force

$Thr_{min}$ minimum aircraft thrust force

$V$ true air speed

$V_s$ stall speed

$V_{M0}$ maximum operating calibrated airspeed

$W$ weight

# BIBLIOGRAPHY


Agency, U. S. D. M., *Supplement to Department of Defense World Geodetic System 1984 Technical Report*, ser. Supplement to Department of Defense World Geodetic System 1984 Technical Report. Defense Mapping Agency, 1987, no. v. 2.

Alarcón, J. F. A., Nieto, F. J. S., and Carretero, J. G.-H., "Aircraft used as a sensor for atmospheric behaviour determination. practical case: pressure estimation using automatic dependent surveillance-broadcast," *Proceedings of the Institution of Mechanical Engineers, Part G: Journal of Aerospace Engineering*, vol. 227, no. 5, pp. 778–797, 2013. [Online]. Available: http://pig.sagepub.com/content/227/5/778.abstract

Ascher, U., Christiansen, J., and Russell, R., "A collocation solver for mixed order systems of boundary value problems," *Mathematics of Computation*, vol. 33, no. 146, pp. 659–679, 1979.

Ascher, U., Mattheij, R., and Russell, R., *Numerical solution of boundary value Problems for Ordinary Differential Equations*. Society for Industrial and Applied Mathematics, 1995.

Bellman, R., *Dynamic Programming*. Princeton UP, 1957.

Belytschko, T., Lu, Y. Y., and Gu, L., "Element-free galerkin methods," *International Journal for Numerical Methods in Engineering*, vol. 37, no. 2, pp. 229–256, 1994. [Online]. Available: http://dx.doi.org/10.1002/nme.1620370205

Benjamin, S. G., Schwartz, B. E., and Cole, R. E., "Accuracy of acars wind and temperature observations determined by collocation," *Weather and Forecasting*, vol. 14, no. 6, pp. 1032–1038, 2014/05/05 1999. [Online]. Available: http://dx.doi.org/10.1175/1520-0434(1999)014⟨1032:AOAWAT⟩2.0.CO;2

Benoît Roturier, M. C., "Analysis of baro vnav safety issues," in *Proc. Navigation Systems Panel (NSP) meeting, Working Group 1&2*, Brussels, BE, 8-19 May 2006, pp. 1–10.

Betts, J. T., *Practical Methods for Optimal Control and Estimation using Nonlinear Programming*. Advances in Design and Control. Society for Industrial and Applied Mathematics, 2010.

Betts, J. T. and Cramer, E. J., "Application of direct transcription to commercial aircraft trajectory optimization," *Journal of Guidance, Control, and Dynamics*, vol. 18, no. 1, pp. 151–159, 1995.

Bhattacharya, R., "Optragen: A matlab toolbox for optimal trajectory generation," in *Decision and Control, 2006 45th IEEE Conference on*, 2006, pp. 6832–6836.

Bliss, G., *Lectures on the calculus of variations*, ser. Phoenix science series. University of Chicago Press, 1963.

Bock, H. G. and Plitt, K. J., "A multiple shooting algorithm for direct solution of optimal control problems," in *In Proceedings of the 9th International Federation of Automatic Control World Congress*, Budapest, Hungary. Pergamon Press, 1984, pp. 242–247.

Bolza, O., *Lectures on the Calculus of Variations*. Chelsea Publisher Company, New York, 1904. [Online]. Available: http://hdl.handle.net/2027/uc1.b4359558

Bonami, P., Olivares, A., M.Soler, and Staffetti, E., "Multiphase mixed-integer optimal control approach to aircraft trajectory optimization," *Journal of Guidance, Control, and Dynamics*, vol. 36, no. 5, pp. 1267–1277, 2013.

Canuto, C., *Spectral methods: Fundamentals in single domains*. Springer Verlag, 2006.

Chao, H. and Chen, Y.-Q., "Surface wind profile measurement using multiple small unmanned aerial vehicles," in *American Control Conference (ACC), 2010*, June 2010, pp. 4133–4138.

Chen, S., Qiu, Z., Zhang, Y., Chen, H., and Wang, Y., "A pure rotational raman lidar using double-grating monochromator for temperature profile detection," *Journal of Quantitative Spectroscopy and Radiative Transfer*, vol. 112, no. 2, pp. 304 – 309, 2011, ¡ce:title¿International Symposium on Atmospheric Light Scattering and Remote Sensing (ISALSaRS09)¡/ce:title¿. [Online]. Available: http://www.sciencedirect.com/science/article/pii/S0022407310002815

Clarke, J.-P. B., Ho, N. T., Ren, L., Brown, J. A., Elmer, K. R., Zou, K., Hunting, C., McGregor, D. L., Shivashankara, B. N., Tong, K.-O., *et al.*, "Continuous descent approach: Design and flight test for louisville international airport," *Journal of Aircraft*, vol. 41, no. 5, pp. 1054–1066, 2004.

Cole, R., Green, S., Jardin, M., Schwartz, B., and Benjamin, S., "Wind prediction accuracy for air traffic management decision support tools," in *3rd USA/Europe Air Traffic Management R&D Seminar, Napoli, Italy*, 2000.

Collinson, R., *Introduction to Avionics Systems*. Springer, 2002.

Coppenbarger, R. A., Mead, R. W., and Sweet, D. N., "Field evaluation of the tailored arrivals concept for datalink-enabled continuous descent approach," *Journal of Aircraft*, vol. 46, no. 4, pp. 1200–1209, 2009.

Cuesta Molina, J. L., "Estudio de dos metodos sin malla para la resolucion de ecuaciones elipticas," Ph.D. dissertation, Technical University of Madrid, Madrid, Spain, 2003.

Dalmau, R. and Prats, X., "How much fuel and time can be saved in a perfect flight trajectory?" in *International Conference on Research in Air Transportation (ICRAT)*, 2014.

Davidsson, M., "Optimal Control for Dummies," *Current Research Journal of Economic Theory*, vol. 4, pp. 88–94, 2012. [Online]. Available: http://ssrn.com/abstract=2248368

de Oliveira, R. F. and Büskens, C., *Emergency flight replanning for minimum loss of life risk using a decoupled trajectory optimization approach.* American Institute of Aeronautics and Astronautics, 2014/04/25 2013. [Online]. Available: http://dx.doi.org/10.2514/6.2013-4238

EUROCADE, *ED-102A standard: minimum operational performance standards for 1090MHz extended squatter ADS-B and Traffic Information Services-Broadcast (TIS-B)*, 2009.

EUROCONTROL, "Automatic dependent surveillance requirements," EUROCONTROL, Tech. Rep. Edition number 0.65, Jan. 2000.

EUROCONTROL, "EUROCONTROL Medium-Term Forecast: IFR Flight Movements 2011–2017," STATFOR, the EUROCONTROL Statistics and Forecast Service, Tech. Rep. Doc 442, Oct. 2011.

Eurocontrol, Performance Review Comission, "Performance review report an assessment of air traffic management in europe during the calendar year 2011: Eurocontrol PRR 2011," Eurocontrol, Tech. Rep., May 2012. http://www.eurocontrol.int/prc [Retrieved 01/09/2012].

European Comission, the FAA and the project AIRE, "North atlantic cruise climb, lateral deviation, and mach number flight trials demonstration. Final Report (D1)," SESAR Joint Undertaking, Tech. Rep., 2010.

European Comission, the FAA and the project AIRE, "Reduction of Emissions on the North Atlantic by the Implementation of ADS-B. Final Report," SESAR Joint Undertaking, Tech. Rep., 2010.

European Comission, the FAA and the project AIRE, "Atlantic Interoperability Initiative to Reduce Emission (AIRE). Summary results 2010/2011," SESAR Joint Undertaking, Tech. Rep., 2012.

Fahroo, F. and Ross, I., "Direct trajectory optimization by a Chebyshev pseudospectral method," *Journal of Guidance, Control, and Dynamics*, vol. 25, no. 1, pp. 160–166, 2002.

Fahroo, F. and Ross, I., "On discrete-time optimality conditions for pseudospectral methods," in *AIAA/AAS Astrodynamics Specialist Conference and Exhibit*, 2006, pp. 21–24.

Fahroo, F. and Ross, I. M., *Advances in Pseudospectral Methods for Optimal Control.* American Institute of Aeronautics and Astronautics, 2014/04/15 2008. [Online]. Available: http://dx.doi.org/10.2514/6.2008-7309

Fahroo, F. and Ross, I. M., "Pseudospectral methods for infinite-horizon nonlinear optimal control problems," *Journal of Guidance, Control, and Dynamics*, vol. 31, no. 4, pp. 927–936, 2014/04/15 2008. [Online]. Available: http://dx.doi.org/10.2514/1.33117

Falk, C., Gonzalez, J., and Perez, J., "Using automatic dependent surveillance-broadcast data for monitoring aircraft altimetry system error," in *Proceedings of the AIAA guidance, navigation, and control conference*, 2010, pp. 2–5.

Federal Aviation Administration Office of NextGen, *NextGen Implementation Plan*, Washington, DC 20591, 2013.

F.J., Y. and Z.M., B., "Weather data obtaining and dissemination using ads-b," in *Proceedings of the 9th Innovative Research Workshop & Exhibition, Eurocontrol Experimental Centre Brétigny-sur-Orge, France*, 2010.

Franco, A., Rivas, D., and Valenzuela, A., "Minimum-fuel cruise at constant altitude with fixed arrival time," *Journal of Guidance, Control, and Dynamics*, vol. 33, no. 1, pp. 280–285, 2010.

Frehlich, R. and Sharman, R., "Climatology of velocity and temperature turbulence statistics determined from rawinsonde and acars/amdar data," *Journal of Applied Meteorology and Climatology*, vol. 49, no. 6, pp. 1149–1169, 2014/05/06 2010. [Online]. Available: http://dx.doi.org/10.1175/2010JAMC2196.1

G., D., "Use of mode s extended squitter in automatic met air-reporting," in *Proceedings of the 5th meeting of Automatic Dependent Surveillance-Broadcast (ADS-B) Study and Implementation Task Force (ADS-B SITF/5), New Delhi, India*, 2006.

Galerkin, B., *On electrical circuits for the approximate solution of the Laplace equation citation.* Vestnik Inzh, 1915, vol. 19.

Garg, D., Patterson, M., Hager, W., Rao, A., Benson, D., and Huntington, G., "A unified framework for the numerical solution of optimal control problems using pseudospectral methods," *Automatica*, vol. 46, no. 11, pp. 1843–1851, 2010.

Garg, D., "Advances in global pseudospectral methods for optimal control," Ph.D. dissertation, University of Florida, 2011.

Garrido-López, D., Ledesma, R. G., Gershzohn, G., and Moore, S., *Analysis of Aircraft Descent Predictability: Implications for Continuous Four-Dimensional Navigation.* American Institute of Aeronautics and Astronautics, 2013/05/02 2011. [Online]. Available: http://dx.doi.org/10.2514/6.2011-6217

Gelfand, I. M. and Fomin, S. V., *Calculus of Variations.* Dover Publications, Oct. 2000. [Online]. Available: http://www.amazon.com/exec/obidos/redirect?tag=citeulike07-20&path=ASIN/0486414485

Gill, P., Murray, W., and Wright, M., *Practical Optimization.* Academic Press, 1981.

Gómez-Aíza, S., Gómez, R. W., and Marquina, V., "A simplified approach to the brachistochrone problem," *European Journal of Physics*, vol. 27, no. 5, p. 1091, 2006. [Online]. Available: http://stacks.iop.org/0143-0807/27/i=5/a=008

Gray, R. and Maybeck, P., "An integrated gps/ins/baro and radar altimeter system for aircraft precision approach landings," in *Aerospace and Electronics Conference, 1995. NAECON 1995., Proceedings of the IEEE 1995 National*, vol. 1, 1995, pp. 161–168 vol.1.

GRIB.US, "(accessed february 2011)," http://www.GRIB.US/, 2005.

GuoYing, J., JiYao, X., DongBo, S., Feng, W., and LianZhong, W., "Observations of the first meteorological rocket of the meridian space weather monitoring project," *Chinese Science Bulletin*, vol. 56, no. 20, p. 2131, 2011. [Online]. Available: http://csb.scichina.com:8080/kxtbe/EN/abstract/article_503801.shtml

Hargraves, C. R. and Paris, S. W., "Direct trajectory optimization using nonlinear programming and collocation," *Journal of Guidance, Control, and Dynamics*, vol. 10, no. 4, pp. 338–342, 1987.

Hayen, J. C., "Brachistochrone with coulomb friction," *International Journal of Non-Linear Mechanics*, vol. 40, no. 8, pp. 1057 – 1075, 2005. [Online]. Available: http://www.sciencedirect.com/science/article/pii/S0020746205000284

Howe-Veenstra, R., "Commercial aircraft trajectory optimization and efficiency of air traffic control procedures," Master's thesis, University of Minnesota, 2011.

Hull, D. G., *Fundamentals of Airplane Flight Mechanics, 1st. edn.* New York, United States of America: Springer-Verlag Berlin and Heidelberg GmbH & Co. K, 2007.

Hussain, M., "Dependence of power law index on surface wind speed," *Energy conversion and management*, vol. 43, no. 4, pp. 467–472, 2002.

ICAO, *Manual of the ICAO Standard Atmosphere. ICAO-Doc 7488/3*, Montreal, Canada, 1993.

ICAO, *Aeronautical telecommunication*, Montreal, Canada, 2007.

ICAO, *Operation of Aircraft*, Montreal, Canada, 2010.

Inc, A. R. and Committee, A. E. E., *Air-ground Character-oriented Protocol Specification*, ser. ARINC specification. Aeronautical Radio, Incorporated, 1993.

Inc, A. R. and Committee, A. E. E., *ATS data link applications over ACARS air-ground network*, ser. ARINC specification. Aeronautical Radio, Incorporated, 2001.

Inc, A. R. and Committee, A. E. E., *Character-oriented Air Traffic Service (ATS) applications*, ser. ARINC specification. Aeronautical Radio, Incorporated, 2005.

Inc, A. R. and Committee, A. E. E., *ACARS protocols for avionics end systems*, ser. ARINC specification. Aeronautical Radio, Incorporated, 2009.

International Civil Aviation Organization (ICAO), "Rules of the Air," ICAO, Tech. Rep., 10th Edtion. 2005.

Jin, L., Cao, Y., and Sun, D., "Investigation of potential fuel savings due to continuous-descent approach," *Journal of Aircraft*, vol. 50, no. 3, pp. 807–816, 2013.

Kelley, H., "Gradient theory of optimal flight paths," *AIAA Journal*, vol. 30, no. 10, pp. 947–954, 1960.

Khardi, S., "Aircraft flight path optimization. the hamilton-jacobi-bellman considerations," *Applied Mathematical Sciences*, vol. 6, no. 25, pp. 1221–1249, 2012.

Klooster, J. K., *4D Trajectory based operations*. GE Aviation Systems, 2009.

Kraft, D., "On converting optimal control problems into nonlinear programming problems," *Computational Mathematical Programming*, vol. 15, pp. 261–280, 1985.

Malwitz, A., Balasubramanian, S., Fleming, G., Yoder, T., and Waitz, I., "Impact of the reduced vertical separation minimum on the domestic united states," *Journal of Aircraft*, vol. 46, no. 1, pp. 148–156, 2013/05/02 2009. [Online]. Available: http://arc.aiaa.org/doi/abs/10.2514/1.36776

Martin, L., Falk, C., and Perez, J. L., "Investigation into the use of automatic dependent surveillance-broadcast data for monitoring aircraft altimetry system error," in *AIAA Guidance, Navigation and Control Conference and Exhibit*, 2008, pp. 18–21.

MATLAB, *version 7.10.0 (R2010a)*. Natick, Massachusetts: The MathWorks Inc., 2010.

Ministère des Transports, de L'Équipement, du Tourisme et de la mer Bureau D'Enquetes et D'Analyses Pour la Securite de L'Aviation Civile, *Flight Data Recorder Read-Out Technical and Regulatory Aspects*, France, 2005.

Miyazawa, Y., Wickramashinghe, N. K., Harada, A., and Miyamoto, Y., "Dynamic programming application to airliner four dimensional optimal flight trajectory," in *Guidance, Navigation, and Control Conference*, 2013.

Montero, G. and Sanin, N., "3-d modelling of wind field adjustment using finite differences in a terrain conformal coordinate system," *Journal of Wind Engineering and Industrial Aerodynamics*, vol. 89, no. 5, pp. 471 – 488, 2001. [Online]. Available: http://www.sciencedirect.com/science/article/pii/S0167610500000751

National Aeronautics and Space Administration. "Radiosonde stations information." Last checked: 09 March 2012. 1996. [Online]. Available: ftp://ftp-gte.larc.nasa.gov/pub/PEMTROPICSA/RADIOSONDES/

National Imagery and Mapping Agency (NIMA), *Department of Defense World Geodetic System 1984, Its Definition and Relationships With Local Geodetic Systems. Report TR8350.2*, Virginia, 22150-7500.

Nayroles, B., Touzot, G., and Villon, P., "Generalizing the finite element method: Diffuse approximation and diffuse elements," *Computational Mechanics*, vol. 10, no. 5, pp. 307–318, 1992. [Online]. Available: http://dx.doi.org/10.1007/BF00364252

Nguyen, N., *Singular Arc Time-Optimal Climb Trajectory of Aircraft in a Two-Dimensional Wind Field*. American Institute of Aeronautics and Astronautics, 2013/09/16 2006.

Nocedal, J. and Wright, S., *Numerical Optimization*. Springer Verlag, 1999.

Nuic A., *User Manual for the base of Aircraft Data (BADA) Revision 3.9*, Eurocontrol Experimental Cente, 2008.

Oceanic, U. S. N., Administration, A., on Extension to the Standard Atmosphere, U. S. C., Aeronautics, U. S. N., Administration, S., and Force, U. S. A., *U.S. standard atmosphere, 1976*, ser. NOAA–S/T. U.S. Govt. Print. Off., 1976.

Office of Research and Engineering Natinal Transportation Sagety Board, *Flight Data Recorder Handbook for Aviation Accident Investigations*, Washington, DC 20594, 2002.

Organization, I. C. A., *Technical Provisions for Mode S Services and Extended Squitter. Doc 9871*, ser. Doc (International Civil Aviation Organization). International Civil Aviation Organization, 2008.

Pan, X. and Yuan, H., "Computational algorithms and applications of element-free galerkin methods for nonlocal damage models," *Engineering Fracture Mechanics*, vol. 77, no. 14, pp. 2640 – 2653, 2010. [Online]. Available: http://www.sciencedirect.com/science/article/pii/S001379441000353X

Pant, M., Singh, I., and Mishra, B., "Numerical simulation of thermo-elastic fracture problems using element free galerkin method," *International Journal of Mechanical Sciences*, vol. 52, no. 12, pp. 1745 – 1755, 2010. [Online]. Available: http://www.sciencedirect.com/science/article/pii/S0020740310002195

Pinch, E., *Optimal Control and the Calculus of Variations*. Oxford University Press, UK, 1993.

Pontryagin, L. S., Boltyanskii, V., Gamkrelidze, R. V., and Mishchenko, E. F., *The Mathematical Theory of Optimal Processes*. Interscience Publishers, 1962.

Pontryagin, L., Boltyanskii, V., Gamkrelidze, R., and Mishchenko, E., *The mathematical theory of optimal processes*. Interscience Publisher, 1962.

Puechmorel, S. and Delahaye, D., "4d trajectories: A functional data perspective," in *Digital Avionics Systems Conference, 2007. DASC '07. IEEE/AIAA 26th*, Oct 2007, pp. 1.C.6–1–1.C.6–12.

R., H., "Meteorological information data link study group (metlinksg) ninth meeting," in *Proceedings of the ninth meeting of Meteorological Information Data Link Study Group (METLINKSG)*, 2006.

Rao, A. V., Benson, D. A., Darby, C., Patterson, M. A., Francolin, C., Sanders, I., and Huntington, G. T., "Algorithm 902: Gpops, a matlab software for solving multiple-phase optimal control problems using the gauss pseudospectral method," *ACM Transactions on Mathematical Software (TOMS)*, vol. 37, no. 2, p. 22, 2010.

RETA-CDA Consortium, "RETA-CDA: Reduction of Emissions in Terminal Areas using Continuous Descent Apporaches. Final Report." SESAR Joint Undertaking, Tech. Rep., 2010.

Rivas, D., Valenzuela, A., and de Augusto, J. L., "Computation of global trajectories of commercial transport aircraft," *Proceedings of the Institution of Mechanical Engineers, Part G: Journal of Aerospace Engineering*, 2012. [Online]. Available: http://pig.sagepub.com/content/early/2012/01/11/0954410011427107.abstract

Romero, A. V., "Aircraft trajectory optimization using parametric optimization theory," Ph.D. dissertation, University of Seville, Seville, Spain, 2012.

Ross, I. M., *A Beginner's Guide to DIDO. A MATLAB Application Package for Solving Optimal Control Problems*, September 2010.

Ross, I. and Karpenko, M., "A review of pseudospectral optimal control: from theory to flight," *Annual Reviews in Control*, vol. 36, no. 2, pp. 182–197, 2012.

Ross, I. and Fahroo, F., "Legendre pseudospectral approximations of optimal control problems," in *New Trends in Nonlinear Dynamics and Control and their Applications*, ser. Lecture Notes in Control and Information Science, Kang, W., Borges, C., and Xiao, M., Eds. Springer Berlin Heidelberg, 2003, vol. 295, pp. 327–342. [Online]. Available: http://dx.doi.org/10.1007/978-3-540-45056-6_21

RTCA, *DO 260B standard: minimum operational performance standards for 1090MHz extended squatter ADS-B and Traffic Information Services-Broadcast (TIS-B)*, Washington, USA, 2009.

Sanín, N. and Montero, G., "A finite difference model for air pollution simulation," *Advances in Engineering Software*, vol. 38, no. 6, pp. 358 – 365, 2007, advances in Numerical Methods for Environmental Engineering. [Online]. Available: http://www.sciencedirect.com/science/article/pii/S0965997806001372

Schwartz, B. E., Benjamin, S. G., Green, S. M., and Jardin, M. R., "Accuracy of ruc-1 and ruc-2 wind and aircraft trajectory forecasts by comparison with acars observations," *Weather and Forecasting*, vol. 15, no. 3, pp. 313–326, 2014/05/05 2000. [Online]. Available: http://dx.doi.org/10.1175/1520-0434(2000)015⟨0313:AORARW⟩2.0.CO;2

Sesar Consortium, "The ATM target concept, SESAR definition phase milestone deliverable 3," September 2007.

Shresta, S., Neskovic, D., and Williams, S., "Analysis of continuous descent benefits and impacts during daytime operations," in *8th USA/Europe Air Traffic Management Research and Development Seminar (ATM2009), Napa, CA*, 2009.

Soler, M., Olivares, A., and Staffetti, E., "Hybrid optimal control approach to commercial aircraft trajectory optimization," *Journal of Guidance, Control, and Dynamics*, vol. 33, no. 3, pp. 985–991, 2010.

Soler, M., Olivares, A., and Staffetti, E., "Hybrid Optimal Control Approach to Commercial Aircraft Trajectory Planning," *Journal of Guidance Control and Dynamics*, vol. 33, pp. 985–991, 2010.

Soler, M., Zapata, D., Olivares, A., and Staffetti, E., "Framework for aircraft 4D trajectory planning towards an efficient air traffic management," *Journal of Aircraft*, vol. 49, no. 1, pp. 341–348, 2012.

Soler, M., "Commercial aircraft trajectory planning based on multiphase mixed-integer optimal control," Ph.D. dissertation, Universidad Rey Juan Carlos, 2013. [Online]. Available: http://www.aerospaceengineering.es/publications/phd-thesis/

Soler, M., Olivares, A., and Staffetti, E., "Multiphase optimal control framework for commercial aircraft four dimensional flight planning problems," *Journal of Aircraft*, Acceppted for publicaton. DOI:10.2514/1.C032697.

Steen, M., Schönhals, S., Polvinen, J., Drake, P., Cariou, J.-P., and Barbaresco, F., "Candidate technologies survey of airport wind & wake-vortex monitoring sensors," in *9th Innovative Research Workshop & Exhibition, Eurocontrol Experimental Centre Brétigny-sur-Orge, France*, 2010, pp. 7–9.

Steve Creamer, S. E. and Haase, N., "Reduced vertical separation minima in u.s. airspace: Air traffic control issues and answers," *Journal of Air Traffic Control*, 2003.

Stevens, B. L. and Lewis, F. L., *Aircraft Control and Simulation*. Wiley-Interscience, Oct. 2003. [Online]. Available: http://www.amazon.com/exec/obidos/redirect?tag=citeulike07-20&path=ASIN/0471371459

Stoer, J. and Bulirsch, R., *Introduction to Numerical Analysis*. Springer Verlag, 2002.

Sussmann, H. J. and Willems, J. C., "The Brachistochrone Problem and Modern Control Theory," *Contemporary trends in non-linear geometric control theory and its applications*, pp. 113–165, 2002. [Online]. Available: http://math.rutgers.edu/~sussmann/papers/brachistochrone-mex.pdf

Sussmann, H. and Willems, J., "300 years of optimal control: from the brachystochrone to the maximum principle," *Control Systems, IEEE*, vol. 17, no. 3, pp. 32–44, Jun.

Thales ATM, "Analysis of sesar 4d trajectory activities-trajectory decomposition for se-2020 task order 0022 international harmonization of 4d trajectory activities," September 2012.

Tsang, T., Himmelblau, D., and Edgar, T., "Optimal control via collocation and non-linear programming," *International Journal of Control*, vol. 21, no. 5, pp. 763–768, 1975.

Tullot, I., *Climatología de España y Portugal*, ser. Acta Salmanticensia. Ediciones Universidad de Salamanca, 2000.

Undertaking., S. J., "Sesar (single european sky atm research)," http://www.sesarju.eu/, 2007.

Vallis, G. K., *Atmospheric and oceanic fluid dynamics: fundamentals and large-scale circulation*. Cambridge University Press, 2006.

Williams, P., "Hermite-Legendre-Gauss-Lobatto direct transcription methods in trajectory optimization," *Advances in the Astronautical Sciences*, vol. 120, Part I, pp. 465–484, 2005.

Wilson, R., Luce, H., Dalaudier, F., and Lefrère, J., "Turbulence patch identification in potential density or temperature profiles," *Journal of Atmospheric and Oceanic Technology*, vol. 27, no. 6, pp. 977–993, 2013/05/02 2010. [Online]. Available: http://dx.doi.org/10.1175/2010JTECHA1357.1

WindStation, "Windstation - a software for the numerical simulation of wind flow over complex topography. easycfd - educational user-friendly ccd (computational fluid dynamics) software," http://www.easycfd.net/wind-station/, 2011 (accessed May 2011).

Young Yee, E. Y., "A study of barometric altimeter in high latitude regions," in *A13th conference on aviation, range and aerospace meteorology (ARAM)*, New Orleans, LA, 2008.

Zhang, L., Ouyang, J., Wang, X., and Zhang, X., "Variational multiscale element-free galerkin method for 2d burgers' equation," *Journal of Computational Physics*, vol. 229, no. 19, pp. 7147 – 7161, 2010. [Online]. Available: http://www.sciencedirect.com/science/article/pii/S0021999110003190

Zhang, Z., "Numerical development of an improved element-free galerkin method for engineering analysis," Ph.D. dissertation, City University of Hong Kong, Hong Kong, China, 2009.